Mechanisms of Longevity Extension by Caloric Restriction and Lithocholic Acid in the Yeast *Saccharomyces Cerevisiae*

Anthony Arlia-Ciommo

A Thesis
in
The Department
of
Biology

Presented in Partial Fulfillment of the Requirements
For the Degree of
Doctor of Philosophy (Biology) at
Concordia University
Montreal, Quebec, Canada

November 2018

CONCORDIA UNIVERSITY

SCHOOL OF GRADUATE STUDIES

This is to certify that the thesis prepared

By: Anthony Arlia-Ciommo

Entitled: Mechanisms of Longevity Extension by Caloric Restriction and Lithocholic Acid in the Yeast Saccharomyces Cerevisiae

and submitted in partial fulfillment of the requirements for the degree of

Doctor Of Philosophy (Biology)

complies with the regulations of the University and meets the accepted standards with respect to originality and quality.

Signed by the final examining committee:

_____ Chair
Dr. Roisin O'Connor

_____ External Examiner
Dr. Dusica Maysinger

_____ External to Program
Dr. Peter Darlington

_____ Examiner
Dr. Alisa Piekny

_____ Examiner
Dr. Dajana Vuckovic

_____ Thesis Supervisor
Dr. Vladimir Titorenko

Approved by _____
Dr. Robert Bertrand Weladji, Graduate Program Director

December 19, 2018

_____
Dr. André Roy, Dean, Faculty of Arts and Science

ABSTRACT

Mechanisms of Longevity Extension by Caloric Restriction and Lithocholic Acid in the Yeast *Saccharomyces Cerevisiae*

Anthony Arlia-Ciommo, Ph.D.

Concordia University, 2018

The objective of studies described in this thesis was to elucidate molecular and cellular mechanisms by which caloric restriction (CR) and lithocholic acid (LCA) extend longevity of the budding yeast *Saccharomyces cerevisiae*. Recent studies of how CR influences a pattern of metabolism and organelle dynamics in the chronologically aging yeast *S. cerevisiae* have revealed that this low-calorie diet alters age-related dynamics of ethanol metabolism, lipid synthesis and degradation, trehalose metabolism, ROS homeostasis maintenance, mitochondrial morphology control, mitochondrial functionality preservation, stress response control, cell cycle regulation, quiescence maintenance, and apoptotic and liponecrotic death subroutines. Our hypothesis was that CR may delay yeast chronological aging by altering the age-related dynamics of some or all these cellular processes. Findings presented here support this hypothesis. Indeed, we found that CR slows yeast chronological aging by mechanisms that coordinate the spatiotemporal dynamics of various cellular processes before entry into a non-proliferative state and after such entry. CR causes a stepwise establishment of an aging-delaying cellular pattern by tuning a network that assimilates the following: 1) pathways of carbohydrate and lipid metabolism; 2) communications between the endoplasmic reticulum, lipid droplets, peroxisomes, mitochondria and the cytosol; and 3) a balance between the processes of mitochondrial fusion and fission. Through different phases of the aging process, the CR-dependent remodeling of this intricate network 1) postpones

the age-related onsets of apoptotic and liponecrotic modes of regulated cell death; and 2) actively increases the chance of cell survival by supporting the maintenance of cellular proteostasis. Because CR decreases the risk of cell death and actively increases the chance of cell survival throughout chronological lifespan, this dietary intervention extends longevity of chronologically aging yeast.

We also used a mass spectrometry-based quantitative analysis of the water-soluble cellular metabolome for the investigation of how CR and the longevity-extending *tor1Δ* mutation (which eliminates the Tor1 protein kinase known to orchestrate the nutrient- and energy-sensing TOR [target of rapamycin] pro-aging signaling pathway) influence the concentrations of various water-soluble metabolites at consecutive stages of the chronological aging process in *S. cerevisiae*. Our investigation provided the first evidence that both the longevity-extending diet CR and the-longevity extending mutation *tor1Δ* establish a similar pattern of relative concentrations of methionine metabolism intermediates through the entire process of chronological aging in *S. cerevisiae*. We proposed a hypothesis that the observed redirection of metabolite flow from the biosynthesis of methionine and spermidine to the biosynthesis of cysteine and glutathione may represent an anti-aging pattern characteristic of the ″metabolic signature″ of longevity extension in chronologically aging yeast cells placed on the CR diet or having the TOR pro-aging signaling pathway being inactivated.

Based on recent findings from the Titorenko laboratory, we hypothesized that the LCA-driven changes in mitochondrial lipidome may have a causal role in the age-related remodeling of proteome, thus eliciting changes in mitochondrial functionality and delaying yeast chronological aging. To test this hypothesis, we used a mass spectrometry-based quantitative analysis to investigate how certain mutations that eliminate enzymes involved in mitochondrial phospholipid

metabolism influence the mitochondrial proteome and how they affect the geroprotective efficiency of LCA in chronologically aging yeast. Our investigation provided the first evidence that LCA-driven specific changes in the composition of mitochondrial membrane lipids cause a distinct remodeling of mitochondrial proteome by decreasing and increasing concentration of many mitochondrial proteins. These proteins have been implicated in such vital mitochondrial functions as the ETC and respiration, the TCA cycle, ribosome assembly, amino acid metabolism, carbohydrate metabolism, protein import, proteostasis, metabolite synthesis, protein synthesis, ATP synthesis, metabolite transport, lipid metabolism, contact sites and cristae maintenance, redox homeostasis, mtDNA maintenance, stress response, mRNA synthesis and processing, the maintenance of contact sites between mitochondria and vacuoles, and mitochondrial fusion. We provided evidence that the LCA-dependent remodeling of mitochondrial lipidome and the resulting changes in mitochondrial proteome are essential for the ability of LCA to delay aging.

Our recent studies have indicated that under CR conditions LCA influences not only the composition and functionality of mitochondria but also some cellular processes confined to other cellular compartments. We therefore hypothesized that LCA may delay chronological aging of yeast limited in calorie supply also because it affects these other cellular processes taking place in various cellular locations. To test this hypothesis, we investigated mechanisms through which LCA controls the spatiotemporal dynamics of these other cellular processes in different cellular locations under CR conditions. Our investigation provided important new insights into the mechanisms by which LCA delays yeast chronological aging under CR conditions by altering the spatiotemporal dynamics of a cellular network that integrates certain pathways of lipid and carbohydrate metabolism, some intercompartmental communications, specific aspects of mitochondrial morphology and functionality, and liponecrotic and apoptotic modes of regulated cell death.

Because LCA triggers major changes in the age-related chronology of several vital processes taking place in mitochondria, we hypothesized that LCA may cause these changes by eliciting a reversible phosphorylation of some mitochondrial proteins. To test this hypothesis, we investigated if an exposure of chronologically aging yeast to exogenous LCA can trigger such phosphorylation. We found that LCA elicits the establishment of a distinct phosphoprotein profile of mitochondria, which significantly differs from the phosphoprotein profile of mitochondria in yeast cells cultured without LCA.

Acknowledgements

I am grateful to my supervisor, Dr. Vladimir Titorenko, for his guidance and support during the years I spent in his laboratory. I would like to thank the members of my committee, Dr. Dajana Vuckovic and Dr. Alisa Piekny, for their valuable suggestions during my graduate research and studies. In addition, I would like to thank the Center for Biological Applications of Mass Spectrometry (CBAMS) and especially Heng Jiang and Alain Tessier for invaluable assistance and expertise with training and assistance in method development and instrumentation for my various uses of mass spectrometry. I would like to thank my friends and fellow graduate students Adam Beach, Michelle Burstein, Paméla Dakik, Rachel Feldman, Vicky Lutchman, Mélissa McAuley, Younes Medkour, Darya Mitrofanova, Karamat Mohammad, Amanda Piano, Vincent Richard and Veronika Svistkova. I would also like to acknowledge the large number of undergraduate students, volunteers, summer research students, and international exchange students who made the laboratory a vibrant and diverse work environment. My doctoral studies were funded by the Fonds de la recherche en santé du Québec (FRSQ) and Natural Sciences and Engineering Research Council of Canada (NSERC).

Table of Contents

List of Figures and Tables

List of Abbreviations

ACN, acetonitrile

CDP-DAG, cytidine diphosphate-diacylglycerol

CDK, cyclin-dependent kinase

CFU, colony forming units

CLS, chronological lifespan

CL, cardiolipin

CR, caloric restriction

CW, Calcofluor White M2R

DAG, diacylglycerol

DHR, Dihydrorhodamine 123

DIC, differential interference contrast

DTT, dithiothreitol

ER, the endoplasmic reticulum

ETC, electron transport chain

IAA, iodoacetamide

IMM, inner mitochondrial membrane

IMS, the intermembrane space

LCA, lithocholic bile acid

MAM, the mitochondria-associated membrane domain of the endoplasmic reticulum

MFQL, Molecular Fragmentation Query Language

MICOS, the mitochondrial contact site protein complex

MS, mass spectrometry

mtDNA, mitochondrial DNA

nDNA, nuclear DNA

OMM, outer mitochondrial membrane

PA, phosphatidic acid

PC, phosphatidylcholine

PCD, programmed cell death

PG, phosphatidylglycerol

PGP, phosphatidylglycerol-phosphate

Pho85, phosphate metabolism, protein 85

PI, phosphatidylinositol

PKA, protein kinase A

POA, palmitoleic acid

PS, phosphatidylserine

PP2ACdc55, the Cdc55 protein phosphatase 2A

RLS, replicative lifespan

ROS, reactive oxygen species

RP-HPLC/MS, reverse phase high performance liquid chromatography coupled to mass spectrometry

R123, Rhodamine 123

Snf1, sucrose non-fermenting, protein 1

SSC, statistically significantly changed

SU, statistically unchanged

TCA, tricarboxylic acid

TORC1, target of rapamycin complex 1

1.1 Introduction

The budding yeast *Saccharomyces cerevisiae* is an advantageous model organism for unveiling fundamental mechanisms and biological principles underlying the inherent complexity of cellular aging in multicellular eukaryotes [1-6]. Because this unicellular eukaryote is amenable to comprehensive biochemical, genetic, cell biological, chemical biological, system biological and microfluidic dissection analyses [7-12], its use as a model in aging research provided deep mechanistic insights into cellular processes essential for longevity regulation in evolutionarily distant eukaryotic organisms. Due to the relatively short and easily monitored chronological and replicative lifespans of the yeast *S. cerevisiae*, it played a pivotal role in discovering: 1) numerous genes that impact cellular aging and define organismal longevity not only in yeast but also in eukaryotic organisms across phyla; 2) some key nutrient- and energy-sensing signaling pathways that orchestrate an evolutionarily conserved set of longevity-defining cellular processes across species; and 3) several aging-decelerating and longevity-extending small molecules, many of which slow down aging, improve health, attenuate age-related pathologies and delay the onset of age-related diseases in evolutionarily distant multicellular eukaryotic organisms [1-6, 13-22]. These studies convincingly demonstrated that the signaling pathways governing cellular aging and mechanisms of their modulation by longevity-extending genetic, dietary and pharmacological interventions are conserved across species.

1.1.1 Two ways of studying *S. cerevisiae* aging and two groups of mechanisms underlying aging of this yeast

There are two different paradigms of yeast aging. Each of them is traditionally investigated separately from each other with the help of robust assays; these assays are conducted under controllable laboratory conditions [23-26] and have been recently automated to enable a systems-level analysis of the aging process in a high-throughput format [9-12, 27-29].

In the chronological aging paradigm, yeast aging is defined by the length of time during which a cell remains viable after an arrest of its growth and division [23, 30, 31]. Yeast chronological aging under laboratory conditions is assessed using a simple clonogenic assay. This assay measures the percentage of yeast cells that in liquid cultures remain viable at different time points following entry of a cell population into the non-proliferative stationary phase; cell viability in the clonogenic assay is assessed by monitoring the ability of a cell to form a colony on the

surface of a solid nutrient-rich medium [3, 25, 30]. Chronological aging in yeast is believed: 1) to mimic aging of non-dividing, post-mitotic cells (such as neurons) in a multicellular eukaryotic organism; and 2) to serve as a simple model for organismal aging [32, 33].

In the replicative aging paradigm, yeast aging is defined by the maximum number of daughter cells that a mother cell can produce before becoming senescent [24, 34, 35]. *S. cerevisiae* reproduces by asymmetric cell division; therefore, its replicative aging under laboratory conditions is typically assessed by using a micromanipulator to remove the budding progeny of a mother cell and counting the cumulative number of asymmetric mitotic divisions this mother cell could undergo [24, 35]. Replicative aging in yeast is thought to mimic aging of dividing, mitotically active cells (such as lymphocytes) in a multicellular eukaryotic organism [2, 32].

The use of robust assays for elucidating longevity regulation in chronologically or replicatively aging yeast under controllable laboratory conditions has significantly advanced our understanding of cell-autonomous mechanisms that orchestrate longevity-defining cellular processes within an individual cell in eukaryotic organisms across phyla [1-3, 5, 6, 10]. Recent studies in yeast also advanced fundamental knowledge about cell-non-autonomous intraspecies mechanisms of longevity regulation. Such mechanisms operate within organized populations of yeast cells that are attached to solid surfaces to form a colony or a biofilm; these cells: 1) communicate with each other and cells in surrounding colonies or biofilms; 2) age chronologically and replicatively; and 3) undergo spatially organized growth, differentiation, aging or death, depending on their position within the colony [4, 36-43].

It seems that cell-autonomous and cell-non-autonomous intraspecies mechanisms regulating yeast longevity have evolved in the process of natural selection within an ecosystem [44-46]. It has been recently proposed that this process: 1) is governed by ecosystemic interspecies mechanisms of lifespan regulation operating within the ecosystem; and 2) is driven by the ability of yeast cells to undergo specific pro-survival changes to their metabolism and physiology in response to some chemical compounds that, after being released to the ecosystem by other groups of organisms, may trigger a hormetic and/or cytostatic response in yeast [44-48].

1.1.2 Cell-autonomous mechanisms orchestrate longevity-defining cellular processes in chronologically aging yeast prior to an arrest of cell growth and division

A body of recent evidence supports the view that certain cellular processes taking place early in life of a chronologically aging yeast cell, prior to entry into a non-proliferative state, define the length of time during which this cell remains viable after such entry - i.e., define longevity of chronologically aging yeast grown under controllable laboratory conditions in liquid media [3, 20, 23, 49-73]. These longevity-defining cellular processes: 1) are essential for metabolism, growth, proliferation, stress resistance, macromolecular homeostasis, survival and death of individual yeast cells that age chronologically; and 2) are orchestrated via cell-autonomous mechanisms of lifespan regulation operating within these cells. The longevity-defining cellular processes and mechanisms orchestrating their progression in chronologically aging yeast prior to entry into a non-proliferative state (and, for some of them, after such entry) are outlined below in sections 1.1.3-1.1.6.

1.1.3 Intracellular trehalose modulates cellular protein homeostasis (proteostasis)

Recent studies revealed that the intracellular concentrations of trehalose prior to cell entry into a non-proliferative state and following such entry play essential and differing roles in defining longevity of chronologically aging yeast; this is because trehalose is involved in modulating protein folding, misfolding, unfolding, refolding, oxidative damage, solubility and aggregation throughout lifespan [23, 61] (Figure 1.1A). In chronologically ″young″ yeast cells, which undergo growth and division, trehalose plays an essential longevity-extending role because this non-reducing disaccharide: 1) binds to newly synthesized cellular proteins, thereby stabilizing their native folding states and attenuating their conversion into aberrantly folded and/or unfolded protein species; 2) shields the contiguous exposed hydrophobic side chains of amino acids that are abundant in misfolded, partially folded and unfolded protein species and that are known to promote their aggregation, thereby eliciting a direct inhibitory effect on the formation of insoluble protein aggregates; and 3) protects cellular proteins from oxidative carbonylation by interacting with their carbonylation-prone aberrantly folded species, thus having an indirect inhibitory effect on the aggregation of oxidatively damaged proteins [23, 61] (Figure 1.1A). In contrast, in chronologically ″old″ yeast cells, which do not grow or divide, trehalose plays a key role in shortening longevity. This is because in such cells trehalose shields the patches of hydrophobic amino acid residues that are abundant in aberrantly folded protein species [61]. Thus, in chronologically ″old″ yeast cells trehalose competes with molecular chaperones for binding with these patches of hydrophobic amino acid residues known to be required for the chaperone-assisted refolding of misfolded,

partially folded and unfolded protein species [74-77] - either soluble or extracted from protein aggregates with the help of molecular chaperones [61] (Figure 1.1A). Importantly, it has been demonstrated that a caloric restriction (CR) diet and certain genetic interventions affecting trehalose synthesis or degradation extend longevity of chronologically aging yeast because they simultaneously: 1) increase the intracellular concentration of trehalose by 70-160% (above its level detected in yeast cultured under non-CR conditions) in chronologically ″young″, proliferating cells; and 2) reduce the intracellular concentration of trehalose by 60-80% (below a threshold observed in yeast cultured under non-CR conditions) in chronologically ″old″, non-proliferating cells [61]. These findings suggest the existence of at least two ″checkpoints″ during the lifespan of a chronologically aging yeast cell at which the intracellular concentration of trehalose (which depends on a balance between trehalose synthesis and degradation) defines its longevity by modulating cellular proteostasis. It seems that one of these checkpoints exists early in life of a chronologically aging yeast cell (i.e., prior to entry into a non-proliferative state), whereas the other checkpoint occurs late in its life (i.e., after such cell enters a non-proliferative state).

1.1.4 Protein import into the peroxisome impacts longevity-defining processes in other cellular compartments

The efficiency of peroxisomal protein import has been shown to decline with the chronological age of a eukaryotic cell [57, 58, 78, 79]; such import is driven by Pex5p and Pex7p, the peroxisomal targeting signal type 1 (PTS1) and PTS2 cytosolic shuttling receptors, respectively [80-82]. Recent findings support the view that the age-dependent efficiency of protein import into the peroxisome defines the efficiencies of fatty acid oxidation, hydrogen peroxide turnover and anaplerotic metabolism within this organelle; these metabolic processes are known to modulate the dynamic communications of peroxisomes with other cellular compartments via a unidirectional or bidirectional flow of certain soluble metabolites and lipids [20, 57, 58, 65, 85-89]. By influencing longevity-defining cellular processes confined to these other compartments, the metabolic processes within the peroxisome cause the development of a pro- or anti-aging cellular pattern [20, 54, 57, 58, 65, 83-89].

Altogether, these findings suggest a model for how the age-dependent efficiency of peroxisomal protein import in chronologically aging yeast defines the age-related metabolic pattern of peroxisomes, thus impacting longevity-defining processes in other cellular

compartments and ultimately establishing a pro- or anti-aging cellular pattern (Figure 1.1B). The model envisions that chronologically ″young″ yeast cells develop and maintain an anti-aging cellular pattern in part because in these cells the efficiency of Pex5p- and Pex7p-dependent peroxisomal protein import exceeds a threshold. Specifically, such ″young″ cells are proficient in peroxisomal import of the following proteins: 1) catalase Cta1p and peroxiredoxin Pmp20p, both required for decomposition of hydrogen peroxide and other reactive oxygen species (ROS) within the peroxisome; 2) Fox1p, Fox2p and Fox3p, enzymes involved in peroxisomal β-oxidation of fatty acids to acetyl-CoA; and 3) the citrate synthase Cit2p and acetyl-carnitine synthase Cat2p, both facilitating the replenishment of tricarboxylic acid (TCA) cycle intermediates destined for mitochondria by catalyzing the anaplerotic conversion of acetyl-CoA to citrate and acetyl-carnitine, respectively [14, 20, 57, 58, 85, 90-92] (Figure 1.1B). The efficient peroxisomal import of all these proteins in chronologically ″young″ yeast cells enables the establishment of an anti-aging cellular pattern by: 1) minimizing the oxidative damage to peroxisomal proteins and membrane lipids; 2) maintaining the intracellular concentration of peroxisomally produced hydrogen peroxide at a threshold which is insufficient to damage cellular macromolecules but can activate transcription of nuclear genes essential for cell survival, thus promoting the longevity-extending cellular process of “stress-response hormesis”; 3) stimulating the TCA cycle and electron transport chain (ETC) in mitochondria, thus enabling to sustain mitochondrially generated ROS at a non-toxic level which is sufficient to stimulate transcription of nuclear genes encoding stress-protecting and other anti-aging proteins [20, 23, 57, 58, 65, 92] (Figure 1.1B).

Noteworthy, peroxisomes in yeast house the polyamine oxidase Fms1p, an enzyme involved in the synthesis of spermidine [17, 93]. This natural polyamine has been shown to extend longevity of chronologically aging yeast by stimulating the essential cytoprotective cellular process of autophagy [13, 94, 95] (Figure 1.1B). Because the intracellular concentration of spermidine in chronologically ″young″ yeast exceeds that in chronologically ″old″ yeast [13], one could speculate that peroxisomal import of Fms1p early in life of a chronologically aging yeast cell is more efficient than it is late in life, after entry of a chronologically aging yeast cell population into a non-proliferative state. In this scenario, chronologically ″young″ yeast cells develop and maintain an anti-aging cellular pattern in part because they are proficient in peroxisomal import of a protein needed for the synthesis of a natural polyamine which promotes the longevity-extending cellular process of autophagy (Figure 1.1B).

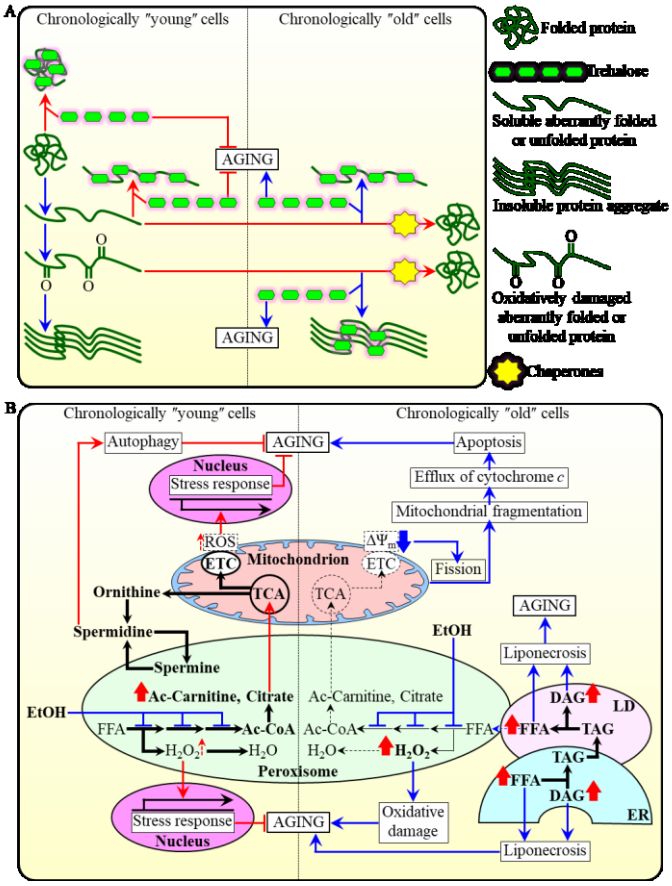

Figure 1.1. Cell-autonomous mechanisms define longevity of chronologically aging yeast by orchestrating trehalose metabolism and metabolic processes confined to peroxisomes. (A) A model for molecular mechanisms through which trehalose regulates the process of cellular aging in yeast by modulating protein folding, misfolding, unfolding, refolding, oxidative damage, solubility and aggregation in chronologically ″young″ and ″old″ cells. (**B**) A model for how the age-dependent efficiency of peroxisomal protein import in chronologically aging yeast defines the age-related metabolic pattern of peroxisomes, thus impacting longevity-defining processes in other cellular compartments and ultimately establishing a pro- or anti-aging cellular pattern. Activation arrows and inhibition bars denote pro-aging processes (displayed in blue color) or anti-aging processes (displayed in red color). Please see text for additional details. Ac-Carnitine, acetyl-carnitine; Ac-CoA, acetyl-CoA; DAG, diacylglycerol; ER, endoplasmic reticulum; ETC, electron transport chain; EtOH, ethanol; FFA, non-esterified (″free″) fatty acids; LD, lipid droplet; ROS, reactive oxygen species; TAG, triacylglycerols; TCA, tricarboxylic acid cycle; ΔΨm, electrochemical potential across the inner mitochondrial membrane. This figure is prepared by Anna Leonov, Amanda Piano and Veronika Svistkova and has been published in Arlia-Ciommo A, Leonov A, Piano A, Svistkova V, Titorenko VI. Cell-autonomous mechanisms of chronological aging in the yeast Saccharomyces cerevisiae. Microb Cell. 2014; 1(6):163-178.

Our model further posits that in chronologically ″old″ yeast cells the efficiencies of Pex5p- and Pex7p-dependent peroxisomal import of Cta1p, Pmp20p, Fox1p, Fox2p, Fox3p, Cit2p and Cat2p markedly decline (Figure 1.1B). Such deterioration of peroxisomal protein import below a threshold in these cells causes the development of a pro-aging cellular pattern by: 1) elevating the intracellular concentration of peroxisomally produced hydrogen peroxide above a cytotoxic level, thus increasing the extent of oxidative damage to cellular macromolecules; 2) reducing the efficiency of Fox1p-, Fox2p- and Fox3p-driven peroxisomal oxidation of fatty acids derived from triacylglycerols that are synthesized in the endoplasmic reticulum (ER) and deposited within lipid droplets (LD) – thus elevating the concentrations of non-esterified (″free″) fatty acids and diacylglycerol, both of which are known to elicit an age-related form of liponecrotic programmed cell death (PCD); 3) diminishing the replenishment of TCA cycle intermediates destined for the TCA cycle in mitochondria – thus triggering a cascade of events that reduce the ETC in

mitochondria, lower electrochemical potential across the inner mitochondrial membrane (IMM), promote mitochondrial fragmentation, cause the efflux of cytochrome c and other pro-apoptotic proteins from fragmented mitochondria, and ultimately elicit an age-related form of apoptotic PCD [14, 20, 23, 54, 57, 58, 65, 84, 91, 92, 96-103] (Figure 1.1B).

Furthermore, our model envisions that chronologically ″old″ yeast cells develop and maintain a pro-aging cellular pattern in part because they exhibit a low efficiency of peroxisomal import of the polyamine oxidase Fms1p; this enzyme is known to be required for the synthesis of spermidine, a natural polyamine which promotes an aging-decelerating cellular process of autophagy [13, 17, 93-95] (Figure 1.1B).

Noteworthy, both chronologically ″young″ and ″old″ yeast cells grown in a nutrient-rich medium under longevity-shortening non-CR conditions have been shown to accumulate ethanol, a product of glucose fermentation [23, 84]. Ethanol is known to repress the synthesis of Fox1p, Fox2p and Fox3p, thereby suppressing Fox1p-, Fox2p- and Fox3p-driven peroxisomal oxidation of fatty acids [90, 104] (Figure 1.1B). By suppressing peroxisomal oxidation of fatty acids to acetyl-CoA in chronologically ″young″ cells under non-CR conditions, the accumulated ethanol attenuates the anaplerotic conversion of acetyl-CoA to citrate and acetyl-carnitine - thus inhibiting an aging-decelerating cellular process of the replenishment of TCA cycle intermediates destined for mitochondria [57, 58, 90, 104] (Figure 1.1B). Moreover, by suppressing peroxisomal oxidation of fatty acids to acetyl-CoA in chronologically ″old″ cells under non-CR conditions, the accumulated ethanol also elevates the concentrations of non-esterified (″free″) fatty acids and diacylglycerol - thus triggering an age-related form of liponecrotic PCD (Figure 1.1B) [14, 23, 54, 57, 58, 84, 103]. It should be stressed that neither chronologically ″young″ nor chronologically ″old″ yeast cells grown under longevity-extending CR conditions amass ethanol [23, 84]. Such inability of yeast cells limited in calorie supply to accumulate ethanol is one of the reasons of why they can develop and maintain an anti-aging cellular pattern throughout lifespan [23, 54, 57, 58, 84] (Figure 1.1B).

In sum, it is conceivable that there are at least two checkpoints during the lifespan of a chronologically aging yeast cell at which the age-dependent efficiency of peroxisomal protein import defines the age-related metabolic pattern of peroxisomes, thus impacting longevity-defining processes in other cellular compartments and ultimately establishing a pro- or anti-aging cellular pattern. It seems that one of these checkpoints occurs early in life of a chronologically

aging yeast cell (i.e., prior to an arrest of cell growth and division), whereas the other checkpoint exists late in its life (i.e., following such arrest).

1.1.5 Coupled mitochondrial respiration, mitochondrial membrane potential and mitochondrial ROS production affect longevity-defining processes in other cellular locations

The functional state of mitochondria and mitochondrial ROS production early in life of a chronologically aging yeast cell, prior to entry into a non-proliferative state, have been shown to define the length of time during which this cell remains viable after such entry - i.e., define longevity of chronologically aging yeast [3, 14, 23, 31, 49-51, 53, 55, 56, 62, 64, 68, 69, 70-73, 105-108]. One key feature of the longevity-defining functional state of mitochondria in chronologically ″young″, proliferating yeast cells is the capacity of electron transport along the respiratory chain coupled to ATP synthesis [3, 14, 23, 49-51, 62, 64, 70, 72, 73, 106, 107]. Another such key feature is the value of mitochondrial membrane potential; it depends on a balance between the capacities of ETC-driven proton transport from the matrix to the intermembrane space and proton translocation across the IMM in the opposite direction [3, 14, 23, 50, 51, 56, 64, 70]. Moreover, the longevity-defining process of mitochondrial ROS production in chronologically ″young″ yeast cells depends on the efficiency of coupling between the ETC and oxidative phosphorylation (OXPHOS) system in mitochondria [50, 51].

Recent studies revealed how various genetic, dietary and pharmacological interventions having diverse effects on the ETC, OXPHOS system and/or ROS production in mitochondria of chronologically ″young″ yeast impact yeast longevity [3, 14, 23, 31, 49-51, 53, 55, 56, 62, 64, 68, 69, 70-73, 105-108]. These studies suggest a model for how coupled mitochondrial respiration, mitochondrial membrane potential maintenance and mitochondrial ROS production early in life of chronologically aging yeast cells define their longevity. This model is depicted schematically in Figure 1.2. The model envisions that chronologically ″young″ yeast cells cultured under non-CR conditions develop and maintain a pro-aging cellular pattern because the capacities of these mitochondrial processes in such cells are below a certain level (Figure 1.2; these capacities are displayed in green color) [23, 53, 62, 72, 73]. Furthermore, the model posits that chronologically ″young″ yeast cells in which the capacities of these mitochondrial processes exceed a critical threshold develop and maintain an anti-aging cellular pattern; this is because such capacities have specific impacts on: 1) some longevity-defining processes confined to mitochondria; and 2) certain

longevity-defining processes in other cellular locations (Figure 1.2; these capacities are displayed in red color) [14, 23, 50, 51, 56, 62, 64, 70, 73, 107]. The model also predicts that a significant further increase in the capacities of coupled mitochondrial respiration, mitochondrial membrane potential maintenance and mitochondrial ROS production above a critical threshold in chronologically ″young″ yeast cells has a negative impact on their longevity (Figure 1.2; these capacities are displayed in blue color) [14, 23, 64, 107].

The capacities of coupled mitochondrial respiration, mitochondrial membrane potential maintenance and mitochondrial ROS production in chronologically ″young″ yeast cells are modulated by several ″upstream″ pathways (Figure 1.2). These longevity-defining pathways include: 1) the nutrient- and energy-sensing TOR (target of rapamycin) signaling pathway, which through the rapamycin-sensitive protein kinase Tor1p inhibits mitochondrial translation of the OXPHOS enzymes encoded by mitochondrial DNA (mtDNA) [14, 50, 51, 56, 62]; 2) a CR pathway, whose ability to modulate coupled mitochondrial respiration, mitochondrial membrane potential maintenance and mitochondrial ROS production in chronologically ″young″ yeast cells is mediated in part by Tor1p [3, 14, 23, 33, 50-52, 56, 62]; 3) a pathway for the maintenance of mitochondrial genome integrity and copy number, which is orchestrated by the mitochondrial base-excision repair enzyme Ntg1p [108]; 4) the mitophagy pathway of mitochondrial quality control responsible for autophagic degradation of aged, dysfunctional or damaged mitochondria - which requires the receptor protein Atg32p on the surface of mitochondria destined for such degradation [70]; and 5) a pathway for specific remodeling of the membrane lipidome of mitochondria - which is stimulated in response to accumulation of the exogenously added lithocholic acid (LCA), an anti-aging natural compound, predominantly in the IMM [64, 107] (Figure 1.2). Noteworthy, some of these ″upstream″ pathways overlap; such convergent pathways modulating the capacities of coupled mitochondrial respiration, mitochondrial membrane potential maintenance and mitochondrial ROS production in chronologically ″young″ yeast include the TOR and CR pathways [3, 14, 23, 33, 50-52, 56, 62], as well as the TOR and Ntg1p-governed pathways [108]. In contrast, it seems that other ″upstream″ pathways modulating the capacities of these three longevity-defining mitochondrial processes do not converge and act in synergy; such ″parallel″ pathways include: 1) a CR pathway and an LCA-driven pathway for remodeling of the membrane lipidome of mitochondria [64, 107]; and 2) a CR pathway and the Ntg1p-governed pathway [108].

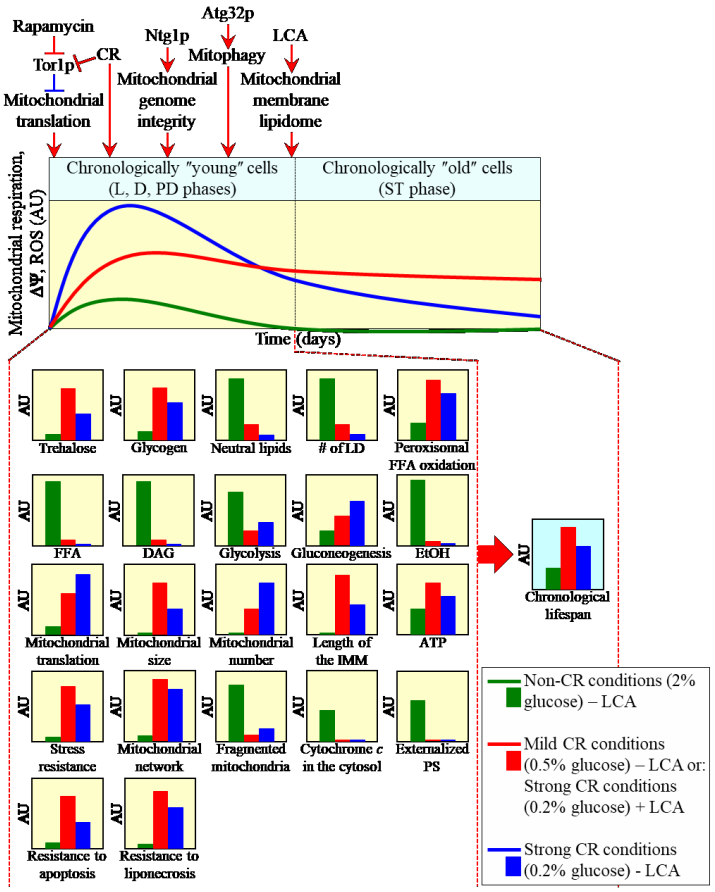

Figure 1.2. The functional state of mitochondria and mitochondrial ROS production in chronologically "young" yeast cells define their longevity by orchestrating numerous "downstream" cellular processes. A model for how coupled mitochondrial respiration, mitochondrial membrane potential maintenance and mitochondrial ROS production early in life of chronologically aging yeast cells, prior to entry into a non-proliferative state, define their viability after such entry - i.e., define their longevity. Activation arrows and inhibition bars denote pro-aging processes (displayed in blue color) or anti-aging processes (displayed in red color). Please see text for additional details. CR, caloric restriction; D, diauxic growth phase; DAG, diacylglycerol; EtOH, ethanol; FFA, non-esterified ("free") fatty acids; IMM, inner mitochondrial membrane; L, logarithmic growth phase; LCA, lithocholic acid; LD, lipid droplet; PD, post-diauxic growth phase; PS, phosphatidylserine; ROS, reactive oxygen species; ST, stationary growth phase; ΔΨm, electrochemical potential across the IMM.

The capacities of coupled mitochondrial respiration, mitochondrial membrane potential maintenance and mitochondrial ROS production in chronologically "young" yeast cells define their longevity by orchestrating numerous "downstream" cellular processes throughout lifespan - i.e., prior to entry into a non-proliferative state and after such entry (Figure 1.2). Among them are the following "downstream" processes (Figure 1.2): 1) the maintenance of trehalose homeostasis, a longevity-defining process known to modulate proteostasis in chronologically "young" and "old" cells [23, 61] (Figure 1.1A); 2) the maintenance of the homeostasis of glycogen, a reserve carbohydrate whose elevated level in chronologically "young" and "old" cells is a hallmark of carbohydrate metabolism remodeling in yeast cultured under CR [23]; 3) the maintenance of the homeostasis of neutral lipids deposited within LD, a process known to play an essential role in regulating longevity of chronologically aging yeast [14, 23, 92] (Figure 1.1B); 4) peroxisomal

oxidation of fatty acids, a process implicated in yeast chronological aging [14, 23, 91, 92] (Figure 1.1B); 5) the maintenance of the homeostasis of non-esterified (″free″) fatty acids and diacylglycerol, whose reduced levels in chronologically ″young″ and ″old″ cells are characteristic of lipid metabolism remodeling in yeast cultured under CR - a pattern likely linked to the demonstrated abilities of both lipid species to elicit an age-related form of liponecrotic PCD [14, 23, 103] (Figure 1.1B); 6) the maintenance of a balance between the relative rates of glycolysis and gluconeogenesis, a process known to impact the level of ethanol in chronologically ″young″ and ″old″ yeast - thus defining the extent to which this product of glucose fermentation suppresses the longevity-extending process of peroxisomal oxidation of fatty acids [14, 23] (Figure 1.1B); 7) the longevity-extending process of mitochondrial translation [23, 50, 51, 56]; 8) the maintenance of a balance between the relative rates of mitochondrial fusion and fission, a process known to define the size and number of mitochondria, the length of mitochondrial cristae extending from the IMM, and the level of ATP synthesized in mitochondria of chronologically ″young″ and ″old″ yeast [14, 23, 64, 70]; 9) the development of an age-related pattern of susceptibility to chronic oxidative, thermal and osmotic stresses [3, 14, 23, 33, 50, 56, 59, 62]; 10) an age-related form of apoptotic PCD, which in chronologically ″young″ yeast is manifested in such early hallmark events of this PCD as the fragmentation of a tubular mitochondrial network into individual mitochondria, release of cytochrome c from mitochondria into the cytosol and phosphatidylserine (PS) translocation from the inner to the outer leaflet of the plasma membrane [14, 23] (Figure 1.1B); and 11) the development of a pattern of cell susceptibility to an age-related forms of apoptotic and liponecrotic PCD elicited by an exposure to exogenous hydrogen peroxide or palmitoleic acid, respectively [14, 23, 59, 103].

The molecular mechanisms through which the capacity of mitochondrial ROS production in chronologically ″young″ yeast cells defines their longevity have begun to emerge; they involve communication between mitochondria and the nucleus via two signaling pathways [71, 108]. In one of these signaling pathways, hormetic concentrations of ROS released from mitochondria trigger a pro-longevity transcriptional program in the nucleus by stimulating Gis1p, Msn2p and Msn4p [68, 71, 108]; these transcriptional factors are known to activate expression of numerous genes essential for the resistance to various stresses, stationary phase survival, carbohydrate metabolism, nutrient sensing and chronological longevity assurance [109-111]. Another mitochondria-to-nucleus signaling pathway initiated by hormetic concentrations of ROS in

chronologically ″young″ yeast cells involves a cascade of events within the nucleus. In this cascade, the DNA damage response (DDR) kinase Tel1p responds to hormetic concentrations of ROS released from mitochondria by phosphorylating and activating the DDR kinase Rad53p. Active Rad53p then phosphorylates and inactivates the histone demethylase Rph1p confined to subtelomeric chromatin regions, thereby repressing their transcription, minimizing telomeric DNA damage and ultimately extending longevity of chronologically aging yeast [68, 71]. Noteworthy, it seems that the Tel1p-Rad53p-Rph1p signaling pathway overlaps with and is regulated by the ″upstream″ Ntg1p-governed pathway (Figure 1.2) for the maintenance of mitochondrial genome integrity and copy number [108].

Altogether, these findings suggest that there is a checkpoint early in life of chronologically aging yeast cells (i.e., prior to entry into a non-proliferative state) at which the capacities of coupled mitochondrial respiration, mitochondrial membrane potential maintenance and mitochondrial ROS production define their viability after such entry - i.e., define their longevity. It seems that the capacities of these three mitochondrial processes at such checkpoint define yeast longevity by orchestrating several ″downstream″ processes taking place in various cellular locations throughout lifespan, before an arrest of cell growth and division and following such arrest.

1.1.6 Metabolite flow within glycolytic and non-glycolytic pathways of carbohydrate metabolism defines the establishment of a pro- or anti-aging cellular pattern

Recent studies provided evidence that the relative rates of reactions comprising glycolytic and non-glycolytic pathways of carbohydrate metabolism, as well as the intracellular concentrations of some key intermediates in these pathways, define the development and maintenance of a pro- or anti-aging cellular pattern in chronologically aging yeast [3, 10, 23, 33, 52, 54, 57, 58, 63, 65-67, 69, 84, 112-117]. The major findings of these studies can be summarized as follows: 1) the establishment of a certain metabolic pattern of such coordinated pathways early in life of chronologically aging yeast cells, prior to entry into a non-proliferative state, defines their longevity; and 2) some dietary, genetic and pharmacological interventions extend yeast longevity by causing a specific remodeling of such metabolic pathways in chronologically ″young″, proliferating cells [23, 52, 66, 67, 69, 112-117]. These findings suggest a model for how metabolic flux within the network integrating glycolytic and non-glycolytic pathways of carbohydrate

metabolism modulates longevity-defining cellular processes. This model is depicted schematically in Figure 1.3.

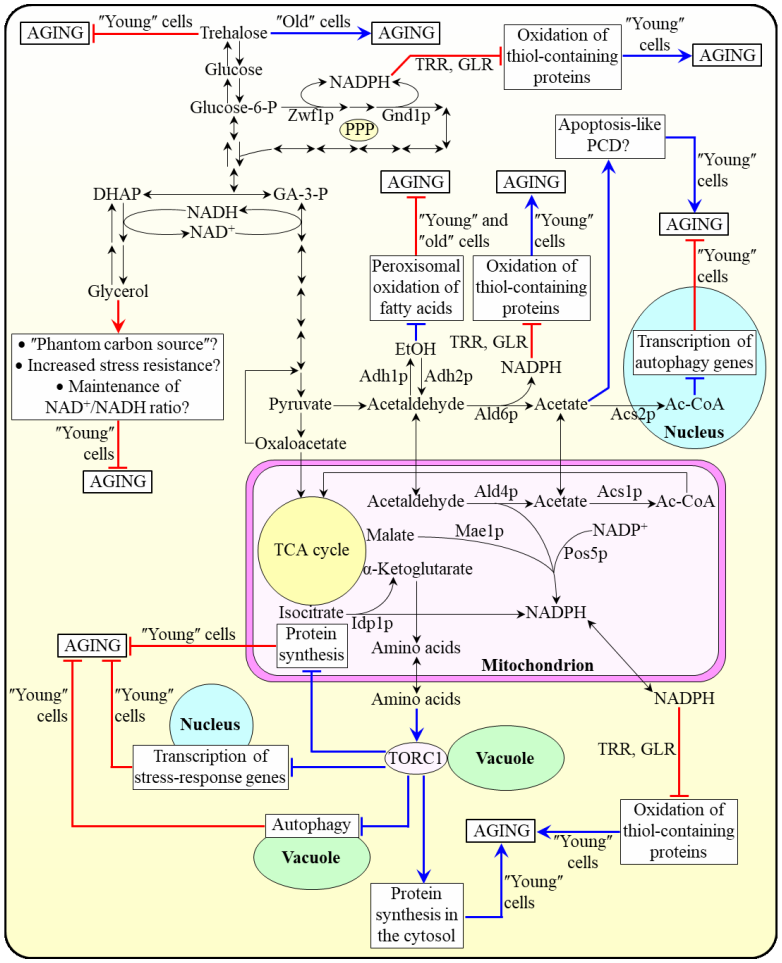

Figure 1.3. The coordinated metabolite flow within glycolytic and non-glycolytic pathways of carbohydrate metabolism defines yeast longevity by modulating vital cellular processes. A model for how metabolic flux within the network integrating glycolytic and non-glycolytic pathways of carbohydrate metabolism in chronologically ″young″, proliferating yeast cells define the development and maintenance of a pro- or anti-aging cellular pattern throughout lifespan before an arrest of cell growth and division and after such arrest. Activation arrows and inhibition bars denote pro-aging processes (displayed in blue color) or anti-aging processes (displayed in red color). Please see text for additional details. Ac-CoA, acetyl-CoA; DHAP, dihydroxyacetone phosphate; EtOH, ethanol; GA-3-P, glyceraldehyde-3-phosphate; GLR, glutathione reductase; PCD, programmed cell death; TCA, tricarboxylic acid; TORC1, target of rapamycin complex 1; TRR, thioredoxin reductase.

The model posits that glucose, the primary carbon source used in most assays for investigating yeast chronological aging under laboratory conditions, is initially converted to pyruvate via the glycolytic pathway and enters the pentose phosphate pathway (PPP) [23, 25, 27, 30, 33, 57, 66] (Figure 1.3). In chronologically ″young″ yeast cells progressing through logarithmic (L) phase, the PPP generates not only ribose-5-phosphate for nucleic acid synthesis but also NADPH, the primary source of cellular reducing equivalents required for the reductive synthesis of fatty acids, sterols and some amino acids [60, 63, 66, 118]. Importantly, NADPH - which is produced in the Zwf1p- and Gnd1p-driven oxidative reactions of the PPP - also functions as the

electron donor essential for sustaining cellular redox homeostasis via thioredoxin and glutathione reductase systems [63, 66, 118] (Figure 1.3). These two NADPH-dependent systems have been shown to reduce the extent of oxidative damage to numerous thiol-containing cytosolic, nuclear and mitochondrial proteins in chronologically ″young″ yeast cells; as such, both reductase systems play essential roles in longevity assurance and underlie, in part, the robust longevity-extending effect of CR [63, 66] (Figure 1.3).

After chronologically aging yeast cells consume glucose during L phase, they enter diauxic (D) and then post-diauxic (PD) phases of slow growth [23, 25, 30, 33]. During D and PD phases, prior to an arrest of cell growth and division and entry into the non-proliferative stationary (ST) phase, the pyruvate formed by glycolysis can enter several alternative pathways of carbon metabolism; all these pathways have been implicated in modulating various longevity-defining cellular processes [3, 10, 23, 33, 52, 54, 57, 58, 63, 65-67, 69, 84, 112-117]. One of these alternative metabolic pathways is fermentation leading to the formation of ethanol and/or acetic acid in the cytosol of a chronologically ″young″ yeast cell; the nature of a product of such fermentation depends on the type of a synthetic or nutrient-rich growth medium used and/or aeration conditions applied [3, 10, 23, 33, 52, 112-115, 117] (Figure 1.3). As discussed above, the level of ethanol in chronologically aging yeast defines the extent to which it suppresses the longevity-extending process of peroxisomal oxidation of fatty acids [14, 23] (Figure 1.1B); the steady-steady state level of this product of glucose fermentation depends on the relative enzymatic activities of Adh1p and Adh2p, which are required for ethanol formation or oxidation, respectively [3, 23, 52, 112, 117] (Figure 1.3). Acetic acid, the alternative product of glucose fermentation in the cytosol of chronologically ″young″ yeast cells, shortens their longevity – likely because it can elicit an age-related form of apoptotic PCD [3, 27, 113-115] (Figure 1.3). Of note, the Ald6p-dependent acetaldehyde dehydrogenase reaction in the cytosol of these cells yields not only acetic acid but also NADPH [60, 66, 118] (Figure 1.3). As discussed above, the NADPH-dependent thioredoxin and glutathione reductase systems are vital for longevity assurance and are essential for the longevity-extending effect of CR because they reduce the extent of oxidative damage to many thiol-containing cellular proteins in chronologically ″young″ yeast cells [63, 66, 118] (Figure 1.3). Moreover, acetic acid can be converted to acetyl-CoA in the nucleo-cytosolic Acs2p-dependent reaction [116, 118]. The acetyl-CoA formed in the nucleus has been shown to shorten longevity of chronologically aging yeast by causing histone H3 hyperacetylation, thereby

selectively suppressing transcription of the ATG5, ATG7, ATG11 and ATG14 genes; these genes encode proteins needed for the longevity-extending process of autophagy [116] (Figure 1.3). It remains to be determine what are the relative impacts of acetic acid (a pro-aging metabolite), NADPH (an anti-aging metabolite) and acetyl-CoA (a pro-aging metabolite) on longevity of chronologically aging yeast.

The model depicted in Figure 1.3 further envisions that glucose fermentation to glycerol in the cytosol of a chronologically ″young″ yeast cell operates as a longevity-extending cellular process - likely because it reduces metabolite flow into the longevity-shortening cellular process of glucose fermentation to ethanol and/or acetic acid [52, 113] (Figure 1.3). The term ″phantom carbon source″ has been coined for defining this aspect of the essential longevity-extending role of glycerol in yeast [52]. Glycerol formed by glucose fermentation in the cytosol of a chronologically ″young″ yeast cell has been proposed to extend it lifespan also because it is known to reduce cell susceptibility to chronic oxidative, thermal and osmotic stresses [52] (Figure 1.3). Furthermore, glucose fermentation to glycerol in chronologically ″young″ yeast cells may also play an essential role in longevity assurance by maintaining an NAD^+/NADH ratio characteristic of an anti-aging cellular pattern [52] (Figure 1.3).

In addition to being converted to ethanol, acetic acid, NADPH and/or acetyl-CoA, the pyruvate formed by glycolysis can enter the gluconeogenesis pathway leading to the formation of glucose; in chronologically aging yeast, this newly synthesized glucose can be further used for the synthesis of trehalose [23, 61, 62, 117] (Figure 1.3). As discussed above [23, 61] (Figure 1.1A): 1) in chronologically ″young″ yeast cells progressing through D and PD growth phases, trehalose plays an essential longevity-extending role by promoting the maintenance of cellular proteostasis, whereas 2) in chronologically ″old″, non-proliferating cells, trehalose plays a key role in shortening longevity because it impairs the chaperone-assisted refolding of misfolded, partially folded and unfolded protein species (Figure 1.3).

In chronologically ″young″ yeast cells progressing through D and PD growth phases, the pyruvate formed by glycolysis - as well as the acetaldehyde and acetate derived from it - can also fuel several longevity-defining metabolic processes in mitochondria. One of these metabolic processes is the TCA cycle. Two intermediates of the cycle, malate and isocitrate, can be used to form NADPH in the Mae1p- and Idp1p-dependent reactions, respectively [60, 66, 118] (Figure 1.3). NADPH in mitochondria of chronologically ″young″ yeast cells progressing through D and

PD growth phases can also be formed in the Ald4p-dependent acetaldehyde dehydrogenase reaction and in the Pos5p-dependent NADH kinase reaction [60, 66, 118] (Figure 1.3). As discussed above, NADPH can play a vital longevity-extending role by being used for a thioredoxin- and glutathione reductase-driven decrease in the extent of oxidative damage to thiol-containing mitochondrial proteins and proteins in other cellular locations [63, 66, 118] (Figure 1.3). Moreover, the oxaloacetate and α-ketoglutarate intermediates of the TCA cycle in mitochondria of chronologically ″young″ yeast cells progressing through D and PD growth phases are known to be used for the synthesis of amino acids [60, 118, 119] (Figure 1.3). After their exit from mitochondria to the cytosol, some of these amino acids - including aspartate, asparagine, glutamate and glutamine - cause a significant increase in protein kinase activity of the TOR complex 1 (TORC1) on the surface of vacuoles [20, 119-124] (Figure 1.3). The resulting stimulation of the TOR signaling pathway in chronologically ″young″ yeast cells is known to initiate the establishment of a pro-aging cellular pattern by: 1) activating the longevity-shortening process of protein synthesis in the cytosol; 2) suppressing the longevity-extending process of autophagy in vacuoles; 3) inhibiting the longevity-extending process of transcription of numerous stress-response genes in the nucleus; and 4) suppressing the longevity-extending process of protein synthesis in mitochondria [20, 50, 51, 119-124] (Figure 1.3).

Taken together, these findings strongly suggest that there are several checkpoints early in life of chronologically aging yeast cells - during L, D and PD phases preceding entry into the non-proliferative ST phase - at which the coordinated metabolite flow within glycolytic and non-glycolytic pathways of carbohydrate metabolism defines yeast longevity. It seems that at each of these early-life checkpoints some key intermediates in such pathways affect - in a different manner and in a concentration-dependent fashion - the vital processes of cell metabolism, growth, proliferation, stress resistance, macromolecular homeostasis, survival and death. By modulating such longevity-defining cellular processes throughout lifespan - prior to an arrest of cell growth and division and following such arrest - these key metabolic intermediates define the development and maintenance of a pro- or anti-aging cellular pattern.

1.1.7 A stepwise progression of a biomolecular network of cellular aging through a series of lifespan checkpoints defines longevity of chronologically aging yeast

The above analysis of the current knowledge about cell-autonomous mechanisms underlying chronological aging in yeast suggests the existence of several lifespan checkpoints that are critically important for establishing the pace of such aging. A recently reported ability of a natural chemical compound to extend longevity of chronologically aging yeast only if added at some of these checkpoints [59] supports the notion that a stepwise progression through such checkpoints may define the development and maintenance of a pro- or anti-aging cellular pattern. Therefore, we extend the recently proposed network theories of yeast chronological aging [3, 20, 23, 58, 59, 61, 62, 125-127] by putting forward a concept of a biomolecular network underlying the chronology of cellular aging in yeast. This concept is depicted schematically in Figure 1.4. The concept posits that the network progresses through a series of the early-life checkpoints (that exist in L, D and PD phases) and late-life checkpoints (that exist in ST phase). At each of these checkpoints, the intracellular concentrations of some key intermediates and products of certain metabolic pathways - as well as the rates of coordinated flow of such metabolites within an intricate network of intercompartmental (i.e., organelle-organelle and organelle-cytosol) communications - are monitored by some checkpoint-specific ″master regulator″ proteins (Figure 1.4). The concept further envisions that, because each of these master regulator proteins is known for its essential role in longevity regulation, their synergistic action at certain early-life and late-life checkpoints modulates the rates and efficiencies of progression of such essential processes as cell metabolism, growth, proliferation, stress resistance, macromolecular homeostasis, survival and death (Figure 1.4). The concept predicts that, by modulating these vital cellular processes throughout lifespan - prior to an arrest of cell growth and division and following such arrest - the checkpoint-specific master regulator proteins orchestrate the development and maintenance of a pro- or anti-aging cellular pattern and, thus, define longevity of chronologically aging yeast (Figure 1.4).

In the proposed concept of a biomolecular network underlying the chronology of cellular aging in yeast, the key intermediates and products of longevity-defining metabolic pathways include the following metabolites: NADPH (an anti-aging metabolite), glycerol (an anti-aging metabolite), trehalose (an anti-aging metabolite in ″young″ cells but a pro-aging metabolite in ″old″ cells), acetyl-carnitine (an anti-aging metabolite), citrate (an anti-aging metabolite), hydrogen peroxide (an anti-aging metabolite if it is maintained at an ″adaptive″ level eliciting a hormetic response but a pro-aging metabolite if it amasses above a cytotoxic level), spermidine (an anti-aging metabolite), ethanol (a pro-aging metabolite), acetic acid (a pro-aging metabolite), acetyl-

CoA (a pro-aging metabolite), non-esterified fatty acids (pro-aging metabolites), diacylglycerol (a pro-aging metabolite) and amino acids (pro-aging metabolites) (Figure 1.4). The proposed concept posits that these key metabolites undergo an age-related flow within an intricate network of intercompartmental communications; such unidirectional and bidirectional flow of the critical metabolites between different cellular compartments connects mitochondria and the nucleus, peroxisomes and the nucleus, vacuoles and the nucleus, the cytosol and the nucleus, mitochondria and peroxisomes, lipid droplets and peroxisomes, mitochondria and vacuoles, peroxisomes and the cytosol, mitochondria and the cytosol, and vacuoles and the cytosol (Figure 1.4). In the proposed concept, a CR diet and some pharmacological interventions (such as rapamycin and LCA) - as well as some other environmental cues (such as the intake of certain dietary supplements and hormetic environmental stresses) - extend longevity of chronologically aging yeast by altering the age-related dynamics of changes in the intracellular concentrations of the key metabolites and/or by modulating the intercompartmental flow of these critical metabolites (Figure 1.4). The following proteins and protein complexes operate as checkpoint-specific master regulators that - according to the proposed concept - respond to age-related changes in the intracellular concentrations of the key metabolites and in the intensity of their intercompartmental flow by modulating the longevity-defining processes of cell metabolism, growth, proliferation, stress resistance, macromolecular homeostasis, survival and death: 1) thioredoxin and glutathione reductase systems (anti-aging master regulators); 2) Rim15p, Msn2p, Msn4p and Gis1p (anti-aging master regulators); 3) Tel1p and Rad53p (anti-aging master regulators); 4) components of the ATG protein machinery involved in the essential cytoprotective cellular process of autophagy (anti-aging master regulators); 5) Rph1p (a pro-aging master regulator); 6) Iki3p and Sas3p (pro-aging master regulators); and 7) TORC1 and protein kinase A (PKA) (pro-aging master regulators) (Figure 1.4). Future studies are likely to reveal some other checkpoint-specific master regulator proteins. Finally, the proposed concept posits that the checkpoint-specific master regulators define longevity of chronologically aging yeast by orchestrating certain ″downstream″ cellular processes and features throughout lifespan - i.e., prior to entry into a non-proliferative state and after such entry (Figure 1.4). These ″downstream″ processes and features include (Figure 1.4): 1) susceptibility to chronic oxidative, thermal and osmotic stresses; 2) oxidative damage to numerous thiol-containing cytosolic, nuclear and mitochondrial proteins; 3) cellular proteostasis, which depends on the relative rates and efficiencies of protein folding, misfolding, unfolding, refolding,

oxidative damage, solubility and aggregation; 4) transcription of subtelomeric chromatin regions, which defines the extent of age-related telomeric DNA damage; 5) protein synthesis in the cytosol; 6) protein synthesis in mitochondria; 7) autophagy, an essential mechanism of cellular quality control responsible for the autophagic degradation of aged, dysfunctional and damaged macromolecules and organelles; and 8) liponecrotic and apoptotic forms of age-related PCD.

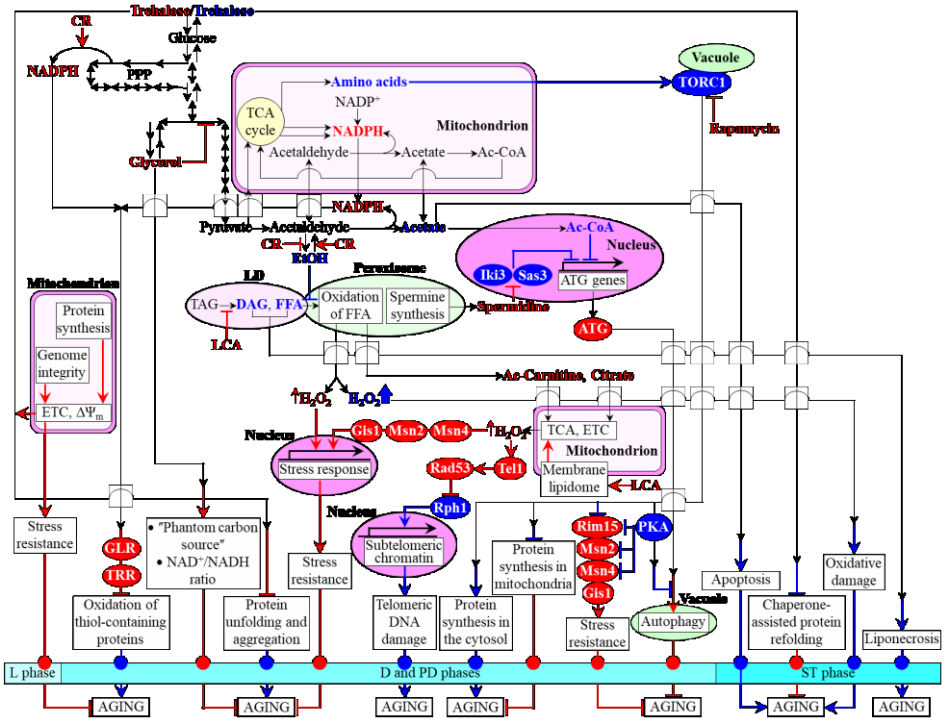

Figure 1.4. A concept of a biomolecular network underlying chronological aging in yeast. A model for how a stepwise progression of a biomolecular network of cellular aging through a series of lifespan checkpoints is monitored by some checkpoint-specific "master regulator" proteins. The model posits that a synergistic action of these master regulator proteins at several early-life and late-life checkpoints modulates certain vital cellular processes throughout lifespan - thereby orchestrating the development and maintenance of a pro- or anti-aging cellular pattern and, thus, defining longevity of chronologically aging yeast. Activation arrows and inhibition bars denote pro-aging processes (displayed in blue color) or anti-aging processes (displayed in red color). Pro-aging or anti-aging master regulator proteins are displayed in blue color or red color, respectively. Ac-Carnitine, acetyl-carnitine; Ac-CoA, acetyl-CoA; CR, caloric restriction; D, diauxic growth phase; DAG, diacylglycerol; ETC, electron transport chain; EtOH, ethanol; FFA, non-esterified ("free") fatty acids; GLR, glutathione reductase; L, logarithmic growth phase; LCA, lithocholic acid; LD, lipid droplet; PD, post-diauxic growth phase; PKA, protein kinase A; TAG, triacylglycerols; TCA, tricarboxylic acid cycle; ST, stationary growth phase; TORC1, target of rapamycin complex 1; TRR, thioredoxin reductase; ΔΨm, electrochemical potential across the inner mitochondrial membrane.

In sum, emergent evidence supports the view that the processes of cell metabolism, growth, proliferation, stress resistance, macromolecular homeostasis, survival and death in chronologically aging yeast are integrated into a biomolecular network of cellular aging. Recent findings imply that a stepwise progression of this network through a series of the early-life and late-life checkpoints is monitored by some checkpoint-specific master regulator proteins; these proteins act in synergy to orchestrate the development and maintenance of a pro- or anti-aging cellular pattern and, thus, to define longevity of chronologically aging yeast. The major challenge now is to understand if a process of yeast chronological aging - whose progression through a series of

lifespan checkpoints is monitored and controlled by a distinct set of master regulator proteins - is a program. We hypothesize that, although yeast chronological aging is a gradual and controllable process progressing through a series of consecutive lifespan checkpoints, it is not a program aimed at the termination of lives of individual yeast cells and of their organized populations. Rather, chronological aging in yeast is probably due to the inability of chronologically ″young″, proliferating cells to maintain the capacities of some crucial cellular processes above a critical threshold; these key cellular processes may include ones that ensure robust cell growth and proliferation, implement a spatiotemporal control of cell development and differentiation into quiescent and non-quiescent cell populations, and limit an age-related accumulation of molecular and cellular damage. The proposed here hypothesis also posits that the extreme cellular stress caused by the excessive accumulation of such damage in chronologically ″old″, non-proliferating cells may activate pathways known to orchestrate the apoptotic, regulated necrotic, autophagic and/or liponecrotic subroutines of PCD; these subroutines are believed to constitute modules that are dynamically integrated into a so-called PCD network [103, 128-135]. In sum, the hypothesis of non-programmed chronological aging in yeast envisions that: 1) the processes of cell metabolism, growth, proliferation, stress response, macromolecular homeostasis, development and differentiation have evolved in the course of natural selection within diverse ecosystems (and perhaps under laboratory conditions) as programs aimed at sustaining the long-term survival of individual yeast cells under various environmental conditions; 2) the processes of various subroutines of PCD have evolved throughout natural selection within different ecosystems (and perhaps under laboratory conditions) as ″altruistic″ programs aimed at sustaining the long-term survival of organized yeast populations (such as colonies and biofilms of yeast cells attached to solid surfaces) by eliminating individual yeast cells that are damaged, unable to mate and reproduce, poorly adapted to diverse environmental conditions, and/or release excessive quantities of ROS and other harmful metabolites (for a comprehensive discussion of this topic, see refs. [136, 137]); and 3) a trade-off between these programs aimed at sustaining the long-term survival of individual yeast cells or that of organized yeast populations under diverse environmental conditions drives the evolution of yeast longevity towards maintaining a finite yeast chronological lifespan within an ecosystem. The proposed here hypothesis of non-programmed chronological aging in yeast provides a framework for future studies aimed at testing its validity.

1.1.8 Caloric restriction and dietary restriction delay aging in evolutionarily distant eukaryotes, including *S. cerevisiae*, by remodeling metabolism and organelle dynamics

Aging of unicellular and multicellular eukaryotic organisms is an intricate biological phenomenon [138, 139]. It is believed to be caused by an age-dependent, progressive dysregulation of many processes within a eukaryotic cell [1, 2, 20, 23, 57, 61, 84, 138-140]. The rates, efficiencies and spatiotemporal organization of all these cellular processes throughout the organismal lifespan are modulated by only a few nutrient- and energy-sensing signaling pathways that converge into a network; this evolutionarily conserved network integrates the insulin/insulin-like growth factor 1, AMP-activated protein kinase/target of rapamycin and cAMP/protein kinase A (cAMP/PKA) pathways [1, 2, 20, 140]. The flow of information along the signaling network of cellular aging can be modulated by certain dietary interventions that can extend lifespan and/or delay the onset of various age-related physiological changes in yeast, nematodes, fruit flies, mice and primates. These dietary interventions are known to prolong both longevity and healthspan in organisms across phyla by beneficially influencing pathologies and diseases of old age [1, 2, 138-141]. These interventions include: 1) caloric restriction (CR), a dietary regimen that limits the intake of calories without reducing the supply of amino acids, vitamins and other nutrients [1, 2, 57, 140, 141]; and 2) dietary restriction (DR), a group of nutrient intake interventions that limit the supply of certain amino acids or vitamins and/or alter the balance of dietary components, but do not reduce overall food or calorie intake [1, 138-141].

The molecular and cellular mechanisms underlying the robust longevity-extending and health-improving effects of CR and certain DR regimens have begun to emerge. These mechanisms involve several distinct, evolutionarily conserved ways of modulating the flow of information along the signaling network, which orchestrates a pro- or anti-aging cellular pattern by controlling numerous longevity-defining cellular processes [1, 2, 20, 138-141]. Among these cellular processes are certain pathways of lipid metabolism and interorganellar transport [14, 23, 57, 84, 142, 143]. Although it remains to be seen if these various pathways can play casual roles in defining longevity and/or healthspan, recent findings suggest that at least some of them can. In fact, it has been demonstrated that: 1) sphingolipid metabolism defines yeast chronological lifespan by modulating many vital cellular processes [144, 145]; 2) the lipolysis of triacylglycerols (TAG), a major class of neutral lipids, defines the longevity of the nematode *Caenorhabditis elegans* by providing arachidonic fatty acid, which extends lifespan by stimulating the essential

pro-longevity process of autophagy [146, 147]; and 3) the concentration of long-chain fatty acids in plasma is a probable biomarker of longevity in various species of mammals [148].

It needs to be emphasized that: 1) lipid metabolism and transport within a cell are governed by an intricate network of interorganellar communications integrating the endoplasmic reticulum (ER), lipid droplets (LD), peroxisomes, mitochondria and the plasma membrane (PM) [20, 57, 145] (Figure 1.5); 2) the proper functioning of this network is essential for maintaining lipid homeostasis in all of these cellular organelles and membranes [20, 57, 145] (Figure 1.5); and 3) the efficacy of maintaining lipid homeostasis in some or all of these cellular organelles and membranes defines the lifespan of chronologically aging yeast [20, 57, 145]. A current view of how the network integrating lipid metabolism and transport in different cellular locations maintains lipid homeostasis in various cellular organelles and membranes is summarized in a model; this model is depicted schematically in Figure 1.5.

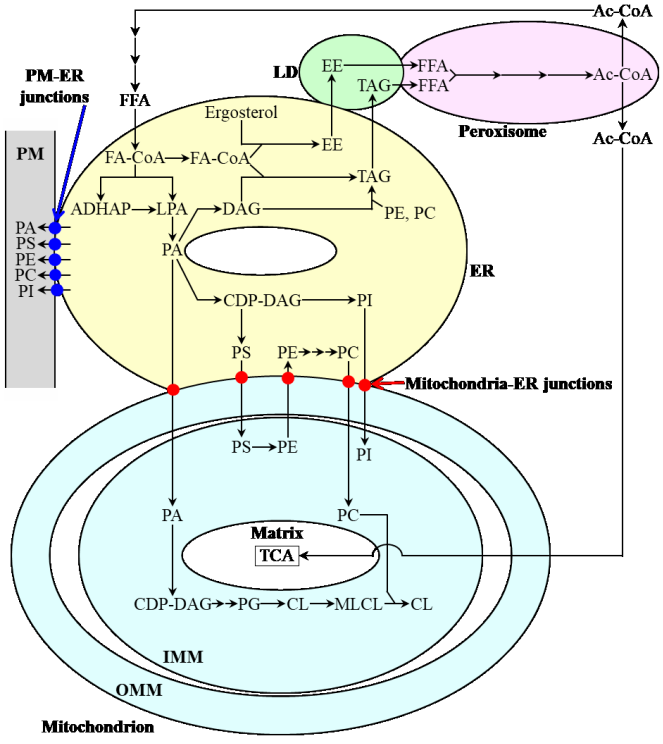

Figure 1.5. Outline of a network governing lipid metabolism and transport within the endoplasmic reticulum (ER), lipid droplets (LD), peroxisomes, mitochondria and the plasma membrane (PM). The proper functioning of this intricate network is necessary for maintaining lipid homeostasis in all these cellular organelles and membranes. The PA, PS, PC and PI classes of phospholipids are synthesized exclusively in the ER; these are then transported to mitochondria via mitochondria-ER junctions and to the PM via PM-ER junctions. The PE and CL classes of phospholipids are formed only in the inner mitochondrial membrane (IMM); PE is then transported from mitochondria to the ER via mitochondria-ER junctions and from the ER to the PM via PM-ER junctions. The neutral lipids TAG and EE are synthesized in the ER and then deposited within LD. The lipolytic hydrolysis of TAG and EE in LD generates FFA; these are then get imported and oxidized by peroxisomes. Peroxisomally produced acetyl-CoA is converted to citrate and acetyl-carnitine, whose subsequent delivery to mitochondria enables to maintain the efficient synthesis of PE and CL in the IMM. The use of peroxisomally produced acetyl-CoA for the synthesis of FFA in the cytosol allows FFA to enter the biosynthetic pathways for phospholipids and neutral lipids in the ER. See text for additional details. Abbreviations: Ac-CoA, acetyl-CoA; ADHAP, acyl dihydroxyacetone phosphate; CDP-DAG, cytidine diphosphate-diacylglycerol; CL, cardiolipin; EE, ergosteryl esters; FA-CoA, fatty acid-CoA; FFA, non-esterified (free) fatty acids; LPA, lysophosphatidic acid; MLCL, monolysocardiolipin; OMM, outer mitochondrial membrane; PA, phosphatidic acid; PC, phosphatidylcholine; PE, phosphatidylethanolamine; PG, phosphatidylglycerol; PI, phosphatidylinositol; PS, phosphatidylserine; TAG, triacylglycerols; WT, wild type.

The model posits that: 1) after being synthesized in the ER, the phosphatidic acid (PA), phosphatidylserine (PS), phosphatidylcholine (PC) and phosphatidylinositol (PI) classes of phospholipids are transported to mitochondria via mitochondria-ER junctions and to the PM via PM-ER junctions; 2) following the synthesis of the phosphatidylethanolamine (PE) class of phospholipids in the inner mitochondrial membrane (IMM) from PS formed in the ER, PE is transported from mitochondria to the ER via mitochondria-ER junctions and subsequently from the ER to the PM via PM-ER junctions; 3) cardiolipin (CL), a signature phospholipid class of the mitochondrion, is synthesized in the IMM from PA, which is formed in the ER and then delivered to mitochondria via mitochondria-ER junctions; 4) after being synthesized in the ER, the neutral lipids triacylglycerols (TAG) and ergosteryl esters (EE) are deposited within LD; 5) the physical contact existing between peroxisomes and LD stimulates the lipolytic conversion of TAG and EE to free fatty acids, which then get imported and oxidized by peroxisomes; 6) the anaplerotic conversion of acetyl-CoA to citrate and acetyl-carnitine in peroxisomes enables the replenishment of tricarboxylic acid (TCA) cycle intermediates destined for mitochondria, thereby allowing one to maintain the efficient synthesis of PE and CL in the IMM; and 7) a pool of peroxisomally produced acetyl-CoA is also used in the cytosol for the synthesis of fatty acids, which then get imported by the ER, where they enter the biosynthetic pathways for phospholipids and neutral lipids [20, 57, 145] (Figure 1.5).

Recent studies in the Titorenko laboratory of how CR influences a pattern of metabolism and organelle dynamics in the chronologically aging yeast *S. cerevisiae* have revealed that this low-calorie diet alters age-related dynamics of certain cellular processes [20, 23, 61, 84, 149, 150]. Among these cellular processes are ethanol metabolism, glycogen and trehalose metabolism, lipid synthesis and degradation, ROS homeostasis maintenance, mitochondrial morphology control, mitochondrial functionality preservation, stress response control, cell cycle regulation, quiescence maintenance, and apoptotic and liponecrotic death subroutines [20, 23, 61, 84, 149, 150]. It remained unclear how CR coordinates the spatiotemporal dynamics of all these cellular processes to delay yeast chronological aging. One of the objectives of my thesis work was therefore to investigate mechanisms through which CR orchestrates these various processes to slow down yeast chronological aging.

1.1.9 A mechanism underlying the longevity-extending effect of lithocholic acid in chronologically aging yeast

In a high-throughput screen for chemical compounds that can slow down aging in *S. cerevisiae* by specifically targeting lipid metabolism and interorganellar transport, the Titorenko laboratory identified lithocholic acid (LCA), a bile acid, as one of them [14]. Studies in the laboratory suggested a mechanism through which LCA prolongs the longevity of chronologically aging yeast under CR conditions by altering mitochondrial lipidome and functionality [14, 64, 103, 107). With the help of subcellular fractionation by differential centrifugation, organelle separation by equilibrium density gradient centrifugation and subsequent mass spectrometric measurement of LCA in purified cellular organelles, it was demonstrated that exogenously added LCA enters yeast cells and accumulates in mitochondria, but not in any other organelle [64, 103] (Figure 1.6). Using subfractionation of purified mitochondria followed by mass spectrometric quantitation of LCA in different mitochondrial subcompartments, it was revealed that confined to the mitochondria, LCA resides mainly in the IMM; a smaller portion of this bile acid also associates with the outer mitochondrial membrane (OMM) [64,103] (Figure 1.6). Mass spectrometric analyses of mitochondrial membrane lipidomes provided evidence that the pools of LCA confined to the IMM and OMM alter the phospholipid composition of mitochondrial membranes. Specifically, LCA elicits a rise in the relative level of PS and a decline in the relative level of PE within mitochondrial membranes; it was proposed that LCA may cause these changes by decelerating the Psd1-dependent reaction, leading to the conversion of PS to PE [64, 103] (Figure 1.6). Furthermore, LCA causes a rise in the relative level of PG and a decline in the relative level of CL within mitochondrial membranes; it is believed that LCA may trigger these changes by slowing down the Crd1-dependent reaction resulting in the synthesis of CL from PG [64, 103] (Figure 1.6). Moreover, LCA increases the relative level of PC, as well as reduces the relative levels of both CL and monolysocardiolipin (MLCL) within mitochondrial membranes; one could envisage that LCA may elicit these changes by reducing the availability of newly synthesized CL for the Cld1- and Taz1-driven reactions that enable a PC-dependent remodeling of the acyl chains of CL [64, 103] (Figure 1.6). In addition, LCA was found to increase the relative level of PA within mitochondrial membranes [64, 103] (Figure 1.6). It was suggested that the observed LCA-driven reduction in the relative level of CL within the IMM may cause such an effect by mitigating a CL-dependent inhibition of PA translocation from the OMM to the IMM; this translocation is known

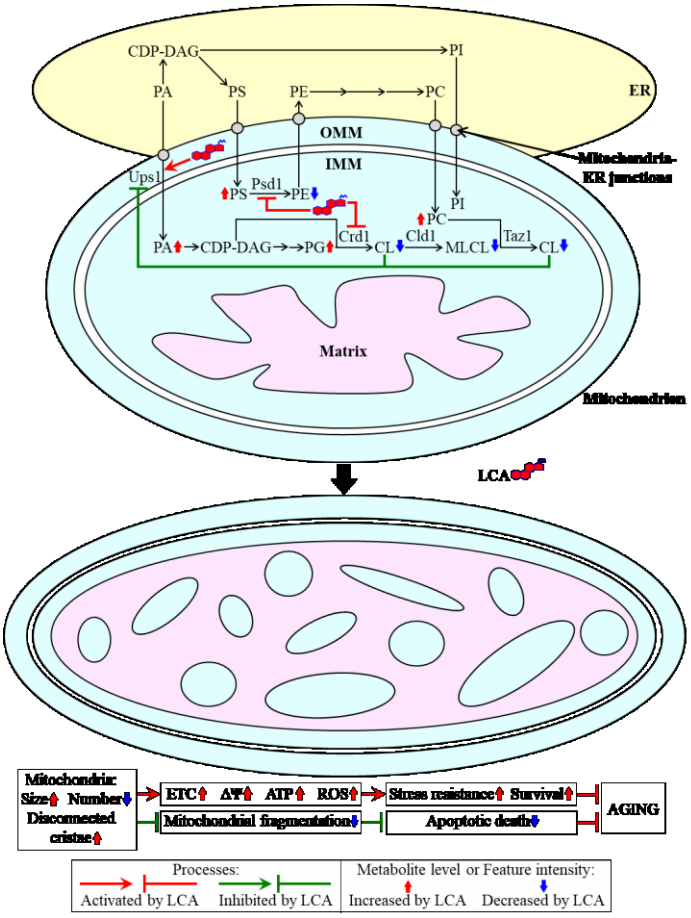

Figure 1.6. A mitochondria-based mechanism through which LCA prolongs the longevity of chronologically aging yeast. Exogenously added LCA enters a yeast cell, where it is sorted to mitochondria, but not to any other organelle. Mitochondria-associated LCA is located predominantly in the inner mitochondrial membrane (IMM) and resides in the outer mitochondrial membrane (OMM). LCA drives a remodeling of the mitochondrial membrane lipidome, thereby enlarging mitochondria, reducing their number and causing a build-up within their matrix of cristae disconnected from the IMM. These major changes in mitochondrial abundance and morphology elevate mitochondrial respiration, membrane potential, ATP synthesis and reactive oxygen species (ROS) levels in chronologically "old" cells, thereby enhancing their long-term stress resistance and viability. Moreover, the LCA-elicited remodeling of the mitochondrial membrane lipidome mitigates mitochondrial fragmentation, thus slowing down an age-related form of apoptotic programmed cell death. All these distinctive alterations in vital mitochondrial processes and features seen in yeast cells permanently exposed to exogenous LCA extend their chronological lifespan. See the text for additional details. Abbreviations: CDP-DAG, cytidine diphosphate-diacylglycerol; CL, cardiolipin; ER, endoplasmic reticulum; ETC, electron transport chain; MLCL, monolysocardiolipin; PA, phosphatidic acid; PC, phosphatidylcholine; PE, phosphatidylethanolamine; PG, phosphatidylglycerol; PI, phosphatidylinositol; PS, phosphatidylserine; ΔΨ, electrochemical membrane potential.

to be promoted by the Ups1 protein, which shuttles PA between the two mitochondrial membranes [151-153] (Figure 1.6). The resulting acceleration of PA transport from the OMM to the IMM, in synergy with the LCA-stimulated movement of PA from the ER to the OMM via mitochondria-ER junctions, may elicit the observed rise in the relative level of PA within mitochondrial membranes [64, 103] (Figure 1.6). The observed remodeling of the mitochondrial membrane lipidome in yeast cells permanently exposed to LCA progresses with their chronological age and triggers major age-related changes in mitochondrial abundance and morphology, including: 1) an expansion of both mitochondrial membranes, which leads to a considerable enlargement of mitochondria; 2) a shift in the balance between the opposing processes of mitochondrial fission and fusion towards fusion, which causes a substantial decline in mitochondrial number; 3) a significant decrease in the fraction of mitochondria with cristae that extend from the inner boundary membrane; and 4) a massive accumulation within the

mitochondrial matrix of cristae disconnected from the inner boundary membrane [64, 103] (Figure 1.6). In synergy, the major changes triggered by LCA in the mitochondrial membrane lipidome and the ensuing vast changes in mitochondrial morphology elicit a distinct set of alterations in the age-related chronology of several mitochondrial processes; these vital mitochondrial processes include respiration, the preservation of electrochemical membrane potential, the synthesis of ATP and the maintenance of ROS homeostasis [64, 103] (Figure 1.6). Because a permanent exposure of yeast to LCA stimulates all these mitochondrial processes in chronologically "old" cells, they exhibit higher long-term stress resistance and viability than yeast cells cultured without LCA [64, 103] (Figure 1.6). Moreover, a shift is elicited by LCA in the balance between the opposing processes of mitochondrial fission and fusion towards fusion attenuates mitochondrial fragmentation, thus slowing down the release of pro-apoptotic proteins from mitochondria and decelerating an age-related form of apoptotic programmed cell death [64, 103, 107] (Figure 1.6). By promoting the long-term stress resistance and viability of chronologically aging yeast cells and by slowing down their age-related apoptotic death, the permanent exposure of these cells to LCA extends their longevity [64, 103, 107] (Figure 1.6).

Based on the above findings, we hypothesized that the LCA-driven changes in mitochondrial lipidome may alter mitochondrial proteome, thus eliciting changes in mitochondrial functionality and delaying yeast chronological aging. One of the objectives of my thesis work was therefore to test this hypothesis by investigating how certain mutations that eliminate enzymes involved in mitochondrial phospholipid metabolism influence the mitochondrial proteome. Moreover, as detailed below in the thesis, our recent studies have indicated that under CR conditions LCA influences not only the aforesaid processes in mitochondria but also some other cellular processes that take place in several cellular compartments. Based on these recent studies, we hypothesized that LCA may delay chronological aging of yeast limited in calorie supply also because it affects these other cellular processes confined to various cellular locations. My other objective was therefore to test this hypothesis by investigating mechanisms through which LCA controls the spatiotemporal dynamics of these other cellular processes in different cellular locations under CR conditions.

1.1.10 Reversible phosphorylation of mitochondrial proteins regulates various processes taking place in mitochondria

The phosphorylation of cellular proteins is the most common reversible post-translational modification that 1) is controlled by a balance between activities of numerous protein kinases and phosphatases; 2) influences protein activity, stability, ligand interaction and localization; and 3) is involved in the maintenance of cellular homeostasis in response to various changes in metabolic, energy or stress status of a cell [154]. The dysregulation of reversible protein phosphorylation is known to be a cause or consequence of many human diseases, including muscular dystrophy, diabetes, stroke, inflammatory and autoimmune diseases, neurodegenerative diseases, and different forms of cancer [155]. Reversible protein phosphorylation has been implicated in almost every process confined to mitochondria, including mitochondrial protein import, oxidative phosphorylation, TCA cycle, steroid biosynthesis, DNA replication, fission, mitophagic degradation, and mitochondria-controlled apoptosis [156-162].

Several mitochondrial processes in animal cells are regulated by protein kinase A (PKA), which can be found both on the mitochondrial surface and in the mitochondrial matrix [160]. PKA that is attached to the outer face of metazoan mitochondria with the help of AKAP121 (the PKA-anchoring protein 121) and some AKAPs can phosphorylate the following mitochondrial proteins: 1) the dynamin-like GTPase Drp1, thereby attenuating the recruitment of Drp1 to mitochondrial fission sites on the organelle surface, weakening mitochondrial fission and stimulating cell survival; 2) the pro-apoptotic protein Bad on the outer mitochondrial membrane, thus inhibiting the apoptotic activity of Bad in mammalian cells; 3) the pro-apoptotic protein Bax, therefore stimulating its recruitment to mitochondrial surface, eliciting the efflux of cytochrome *c* and promoting apoptotic cell death of mammalian cells; 4) the pro-apoptotic protein Bim, as a result protecting it from proteasomal degradation and accelerating apoptosis in cells of mammals; and 5) the steroidogenic acute regulatory (StAR) protein, thereby promoting cholesterol transport from cytosol to mitochondria (Figure 1.7A) [157, 160, 161]. PKA that resides in the matrix of mammalian mitochondria can phosphorylate the following mitochondrial proteins: 1) several protein components of the electron transport chain (ETC) and TCA cycle enzymes, thereby modulating oxidative phosphorylation and ATP synthesis; 2) IF1 (an ATPase inhibitory factor 1), thus increasing both the ATP hydrolytic and ATP synthetic activities of respiratory complex V, and adjusting the glycolytic and mitochondrial oxidative phosphorylation fluxes to physiological demands of a cell; and 3) TFAM (a mitochondrial transcription factor A), therefore promoting

TFAM degradation and attenuating the TFAM-dependent replication of mitochondrial DNA (Figure 1.7B) [157, 160, 161].

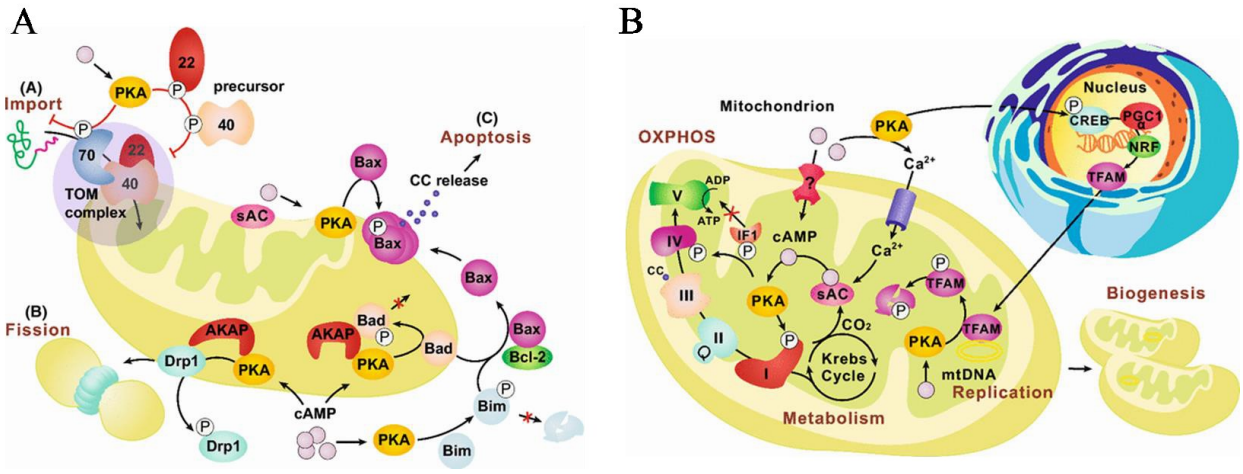

Figure 1.7. Several mitochondrial processes in animal cells are regulated by protein kinase A (PKA), which can be found both on the mitochondrial surface (A) and in the mitochondrial matrix (B). See text for more details. Abbreviations: AKAP, PKA-anchoring protein; CC, cytochrome *c*; mtDNA, mitochondrial DNA; sAC, soluble adenylyl cyclase; TFAM, mitochondrial transcription factor A). From reference [160].

In the yeast *S. cerevisiae*, reversible protein phosphorylation has been implicated in adjusting the rates and efficiencies of mitochondrial protein import [156, 158, 159, 162] and autophagic degradation of mitochondria [157] to physiological demands of a cell in response to various changes in its metabolic, energy or stress status. At high concentrations of glucose in culture medium, *S. cerevisiae* cells use mainly glycolysis to metabolize this fermentable carbon source and maintain mitochondrial respiration at low level [158]. Under such glucose-rich conditions, a catalytic activity of the adenylyl cyclase is amplified and the resulting rise in the concentration of cAMP stimulates PKA in the cytosol [158, 159]. Active PKA phosphorylates the cytosolic precursors of Tom40 (which is phosphorylated at serine 54) and Tom22 (which is phosphorylated at threonine 76), two core protein components of the translocase of the outer membrane (TOM) complex that is responsible for the import of most mitochondrial proteins (Figure 1.8A) [156-159]. Such PKA-dependent phosphorylation of Tom40 and Tom22 diminishes their delivery to and/or integration into the outer mitochondrial membrane, thus precluding the assembly of the mature TOM complex and impairing mitochondrial import of most mitochondrial proteins (Figure 1.8A) [156-159]. Furthermore, active PKA phosphorylates the Tom70 import receptor for the metabolite carrier proteins of the inner mitochondrial membrane [156-160]. Because the phosphorylated form of Tom70, Tom70^{S174}, does not interact efficiently with the

complexes formed between cytosolic metabolite carrier precursors and the cytosolic chaperone Hsp70, the delivery of these metabolite carriers into the inner mitochondrial membrane is impeded (Figure 1.8B) [156-159].

Yeast cells cultured in glucose-rich media undergo not only the activation of cytosolic PKA but also the palmitoylation of Yck1 and Yck2, two homologous isoforms of the casein kinase type 1 (CK1) [156-159, 162]. After being attached to the plasma membrane, a substantial fraction of the palmitoylated Yck1 and Yck2 re-locates to the outer mitochondrial membrane (Figure 1.8C) [156-159, 162]. Yck1 on the mitochondrial surface phosphorylates the Tom22 component of the TOM complex at threonine 57, thereby enhancing Tom22 interaction with the Tom20 component of this complex, promoting TOM complex assembly and stimulating mitochondrial protein import (Figure 1.8C) [156-159, 162]. Thus, the PKA-dependent impairment of mitochondrial protein import in yeast cells cultured in glucose-rich media is balanced by the Yck1-driven activation of this import; it is conceivable that the existence of such balance allows to adjust the rate and efficiency of mitochondrial protein import to metabolic requirements of cells that ferment glucose (Figure 1.8C) [156-159, 162].

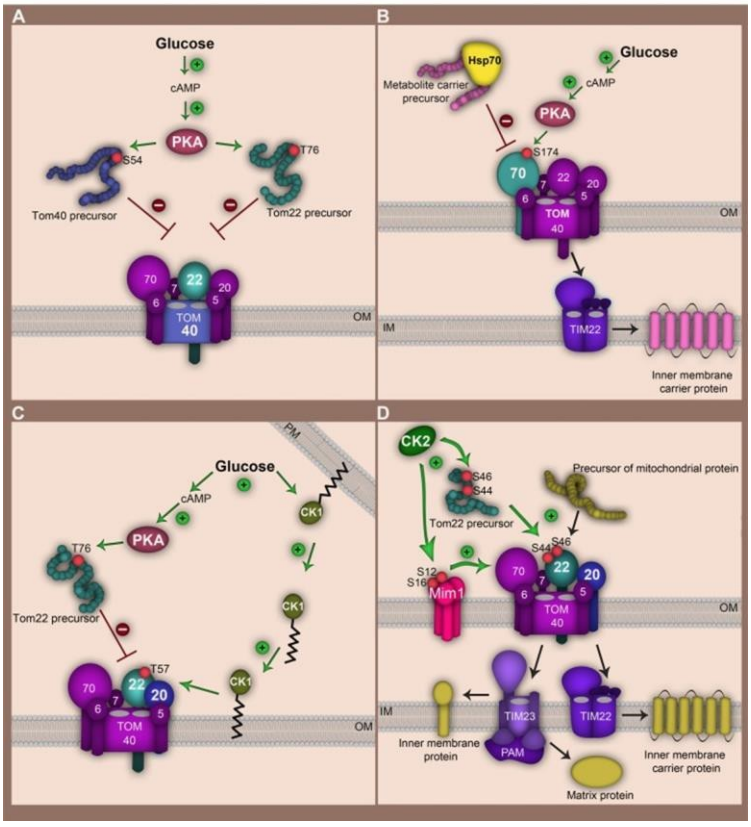

Figure 1.8. Cytosolic protein kinase A (PKA), the Yck1 isoform of the casein kinase type 1 (CK1) attached to the mitochondrial surface and the α catalytic subunit Cka2 of cytosolic casein kinase type 2 (CK2) regulate mitochondrial protein import by phosphorylating some protein subunits of the translocase of the outer membrane (TOM) complex or the Mim1 protein component of the MIM (Mim1-containing) complex. See text for more details. From reference [158].

The reversible phosphorylation of mitochondrial proteins (and, thus, mitochondrial functionality) is linked not only to metabolic requirements of yeast cells but also to the proliferation and regulated death of these cells [159]. This link is mediated by the α catalytic subunit Cka2 of casein kinase type 2 (CK2); Cka2 phosphorylates the following two mitochondrial proteins: 1) the cytosolic precursors of the Tom22 component of the TOM complex (as well as the assembled form of Tom22) at serine 44 and serine 46, thus augmenting Tom22 interaction with the Tom20 component of this complex, enhancing TOM complex assembly and activating mitochondrial protein import; and 2) the Mim1 component of the MIM complex at serine 16 and serine 14, thereby stabilizing Mim1, activating Mim1-dependent mitochondrial import of Tom20 and Tom70 precursors, promoting TOM complex assembly and stimulating mitochondrial protein import (Figure 1.8D) [156-159, 162]. Thus, akin to mitochondrial protein phosphorylation by Yck1 bound to the outer mitochondrial membrane, mitochondrial protein phosphorylation by cytosolic Cka2 activates protein import into mitochondria and promote mitochondrial biogenesis.

The Cka2-dependent phosphorylation of the Atg32 protein attached to the outer surface of yeast mitochondria also regulates mitophagy, an essential mechanism of mitochondrial quality and quantity control that is responsible for the selective autophagic degradation of aged, dysfunctional, damaged or excessive mitochondria [157]. Atg32 is a mitochondrial receptor for mitophagic removal of yeast mitochondria under nitrogen starvation conditions and in chronologically old cells [163]. Mitophagy-promoting stimuli are detected by the cell-surface stress sensor Sln1, which in response activates the high osmolarity glycerol (HOG) signaling pathway; the HOG pathway is an evolutionarily conserved mitogen-activated protein kinase (MAPK) cascade also known for its essential role in hyperosmotic stress response (Figure 1.9) [163]. After being phosphorylated and activated by the MAPK kinase (MAPKK) Pbs2, the MAPK Hog1 stimulates the α catalytic subunit Cka2 of CK2; Cka2 then phosphorylates Atg32 at serine 114 and serine 119 (Figure 1.9) [163]. The Cka2-dependent phosphorylation of Atg32 at serine 114 is needed for its interaction with Atg11, which then recruits mitochondria to the pre-autophagosomal structure where the mitochondria-enclosing autophagosome is generated in preparation to its degradation by vacuolar hydrolases (Figure 1.9) [163].

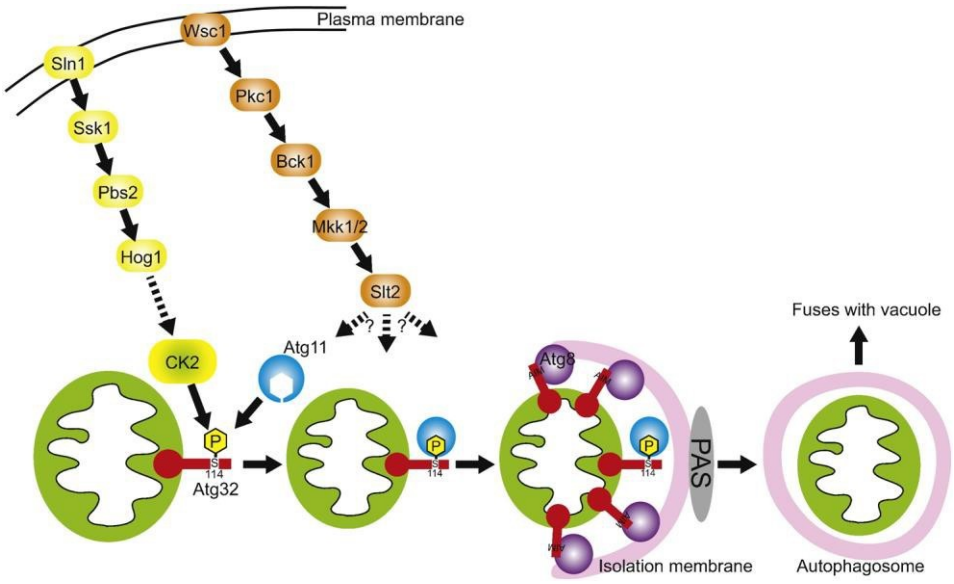

Figure 1.9. The Cka2-dependent phosphorylation of the Atg32 protein attached to the outer surface of yeast mitochondria also regulates mitophagy, an essential mechanism of mitochondrial quality and quantity control. See text for more details. From reference [163].

Recent proteomics analyses of mitochondria purified from *S. cerevisiae* cells have revealed numerous protein kinases, protein phosphatases and their accessory proteins associated with these organelles (Table 1.1) [156]. Some of these proteins have been found only in mitochondria of yeast cells; they include the following proteins: 1) two redundant protein kinases (i.e. Pkp1 and Pkp2) and two redundant protein phosphatases (i.e. Ptc5 and Ptc6) essential for the regulation of the pyruvate dehydrogenase complex in the mitochondrial matrix; 2) the protein kinase Fmp48 and the protein phosphatase Ptc7 of presently unknown function (Table 1.1) [156, 164, 165]. In contrast, many of these mitochondria-associated protein kinases, protein phosphatases and their accessory proteins 1) have also been found in other cellular locations; and 2) have been shown to participate in essential cellular processes most of which have not been directly linked to mitochondria. They include the following proteins: 1) the nutrient-sensing protein kinases Psk2, Snf1 and Tor2 that have been implicated in the regulation of carbohydrate and lipid metabolism, cell growth and stress response; 2) Fus3 and Smk1, two MAPKs implicated in mating and sporulation (respectively); 3) Mec1 and Tel1, two protein kinases involved in the regulation of telomere length and the DNA-damage response checkpoint; 4) Vps15, a protein kinase implicated in vacuolar protein sorting; and 5) Yck1 and Yck2, two protein kinases involved in cell morphogenesis, septin assembly, endocytic trafficking, glucose sensing and glucose repression of respiratory metabolism (as discussed above, Yck1 has recently been implicated in adjusting the rate and efficiency of mitochondrial protein import to metabolic requirements of cells) (Table 1.1)

[156, 164, 165]. Altogether, these findings allow to speculate that some (or many) of these mitochondria-associated protein kinases, protein phosphatases and their accessory proteins 1) may somehow regulate mitochondrial functionality in yeast cells (in addition to their established involvement in regulating cellular proteins not directly linked to mitochondria); and 2) may control communications between mitochondria and various other compartments of a yeast cell [156].

Name	Gene	Primary function (SGD)
Protein Kinases		
Fmp48	YGR052W	Putative Ser/Thr kinase of unknown function
Fus3	YBL016W	Mitogen-activated protein kinase (MAPK) regulating mating-pheromone induced gene expression, homolog of MAPK1
Mec1	YBR136W	Cell cycle checkpoint control after DNA damage, homolog of human Ataxia telangiectasia mutated-related kinase (ATR)
Pkp1	YIL042C	Regulation of pyruvate dehydrogenase complex activity
Pkp2	YGL059W	Regulation of pyruvate dehydrogenase complex activity
Psk2	YOL045W	Control of sugar metabolism
Smk1	YPR054W	MAPK involved in spore wall assembly during sporulation
Snf1	YDR477W	Nutrient sensing, cellular adaption to glucose limitations, homolog of adenosine monophosphate-activated protein kinase (AMPK)
Tel1	YBL088C	Telomere length regulation, cell cycle checkpoint control after DNA damage, homolog of human Ataxia telangiectasia mutated (ATM)
Tor2	YKL203C	Regulation of cell growth in response to nutrient availability and stress, subunit of target of rapamycin complex 1 (TORC1) and TORC2
Vps15	YBR097W	Myristoylated, membrane associated kinase involved in vacuolar protein sorting
Yck1	YHR135C	Palmitoylated, membrane-associated kinase involved in cell morphogenesis and endocytosis, isoform of casein kinase 1 (CK1)
Protein Phosphatases		
Ptc5	YOR090C	Regulation of pyruvate dehydrogenase complex activity
Ptc6	YCR079W	Regulation of pyruvate dehydrogenase complex activity, role in autophagy
Ptc7	YHR076W	Protein Ser/Thr phosphatase of unkown function, short splice variant localizes to mitochondria
Ptp1	YDL230W	Protein tyrosine phosphatase of unkown function
Accessory Proteins		
Sap4	YGL229C	Component of Sit4 protein phosphatase complex
Sap185	YJL098W	Component of Sit4 protein phosphatase complex

Table 1.1. Protein kinases, protein phosphatases and their accessory proteins found in the mitochondrial proteome of *Saccharomyces cerevisiae*. See text for more details. From reference [156].

Because LCA triggers major changes in the age-related chronology of several vital processes taking place in mitochondria, we hypothesized that LCA may cause these changes by eliciting a reversible phosphorylation of some mitochondrial proteins. One of the objectives of my thesis work was therefore to test this hypothesis by investigating if an exposure of chronologically aging yeast to LCA prompts such phosphorylation.

1.2 Thesis outline and contributions of colleagues

Chapter 1 outlines two ways of studying yeast aging, two groups of mechanisms underlying yeast chronological and replicative aging, the essential role of intracellular trehalose in maintaining cellular protein homeostasis (proteostasis), the key roles of peroxisomal protein import in

longevity-defining processes that take place in other cellular compartments, the importance of several mitochondrial processes in orchestrating longevity-defining processes in other cellular locations, the essential role of metabolite flow within glycolytic and non-glycolytic pathways of carbohydrate metabolism in establishing a pro- or anti-aging cellular pattern, a stepwise progression of a biomolecular network of cellular aging through a series of lifespan checkpoints defines longevity of chronologically aging yeast, mechanisms through which CR and DR delay aging in evolutionarily distant eukaryotes by remodeling metabolism and organelle dynamics, and a mitochondria-based mechanism underlying the longevity-extending effect of LCA in chronologically aging yeast. I wrote sections 1.1, 1.1.1, 1.1.4, 1.1.5, 1.1.6, 1.1.7 and prepared Figures 1.2-1.4 for Chapter 1; Anna Leonov, Amanda Piano and Veronika Svistkova wrote sections 1.1.2, 1.1.3 and prepared Figure 1.1 for Chapter 1; all these sections and figures of Chapter 1 have been published in Arlia-Ciommo A, Leonov A, Piano A, Svistkova V, Titorenko VI. Cell-autonomous mechanisms of chronological aging in the yeast *Saccharomyces cerevisiae*. Microb Cell. 2014; 1(6):163-178. I also wrote sections 1.1.8, 1.1.9 and prepared Figures 1.5, 1.6 for Chapter 1; these sections and figures of Chapter 1 have been published in Arlia-Ciommo A, Piano A, Svistkova V, Mohtashami S, Titorenko VI. Mechanisms underlying the anti-aging and anti-tumor effects of lithocholic bile acid. Int J Mol Sci. 2014;15(9):16522-43.

The objective of studies described in Chapter 2 was to investigate mechanisms through which CR slows down yeast chronological aging by orchestrating age-related dynamics of ethanol metabolism, glycogen and trehalose metabolism, lipid synthesis and degradation, ROS homeostasis maintenance, mitochondrial morphology control, mitochondrial functionality preservation, and apoptotic and liponecrotic death subroutines. Our investigation revealed that CR extends longevity of chronologically aging yeast by remodeling carbohydrate and lipid metabolism, affecting certain interorganellar communications, changing morphologies and functional states of peroxisomes and mitochondria, and delaying the age-related onsets of apoptotic and liponecrotic forms of regulated cell death (RCD). I conducted experiments shown in figures 2.1, 2.2, 2.3, 2.5, 2.6, 2.7, 2.8, 2.9, 2.11, 2.14, 2.15, 2.17, 2.19, and prepared these figures. The experiments shown in figures 2.2E-2.2H, 2.4, 2.6A-2.6C, 2.10, 2.11B, 2.12, 2.13, 2.16, 2.18 were carried out by Simon Bourque, Anna Leonov, Adam Beach, Vincent Richard, Simon Bourque, Michelle Burstein, Pavlo Kyryakov, Alejandra Gomez-Perez, Olivia Koupaki and Rachel Feldman. All findings described in Chapter 2 have been published in Arlia-Ciommo A,

Leonov A, Beach A, Richard VR, Bourque SD, Burstein MT, Kyryakov P, Gomez-Perez A, Koupaki O, Feldman R, Titorenko VI. Caloric restriction delays yeast chronological aging by remodeling carbohydrate and lipid metabolism, altering peroxisomal and mitochondrial functionalities, and postponing the onsets of apoptotic and liponecrotic modes of regulated cell death. Oncotarget. 2018; 9(22):16163-84. Dr. Titorenko provided intellectual leadership of this project; he also edited the first draft of Chapter 2 and the entire manuscript of the above article.

The objective of studies described in Chapter 3 was to use a mass spectrometry-based quantitative analysis of the water-soluble cellular metabolome for the investigation of how CR and the longevity-extending *tor1Δ* mutation (which eliminates the Tor1 protein kinase known to orchestrate the nutrient- and energy-sensing TOR [target of rapamycin] pro-aging signaling pathway) affect the concentrations of various water-soluble metabolites at consecutive stages of the chronological aging process in *S. cerevisiae*. Our investigation provided the first evidence that both the longevity-extending diet CR and the-longevity extending mutation *tor1Δ* establish a similar pattern of relative concentrations of methionine metabolism intermediates through the entire process of chronological aging in *S. cerevisiae*. We hypothesized that the observed redirection of metabolite flow from the biosynthesis of methionine and spermidine to the biosynthesis of cysteine and glutathione may represent an anti-aging pattern characteristic of the ″metabolic signature″ of longevity extension in chronologically aging yeast cells placed on the CR diet or having the TOR pro-aging signaling pathway inhibited. We also proposed future studies to test this hypothesis. I conducted all experiments described in this Chapter and prepared all figures and tables. Dr. Titorenko provided intellectual leadership of this project; he also edited the first draft of Chapter 3.

The objective of studies described in Chapter 4 was to use a mass spectrometry-based quantitative analysis for the investigation of how certain mutations that eliminate enzymes involved in mitochondrial phospholipid metabolism influence the mitochondrial proteome and how they affect the geroprotective efficiency of LCA in chronologically aging yeast. Based on recent findings by the Titorenko laboratory, we hypothesized that the LCA-driven alterations in mitochondrial lipidome may have a causal role in the age-related remodeling of proteome, thereby altering mitochondrial functionality to delay chronological aging in *S. cerevisiae*. Our investigation revealed that LCA-driven specific changes in the composition of mitochondrial membrane lipids cause a distinctive remodeling of mitochondrial proteome by decreasing and

increasing concentration of many mitochondrial proteins. We also demonstrated that this remodeling of mitochondrial proteome is essential for the ability of LCA to delay aging. I conducted experiments shown in figures 4.2-4.7 and prepared these figures. Figure 4.1 was prepared by Anna Leonov and me. The experiment shown in figure 4.8 were carried out by Pavlo Kyryakov, Pamela Dakik, Melissa McAuley, Younes Medkour and Tamara Di Maulo. All findings described in Chapter 4 have been published in Leonov A, Arlia-Ciommo A, Bourque SD, Koupaki O, Kyryakov P, Dakik P, McAuley M, Medkour Y, Mohammad K, Di Maulo T, Titorenko VI. Specific changes in mitochondrial lipidome alter mitochondrial proteome and increase the geroprotective efficiency of lithocholic acid in chronologically aging yeast. Oncotarget. 2017; 8(19):30672-91. Dr. Titorenko provided intellectual leadership of this project; he also edited the first draft of Chapter 4 and the entire manuscript of the above article.

The objective of studies described in Chapter 5 was to test our hypothesis that LCA may delay chronological aging of yeast limited in calorie supply because it controls the spatiotemporal dynamics of several cellular processes outside of mitochondria. Our investigation revealed mechanisms by which LCA delays yeast chronological aging under CR conditions by altering the spatiotemporal dynamics of a cellular network that integrates certain pathways of lipid and carbohydrate metabolism, some intercompartmental communications, specific aspects of mitochondrial morphology and functionality, and liponecrotic and apoptotic modes of RCD. I conducted experiments shown in figures 5.3, 5.11-5.13, 5.19-5.21 and prepared these figures. I also prepared figures 5.1, 5.2, 5.5, 5.22 that depict various models of cellular processes controlled by LCA. Together with Simon Bourque, Vincent Richard and Karamat Mohammad, I performed experiments shown in figures 5.4, 5.7, 5.10 and prepared these figures. Experiments shown in figures 5.6, 5.8, 5.9, 5.14-5.18 were carried out by Alexander Goldberg, Pavlo Kyryakov, Alejandra Gomez-Perez and Olivia Koupaki. All findings described in Chapter 5 have been published in Arlia-Ciommo A, Leonov A, Mohammad K, Beach A, Richard VR, Bourque SD, Burstein MT, Goldberg AA, Kyryakov P, Gomez-Perez A, Koupaki O, Titorenko VI. Mechanisms through which lithocholic acid delays yeast chronological aging under caloric restriction conditions. Oncotarget (2018) 9 (79):34945-71. Dr. Titorenko provided intellectual leadership of this project; he also edited the first draft of Chapter 5 and the entire manuscript of the above article.

The objective of studies described in Chapter 6 was to test our hypothesis that LCA may trigger a reversible phosphorylation of some mitochondrial proteins. Our investigation revealed

that LCA elicits the establishment of a distinct phosphoprotein profile of mitochondria, which significantly differs from the phosphoprotein profile of mitochondria in yeast cells cultured without LCA. I conducted all experiments described in this Chapter and prepared all figures and tables. Dr. Titorenko provided intellectual leadership of this project; he also edited the first draft of Chapter 6.

2 Caloric restriction delays yeast chronological aging by remodeling carbohydrate and lipid metabolism, altering peroxisomal and mitochondrial functionalities, and postponing the onsets of apoptotic and liponecrotic modes of regulated cell death

2.1 Introduction

As described in the ″Introduction″ section, recent studies in the Titorenko laboratory of how CR influences a pattern of metabolism and organelle dynamics in the chronologically aging yeast *S. cerevisiae* have revealed that this low-calorie diet alters age-related dynamics of ethanol metabolism, lipid synthesis and degradation, trehalose metabolism, ROS homeostasis maintenance, mitochondrial morphology control, mitochondrial functionality preservation, stress response control, cell cycle regulation, quiescence maintenance, and apoptotic and liponecrotic death subroutines. Because it remained unclear how CR coordinates the spatiotemporal dynamics of all these cellular processes to delay yeast chronological aging, the objectives of studies described in this chapter was to investigate mechanisms through which CR orchestrates these various processes to slow down yeast chronological aging.

2.2 Materials and methods

2.2.1 Yeast strains, media and growth conditions

The wild-type strain *Saccharomyces cerevisiae* BY4742 (*MATα his3Δ1 leu2Δ0 lys2Δ0 ura3Δ0*) from Open Biosystems/Dharmacon (a part of GE Healthcare) was grown in YP medium (1% yeast extract, 2% peptone; both from Fisher Scientific; #BP1422-2 and #BP1420-2, respectively) initially containing 0.2% (w/v), 0.5% (w/v), 1% (w/v) or 2% (w/v) glucose (#D16-10; Fisher Scientific) as carbon source. Cells were cultured at 30^{o}C with rotational shaking at 200 rpm in Erlenmeyer flasks at a ″flask volume/medium volume″ ratio of 5:1.

2.2.2 Chronological life span assay

A sample of cells was taken from a culture at a certain time-point. A fraction of the sample was diluted to determine the total number of cells using a hemocytometer. Another fraction of the cell sample was diluted, and serial dilutions of cells were plated in duplicate onto YP plates containing 2% glucose as carbon source. After 2 d of incubation at 30^{o}C, the number of colony forming units (CFU) per plate was counted. The number of CFU was defined as the number of

viable cells in a sample. For each culture, the percentage of viable cells was calculated as follows: (number of viable cells per ml/total number of cells per ml) × 100. The percentage of viable cells in mid-logarithmic phase was set at 100%. The life span curves were validated using a LIVE/DEAD yeast viability kit (Invitrogen) following the manufacturer's instructions.

2.2.3 Ethanol concentration measurement

For measuring ethanol and acetic acid concentrations, 1-ml aliquots of yeast cultures were centrifuged, and supernatants frozen at -80°C. The supernatants were subjected to gas chromatography using an Agilent 6890 Networked GC system equipped with a Supelco Equity-1 (0.32 mm × 30 cm) column and FID detector. Ethanol and acetic acid concentrations were calculated using the Chemstation 3 software (Agilent).

2.2.4 Measurement of trehalose and glycogen concentrations

2×10^9 cells were harvested by centrifugation for 1 min at 16,000 × g at 4°C. The cell pellet was washed three times in ice-cold PBS (20 mM KH_2PO_4/KOH (pH 7.5) and 150 mM NaCl) and then resuspended in 200 µl of ice-cold SHE solution (50 mM NaOH and 1 mM EDTA). 800 µl of ice-cold SHE solution were added to the cell suspension. The resulting alkali extract was incubated at 60°C for 30 min to destroy endogenous enzyme activities and pyridine nucleotides. The extract was neutralized by adding 500 µl of THA solution (100 mM Tris/HCl (pH 8.1) and 50 mM HCl). The extract was then divided into 150 µl aliquots, quickly frozen in liquid nitrogen and stored at -80°C prior to use.

To measure trehalose concentration, 50 µl of alkali extract were added to 150 µl of trehalose reagent (25 mM KH_2PO_4/KOH (pH 7.5) and 0.02% BSA) with or without 15 mU trehalase. The mixture was incubated for 60 min at 37°C. 800 µl of glucose reagent (100 mM Tris/HCl (pH 8.1), 2 mM $MgCl_2$, 1 mM DTT, 1 mM ATP, 0.2 mM $NADP^+$, and mixture of hexokinase (7 U) and glucose-6-phosphate dehydrogenase (8 U)) were added, and the mixture was incubated for 30 min at 25°C. The NADPH generated from $NADP^+$ was measured fluorimetrically (excitation at 365 nm, emission monitored at 460 nm).

To measure glycogen concentration, 50 µl of alkali extract were added to 500 µl of glycogen reagent (50 mM sodium acetate (pH 4.6) and 0.02% BSA; with and without 5 µg/ml amyloglucosidase 14 U/mg). The mixture was incubated for 30 min at 25°C. 500 µl of glucose

reagent (100 mM Tris/HCl (pH 8.1), 2 mM $MgCl_2$, 1 mM DTT, 1 mM ATP, 0.2 mM $NADP^+$, and mixture of hexokinase (7 U) and glucose-6-phosphate dehydrogenase (8 U)) were added, and the mixture was incubated for 30 min at 25ºC. The NADPH generated from $NADP^+$ was measured fluorimetrically (excitation at 365 nm, emission monitored at 460 nm).

2.2.5 Lipid extraction, separation by thin-layer chromatography (TLC), visualization and quantitation

The recovered pellet of membranes (total cellular membranes, membranes of the purified ER or membranes of purified LD) that contained 1 mg of membrane protein was resuspended in 1.0 ml of chloroform/methanol (1:1; vol/vol). After incubation on ice for 15 min with occasional agitation, the samples were subjected to centrifugation at 20,000 × g for 15 min at 4ºC. The chloroform phase was separated and dried under nitrogen. The lipid film was dissolved in 100 µl of chloroform. 25 µl of each sample were spotted on 60-Å silica gel plates for TLC (Whatman). The lipids were developed in the chloroform/acetone (4.6:0.4) [vol/vol] solvent system, detected using 5% phosphomolybdic acid in ethanol and visualized by heating for 30 min at 110°C. The lipids were quantitated by densitometric analysis of TLC plates, using lipid standards in the 0.1–0.5 µg range for calibration.

2.2.6 Electron microscopy and morphometric analysis

Whole cells were fixed in 1.5% $KMnO_4$ for 20 min at room temperature, dehydrated by successive incubations in increasing concentrations of ethanol, and embedded in Poly/Bed 812 epoxy resin (Polysciences). Ultrathin sections were cut using an Ultra-Cut E Microtome (Reichert-Jung). Silver/gold thin sections from the embedded blocks were examined in a transmission electron microscope (JEM-2000FX; JEOL). For morphometric analysis of random electron microscopic sections of cells, 12- × 14-cm prints and 8- × 10-cm negatives of 35–40 cell sections of each strain at 24,000–29,000 magnification were scanned and converted to digitized images with a ScanJet 4400c (Hewlett-Packard) and Photoshop 6.0 software (Adobe Systems, Inc.). Quantitation of digitized images was performed using the Discovery Series Quantity One 1-D Analysis Software (Bio-Rad Laboratories).

2.2.7 Cellular respiration measurement

A sample of cells was taken from a culture at a certain time-point. Cells were pelleted by centrifugation and resuspended in 1 ml of fresh YP medium containing 0.05% glucose. Oxygen uptake by cells was measured continuously in a 2-ml stirred chamber using a custom-designed biological oxygen monitor (Science Technical Center of Concordia University) equipped with a Clark-type oxygen electrode.

2.2.8 Fluorescence microscopy

BODIPY 493/503 (Invitrogen) staining for monitoring neutral lipids deposited in lipid droplets and DHR (Sigma) staining for ROS were performed according to established procedures [23]. The mitochondrial membrane potential ($\Delta\Psi$) was measured in live yeast by fluorescence microscopy of Rhodamine 123 (R123) staining. For R123 staining, 5×10^6 cells were harvested by centrifugation for 1 min at 21,000 × g at room temperature and then resuspended in 100 µl of 50 mM sodium citrate buffer (pH 5.0) containing 2% glucose. R123 (Invitrogen) was added to a final concentration of 10 µM. Following incubation in the dark for 30 min at room temperature, the cells were washed twice in 50 mM sodium citrate buffer (pH 5.0) containing 2% glucose and then analyzed by fluorescence microscopy. Images were collected with a Zeiss Axioplan fluorescence microscope (Zeiss) mounted with a SPOT Insight 2-megapixel color mosaic digital camera (Spot Diagnostic Instruments). For evaluating the percentage of BODIPY 493/503-, DHR- and R123-positive cells, the UTHSCSA Image Tool (Version 3.0) software was used to calculate both the total number of cells and the number of stained cells. Fluorescence of individual DHR- or R123-positive cells in arbitrary units was determined by using the UTHSCSA Image Tool software (Version 3.0). In each of 3 independent experiments, the value of median fluorescence was calculated by analyzing at least 800-1000 cells that were collected at each time-point. The median fluorescence values were plotted as a function of the number of days cells were cultured.

2.2.9 Immunofluorescence microscopy

Cell cultures were fixed in 3.7% formaldehyde for 45 min at room temperature. The cells were washed in solution B (100 mM KH_2PO_4/KOH pH 7.5, 1.2 M sorbitol), treated with Zymolyase 100T (MP Biomedicals, 1 µg Zymolyase 100T/1 mg cells) for 30 min at 30°C and then processed as previously described [166]. Monoclonal antibody raised against porin (Invitrogen,

0.25 μg/μl in TBSB buffer [20 mM Tris/HCl pH 7.5, 150 mM NaCl, 1 mg/ml BSA]) was used as a primary antibody. Alexa Fluor 568 goat anti-mouse IgG (Invitrogen, 2 μg/μl in TBSB buffer) was used as a secondary antibody. The labeled samples were mounted in mounting solution (16.7 mM Tris/HCl pH 9.0, 1.7 mg/ml p-phenylenediamine, 83% glycerol). Images were collected with a Zeiss Axioplan fluorescence microscope (Zeiss) mounted with a SPOT Insight 2-megapixel color mosaic digital camera (Spot Diagnostic Instruments).

2.2.10 ATP measurement

2×10^9 cells were harvested by centrifugation for 1 min at 16,000 × g at 4ºC. The cell pellet was washed three times in ice-cold PBS (20 mM KH_2PO_4/KOH (pH 7.5) and 150 mM NaCl) and then resuspended in 200 μl of ice-cold SHE solution (50 mM NaOH and 1 mM EDTA). 800 μl of ice-cold SHE solution were added to the cell suspension. The resulting alkali extract was incubated at 60ºC for 30 min to destroy endogenous enzyme activities and pyridine nucleotides. The extract was neutralized by adding 500 μl of THA solution (100 mM Tris/HCl (pH 8.1) and 50 mM HCl). The extract was then divided into 150 μl aliquots, quickly frozen in liquid nitrogen and stored at -80ºC prior to use. For ATP measurement, 1 μl of alkali extract was added to 1 μl ATP reagent (50 mM Tris-HCl (pH 8.1), 3 mM $MgCl_2$, 0.2 mM glucose, 0.04% BSA, 0.05 mM $NADP^+$, 10 μg/ml hexokinase, 2 μg/ml glucose-6-phosphate dehydrogenase). Following a 30-min incubation at 25ºC, the reaction was stopped by adding 1 μl of 0.15 M NaOH and heating at 80º C for 20 min. A 1 μl aliquot was transferred 100 μl of reagent containing 100 μg/ml hexokinase and 20 μg/ml glucose-6-phosphate dehydrogenase. The reaction mixture was incubated for 1 h at 38ºC. The NADPH generated from $NADP^+$ was measured fluorimetrically (excitation at 365 nm, emission monitored at 460 nm).

2.2.11 Total cell lysates preparation

Total cell lysates were made by vortexing the cells in TCL buffer (25 mM Tris/HCl pH 8.5, 150 mM NaCl, 1 mM EDTA, 0.1 mM DTT, 4% CHAPS, 1 mM PMSF, protease inhibitor cocktail [Sigma]) with glass beads three times for 1 min. Lysates were then centrifuged for 3 min at 21,000 × g at 4ºC and supernatants collected.

2.2.12 Cell viability assay for monitoring the susceptibility of yeast to a mode of cell death induced by palmitoleic acid (POA)

A sample of cells was taken from a culture on a certain day of culturing. A fraction of the sample was diluted to determine the total number of cells using a hemocytometer. 8×10^7 cells were harvested by centrifugation for 1 min at 21,000 × g at room temperature and resuspended in 8 ml of YP medium containing 0.2% glucose as carbon source. Each cell suspension was divided into 8 equal aliquots. Three pairs of aliquots were supplemented with POA (#P9417; Sigma) from a 50-mM stock solution (in 10% chloroform, 45% hexane and 45% ethanol; #650498, #248878 and #34852, respectively; all from Sigma). The final concentration of POA was 0.05 mM, 0.1 mM or 0.15 mM for each pair of aliquots; in all these aliquots, the final concentrations of chloroform, hexane and ethanol were 0.03%, 0.135% and 0.135%, respectively. One pair of aliquots was supplemented only with chloroform, hexane and ethanol added to the final concentrations of 0.03%, 0.135% and 0.135%, respectively. All aliquots were then incubated for 2 h at 30ºC on a Labquake rotator (#400110; Thermolyne/Barnstead International) set for 360º rotation. Serial dilutions of cells were plated in duplicate onto plates containing YP medium with 2% glucose as carbon source. After 2 d of incubation at 30ºC, the number of colony forming units (CFU) per plate was counted. The number of CFU was defined as the number of viable cells in a sample. For each aliquot of cells exposed to POA, the % of viable cells was calculated as follows: (number of viable cells per ml in the aliquot exposed to POA/number of viable cells per ml in the control aliquot that was not exposed to POA) × 100.

2.2.13 Cell viability assay for monitoring the susceptibility of yeast to a mode of cell death induced by hydrogen peroxide

A sample of cells was taken from a culture on a certain day of culturing. A fraction of the sample was diluted to determine the total number of cells using a hemocytometer. 8×10^7 cells were harvested by centrifugation for 1 min at 21,000 × g at room temperature and resuspended in 8 ml of YP medium containing 0.2% glucose as carbon source. Each cell suspension was divided into 8 equal aliquots. Three pairs of aliquots were supplemented with hydrogen peroxide (#H325-500; Fisher Scientific) to the final concentration of 0.5 mM, 1.5 mM or 2.5 mM for each pair. One pair of aliquots remained untreated. All aliquots were then incubated for 2 h at 30ºC on a Labquake rotator (#400110; Thermolyne/Barnstead International) set for 360º rotation. Serial dilutions of

cells were plated in duplicate onto plates containing YP medium with 2% glucose as carbon source. After 2 d of incubation at 30ºC, the number of CFU per plate was counted. The number of CFU was defined as the number of viable cells in a sample. For each aliquot of cells exposed to hydrogen peroxide, the % of viable cells was calculated as follows: (number of viable cells per ml in the aliquot exposed to hydrogen peroxide/number of viable cells per ml in the control aliquot that was not exposed to hydrogen peroxide) × 100.

2.2.14 Statistical analysis

Statistical analysis was performed using Microsoft Excel's (2010) Analysis ToolPak - VBA. All data on cell survival are presented as mean ± SEM. The p values for comparing the means of two groups using an unpaired two-tailed *t* test were calculated with the help of the GraphPad Prism 7 statistics software. The logrank test for comparing each pair of survival curves was performed with GraphPad Prism 7. Two survival curves were considered statistically different if the *p* value was less than 0.05.

2.2.15 Miscellaneous procedures

Enzymatic activity of cytochrome c oxidase measurement [166], a measurement of succinate dehydrogenase enzymatic activity [167], enzymatic activity of aconitase measurement [168], SDS-PAGE and immunoblotting [169], subcellular fractionation of yeast [170], purification of LD [171], purification of the ER [170] were performed as previously described.

2.3 Results

2.3.1 Rapid consumption of ethanol by yeast cultured under CR conditions is an essential contributing factor to chronological aging delay by CR

The Titorenko laboratory has previously found that wild-type (WT) cells of yeast grown under CR conditions on 0.2% or 0.5% glucose quickly consume ethanol, a product of glucose fermentation by these cells [23]. Because WT yeast cultures grown under non-CR conditions on 1% or 2% glucose did not consume (and therefore accumulated) ethanol for many days of culturing [23], we hypothesized that the fast consumption of ethanol by WT yeast limited in calorie supply may play essential role in the ability of CR to delay yeast chronological aging [23, 84, 149]. In our

hypothesis, ethanol accumulation by yeast cells cultured in calorie-rich medium may be responsible for the accelerated chronological aging of non-CR yeast [23, 84, 149]. This hypothesis posits that 1) a genetic intervention that lowers ethanol concentration in non-CR yeast cultures will extend longevity of chronologically aging yeast; whereas 2) a genetic intervention that rises ethanol concentration in such cultures will shorten yeast chronological lifespan (CLS) [23, 84, 149]. To test this hypothesis, we assessed how a single-gene-deletion mutation eliminating either the Adh1 or the Adh2 isozyme of alcohol dehydrogenase influences ethanol concentrations in CR and non-CR yeast cultures and how each of these mutations affects CLS of CR and non-CR yeast. Adh1 is known to catalyze acetaldehyde conversion to ethanol, whereas Adh2 is involved in the reverse process of ethanol conversion to acetaldehyde (Figure 2.1) [172]. Both these alcohol dehydrogenase isozymes are assimilated into a network of metabolic pathways and interorganellar communications taking place in cells of chronologically aging *S. cerevisiae* (Figure 2.1) [23, 20, 149, 172-175].

We found that, although the *adh1Δ* mutation decreases and the *adh2Δ* mutation increases ethanol concentration in yeast cultures during logarithmic (L) phase of growth under CR on 0.2% or 0.5% glucose, ethanol is rapidly and completely consumed by *adh1Δ* and *adh2Δ* cells (as well as by WT cells) during subsequent diauxic (D) phase of culturing under CR conditions (Figures 2.2A and 2.2B, respectively). Not only the *adh1Δ* and *adh2Δ* mutations had no effect on the rapid consumption of ethanol under CR conditions, but they also did not affect the CLS of yeast placed on a low-calorie diet (Figures 2.2E, 2.2F, 2.2I and 2.2J).

Despite the *adh1Δ* and *adh2Δ* mutations did not influence ethanol concentration in post-logarithmic CR yeast cultures and had no effect on yeast CLS under CR conditions, each of them differently affected ethanol concentration and CLS under non-CR conditions on 1% or 2% glucose. *adh1Δ* significantly decreased ethanol concentration in non-CR yeast during all phases of culturing (Figures 2.2C and 2.2D) and increased the CLS of non-CR yeast (Figures 2.2G, 2.2H, 2.2K and 2.2L). In contrast, *adh2Δ* significantly increased ethanol concentration in non-CR yeast during all phases of culturing (Figures 2.2C and 2.2D) and decreased the CLS of non-CR yeast (Figures 2.2G, 2.2H, 2.2K and 2.2L).

In sum, these findings indicate that CR delays yeast chronological aging in part because this low-calorie diet accelerates the consumption of ethanol, a product of glucose fermentation.

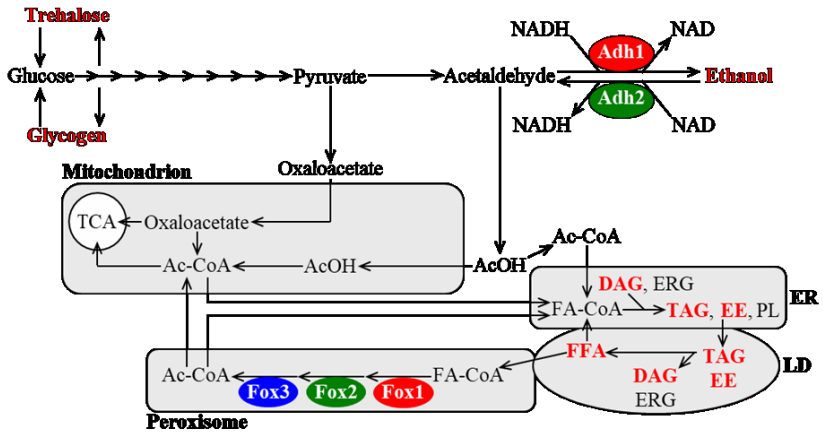

Figure 2.1. The Adh1- and Adh2-dependent metabolism of ethanol is integrated into a network which also assimilates the synthesis and degradation of glycogen and trehalose, the synthesis of neutral lipids TAG and EE in the ER, the lipolytic degradation of TAG and EE in LD, and the Fox1-, Fox2- and Fox3-dependent β-oxidation of FFA in peroxisomes. The names of metabolites integrated into this network and pertinent to this study are displayed in red color. The Adh1 isozyme of alcohol dehydrogenase catalyzes the conversion of acetaldehyde to ethanol, whereas the Adh2 isozyme of alcohol dehydrogenase is involved in a reverse process of ethanol conversion to acetaldehyde. Abbreviations: Ac-CoA, acetyl-CoA; AcOH, acetic acid; DAG, diacylglycerols; EE, ergosteryl esters; ER, endoplasmic reticulum; ERG, ergosterol; FFA, free fatty acids; FA-CoA, fatty acyl-CoA esters; LD, lipid droplets; TAG, triacylglycerols.

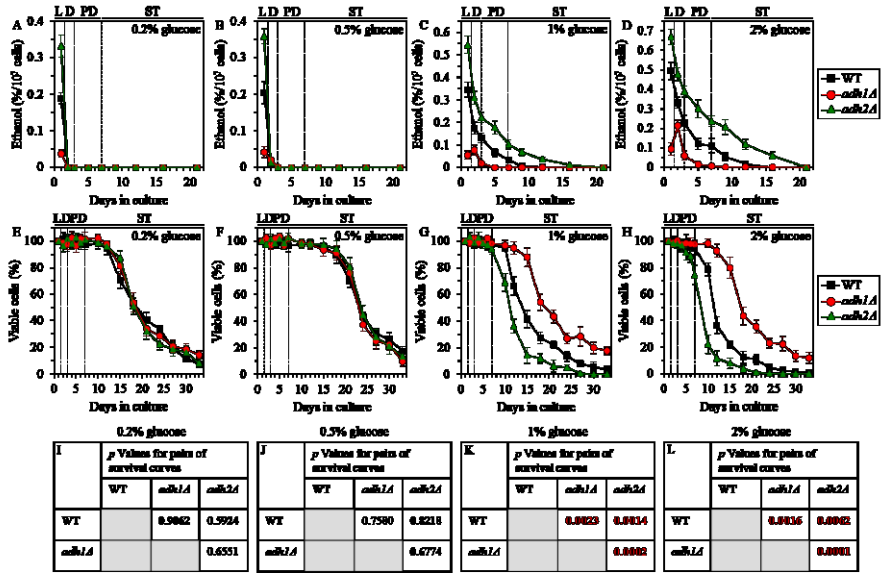

Figure 2.2. Effects of the *adh1Δ* and *adh2Δ* mutations on ethanol concentration and CLS under CR and non-CR conditions. WT, *adh1Δ* and *adh2Δ* cells were cultured in the nutrient-rich YP medium under CR (the initial concentration of glucose was 0.2% or 0.5%) or non-CR (the initial concentration of glucose was 1% or 2%) conditions. **A-D**. Ethanol concentrations in yeast cultures grown under CR or non-CR conditions and recovered on different days of culturing. **E-H**. Survival curves of chronologically aging WT, *adh1Δ* and *adh2Δ* strains. Data are presented as means ± SEM (n = 4). **I-L**. *p* Values for different pairs of survival curves of WT, *adh1Δ* and *adh2Δ* strains cultured under CR or non-CR conditions. Survival curves shown in **E-H** were compared. Two survival curves were considered statistically different if the *p* value was less than 0.05. The *p* values for comparing pairs of survival curves using the logrank test were calculated as described in Materials and Methods. Abbreviations: L, D, PD and ST, logarithmic, diauxic, post-diauxic and stationary growth phases (respectively). Experiments in **E-H** were performed by Pavlo Kyryakov and Alejandra Gomez-Perez.

2.3.2 Ethanol concentration controls the homeostasis of glycogen and trehalose in yeast cultured under non-CR conditions

Both the Adh1-dependent conversion of acetaldehyde to ethanol and the Adh2-driven conversion of ethanol to acetaldehyde are integrated into a network which includes the metabolic

pathways for glycogen and trehalose synthesis and degradation (Figure 2.1) [23, 149, 172, 176]. Glycogen and trehalose are the major stores of glucose in yeast cells [23, 149, 176, 177]. Trehalose in yeast is also involved in the development and maintenance of an anti-aging cellular pattern because this carbohydrate 1) protects cells and proteins from various stresses [19]; 2) preserves cellular proteostasis by suppressing the misfolding, aggregation and oxidative damage of newly synthesized polypeptides [61, 149, 179]; and 3) enables a re-entry of quiescent cells into the proliferative cell cycle in response to a supply of nutrients [150, 180, 181].

Because the pathways of ethanol, glycogen and trehalose metabolism are integrated into a network and play essential roles in yeast chronological aging, we hypothesized that the extent of ethanol accumulation by yeast cells cultured under non-CR conditions may influence glycogen and/or trehalose homeostasis in yeast cells. Our hypothesis posits that genetic interventions that decrease or increase ethanol concentration in non-CR yeast cultures will differently affect the concentrations of glycogen and/or trehalose in yeast cells cultured in calorie-rich medium. To test this hypothesis, we examined how the *adh1Δ* mutation (which decreases ethanol concentration in non-CR yeast; Figures 2.2C and 2.2D) and the *adh2Δ* mutation (which increases ethanol concentration in non-CR yeast; Figures 2.2C and 2.2D) affect glycogen and trehalose abundance in yeast cultured under non-CR conditions.

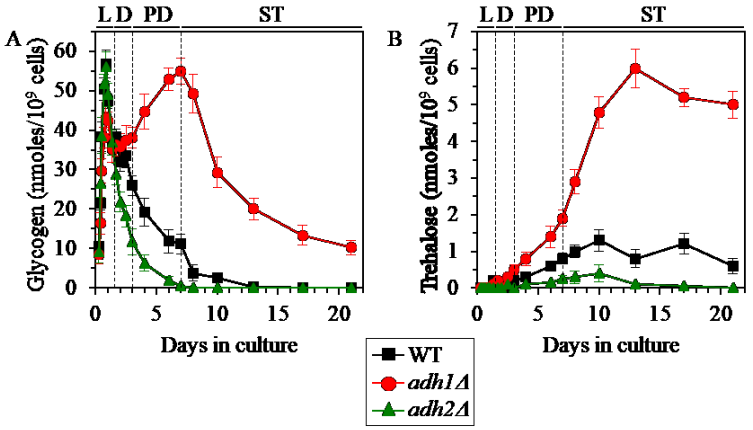

Figure 2.3. Effects of the *adh1Δ* and *adh2Δ* mutations on glycogen and trehalose concentrations in non-CR yeast. WT, *adh1Δ* and *adh2Δ* cells were cultured in the nutrient-rich YP medium under non-CR conditions on 2% glucose. Glycogen (**A**) and trehalose (**B**) concentrations in non-CR yeast recovered on different days of culturing are shown. Glycogen and trehalose concentrations were measured as described in Materials and Methods. Abbreviations: L, D, PD and ST, logarithmic, diauxic, post-diauxic and stationary growth phases (respectively).

We found that the *adh1Δ* mutation has the following effects on glycogen and trehalose in non-CR yeast cultured on 2% glucose: 1) it elicits a buildup of glycogen during post-diauxic (PD) phase of culturing and shifts glycogen consumption by *adh1Δ* cells to stationary (ST) phase (whereas WT cells deplete glycogen store during preceding PD phase) (Figure 2.3A); and 2) it

substantially increases the concentration of trehalose during PD and ST phases (Figure 2.3B). In contrast, the *adh2Δ* mutation affected glycogen and trehalose abundance in non-CR yeast cultured on 2% glucose as follows: 1) it accelerated the consumption of glycogen during D and PD phases (Figure 2.3A); and 2) it significantly decreased trehalose concentration during PD and ST phases (Figure 2.3B).

These findings support our hypothesis that ethanol concentration in non-CR yeast cells regulates glycogen and trehalose homeostasis in these cells.

2.3.3 Ethanol concentration regulates the homeostasis of neutral lipids, free fatty acids and diacylglycerols, in non-CR yeast

The network integrating ethanol, glycogen and trehalose metabolism also incorporates the metabolic pathways for the synthesis and degradation of the following lipid classes: 1) the so-called ″neutral″ (uncharged) lipids triacylglycerols (TAG) and ergosteryl esters (EE), both of which are first synthesized in the endoplasmic reticulum (ER) and then deposited in lipid droplets (LD); and 2) free fatty acids (FFA) and diacylglycerols (DAG), both of which can be used for TAG synthesis in the ER and can also be formed as the products of TAG lipolysis in LD (FFA can also undergo β-oxidation in peroxisomes) (Figure 2.1) [23, 149, 173-175]. TAG synthesis from FFA and DAG in the ER, LD-confined TAG lipolysis into FFA and DAG, and the peroxisomal oxidation of FFA are known to be longevity assurance processes in chronologically aging yeast [20, 23, 149, 173-175].

Given that the metabolic pathways for ethanol, TAG, EE, FFA and DAG synthesis and degradation are assimilated into a network and define longevity of chronologically aging yeast, one may assume that ethanol concentration in non-CR yeast may play an important role in the maintenance of TAG, EE, FFA and DAG homeostasis. To test this assumption, we assessed the effects of the *adh1Δ* and *adh2Δ* mutations on the abundance of LD, TAG, EE, FFA and DAG in non-CR yeast.

We found that in yeast cultured under non-CR conditions on 2% glucose, the *adh1Δ* mutation stimulates LD degradation, promotes TAG and EE lipolysis, and accelerates FFA and DAG consumption during ST phase (Figures 2.4A-2.4E); this mutation decreases ethanol concentration in non-CR yeast (Figures 2.2C and 2.2D). We also noticed that the *adh2Δ* mutation

has the following effects in non-CR yeast cultured on 2% glucose: 1) it suppresses LD degradation during late ST phase; 2) it slows down TAG and EE lipolysis during ST phase; and 3) it rises FFA

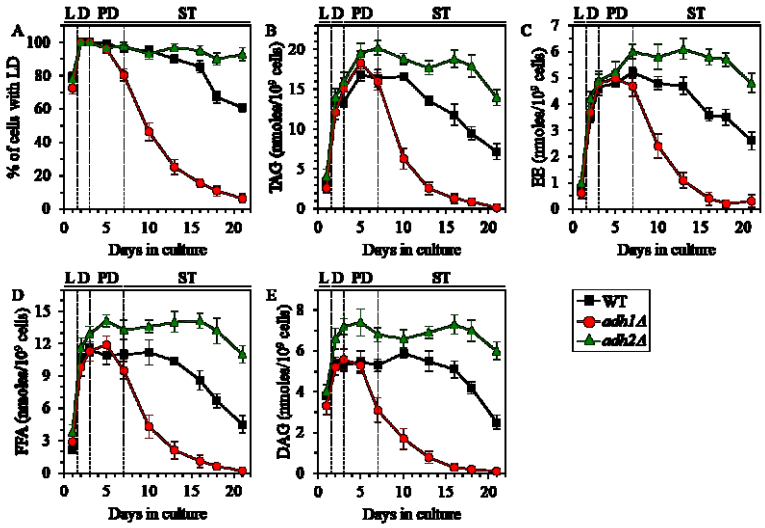

Figure 2.4. Effects of the *adh1Δ* and *adh2Δ* mutations on the abundance of LD, TAG, EE, FFA and DAG in non-CR yeast. WT, *adh1Δ* and *adh2Δ* cells were cultured in the nutrient-rich YP medium under non-CR conditions on 2% glucose. The percentage of cells with LD (**A**) as well as TAG (**B**), EE (**C**), FFA (**D**) and DAG (**E**) concentrations in whole cells recovered on different days of culturing are shown. The abundance of LD and the concentrations of TAG, EE, FFA and DAG in whole cells were measured as described in Materials and Methods. Abbreviations: DAG, diacylglycerols; EE, ergosteryl esters; FFA, free fatty acids; LD, lipid droplets; L, D, PD and ST, logarithmic, diauxic, post-diauxic and stationary growth phases (respectively); TAG, triacylglycerols. These experiments were performed by Simon Bourque, Alexander Goldberg and Pavlo Kyryakov.

and DAG concentrations during PD phase and decelerates their consumption during subsequent ST phase (Figures 2.4A-2.4E); this mutation increases ethanol concentration in non-CR yeast (Figures 2.2C and 2.2D).

In sum, these findings confirm our assumption that ethanol concentration in non-CR yeast cells is an important contributing factor to the maintenance of TAG, EE, FFA and DAG homeostasis.

2.3.4 Ethanol lowers concentrations of enzymes involved in the peroxisomal oxidation of FFA to cause FFA accumulation in non-CR yeast

Our previous study has revealed that in chronologically aging yeast the CR diet 1) elicits a rapid and complete exhaustion of ethanol during D phase; 2) increases the concentrations of the core enzymes of peroxisomal fatty acid β-oxidation Fox1, Fox2 and Fox3 (Figure 2.1) during D, PD and ST phases; and 3) stimulates a fast depletion of FFA during PD phase [23]. Ethanol has been shown to decrease the levels of Fox1, Fox2 and Fox3 in methylotrophic yeast capable of using methanol as sole source of carbon and energy [182, 183]. Altogether, these findings suggested a hypothesis that the observed buildup of ethanol in non-CR yeast cultures (Figures 2.2C

and 2.2D) may decrease the abundance of Fox1, Fox2 and Fox3; the resulting decline in the peroxisomal β-oxidation of FFA may instigate the accumulation of FFA seen in non-CR yeast [23].

If this hypothesis is correct, then 1) a genetic intervention that decreases ethanol concentration in non-CR yeast cultures (such as the *adh1Δ* mutation) will increase the levels of Fox1, Fox2 and Fox3 in yeast cultured in calorie-rich medium; whereas 2) a genetic intervention that increases ethanol concentration in these cultures (such as the *adh2Δ* mutation) will decrease the levels of Fox1, Fox2 and Fox3 in non-CR yeast. In support of this hypothesis, the *adh1Δ* mutation caused an increase in the concentrations of Fox1, Fox2 and Fox3 in non-CR yeast cultured on 1% or 2% glucose, while the *adh2Δ* mutation had the opposite effect on the concentrations of these enzymes in yeast under non-CR conditions (Figures 2.5A, 2.5D, 2.5E, 2.5H, 2.5I, 2.5L and 2.5M).

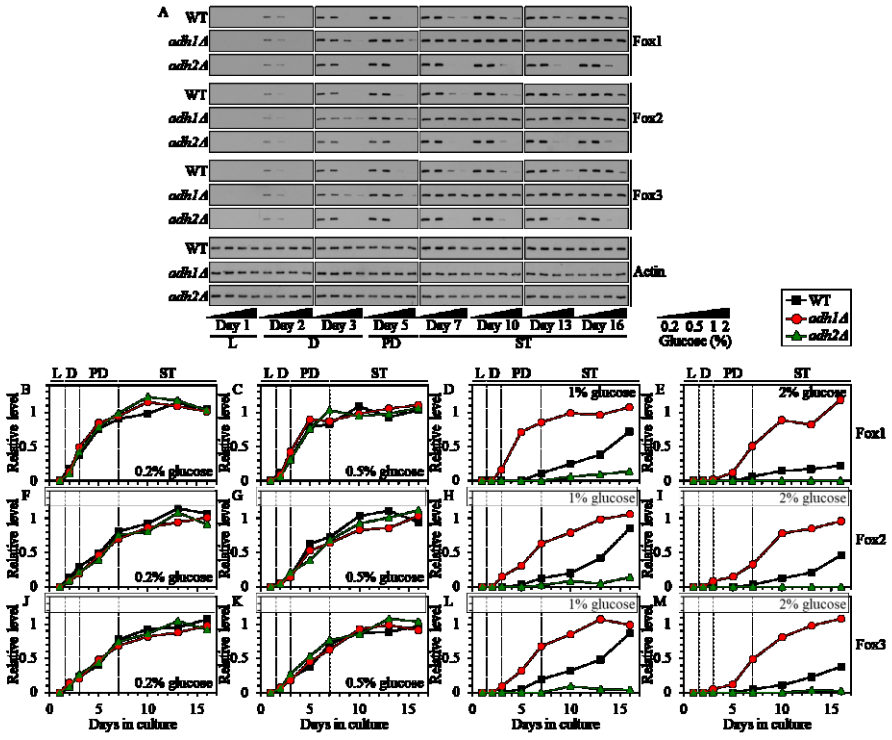

Figure 2.5. Effects of the *adh1Δ* and *adh2Δ* mutations on the concentrations of Fox1, Fox2 and Fox3 in yeast cultured under CR or non-CR conditions. WT, *adh1Δ* and *adh2Δ* cells were cultured in the nutrient-rich YP medium under CR (the initial concentration of glucose was 0.2% or 0.5%) or non-CR (the initial concentration of glucose was 1% or 2%) conditions. **A**. Western blot analysis of Fox1, Fox2, Fox3 and actin in total cell lysates was performed as described in Materials and Methods. **B-M**. Immunoblots shown in A were used to calculate the relative levels of Fox1, Fox2 and Fox3 in total cell lysates as described in Materials and Methods. Abbreviations: L, D, PD and ST, logarithmic, diauxic, post-diauxic and stationary growth phases (respectively).

We therefore concluded that ethanol decreases the concentrations of Fox1, Fox2 and Fox3 in non-CR yeast cells, thus decelerating the peroxisomal β-oxidation of FFA and eliciting a buildup of FFA in these cells.

2.3.5 In CR yeast, the peroxisomal β-oxidation of FFA is a longevity assurance process that controls neutral lipids synthesis in the ER and neutral lipids lipolysis in LD

Since CR diet elicits a substantial increase in the concentrations of the core enzymes of peroxisomal fatty acid β-oxidation Fox1, Fox2 and Fox3 (Figure 2.5) [23], one may assume that the β-oxidation of FFA in peroxisomes may be a longevity assurance process in chronologically aging yeast limited in calorie supply. In support of this assumption, we found that the *fox1Δ*, *fox2Δ* and *fox3Δ* mutations significantly shorten the CLS of yeast cultured under CR on 0.2% glucose (Figures 2.6A and 2.6B).

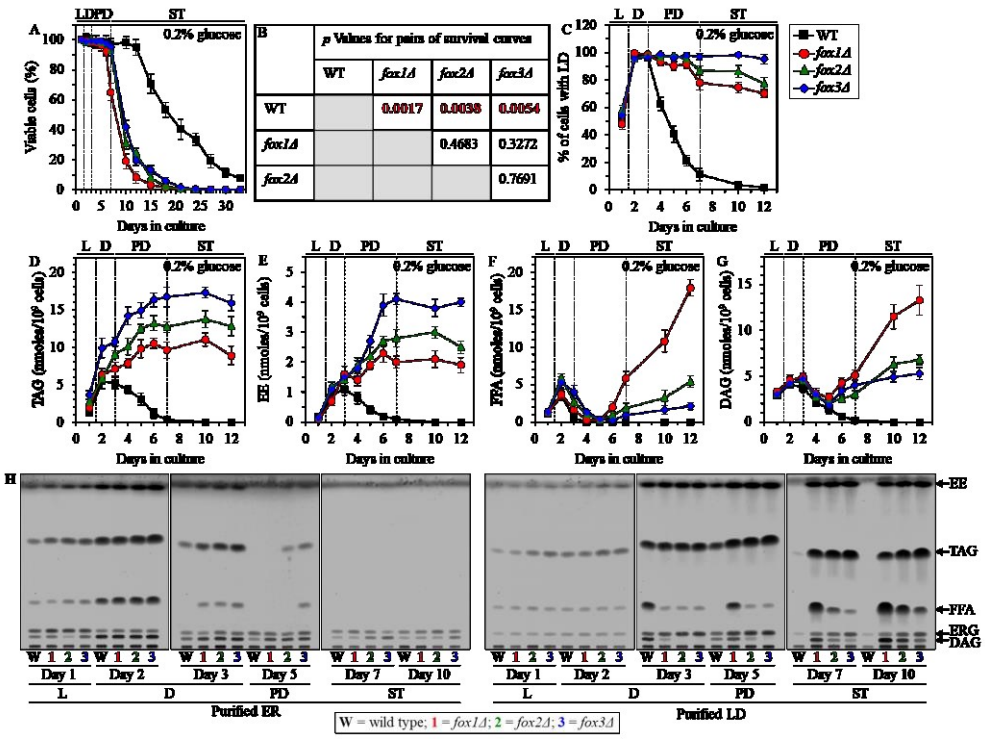

Figure 2.6. Effects of the *fox1Δ*, *fox2Δ* and *fox3Δ* mutations on CLS, LD abundance, and TAG, EE, FFA and DAG concentrations in yeast cultured under CR conditions. WT, *fox1Δ*, *fox2Δ* and *fox3Δ* cells were cultured in the nutrient-rich YP medium under CR conditions on 0.2% glucose. **A**. Survival curves of chronologically aging WT, *fox1Δ*, *fox2Δ* and *fox3Δ* strains. Data are presented as means ± SEM (n = 4). **B**. *p* Values for different pairs of survival curves of WT, *fox1*Δ, *fox2Δ* and *fox3Δ* strains. Survival curves shown in **A** were compared. Two survival curves were considered statistically different if the *p* value was less than 0.05. The *p* values for comparing pairs of survival curves using the logrank test were calculated as described in Materials and Methods. The percentage of cells with LD (**C**) as well as TAG (**D**), EE (**E**), FFA (**F**) and DAG (**G**) concentrations in whole cells recovered on different days of culturing are shown. Data are presented as means ± SEM (n = 4). The abundance of LD and the concentrations of TAG, EE, FFA and DAG in whole cells were measured as described in Materials and Methods. **H**. Spectra of lipids that were extracted from the ER or LD purified from WT, *fox1Δ*, *fox2Δ* and *fox3Δ* cells. Cells were recovered on different days of culturing, and the ER and LD were purified as described in Materials and Methods. The equivalent of 200 μg of ER proteins and the equivalent of 20 μg of LD proteins were used for lipid extraction and analysis by thin-layer chromatography, as described in Materials and Methods. A representative of 3 independent experiments is shown. Abbreviations: DAG, diacylglycerols; EE, ergosteryl esters; ER, endoplasmic reticulum; FFA, free fatty acids; LD, lipid droplets; L, D, PD and ST, logarithmic, diauxic, post-diauxic and stationary growth phases (respectively); TAG, triacylglycerols. Experiments in **A-C** were performed by Pavlo Kyryakov and Alejandra Gomez-Perez.

FFA that undergo the β-oxidation in peroxisomes are formed in LD as the products of neutral lipid lipolysis, a process which also generates DAG and ergosterol (ERG) from TAG and EE (respectively) (Figure 2.1) [23, 149, 173-175]. Moreover, LD-derived FFA are utilized for neutral lipids synthesis in the ER using DAG and ERG as the co-substrates for TAG and EE formation (respectively) (Figure 2.1) [23, 149, 173-175]. Thus, the β-oxidation of FFA in peroxisomes, lipolysis of neutral lipids in LD and synthesis of neutral lipids in the ER are integrated into an intricate metabolic network (Figure 2.1). We therefore hypothesized that the *fox1Δ*, *fox2Δ* and *fox3Δ* mutations may alter the concentrations of all these lipid classes (i.e. FFA, DAG, TAG and EE). Our hypothesis posits that the rate of the peroxisomal β-oxidation of FFA may influence the rates of neutral lipids synthesis in the ER and neutral lipids lipolysis in LD. In support of this hypothesis, we found that in chronologically aging CR yeast the *fox1Δ*, *fox2Δ* and *fox3Δ* mutations 1) prevent an age-related depletion of LD during PD and ST phases (Figure 2.6C); 2) eliminate an age-related decline in the cellular concentrations of TAG and EE during PD and ST phases (Figures 2.6D and 2.6E); 3) elicit an accumulation of TAG and EE in the ER during PD phase (Figure 2.6H); 4) cause a buildup of TAG and EE in LD during ST phase (Figure 2.6H); 5) increase the cellular concentrations of FFA and DAG during PD and ST phases (Figures 2.6F and 2.6G); 6) prompt an accumulation of FFA and DAG in the ER during D and PD phases (Figure 2.6H); and 7) promote a deposition of FFA and DAG in LD during PD and ST phases (Figure 2.6H).

2.3.6 A weakening of peroxisomal fatty acid β-oxidation elicits negative feedback loops that regulate the metabolism and transport of several lipid classes in the ER and LD

A close association of peroxisomes with LD in chronologically aging yeast causes an intrusion of peroxisomes into the neutral lipid core of LD, thus forming so-called ″pexopodia″ (Figures 2.7A-2.7C; Figure 2.8) [184]. Pexopodia stimulate the lipolysis of neutral lipids within LD, thereby increasing the supply of FFA for β-oxidation in peroxisomes [184]. The *fox1Δ*, *fox2Δ* and *fox3Δ* mutations impair peroxisomal fatty acid β-oxidation, thus eliciting a deposition of electron-dense arrays of FFA (termed ″gnarls″) and non-degraded neutral lipids within LD (Figures 2.7A-2.7C; Figure 2.8) [184].

We have used electron microscopy to monitor age-related changes in the abundance of pexopodia and LD-confined gnarls in WT, *fox1Δ*, *fox2Δ* and *fox3Δ* cells cultured under CR on 0.2% glucose.

We found that pexopodia amass in WT, *fox1Δ*, *fox2Δ* and *fox3Δ* cells during L and D phases (Figure 2.7D), concomitantly with an increase of FFA and DAG in whole cells (Figures 2.6F and 2.6G), the ER (Figure 2.6H) and LD (Figure 2.6H).

During the following PD phase, pexopodia disappeared in WT cells (Figure 2.7D); such disappearance of pexopodia in WT cells during PD phase coincided with 1) a depletion of FFA and DAG in whole WT cells (Figures 2.6F and 2.6G), the ER of WT (Figure 2.6H) and LD of WT (Figure 2.6H); 2) an exhaustion of TAG and EE in whole WT cells (Figures 2.6D and 2.6E) and the ER of WT (Figure 2.6H); 3) a decrease of TAG and EE concentrations in LD of WT (Figure 2.6H; both TAG and EE were completely depleted in LD of WT by the beginning of the ensuing ST phase); and 4) a lack of gnarls in LD of WT (Figure 2.7E). In contrast, pexopodia became more abundant in *fox1Δ*, *fox2Δ* and *fox3Δ* mutant cells during PD phase (Figure 2.7D), concomitantly with 1) a rise of FFA and DAG in whole mutant cells (Figures 2.6F and 2.6G), the ER of mutants (Figure 2.6H) and LD of mutants (Figure 2.6H); 2) an increase in TAG and EE concentrations in whole mutant cells (Figures 2.6D and 2.6E), the ER of mutants (Figure 2.6H) and LD of mutants (Figure 2.6H); and 3) an expansion of gnarls in LD of mutants (Figure 2.7E).

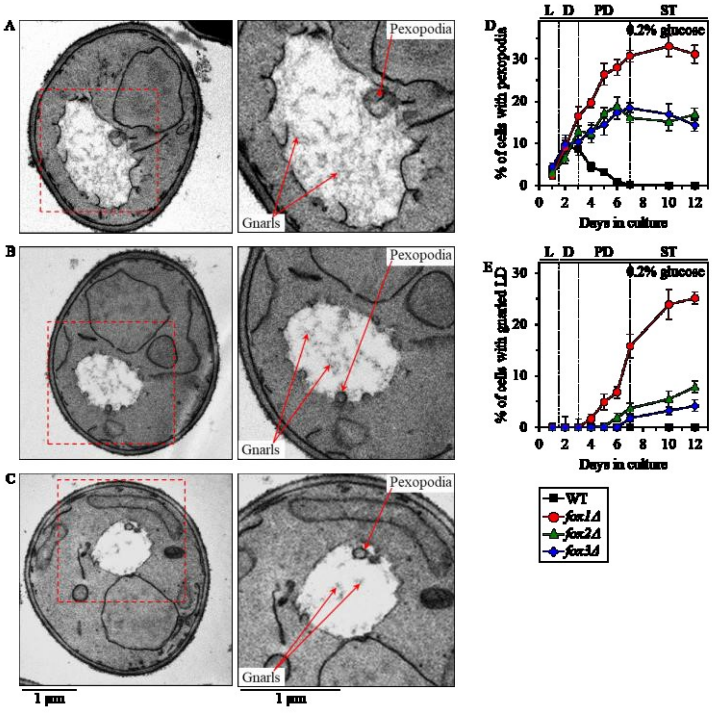

Figure 2.7. Effects of the *fox1Δ*, *fox2Δ* and *fox3Δ* mutations on age-related changes in the abundance of pexopodia and LD-confined gnarls in yeast cultured under CR conditions. WT, *fox1Δ*, *fox2Δ* and *fox3Δ* cells were cultured in the nutrient-rich YP medium under CR conditions on 0.2% glucose. **A-C**. Transmission electron micrographs of chronologically aging *fox1Δ* (**A**), *fox2Δ* (**B**) and *fox3Δ* (**C**) cells recovered on day 7. Each of the two panels for *fox1Δ*, *fox2Δ* and *fox3Δ* cells shows a different magnification of the same electron micrograph. The percentage of WT, *fox1Δ*, *fox2Δ* and *fox3Δ* cells with pexopodia (**D**) and LD-confined gnarls (**E**) in yeast recovered on different days of culturing are presented. Images like the representative images shown in **A**, **B** and **C** were quantified as described in Materials and Methods. Data are presented as means ± SEM (n = 3). Abbreviations: L, D, PD and ST, logarithmic, diauxic, post-diauxic and stationary growth phases (respectively).

During the subsequent ST phase, the abundance of pexopodia in *fox1Δ*, *fox2Δ* and *fox3Δ* mutant cells remained unchanged (Figure 2.7D), whereas the abundance of gnarls within LD of these cells significantly increased (Figure 2.7E). Such deposition of gnarls within LD of *fox1Δ*, *fox2Δ* and *fox3Δ* mutant cells during ST phase coincided with 1) a rise of FFA and DAG in whole mutant cells (Figures 2.6F and 2.6G) and LD of mutants (Figure 2.6H); 2) an increase of ERG in LD of mutants (Figure 2.6H); 3) an absence of FFA in the ER of mutants (Figure 2.6H); 4) a slight increase in DAG concentrations in the ER of mutants (Figure 2.6H); and 5) a lack of significant changes in TAG and EE concentrations in whole mutant cells (Figures 2.6D and 2.6E), the ER of mutants (Figure 2.6H) and LD of mutants (Figure 2.6H).

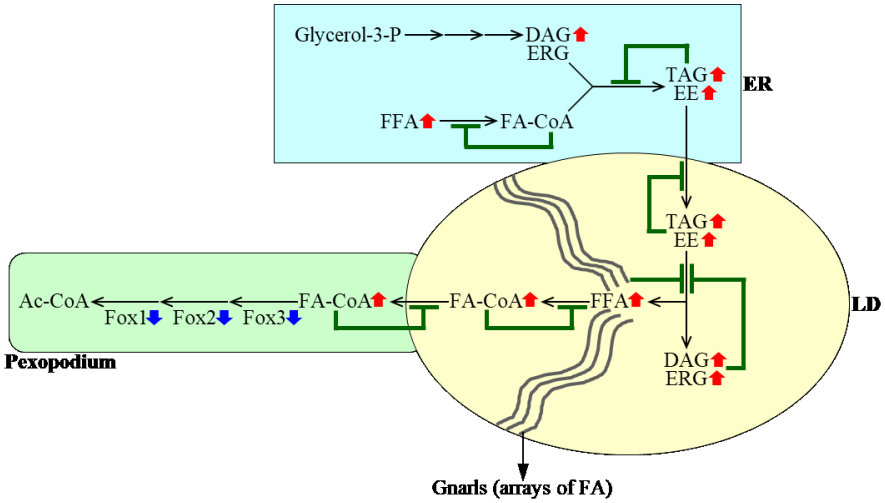

Figure 2.8. A mechanism through which a decline in the peroxisomal β-oxidation of FFA elicits negative feedback loops that regulate the metabolism and transport of several lipid classes in the ER and LD. A weakening of the peroxisomal β-oxidation of FFA causes an accumulation of FA-CoA in pexopodia, which represent intrusions of peroxisomes into the neutral lipid core of LD. This creates several negative feedback loops whose action ultimately causes an age-related build-up of FFA and DAG in the ER and LD. Blue arrows next to the names of Fox1, Fox2 and Fox3 indicate that a decline in the peroxisomal β-oxidation of FFA is due to a decrease in the concentrations of the core enzymes of such oxidation. Red arrows next to the names of lipid classes denote those of them whose concentrations are increased. Inhibition bars displayed in green color signify negative feedback loops. See text for more details. Abbreviations: Ac-CoA, acetyl-CoA; DAG, diacylglycerols; EE, ergosteryl esters; ERG, ergosterol; ER, endoplasmic reticulum; FA-CoA, acyl-CoA esters; FFA, free fatty acids; LD, lipid droplets; LD, lipid droplet; TAG, triacylglycerols.

In sum, these findings suggest that a decline in the peroxisomal β-oxidation of FFA causes a build-up of fatty acyl-CoA esters (FA-CoA) in pexopodia, which represent intrusions of peroxisomes into the neutral lipid core of LD. This creates a negative feedback loop which mitigates the transport of FA-CoA to pexopodia from associated LD, where these FA-CoA are formed from FFA derived from neutral lipids (Figure 2.8). This, in turn, elicits an accumulation of gnarls (the electron-dense arrays of FFA [184]) in LD, thereby instigating a series of negative feedback loops. These feedback loops attenuate the lipolysis of neutral lipids in LD, transport of neutral lipids from the ER to LD, and synthesis of neutral lipids synthesis from FFA, DAG and

ERG in the ER (Figure 2.8). Due to the action of such negative feedback mechanism regulating lipid metabolism and transport in several organelles, a decline in peroxisomal fatty acid β-oxidation in chronologically aging yeast causes an age-related build-up of FFA and DAG in the ER and LD (Figure 2.8).

2.3.7 Three possible mechanisms through which peroxisomal fatty acid β-oxidation may define yeast CLS

As we have found, the β-oxidation of FFA in peroxisomes is a longevity assurance process in chronologically aging yeast cultured under CR-conditions (Figures 2.6A and 2.6B). It is conceivable that there may be at least three different mechanisms by which peroxisomal fatty acid β-oxidation defines longevity of chronologically aging yeast. These possible mechanisms are outlined below.

First mechanism: the final product of peroxisomal fatty acid β-oxidation is acetyl-CoA, which is transported to mitochondria after being formed in peroxisomes (Figure 2.9). Mitochondrial oxidation of the peroxisomally generated pool of acetyl-CoA through the TCA cycle provides reducing equivalents for the synthesis of ATP via oxidative phosphorylation [23, 149, 172, 176]. Acetyl-CoA that is used for the synthesis of ATP in mitochondria is also made within these organelles as the product of oxaloacetate and acetate oxidation (Figure 2.9) [23, 149, 172, 176]. It is feasible that an ample amount of ATP is generated in mitochondria of CR yeast because of the oxidation of acetyl-CoA made in peroxisomes, not due to the oxidation of acetyl-CoA produced in mitochondria. Thus, peroxisomal fatty acid β-oxidation may regulate longevity-defining processes inside and outside of mitochondria and influence yeast CLS under CR conditions because such oxidation may be responsible for the synthesis of the bulk of cellular ATP (Figure 2.9).

Second mechanism: mitochondrial oxidation of the peroxisomally produced pool of acetyl-CoA may also be essential for the demonstrated ability of yeast mitochondria to maintain the shape of a tubular network under CR conditions [23]; in chronologically aging non-CR yeast, this network is fragmented into individual mitochondria [23]. Because mitochondrial morphology depends on a balance between the processes of mitochondrial fission and fusion [185, 186], it is conceivable that mitochondrial oxidation of peroxisomally produced acetyl-CoA in CR yeast may allow to shift this balance toward fusion (Figure 2.9). Moreover, a shift of this balance toward the

opposing process of mitochondrial fission elicits mitochondrial fragmentation and promotes a mitochondria-controlled apoptotic mode of age-related RCD (Figure 2.9) [187-196]. Thus, it is also plausible that mitochondrial oxidation of peroxisomally produced acetyl-CoA may be essential for the demonstrated ability of CR [23, 150] to delay the onset of the apoptotic mode of age-related RCD.

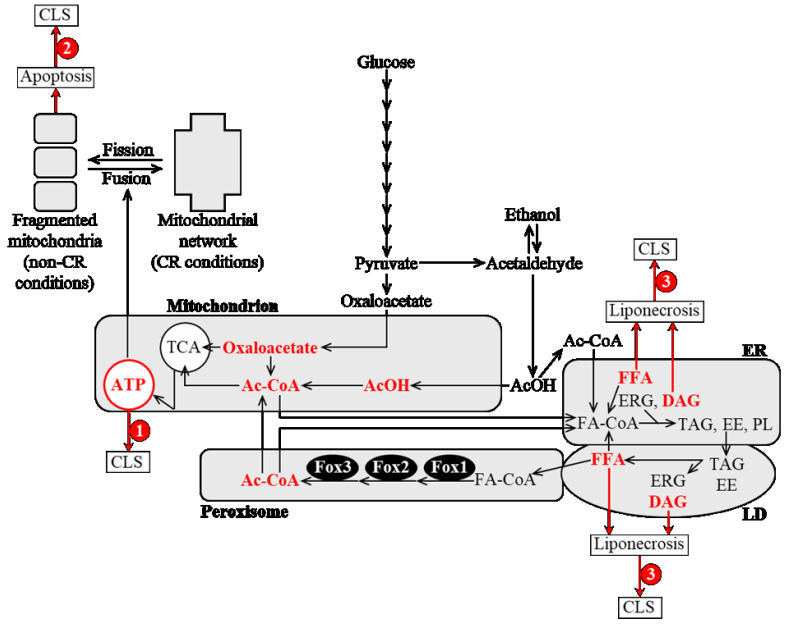

Figure 2.9. Possible mechanisms through which the β-oxidation of FFA in peroxisomes may define longevity of chronologically aging yeast. The names of metabolites whose concentrations depend on the extent of peroxisomal fatty acid β-oxidation are displayed in red color. There may be at least three different mechanisms through which the concentrations of these metabolites may define yeast chronological lifespan (CLS). These mechanisms are numbered. See text for more details. Abbreviations: Ac-CoA, acetyl-CoA; AcOH, acetic acid; CR, caloric restriction; DAG, diacylglycerols; EE, ergosteryl esters; ER, endoplasmic reticulum; ERG, ergosterol; FFA, free fatty acids; FA-CoA, fatty acyl-CoA esters; LD, lipid droplets; TAG, triacylglycerols.

Third mechanism: we have revealed that 1) a decline in peroxisomal fatty acid β-oxidation in chronologically aging yeast causes an age-related build-up of FFA and DAG in the ER and LD (Figure 2.8); and 2) CR stimulates peroxisomal fatty acid β-oxidation and decreases the concentrations of FFA and DAG in chronologically aging yeast [14, 23]. An exposure of yeast cells to exogenous FFA and DAG is known to elicit a ″liponecrotic″ mode of age-related RCD [14, 103, 197, 198]. Therefore, it is possible that the abilities of CR to stimulate peroxisomal fatty acid β-oxidation and to decrease the concentrations of FFA and DAG may delay the age-related onset of the liponecrotic mode of RCD (Figure 2.9).

In a series of experiments outlined below, we assessed how each of the three mechanisms contributes to the extension of yeast CLS by CR.

2.3.8 The β-oxidation of FFA in peroxisomes defines the CLS of CR yeast in part because it is essential for mitochondrial functionality and ATP synthesis in mitochondria

To assess the first proposed mechanism (Figure 2.9), we tested if the *fox1Δ*, *fox2Δ* and *fox3Δ* mutations can alter mitochondrial functionality and decrease the concentration of cellular ATP, which in CR yeast is produced mainly in mitochondria [174, 199]. The *fox1Δ*, *fox2Δ* and *fox3Δ* mutations deplete the peroxisomally generated pool of acetyl-CoA by impairing peroxisomal fatty acid β-oxidation (Figure 2.9) [174, 199]. As we demonstrated, each of these mutations significantly shortens the CLS of yeast cultured under CR on 0.2% glucose (Figures 2.6A and 2.6B).

We assessed how the *fox1Δ*, *fox2Δ* and *fox3Δ* mutations influence age-related changes in the following vital traits of mitochondrial functionality: 1) oxygen consumption by cells, which in yeast cultured in media with low (0.2%) glucose concentration is mainly due to mitochondrial respiration [172, 200]; 2) the electrochemical potential (ΔΨ) across the inner mitochondrial membrane; and 3) cellular concentration of ATP, which in yeast cultured in media with low glucose concentration is generated mainly in mitochondria [172, 200]. We found that in CR yeast cultured on 0.2% glucose, the *fox1Δ*, *fox2Δ* and *fox3Δ* mutations 1) markedly amplify mitochondrial respiration (Figure 2.10A) and ΔΨ (Figure 2.10B) during L and D phases; 2) elicit an abrupt decline in mitochondrial respiration (Figure 2.10A) and ΔΨ (Figure 2.10B) during PD phase. Although neither of these mutations altered the concentration of mitochondrially synthesized ATP during L phase and in the beginning of D phase, all three mutations decreased ATP production in mitochondria by the end of D phase and caused a rapid decline in mitochondrial ATP synthesis during PD and ST phases (Figure 2.10C).

The *fox1Δ*, *fox2Δ* and *fox3Δ* mutations cause a sharp increase of mitochondrially produced ROS during L and D phases in yeast cultured under CR conditions on 0.2% glucose (Figure 2.10D). In agreement with an essential role that excessive concentrations of mitochondrial ROS play in oxidative damage to mitochondrial proteins [200, 201], the sharp increase of mitochondrial ROS seen in *fox1Δ*, *fox2Δ* and *fox3Δ* cells during L and D phases coincided with a rapid inactivation of several enzymes involved in the electron transport chain (ETC) and/or TCA cycle in mitochondria; such inactivation of mitochondrial ETC and TCA enzymes in *fox1Δ*, *fox2Δ* and *fox3Δ* cells continued during the subsequent PD phase (Figures 2.10E-2.10G). The protein components of mitochondrial ETC and TCA undergoing such rapid inactivation in *fox1Δ*, *fox2Δ*

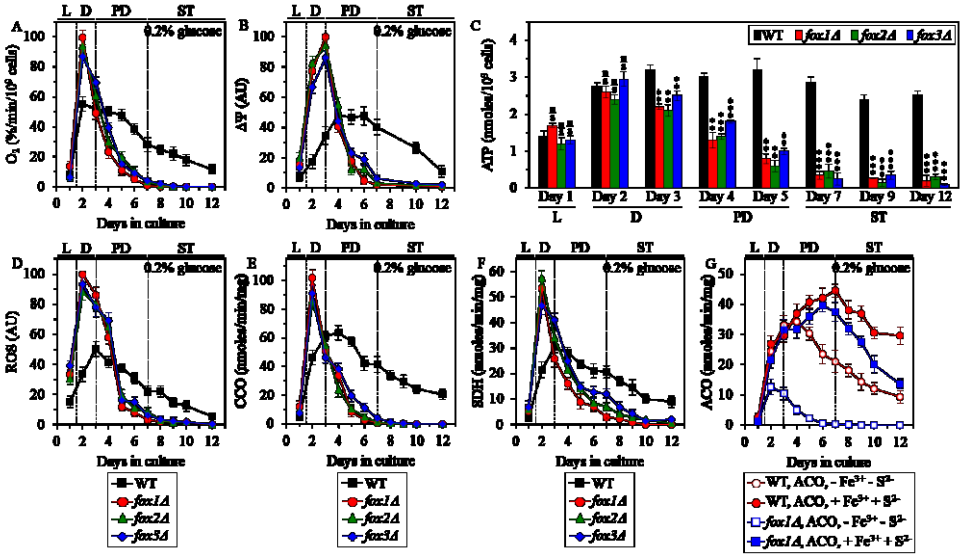

Figure 2.10. Effects of the *fox1Δ*, *fox2Δ* and *fox3Δ* mutations on vital traits of mitochondrial functionality, including ATP synthesis, in yeast cultured under CR conditions. WT, *fox1Δ*, *fox2Δ* and *fox3Δ* cells were cultured in the nutrient-rich YP medium under CR conditions on 0.2% glucose. The rate of oxygen consumption by cells (**A**), electrochemical potential (ΔΨ) across the IMM (**B**), cellular ATP concentration (**C**), cellular ROS concentration (**D**), enzymatic activity of cytochrome c oxidase (CCO) in purified mitochondria (**E**), enzymatic activity of succinate dehydrogenase in purified mitochondria (SDH) (**F**), and enzymatic activity of aconitase (ACO) in total cell lysates (**G**) were measured as described in Materials and Methods. The ACO activity was measured with or without the reactivation agents Fe^{3+} and Na_2S. Data are presented as means ± SEM (n = 5 for **A**; n = 3 for **B-G**; ns, not significant; ** < 0.01; *** < 0.001). Abbreviations: L, D, PD and ST, logarithmic, diauxic, post-diauxic and stationary growth phases (respectively); IMM, inner mitochondrial membrane; ROS, reactive oxygen species. These experiments were performed by Michelle Burstein, Adam Beach, Pavlo Kyryakov, Alejandra Gomez-Perez and Rachel Feldman.

and *fox3Δ* cells included cytochrome *c* oxidase (CCO) (Figure 2.10E), succinate dehydrogenase (SDH) (Figure 2.10F) and aconitase (ACO) (Figure 2.10G), all of which are known to be highly susceptible to ROS-inflicted oxidative damage [23, 200-203]. We found that the enzymatic activity of ACO, which in *fox1Δ*, *fox2Δ* and *fox3Δ* cells is rapidly decreased *in vivo* during D and PD phases, can be markedly increased *in vitro* by incubating lysates of these cells with Fe^{3+} and S^{2-} (Figure 2.10G); such incubation *in vitro* is known to restore the oxidative damage-dependent loss of one iron from the [4Fe-4S] cluster of ACO [204]. This observation confirms our assumption that the rapid inactivation of mitochondrial ACO seen in *fox1Δ*, *fox2Δ* and *fox3Δ* cells is due to ROS-inflicted oxidative damage to mitochondrial proteins in these cells.

Altogether, these findings support the notion that mitochondrial oxidation of acetyl-CoA pool generated in peroxisomal fatty acid β-oxidation is 1) essential for maintaining mitochondrial functionality; and 2) responsible for the synthesis of the bulk of cellular ATP fueled by the TCA cycle, ETC and oxidative phosphorylation in mitochondria.

2.3.9 Peroxisomal fatty acid β-oxidation contributes to yeast CLS extension under CR conditions by weakening the fragmentation of a mitochondrial network and postponing the onset of age-related apoptotic RCD

To assess the second proposed mechanism (Figure 2.9), we initially tested if the *fox1Δ*, *fox2Δ* and *fox3Δ* mutations influence the demonstrated ability [23] of yeast mitochondria to maintain the shape of a continuous tubular network under CR conditions. We found that in CR yeast cultured on 0.2% glucose 1) none of these mutations alters the concentration of porin (an abundant mitochondrial protein) and, thus, none of them influences the abundance of mitochondria (Figure 2.11A); and 2) each of these mutations elicits the fragmentation of the mitochondrial network into individual mitochondria during PD phase (Figures 2.11B and 2.11C), concurrently with an abrupt decline in mitochondrial functionality and ATP synthesis (Figure 2.10).

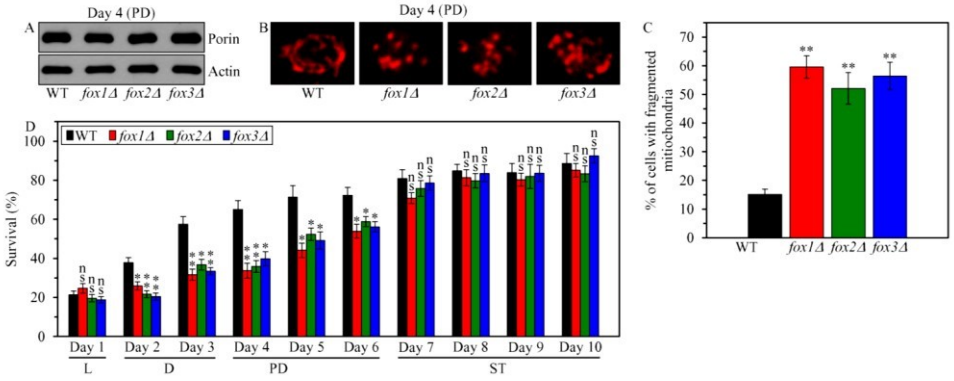

Figure 2.11. Effects of the *fox1Δ*, *fox2Δ* and *fox3Δ* mutations on mitochondrial abundance and morphology, and on cell susceptibility to mitochondria-controlled apoptotic RCD in yeast cultured under CR conditions. WT, *fox1Δ*, *fox2Δ* and *fox3Δ* cells were cultured in the nutrient-rich YP medium under CR conditions on 0.2% glucose. **A**. The concentrations of porin and actin in total cell lysates were assessed by immunoblotting, as described in Materials and Methods. **B**. Mitochondrial morphology was visualized with the help of indirect immunofluorescence microscopy using primary antibodies against porin, as described in Materials and Methods. **C**. The percentage of cells exhibiting fragmented mitochondria was calculated. At least 500 cells of each strain were used for quantitation. Data are presented as means ± SEM (n = 3; ** < 0.01). **D**. An assay for measuring clonogenic survival of cells treated for 2 h with 2.5 mM hydrogen peroxide was performed as described in Materials and Methods. Data are presented as means ± SEM (n = 3; ns, not significant; * < 0.05; ** < 0.01). Abbreviations: L, D, PD and ST, logarithmic, diauxic, post-diauxic and stationary growth phases (respectively). Experiments in **B** were performed by Adam Beach, Pavlo Kyryakov and Alejandra Gomez-Perez.

We then tested how the *fox1Δ*, *fox2Δ* and *fox3Δ* mutations influence the susceptibility of CR yeast to mitochondria-controlled apoptotic RCD induced by a short-term exposure of cells to exogenous hydrogen peroxide; this mode of age-related RCD has been linked to mitochondrial network fragmentation, mitochondrial outer membrane permeabilization and the efflux of several pro-apoptotic proteins from the intermembrane space of fragmented mitochondria [23, 187-196, 205]. We found that in CR yeast cultured on 0.2% glucose, each of these mutations 1) significantly

decreases clonogenic survival of cells briefly (for 2 h) treated with hydrogen peroxide if these cells were recovered during D or PD phase of culturing (Figure 2.11D); and 2) does not alter clonogenic survival of cells subjected to such treatment if these cells were recovered during L or ST phase of culturing (Figure 2.11D).

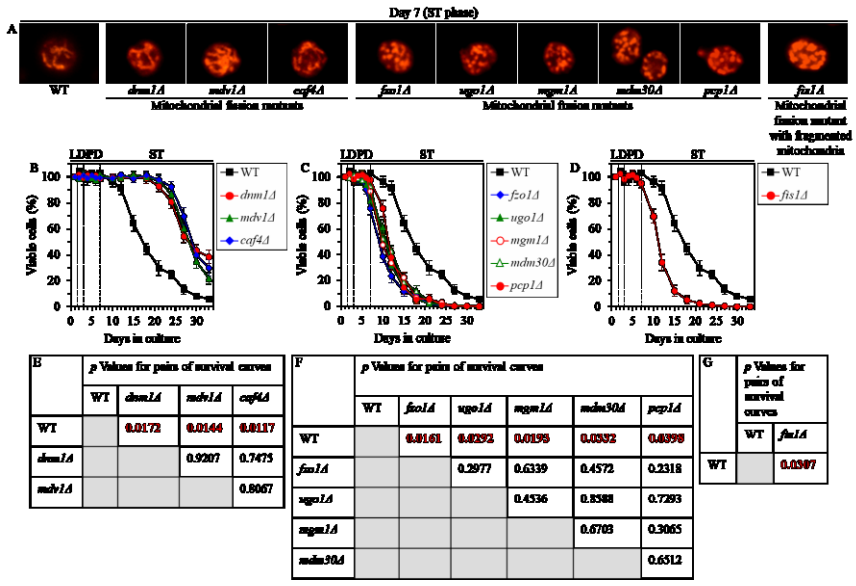

E — *p* Values for pairs of survival curves

	WT	*dnm1Δ*	*mdv1Δ*	*caf4Δ*
WT		0.0172	0.0144	0.0117
dnm1Δ			0.9207	0.7475
mdv1Δ				0.8067

F — *p* Values for pairs of survival curves

	WT	*fzo1Δ*	*ugo1Δ*	*mgm1Δ*	*mdm30Δ*	*pcp1Δ*
WT		0.0161	0.0252	0.0195	0.0332	0.0398
fzo1Δ			0.2977	0.6339	0.4572	0.2318
ugo1Δ				0.4536	0.8588	0.7293
mgm1Δ					0.6703	0.3065
mdm30Δ						0.6512

G — *p* Values for pairs of survival curves

	WT	*fis1Δ*
WT		0.0307

Figure 2.12. Effects of the single-gene-deletion mutations eliminating different protein components of the mitochondrial fission or fusion machine on mitochondrial morphology and CLS in yeast cultured under CR conditions. WT, *dnm1Δ*, *mdv1Δ*, *caf4Δ*, *fzo1Δ*, *ugo1Δ*, *mgm1Δ*, *mdm30Δ*, *pcp1Δ* and *fis1Δ* cells were cultured in the nutrient-rich YP medium under CR conditions on 0.2% glucose. **A.** Mitochondrial morphology was visualized with the help of indirect immunofluorescence microscopy using primary antibodies against porin, as described in Materials and Methods. **B-D.** Survival curves of chronologically aging WT and mutant cells. Data are presented as means ± SEM (n = 3). **E-G.** *p* Values for different pairs of survival curves of WT and mutant strains. Survival curves shown in **B-D** were compared. Two survival curves were considered statistically different if the *p* value was less than 0.05. The *p* values for comparing pairs of survival curves were calculated as described in Materials and Methods. Abbreviations: L, D, PD and ST, logarithmic, diauxic, post-diauxic and stationary growth phases (respectively). These experiments were performed by Michelle Burstein, Pavlo Kyryakov and Alejandra Gomez-Perez.

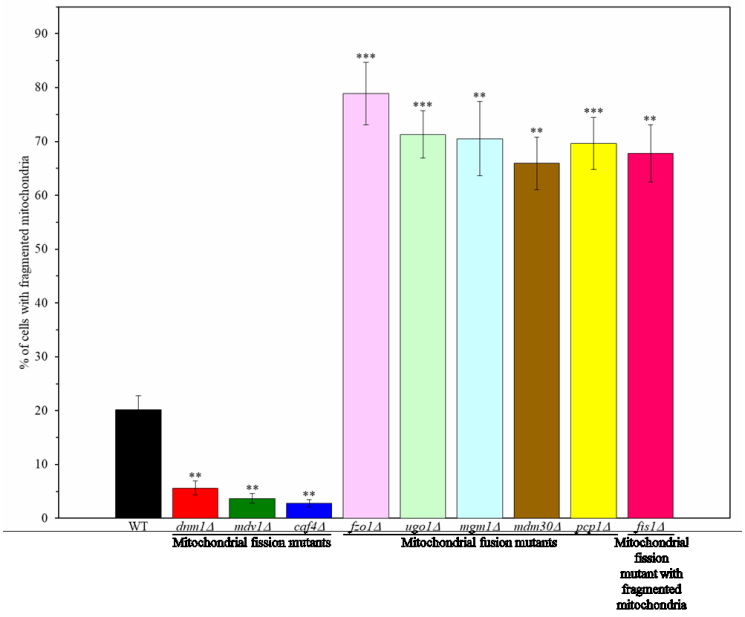

Figure 2.13. Effects of the single-gene-deletion mutations eliminating different protein components of the mitochondrial fission or fusion machine on mitochondrial morphology in yeast cultured under CR conditions. WT, *dnm1Δ*, *mdv1Δ*, *caf4Δ*, *fzo1Δ*, *ugo1Δ*, *mgm1Δ*, *mdm30Δ*, *pcp1Δ* and *fis1Δ* cells were cultured in the nutrient-rich YP medium under CR conditions on 0.2% glucose. Mitochondrial morphology was visualized with the help of indirect immunofluorescence microscopy using primary antibodies against porin, as described in Materials and Methods and shown in Figure 2.12A. The percentage of cells exhibiting fragmented mitochondria was calculated. At least 500 cells of each strain were used for quantitation. Data are presented as means ± SEM (n = 3; ** < 0.01; *** < 0.001). These experiments were performed by Michelle Burstein, Pavlo Kyryakov and Alejandra Gomez-Perez.

These findings suggest that in CR yeast mitochondrial oxidation of acetyl-CoA that is generated in peroxisomal fatty acid β-oxidation 1) is essential for preventing mitochondrial network fragmentation during D and PD phases; and 2) is indispensable for the CR-dependent delay of the onset of age-related apoptotic RCD during these phases of culturing.

We have previously hypothesized that the abilities of CR to attenuate mitochondrial network fragmentation and to delay the onset of a mitochondria-controlled mode of the age-related apoptotic RCD may be required for the ability of this low-calorie diet to extend yeast CLS [23, 205]. To test this hypothesis, we examined how the single-gene-deletion mutations eliminating protein components of the mitochondrial fission or fusion machine influence the extent of yeast CLS extension by CR; a balance between the processes of mitochondrial fission and fusion is known to define mitochondrial morphology [185, 186]. We found that in CR yeast cultured on 0.2% glucose 1) the *dnm1Δ*, *mdv1Δ* and *caf4Δ* mutations, which eliminate different components of the mitochondrial fission machine [191], stimulate the formation of net-like mitochondria (Figure 2.12A; Figure 2.13) and increase the efficiency with which CR extends yeast CLS (Figures 2.12B and 2.12E); 2) the *fzo1Δ*, *ugo1Δ*, *mgm1Δ*, *mdm30Δ* and *pcp1Δ* mutations, which eliminate different components of the mitochondrial fusion machine [191], elicit mitochondrial network fragmentation (Figure 2.12A; Figure 2.13) and decrease the efficiency of yeast CLS extension by CR (Figures 2.12C and 2.12F); and 3) the *fis1Δ* mutation, which eliminates a component of the mitochondrial fission machine (however, impairs mitochondrial fission only in exponentially growing yeast but not in yeast committed to apoptotic RCD) [191], causes mitochondrial network fragmentation (Figure 2.12A; Figure 2.13) and lowers the efficiency with which CR extends yeast CLS (Figures 2.12D and 2.12G).

In sum, these findings support the view that mitochondrial oxidation of acetyl-CoA that is produced during peroxisomal fatty acid β-oxidation makes an essential contribution to the CR-dependent extension of yeast CLS because it averts mitochondrial network fragmentation during D and PD phases, thereby delaying the onset of an age-related mode of apoptotic RCD during these phases of culturing.

2.3.10 Peroxisomal fatty acid β-oxidation contributes to the CR-dependent extension of yeast CLS in part because it slows down the onset of age-related liponecrotic RCD

To assess the third proposed mechanism (Figure 2.9), we initially examined if the *fox1Δ*, *fox2Δ* and *fox3Δ* mutations affect the susceptibility of CR yeast to liponecrotic RCD; this mode of age-related RCD can be elicited by a short-term exposure of yeast cells to exogenous FFA and DAG [14, 103, 197, 198]. We found that in CR yeast cultured on 0.2% glucose, each of these mutations 1) substantially reduces clonogenic survival of cells briefly (for 2 h) treated with palmitoleic acid (POA; a monounsaturated FFA) if these cells were recovered during late PD phase (on day 6 of culturing) or during ST phase (on days 7 to 10 of culturing) (Figure 2.14); and 2) has no effect on clonogenic survival of cells subjected to treatment with POA if these cells were collected during L, D or early PD phase of culturing (Figure 2.14). As we demonstrated, the *fox1Δ*, *fox2Δ* and *fox3Δ* mutations 2) significantly shorten the CLS of CR yeast (Figures 2.6A and 2.6B); and 2) increase the cellular concentrations of FFA and DAG during PD and ST phases (Figures 2.6F and 2.6G).

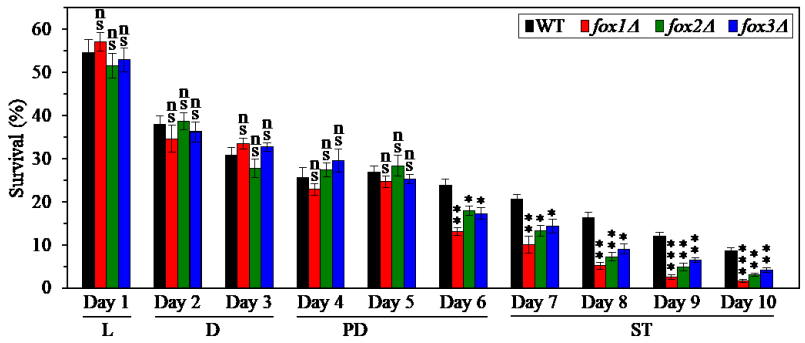

Figure 2.14. Effects of the *fox1Δ*, *fox2Δ* and *fox3Δ* mutations on cell susceptibility to liponecrotic RCD in yeast cultured under CR conditions. WT, *fox1Δ, fox2Δ and fox3Δ* cells were cultured in the nutrient-rich YP medium under CR conditions on 0.2% glucose. An assay for measuring clonogenic survival of cells treated for 2 h with 0.15 mM palmitoleic acid, a monounsaturated FFA, was performed as described in Materials and Methods. Data are presented as means ± SEM (n = 3; ns, not significant; * < 0.05; ** < 0.01; *** < 0.001). Abbreviations: L, D, PD and ST, logarithmic, diauxic, post-diauxic and stationary growth phases (respectively).

Taken together, these findings support the view that the β-oxidation of FFA in peroxisomes is necessary for the CR-dependent extension of yeast CLS in part because it allows to maintain low concentrations of FFA and DAG during PD and ST phases, thereby postponing the onset of an age-related mode of liponecrotic RCD.

We have previously hypothesized that the ability of CR to decrease the cellular concentrations of FFA and DAG during PD and ST phases may be essential for the CR-dependent extension of yeast CLS because it lowers the susceptibility of CR yeast to age-related liponecrotic RCD during these phases of culturing [23, 14, 103, 197, 198, 205]. To test this hypothesis, we examined how the single-gene-deletion mutations eliminating redundant enzymes involved in TAG synthesis or degradation influence age-related changes in the following: 1) the concentrations

of FFA, DAG and TAG in CR yeast; 2) the susceptibility of CR yeast to liponecrotic RCD elicited by a short-term treatment of cells with POA, a monounsaturated FFA; and 3) the extent of yeast CLS extension by CR. The synthesis of TAG from FFA and DAG in the ER is catalyzed by Dga1, Are1 and Are2 (Figure 2.15) [173-175, 206, 207]. The lipolytic degradation of TAG into FFA and DAG in LD is catalyzed by the TAG lipases Tgl1, Tgl3, Tgl4 and Tgl5 (Figure 2.15) [173-175, 206-210].

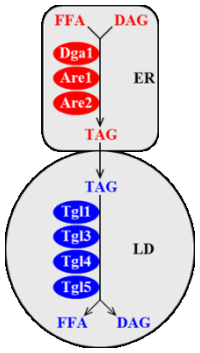

Figure 2.15. TAG synthesis from FFA and DAG in the ER and TAG lipolysis into FFA and DAG in LD are catalyzed by redundant enzymes. See text for more details. Abbreviations: DAG, diacylglycerols; ER, endoplasmic reticulum; FFA, free fatty acids; LD, lipid droplets; TAG, triacylglycerols.

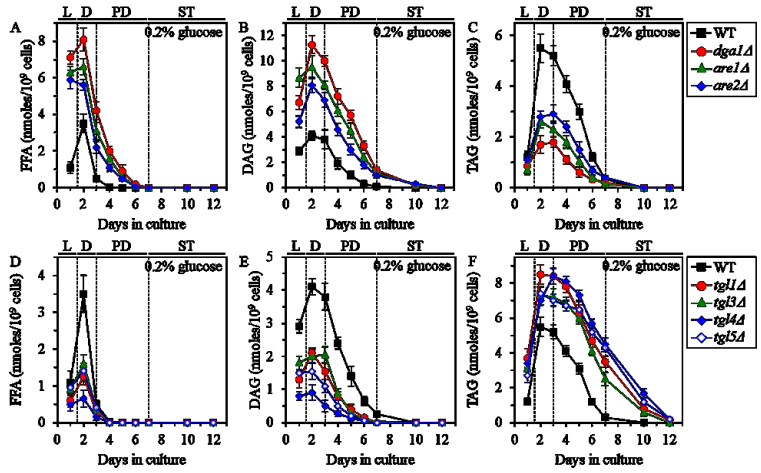

Figure 2.16. Effects of the *dga1Δ*, *are1Δ*, *are2Δ*, *tgl1Δ*, *tgl3Δ*, *tgl4Δ* and *tgl5Δ* mutations on FFA, DAG and TAG concentrations in yeast cultured under CR conditions. WT, *dga1Δ*, *are1Δ*, *are2Δ*, *tgl1Δ*, *tgl3Δ*, *tgl4Δ* and *tgl5Δ* cells were cultured in the nutrient-rich YP medium under CR conditions on 0.2% glucose. FFA (**A** and **D**), DAG (**B** and **E**) and TAG (**C** and **F**) concentrations in whole cells recovered on different days of culturing are shown. Data are presented as means ± SEM (n = 3). The concentrations of FFA, DAG and TAG in whole cells were measured as described in Materials and Methods. Abbreviations: DAG, diacylglycerols; FFA, free fatty acids; L, D, PD and ST, logarithmic, diauxic, post-diauxic and stationary growth phases (respectively); TAG, triacylglycerols. These experiments were performed by Simon Bourque, Adam Beach and Pavlo Kyryakov.

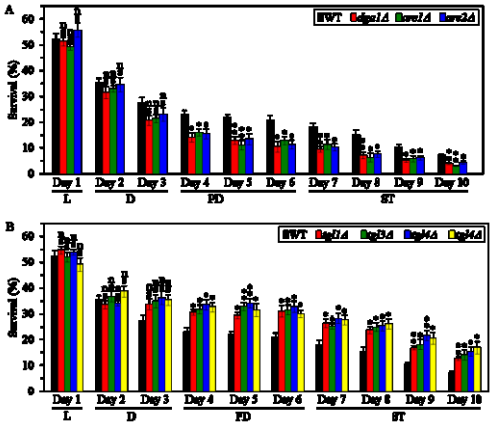

Figure 2.17. Effects of the *dga1Δ*, *are1Δ*, *are2Δ*, *tgl1Δ*, *tgl3Δ*, *tgl4Δ* and *tgl5Δ* mutations on cell susceptibility to liponecrotic RCD in yeast cultured under CR conditions. WT, *dga1Δ*, *are1Δ*, *are2Δ*, *tgl1Δ*, *tgl3Δ*, *tgl4Δ* and *tgl5Δ* cells were cultured in the nutrient-rich YP medium under CR conditions on 0.2% glucose. An assay for measuring clonogenic survival of cells treated for 2 h with 0.15 mM palmitoleic acid, a monounsaturated FFA, was performed as described in Materials and Methods. Data are presented as means ± SEM (n = 3; ns, not significant; * < 0.05; ** < 0.01). Abbreviations: L, D, PD and ST, logarithmic, diauxic, post-diauxic and stationary growth phases (respectively).

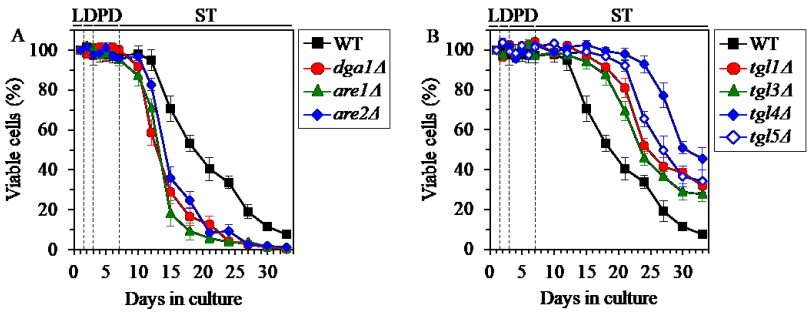

C

	p Values for pairs of survival curves			
	WT	*dga1Δ*	*are1Δ*	*are2Δ*
WT		0.0254	0.0378	0.0417
dga1Δ			0.6822	0.4383
are1Δ				0.5886

D

	p Values for pairs of survival curves				
	WT	*tgl1Δ*	*tgl3Δ*	*tgl4Δ*	*tgl5Δ*
WT		0.0161	0.0234	0.0025	0.0062
tgl1Δ			0.3381	0.0301	0.2904
tgl3Δ				0.0238	0.0626
tgl4Δ					0.1425

Figure 2.18. Effects of the *dga1Δ*, *are1Δ*, *are2Δ*, *tgl1Δ*, *tgl3Δ*, *tgl4Δ* and *tgl5Δ* mutations on CLS in yeast cultured under CR conditions. WT, *dga1Δ*, *are1Δ*, *are2Δ*, *tgl1Δ*, *tgl3Δ*, *tgl4Δ* and *tgl5Δ* cells were cultured in the nutrient-rich YP medium under CR conditions on 0.2% glucose. **A, B.** Survival curves of chronologically aging WT and mutant cells. Data are presented as means ± SEM (n = 3). **C, D.** *p* Values for different pairs of survival curves of WT and mutant strains. Survival curves shown in **A, B** were compared. Two survival curves were considered statistically different if the *p* value was less than 0.05. The *p* values for comparing pairs of survival curves using the logrank test were calculated as described in Materials and Methods. Abbreviations: L, D, PD and ST, logarithmic, diauxic, post-diauxic and stationary growth phases (respectively). These experiments were performed by Pavlo Kyryakov and Alejandra Gomez-Perez.

We found that in CR yeast cultured on 0.2% glucose, the *dga1Δ*, *are1Δ* and *are2Δ* mutations (which eliminate redundant ER enzymes involved in TAG synthesis from FFA and DAG) exhibit the following effects: 1) they increase the concentrations of FFA (Figure 2.16A) and DAG (Figure 2.16B) during L, D and PD phases; 2) they decrease TAG concentration during D and PD phases (Figure 2.16C); 3) they make cells progressing through PD and ST phases more sensitive to liponecrotic RCD (Figure 2.17A); and 4) they significantly shorten yeast CLS (Figures 2.18A and 2.18C). We also found that in CR yeast cultured on 0.2% glucose, the *tgl1Δ*, *tgl3Δ*, *tgl4Δ* and *tgl5Δ* mutations (which eliminate redundant LD lipases catalyzing the degradation of TAG into FFA and DAG) display the following effects: 1) they decrease the concentrations of FFA (Figure 2.16D) and DAG (Figure 2.16E) during L, D and PD phases; 2) they increase TAG concentration during L, D, PD and ST phases (Figure 2.16F); 3) they make cells advancing through PD and ST phases more resistant to liponecrotic RCD (Figure 2.17B); and 4) they significantly extend yeast CLS (Figures 2.18B and 2.18D).

In sum, these findings imply that peroxisomal fatty acid β-oxidation makes an essential contribution to yeast CLS extension by CR in part because it decreases the cellular concentrations of FFA and DAG during PD and ST phases [172, 177], thus slowing down the onset of an age-related mode of liponecrotic RCD during these phases of culturing.

2.4 Discussion

This study revealed that CR delays yeast chronological aging via mechanisms that coordinate the spatiotemporal dynamics of various cellular processes. Our comparative analyzes of morphological, biochemical and cell biological properties of CR and non-CR yeast advancing through different stages of the aging process suggest a hypothetical model for such mechanisms. This model is depicted schematically in Figure 2.19.

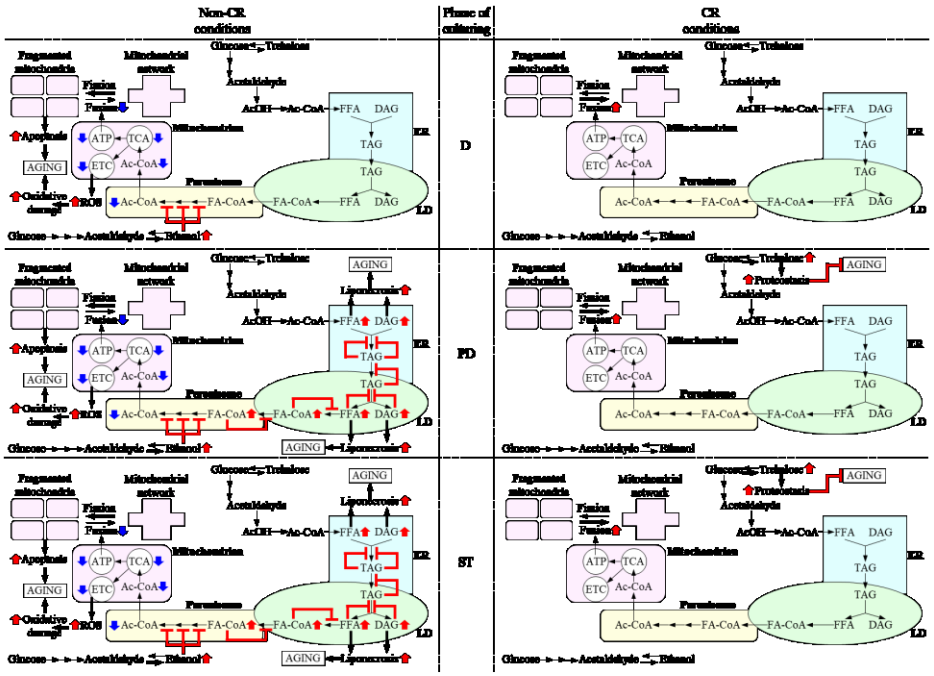

Figure 2.19. Mechanisms through which CR delays yeast chronological aging by coordinating the spatiotemporal dynamics of various cellular processes. CR orchestrates the development and maintenance of distinct patterns of metabolism, interorganellar communications and mitochondrial morphology in yeast cells advancing through D, PD and ST phases of culturing. Throughout different stages of chronological aging, these CR-driven patterns 1) delay the age-related onsets of apoptotic and liponecrotic modes of regulated cell death, thereby decreases the risk of cell death; and 2) preserve cellular proteostasis, thus actively increasing the chance of survival. Because CR decreases the risk of death and actively increases the chance of survival throughout chronological lifespan, this low-calorie diet extends longevity of chronologically aging yeast. The thickness of black arrows is proportional to the rates of processes. Arrows next to the names of affected processes denote those of them that are intensified (red arrows) or weakened (blue arrows). Arrows next to the names of affected metabolites signify those of them whose concentrations are increased (red arrows) or decreased (blue arrows). Inhibition bars are displayed in red color. Please see text for additional details. Abbreviations: Ac-CoA, acetyl-CoA; AcOH, acetic acid; DAG, diacylglycerols; D, PD and ST, diauxic, post-diauxic and stationary growth phases (respectively); ER, endoplasmic reticulum; FA-CoA, acyl-CoA esters; FFA, free fatty acids; LD, lipid droplets; TAG, triacylglycerols; TCA, tricarboxylic cycle.

The model posits that CR orchestrates the development and maintenance of an aging-delaying cellular pattern throughout yeast chronological lifespan before an arrest of cell growth and division (i.e. during D and PD phases of culturing) and after such arrest (i.e. during ST phase of culturing) (Figure 2.19). CR elicits the stepwise development and maintenance of this cellular pattern by modulating a network that integrates the following: 1) pathways of ethanol, trehalose

and lipid metabolism; 2) interorganellar communications involving unidirectional and bidirectional movements of certain metabolites between the ER and the cytosol, the ER and LD, LD and peroxisomes, and peroxisomes and mitochondria; and 3) a balance between the processes of mitochondrial fission and fusion (Figure 2.19). These CR-driven patterns of metabolism, interorganellar communications and mitochondrial morphology delay the age-related onsets of apoptotic and liponecrotic modes of RCD throughout different stages of chronological aging (Figure 2.19). Moreover, CR lowers the concentration of mitochondrially produced ROS and rises trehalose concentration, thereby preserving cellular proteostasis and actively increasing the chance of survival. Because CR decreases the risk of cell death and actively increases the chance of cell survival throughout chronological lifespan (i.e. during D, PD and ST phases of culturing), this low-calorie diet extends yeast CLS.

Specifically, we found that non-CR yeast cells progressing through D phase of culturing accumulate ethanol, a product of glucose fermentation (Figure 2.19). Such accumulation of ethanol in non-CR yeast during D phase elicits a decline in the concentrations of the core enzymes of peroxisomal fatty acid β-oxidation Fox1, Fox2 and Fox3. The decline of Fox1, Fox2 and Fox3 in non-CR yeast during D phase decelerates peroxisomal fatty acid β-oxidation, thus lowering the pool of peroxisomally produced acetyl-CoA available for mitochondrial oxidation (Figure 2.19). The ensuing weakening of mitochondrial functionality in non-CR yeast during D phase is manifested as a decline in mitochondrial respiration, $\Delta\Psi$, TCA and ATP synthesis, as well as a rise in mitochondrially produced ROS. Because of the decline in mitochondrial functionality and ATP synthesis taking place in non-CR cells during D phase, their mitochondrial network undergoes fragmentation; this initiates the onset of the mitochondria-controlled apoptotic mode of RCD and increases the risk of death (Figure 2.19). Due to the rise in mitochondrially produced ROS occurring in non-CR cells during D phase, their proteins undergo oxidative damage; this impairs cellular proteostasis and decreases the chance of survival (Figure 2.19). Owing to the ability of CR to accelerate ethanol consumption and to cause ethanol depletion during D phase, this low-calorie diet 1) preserves mitochondrial respiration, $\Delta\Psi$, TCA and ATP synthesis during D phase; 2) prevents mitochondrial network fragmentation during D phase by shifting a balance between the processes of mitochondrial fission and fusion toward fusion; 3) allows to maintain the concentration of mitochondrially produced ROS during D phase below a toxic threshold (Figure 2.19). This ability of CR to cause ethanol depletion during D phase allows to delay the onset of

apoptotic RCD and to maintain cellular proteostasis, thus decreasing the risk of death and actively increasing the chance of survival for cells advancing through D phase of culturing (Figure 2.19).

Because ethanol concentration remains high in non-CR yeast cells progressing through PD phase of culturing, the risk of death for these cells remains elevated due to the accelerated onset of the mitochondria-controlled apoptotic mode of RCD (Figure 2.19). In contrast, CR decreases the risk of death during PD phase by allowing to delay the onset of this mode of mitochondria-controlled RCD (Figure 2.19). Furthermore, the high concentration of ethanol in non-CR yeast cells advancing through PD phase weakens the β-oxidation of FFA in peroxisomes and causes an accumulation of FA-CoA in pexopodia (Figure 2.19). Such accumulation of FA-CoA in pexopodia of non-CR yeast progressing through PD phase creates several negative feedback loops whose action elicits a build-up of FFA and DAG in the ER and LD (Figure 2.19). This build-up of FFA and DAG in non-CR yeast accelerates the onset of the liponecrotic mode of RCD during PD phase, thus increasing the risk of death during this phase of culturing (Figure 2.19). In contrast, CR decreases the risk of death during PD phase by 1) promoting peroxisomal fatty acid β-oxidation; 2) preventing FA-CoA accumulation in pexopodia; 3) allowing to maintain low concentrations of FFA and DAG; and, ultimately 4) delaying the onset of liponecrotic RCD (Figure 2.19). Moreover, CR actively increases the chance of survival for cells advancing through PD phase of culturing because this low-calorie diet significantly increases the concentration of trehalose, thereby preserving cellular proteostasis (Figure 2.19).

The risk of death for non-CR yeast cells during ST phase remains high because of the accelerated onsets of both apoptotic and liponecrotic modes of RCD (Figure 2.19). However, we found that liponecrotic RCD is a prevailing mode of death in non-CR yeast advancing through ST phase (compare Figures 2.11C and 2.14). This finding indicates that the apoptotic and liponecrotic modes of RCD may have different relative contributions to the age-related death of non-CR yeast at different periods of CLS. The apoptotic mode of RCD predominates during D phase, apoptotic and liponecrotic RCD modes equally increase the risk of death during PD phase, whereas the liponecrotic mode of RCD prevails during ST phase (Figure 2.19). This is like the ″big P″ and ″small p″ modes of death in the nematode *Caenorhabditis elegans*, which define lifespan earlier or later in life (respectively) [211]. Like its effects in yeast progressing through PD phase, CR decreases the risk of death during ST phase by allowing to delay the onsets of both apoptotic and liponecrotic RCD modes (Figure 2.19). In addition, akin to its effect on the survival of yeast during

PD phase, CR increases the chance of survival for yeast progressing through ST phase by rising the concentration of trehalose; this allows CR to maintain cellular proteostasis during ST phase (Figure 2.19).

In conclusion, this study provides important new insights into mechanisms through which CR delays yeast chronological aging by orchestrating a stepwise remodeling of numerous cellular processes that are integrated into an intricate network. These processes are confined to different cellular locations and occur at different periods of yeast chronological lifespan.

3 A possible "metabolic signature" of longevity extension by caloric restriction and the *tor1Δ* mutation in chronologically aging yeast

3.1 Introduction

Recent studies have revealed that a characteristic age-related remodeling of the composition of water-soluble metabolites (which is further referred to as "the water-soluble metabolome") may play essential roles in regulating cellular aging, influencing age-related pathologies and defining organismal longevity in eukaryotic organisms across phyla. It remained unclear how CR and some longevity-extending genetic interventions influence the water-soluble metabolome of chronologically aging yeast cells. The objectives of studies described in this chapter was therefore to use a mass spectrometry-based quantitative analysis of the water-soluble cellular metabolome for the investigation of how CR and the longevity-extending *tor1Δ* mutation (which eliminates the Tor1 protein kinase known to orchestrate the nutrient- and energy-sensing TOR (target of rapamycin) pro-aging signaling pathway) affect the concentrations of various water-soluble metabolites at consecutive stages of the chronological aging process in *S. cerevisiae*.

3.2 Materials and methods

3.2.1 Yeast strains, media and growth conditions

The wild-type (WT) strain *Saccharomyces cerevisiae* BY4742 (*MATα his3Δ1 leu2Δ0 lys2Δ0 ura3Δ0*) and the *tor1Δ* single-gene-deletion mutant strain in the BY4742 genetic background from Open Biosystems/Dharmacon (a part of GE Healthcare) were grown in YP medium (1% yeast extract, 2% peptone; both from Fisher Scientific; #BP1422-2 and #BP1420-2, respectively) initially containing 0.2% (w/v) or 2% (w/v) glucose (#D16-10; Fisher Scientific) as carbon source. Cells were cultured at 30ºC with rotational shaking at 200 rpm in Erlenmeyer flasks at a ″flask volume/medium volume″ ratio of 5:1.

3.2.2 Sample preparation for mass spectrometry-based metabolomics

Cells were collected on days 1, 2, 7 and 10 of culturing. After measuring the cell titer, cells from 50 ml of a culture were harvested by centrifugation at 5,000 × g for 1 min at 4°C. The pelleted cells were rinsed with nanopure water and then collected by centrifugation at 5,000 × g for 1 min at 4°C. Cells are then immediately quenched by the addition of 8 ml of MeOH/H_2O (1:1) stored at

-80°C. After quenching, cells were aliquoted into 1 ml-fractions and stored at -80°C until the extraction of metabolites.

For metabolite extraction, 5 x 10^8 cells were spiked with 50 µl of internal standards (0.2 mg/ml Citric-2,2,4,4-d4, *L*-Ornitihine-2,3,3,4,4,5,5-d7 HCl, *L*-glutamic acid ^{15}N and D-glucose ^{13}C) and disrupted with glass beads for 15 min at 4°C. Lysates were then subjected to centrifugation at 20,000 × g at 4°C to remove cell debris and residual glass beads. The supernatant was concentrated using a SpeedVac at ambient temperature for 2 h. Metabolite extracts were diluted in 40 µl of 1:1 Acetonitrile/H_2O (1:1) for HILIC or MeOH/H_2O (1:1) for RP-C18 HPLC. Samples were kept at 4°C prior to LC-MS/MS.

3.2.3 LC-MS/MS analysis

LC-MS/MS data were acquired using an Agilent 1100 HPLC system (Agilent Technologies, CA, USA) interfaced with an LTQ Orbitrap Velos mass spectrometer (Thermo Fisher Scientific, Waltham, MA, USA).

LC separation was carried out using a ZIC-pHILIC column (Merck SeQuant, Umeå, Sweden; 150 × 2.1 mm, 5 µm particle size). Acetonitrile (A) and 20 mM ammonium bicarbonate buffer, pH 7.8 (B) were used as the mobile phase, with an elution gradient of 90% A to 10% A in 20 min at a flow rate of 200 µl/min. LC separation was also carried out using a reverse phase column (Agilent Technologies, CA, USA; Zorbax C18 SB-300, 150 x 2.1 mm, 5 µm). Nanopure water with 0.1% formic acid (A) and acetonitrile (B) were used as the mobile phase, with an elution gradient of 80% A to 20% A in 15 min at a flow rate of 200 µl/min. Mass spectrometric analyses were performed with a Thermo Orbitrap Velos mass spectrometer equipped with a HESI-II ion source (#10145339; Thermo Scientific). Metabolites were detected by top 5 data dependent FT-MS/MS at a resolution of 60,000 for MS scans and 30,000 for dependent MS/MS. Fragmentation was carried out using HCD at a normalized collision energy of 35. Samples were analyzed in both positive and negative ionization modes.

Acquired mass spectra were converted from proprietary Thermo RAW format to either mzXML using MSConvert as part of the ProteoWizard suite (freely available from http://proteowizard.sourceforge.net/). Data were analyzed using MZmine 2.10. Statistical processing was carried out using Metaboanalyst (http://www.metaboanalyst.ca/MetaboAnalyst/faces/Home.jsp).

3.3 Results

3.3.1 CR elicits major changes in the water-soluble metabolomes of chronologically aging WT and *tor1Δ* cells

WT and *tor1Δ* cells were cultured in the nutrient-rich YP medium initially containing 0.2% glucose (CR conditions) or 2% glucose (non-CR conditions). Cells were collected on days 1 (logarithmic phase), 2 (the beginning of diauxic phase), 7 (the end of post-diauxic phase/the beginning of stationary phase) and 10 (stationary phase) of culturing. Cells were recovered on different days of culturing because we sought to assess how chronological age of these cells influences the effect of CR on the water-soluble metabolome.

The LC-MS/MS analysis of water-soluble metabolites extracted from these cells revealed thousands of metabolites (assigned as well as non-assigned, from both negative and positive ionization modes) in extracts of WT and *tor1Δ* cells. We found that CR causes major changes in the water-soluble metabolomes of WT and *tor1Δ* cells recovered on any of the four consecutive phases of chronological aging; indeed, from 50% to 70% of water-soluble metabolites in these cells were enriched (i.e. their concentrations were increased by at least 2-fold) or depleted (i.e. their concentrations were decreased by at least 2-fold) by the CR diet (Figures 3.1-3.4).

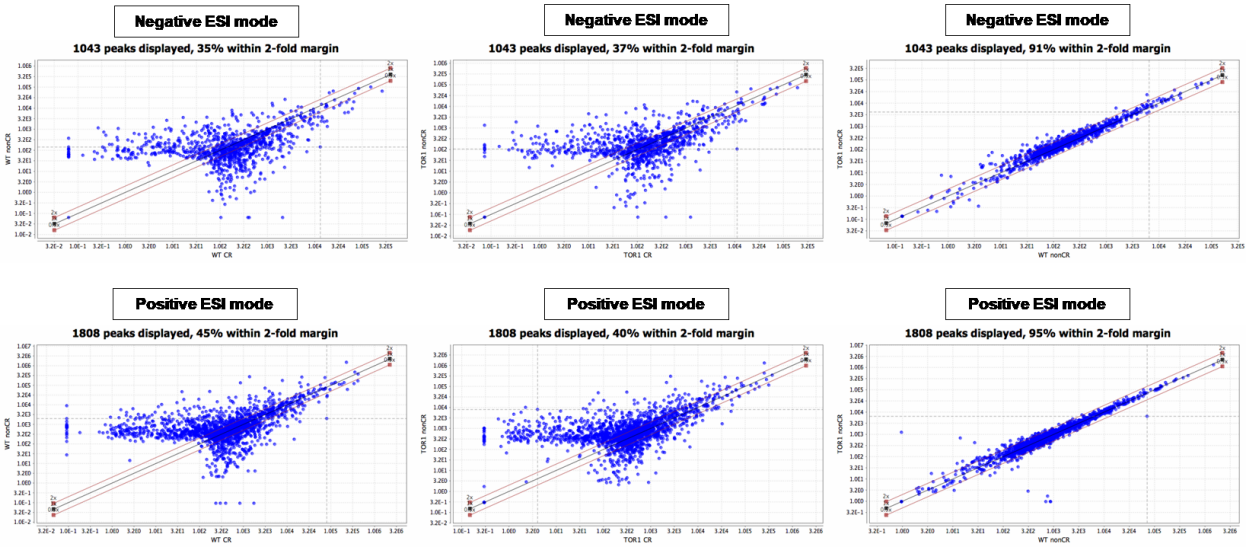

Figure 3.1. Scatter plots of normalized peak areas of all LC-MS peaks detected (assigned as well as non-assigned, from both negative and positive ionization modes) in extracts of WT and *tor1Δ* cells. Cells grown under CR or non-CR conditions were recovered for metabolite extraction on ***Day 1 (logarithmic phase of culturing***).

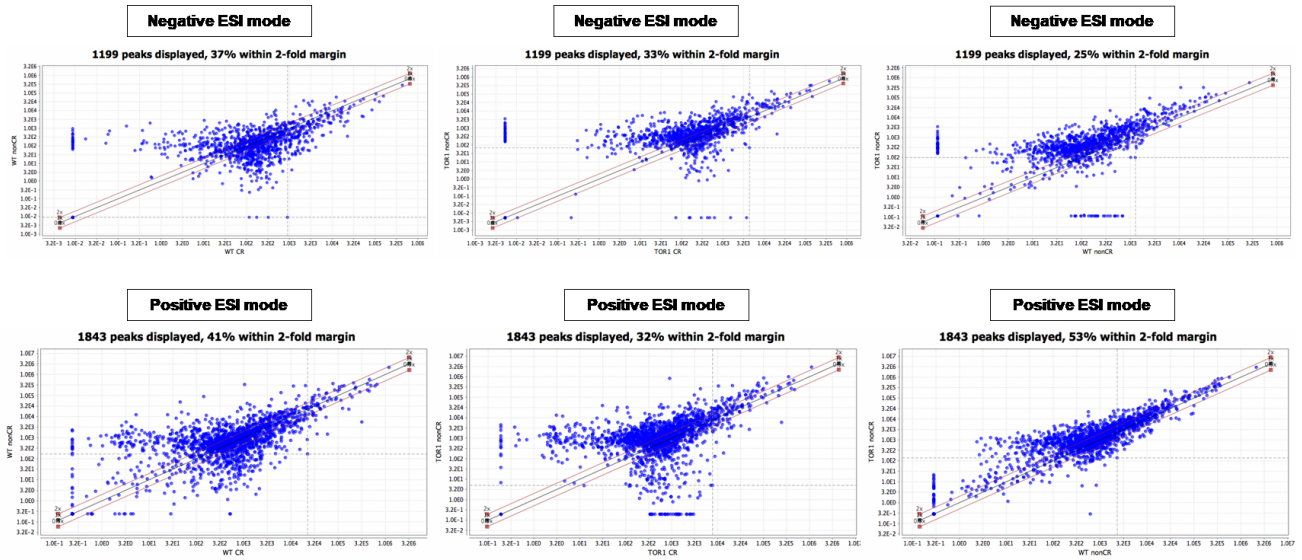

Figure 3.2. Scatter plots of normalized peak areas of all LC-MS peaks detected (assigned as well as non-assigned, from both negative and positive ionization modes) in extracts of WT and *tor1Δ* cells. Cells grown under CR or non-CR conditions were recovered for metabolite extraction on ***Day 2 (the beginning of post-diauxic phase of culturing).***

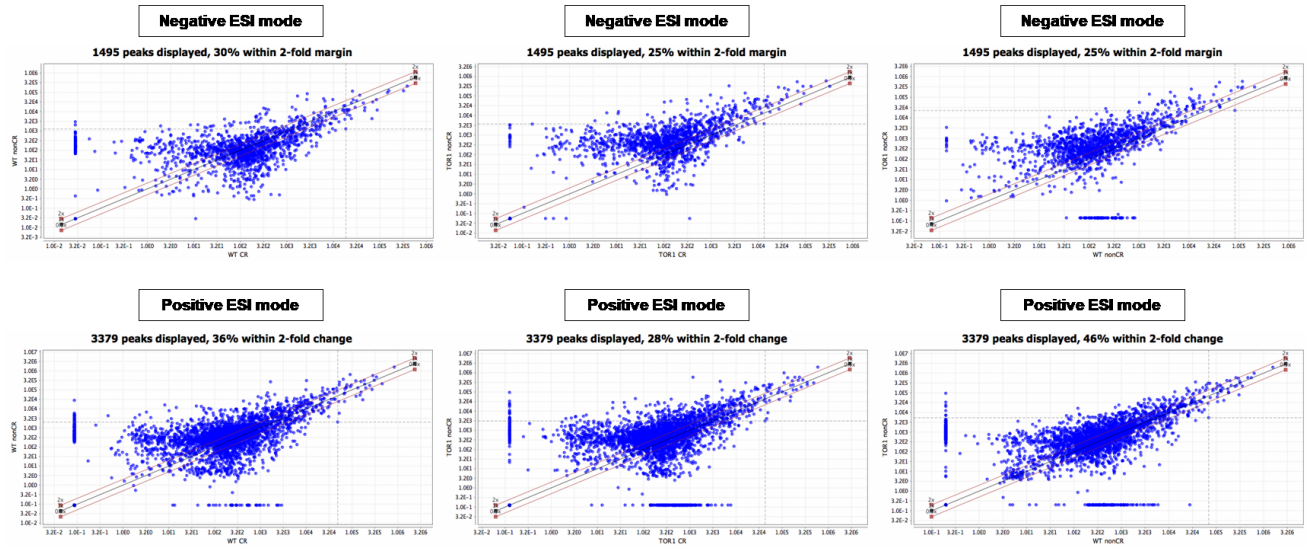

Figure 3.3. Scatter plots of normalized peak areas of all LC-MS peaks detected (assigned as well as non-assigned, from both negative and positive ionization modes) in extracts of WT and *tor1Δ* cells. Cells grown under CR or non-CR conditions were recovered for metabolite extraction on ***Day 7 (the end of post-diauxic phase of culturing/the beginning of stationary phase of culturing).***

Of note, the longevity-extending *tor1Δ* mutation did not cause significant changes in the water-soluble metabolome of cells cultured under non-CR conditions and recovered on day 1 of culturing (only 5%-9% of water-soluble metabolites were enriched or depleted in *tor1Δ* cells as compared to WT cells) (Figure 3.1). However, beginning of day 2 of culturing, from 50% to 70%

of water-soluble metabolites in *tor1Δ* cells were enriched or depleted as compared to WT cells (Figures 3.2-3.4).

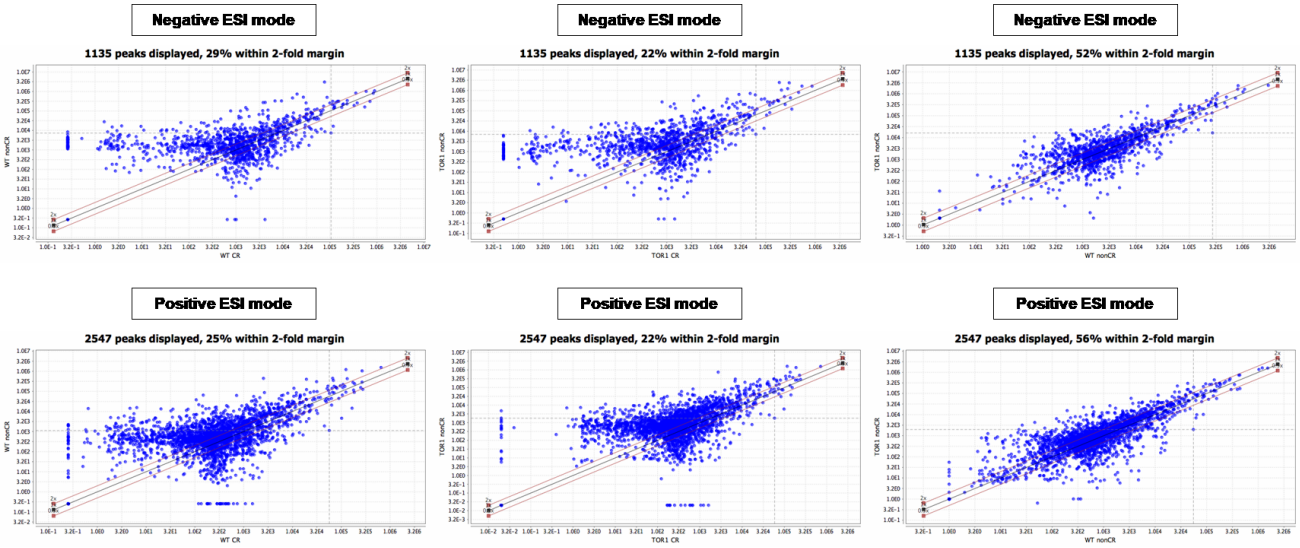

Figure 3.4. Scatter plots of normalized peak areas of all LC-MS peaks detected (assigned as well as non-assigned, from both negative and positive ionization modes) in extracts of WT and *tor1Δ* cells. Cells grown under CR or non-CR conditions were recovered for metabolite extraction on ***Day 10 (stationary phase of culturing).***

3.3.2 In chronologically aging cells, CR establishes a distinct metabolic pattern that significantly differs from that of cells cultured under non-CR conditions

The principal components analysis (PCA) of the metabolite concentrations in extracts of WT and *tor1Δ* cells (the metabolites were normalized to an internal standard and auto-scaled) has revealed that CR elicits a distinct metabolic pattern that significantly differs from the metabolic pattern of these cells cultured under non-CR conditions. Indeed, the PCs of cells cultured under CR or non-CR conditions were well separated from each other in both WT and *tor1Δ* cells recovered at any of the 4 days of culturing (Figures 3.5-3.8). Thus, the CR-specific metabolic pattern exists in both WT and *tor1Δ* cells through all phases of the chronological aging process.

Of note, the longevity-extending *tor1Δ* mutation did not cause a significant change in the pattern of water-soluble metabolites in cells cultured under non-CR conditions and recovered on day 1 of culturing; this conclusion is based on the observation that the PCs of WT and *tor1Δ* cells cultured under non-CR conditions were not separated from each other (Figure 3.5). However, beginning of day 2 of culturing, the PCs of WT and *tor1Δ* cells cultured under non-CR conditions were well separated from each other (Figures 3.6-3.8). Thus, the ability of the *tor1Δ* mutation to

extend longevity under non-CR conditions coincides (and may cause) the ability of this mutation to remodel the pattern of water-soluble metabolites under these conditions.

Furthermore, only in cells recovered on day 1 of culturing, the PCs of WT and *tor1Δ* cells cultured under CR conditions were slightly separated from each other (Figure 3.5). However, beginning of day 2 of culturing, the PCs of WT and *tor1Δ* cells cultured under CR conditions were not separated from each other (Figures 3.6-3.8). Thus, beginning of day 2 of culturing, CR establishes the same metabolic pattern in both WT and *tor1Δ* cells.

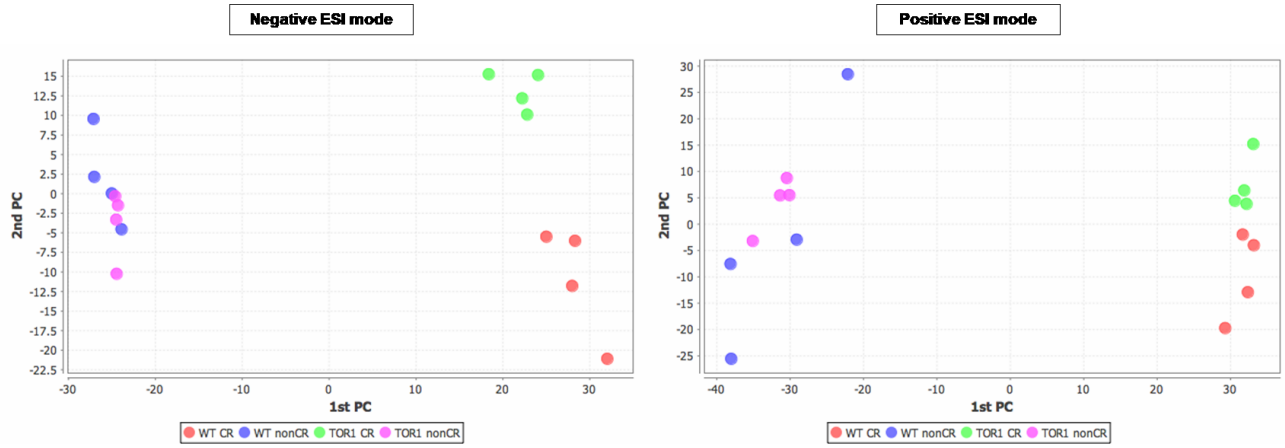

Figure 3.5. Scores plots from the principal components analysis (PCA) of the metabolite concentrations in extracts of WT and *tor1Δ* cells (the metabolites were normalized to an internal standard and auto-scaled). Cells grown under CR or non-CR conditions were recovered for metabolite extraction on ***Day 1 (logarithmic phase of culturing).***

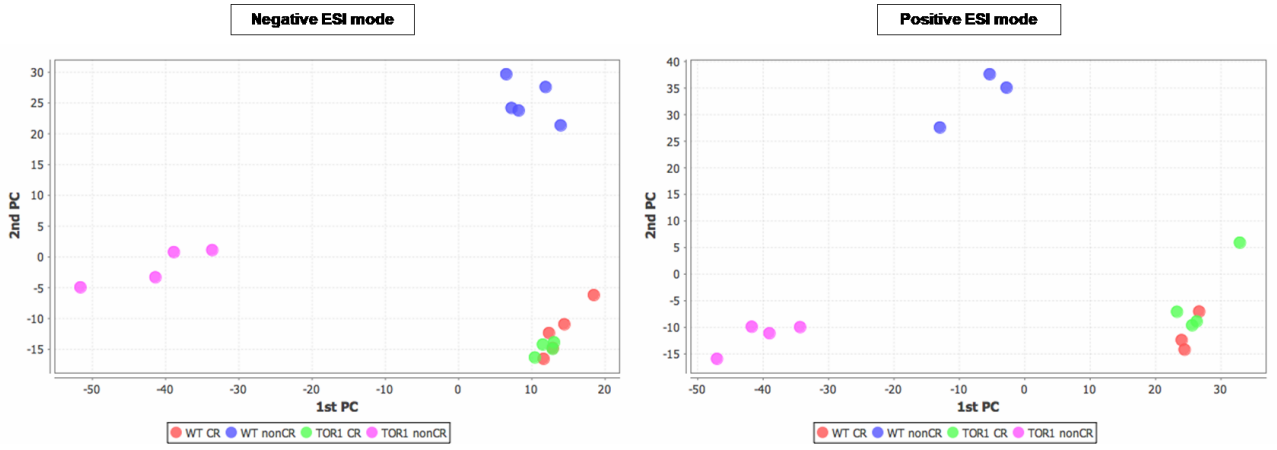

Figure 3.6. Scores plots from the principal components analysis (PCA) of the metabolite concentrations in extracts of WT and *tor1Δ* cells (the metabolites were normalized to an internal standard and auto-scaled). Cells grown under CR or non-CR conditions were recovered for metabolite extraction on ***Day 2 (the beginning of post-diauxic phase of culturing).***

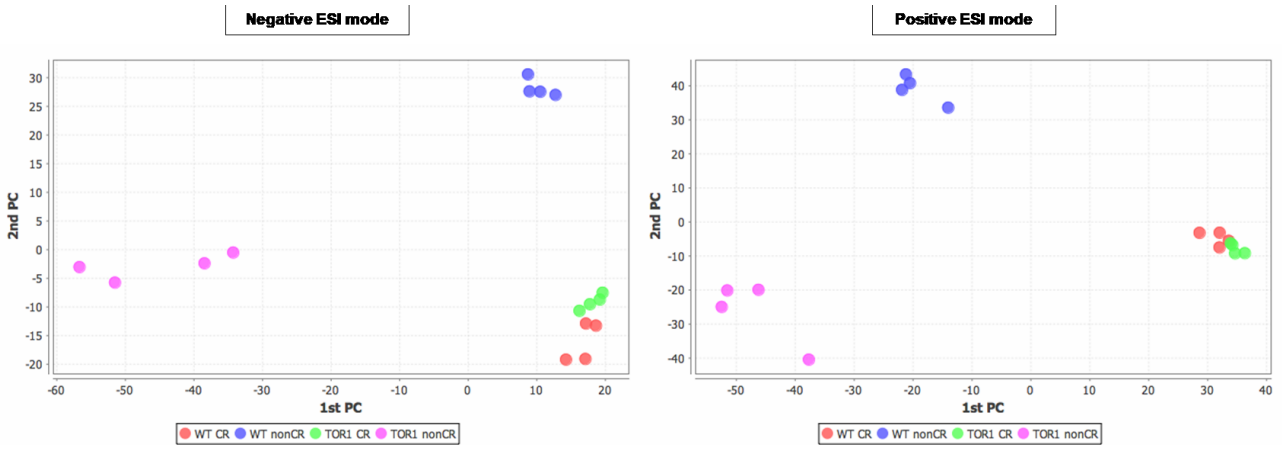

Figure 3.7. Scores plots from the principal components analysis (PCA) of the metabolite concentrations in extracts of WT and *tor1Δ* cells (the metabolites were normalized to an internal standard and auto-scaled). Cells grown under CR or non-CR conditions were recovered for metabolite extraction on ***Day 7 (the end of post-diauxic phase of culturing/the beginning of stationary phase of culturing).***

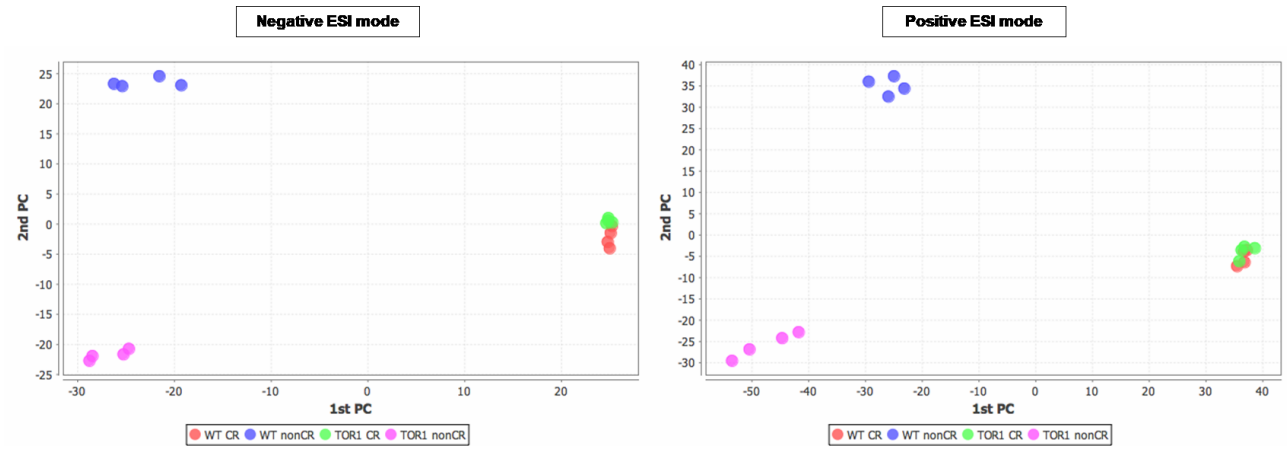

Figure 3.8. Scores plots from the principal components analysis (PCA) of the metabolite concentrations in extracts of WT and *tor1Δ* cells (the metabolites were normalized to an internal standard and auto-scaled). Cells grown under CR or non-CR conditions were recovered for metabolite extraction on ***Day 10 (stationary phase of culturing).***

3.3.3 The *tor1Δ* mutation enriches and depletes distinct sets of metabolites in chronologically aging yeast cultured under non-CR conditions

The *tor1Δ* mutation: 1) extends longevity of chronologically aging yeast cultured under non-CR conditions on 2% glucose [1-3]; and 2) beginning of day 2 of culturing, causes a substantial remodeling of the pattern of water-soluble metabolites in chronologically aging yeast cells cultured under non-CR conditions (see section 3.3.2). Our LC-MS/MS analysis has revealed 12 metabolites whose cellular concentrations are increased or decreased to the highest extent by

the *tor1Δ* mutation (Table 3.1). Many of these metabolites comprise a network which integrates the following pathways of intermediary metabolism: 1) the biosynthesis of methionine from aspartate; 2) the biosynthesis of threonine from aspartate; 3) the biosynthesis of both cysteine and glutathione from homocysteine, an intermediate in the biosynthetic pathway for methionine; and 4) the biosynthesis of spermidine and other polyamines from S-adenosylmethionine, an intermediate in the biosynthetic pathway for methionine (Figure 3.9).

Table 3.1. Loading plots from the PCA of the metabolite concentrations in WT and *tor1Δ* cells. These plots have revealed 12 metabolites whose cellular concentrations are increased or decreased to the highest extent by the *tor1Δ* mutation. Cells cultured under non-CR conditions were recovered for metabolite extraction on Day 7 (the end of post-diauxic phase of culturing/the beginning of stationary phase of culturing).

Metabolites whose concentrations are INCREASED the most	Log2FC
3-phosphoglycerate.1	8.16
UDP-N-acetyl-alpha-D-glucosamine	7.65
UDP-glucose dimer	6.67
UDP-N-acetyl-glucosamine	6.44
cis-Aconitate.1	6.19
3-phosphoglycerate	6.01
Inosine	5.53
Maltotriose	5.42
N-acetyl-glutamate	4.86
D-Glycerate	4.84
cis-Aconitate	4.82
N6-Acetyl-N6-hydroxy-L-lysine	4.75

Metabolites whose concentrations are DECREASED the most	Log2FC
L-Methionine	-2.49
S-adenosyl-homocysteine.1	-2.54
Glutamyl-glutamic acid.2	-2.91
GMP.1	-2.94
N2-Succinyl-L-arginine.1	-2.97
D-Erythrose 4-phosphate.1	-3.27
Trimethyl lysine.2	-3.35
4-Methylene-L-glutamine.2	-3.59
N-Acetyl-L-glutamate 5-semialdehyde	-4.11
Octose-diphosphate	-4.66
1-Pyrroline-5-carboxylic acid.1	-5.23
dTDP-glucose	-8.17

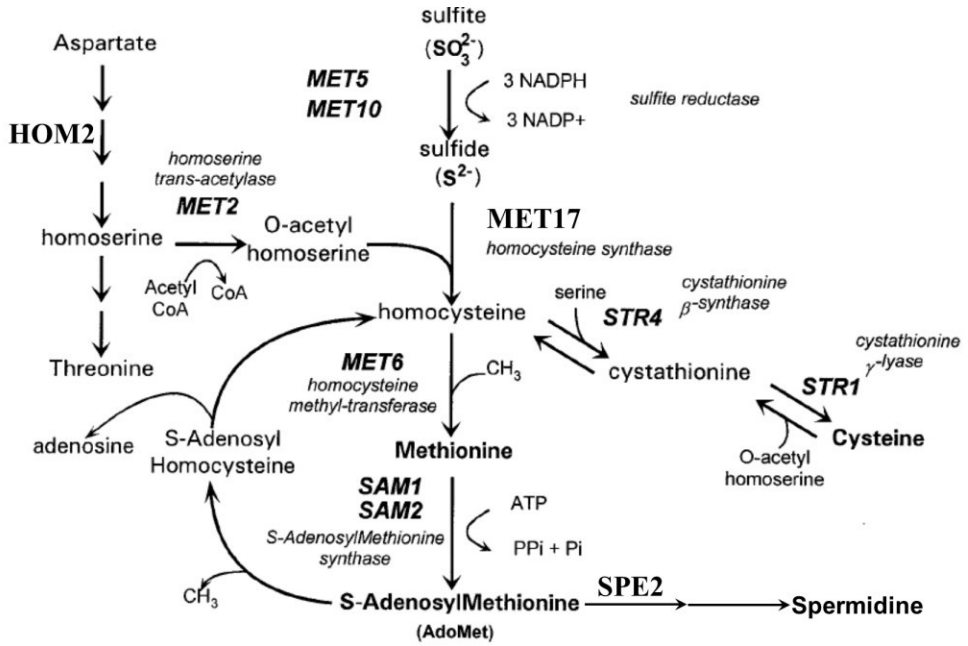

Figure 3.9. Metabolic pathways for the biosynthesis of methionine and other sulfur amino acids in yeast. Modified from [212].

3.3.4 The pathway of methionine metabolism is among metabolic pathways affected the most by both CR and the *tor1Δ* mutation

Our metabolite set enrichment analysis (MSEA; also known as the pathway analysis) of the water-soluble metabolites identified by LC-MS/MS has revealed that the pathway of methionine metabolism is among metabolic pathways affected the most by the extent of calorie availability (i.e. CR vs non-CR conditions) and/or by the *tor1Δ* mutation (Figures 3.10 – 3.33).

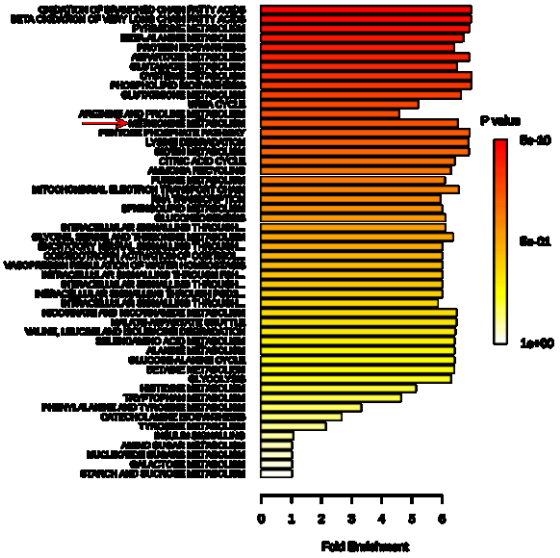

Figure 3.10. The metabolite set enrichment analysis [MSEA] (a.k.a. the pathway analysis) to establish which metabolic pathways are affected the most by the extent of calorie availability (i.e. CR vs non-CR) and/or by the *tor1Δ* mutation. In this example, *tor1Δ* cells grown under CR conditions were compared to *tor1Δ* cells grown under non-CR conditions. Cells were recovered for metabolite extraction on ***Day 1 (logarithmic phase of culturing)***. The metabolites were separated using ***a C18 column***.

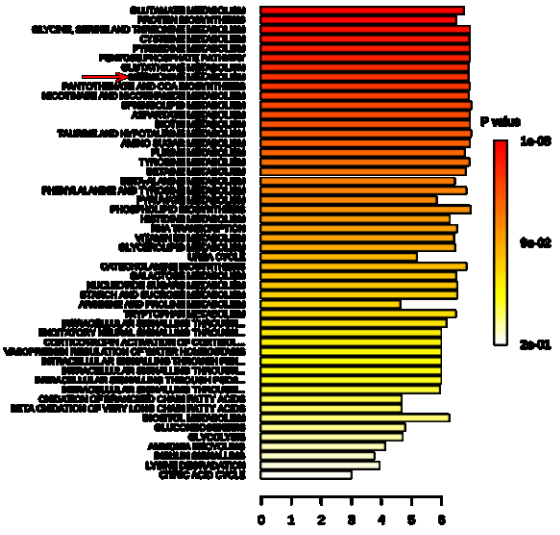

Figure 3.11. The metabolite set enrichment analysis [MSEA] (a.k.a. the pathway analysis) to establish which metabolic pathways are affected the most by the extent of calorie availability (i.e. CR vs non-CR) and/or by the *tor1Δ* mutation. In this example, *tor1Δ* cells grown under CR conditions were compared to *tor1Δ* cells grown under non-CR conditions. Cells were recovered for metabolite extraction on ***Day 1 (logarithmic phase of culturing)***. The metabolites were separated using a ***ZIC-pHILIC column***.

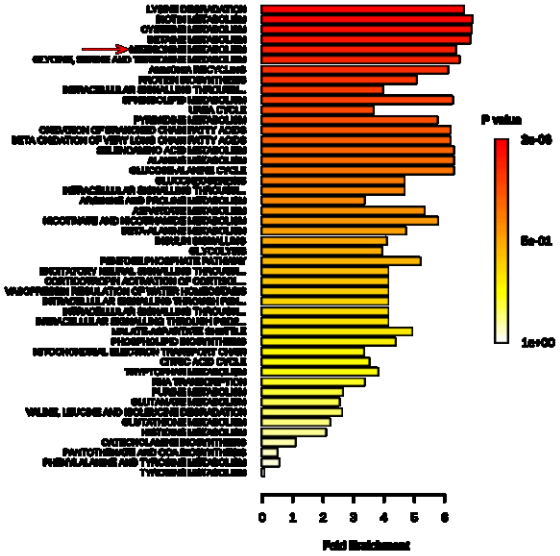

Figure 3.12. The metabolite set enrichment analysis [MSEA] (a.k.a. the pathway analysis) to establish which metabolic pathways are affected the most by the extent of calorie availability (i.e. CR vs non-CR). In this example, WT cells grown under CR conditions were compared to WT cells grown under non-CR conditions. Cells were recovered for metabolite extraction on ***Day 1 (logarithmic phase of culturing)***. The metabolites were separated using a ***C18 column***.

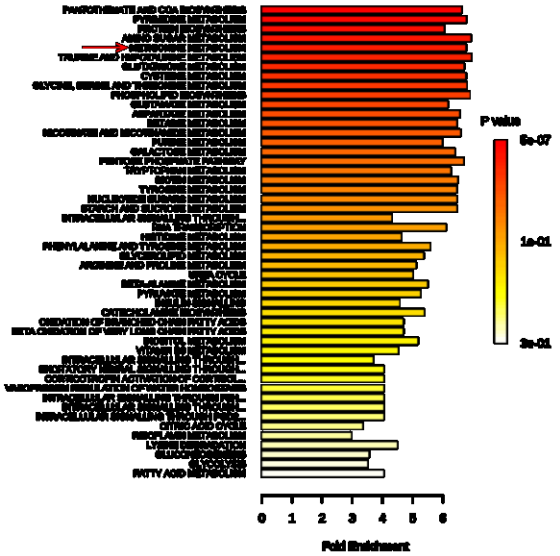

Figure 3.13. The metabolite set enrichment analysis [MSEA] (a.k.a. the pathway analysis) to establish which metabolic pathways are affected the most by the extent of calorie availability (i.e. CR vs non-CR). In this example, WT cells grown under CR conditions were compared to WT cells grown under non-CR conditions. Cells were recovered for metabolite extraction on ***Day 1 (logarithmic phase of culturing)***. The metabolites were separated using a ***ZIC-pHILIC column***.

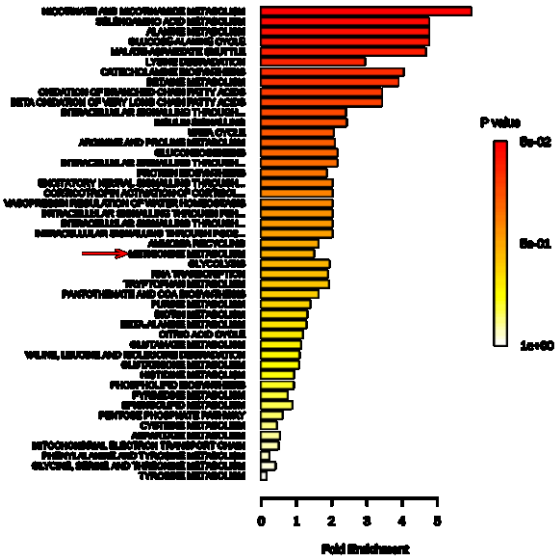

Figure 3.14. The metabolite set enrichment analysis [MSEA] (a.k.a. the pathway analysis) to establish which metabolic pathways are affected the most by the *tor1Δ* mutation. In this example, WT cells grown under non-CR conditions were compared to *tor1Δ* cells grown under non-CR conditions. Cells were recovered for metabolite extraction on ***Day 1 (logarithmic phase of culturing)***. The metabolites were separated using a ***C18 column***.

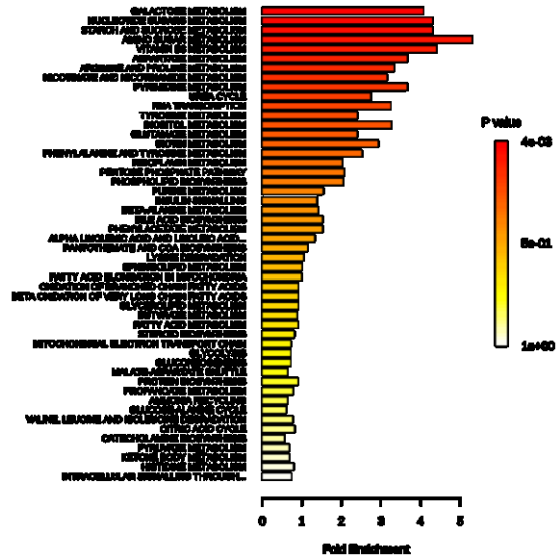

Figure 3.15. The metabolite set enrichment analysis [MSEA] (a.k.a. the pathway analysis) to establish which metabolic pathways are affected the most by the *tor1Δ* mutation. In this example, WT cells grown under non-CR conditions were compared to *tor1Δ* cells grown under non-CR conditions. Cells were recovered for metabolite extraction on ***Day 1 (logarithmic phase of culturing)***. The metabolites were separated using a ***ZIC-pHILIC column***.

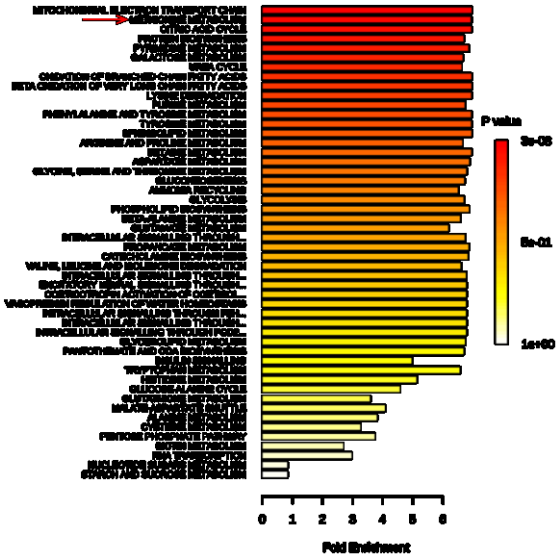

Figure 3.16. The metabolite set enrichment analysis [MSEA] (a.k.a. the pathway analysis) to establish which metabolic pathways are affected the most by the extent of calorie availability (i.e. CR vs non-CR) and/or by the *tor1Δ* mutation. In this example, *tor1Δ* cells grown under CR conditions were compared to *tor1Δ* cells grown under non-CR conditions. Cells were recovered for metabolite extraction on ***Day 2 (post-diauxic phase of culturing)***. The metabolites were separated using a ***C18 column***.

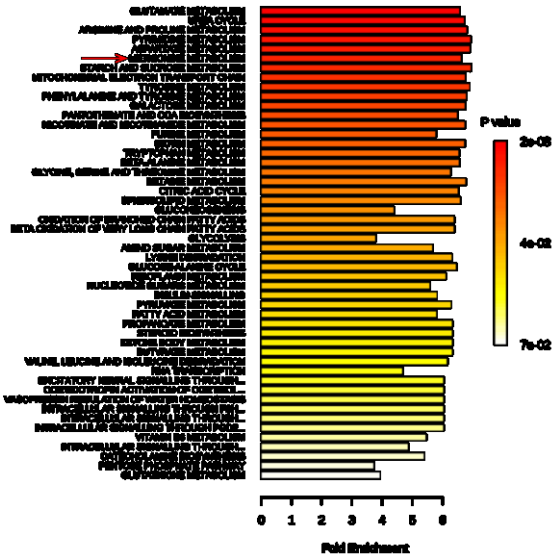

Figure 3.17. The metabolite set enrichment analysis [MSEA] (a.k.a. the pathway analysis) to establish which metabolic pathways are affected the most by the extent of calorie availability (i.e. CR vs non-CR) and/or by the *tor1Δ* mutation. In this example, *tor1Δ* cells grown under CR conditions were compared to *tor1Δ* cells grown under non-CR conditions. Cells were recovered for metabolite extraction on ***Day 2 (post-diauxic phase of culturing)***. The metabolites were separated using a ***ZIC-pHILIC column***.

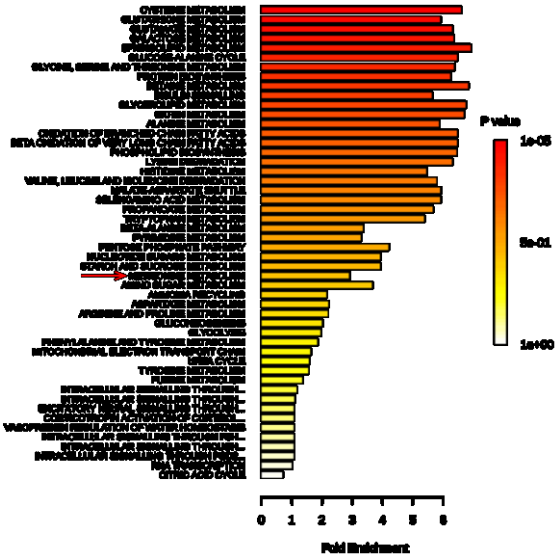

Figure 3.18. The metabolite set enrichment analysis [MSEA] (a.k.a. the pathway analysis) to establish which metabolic pathways are affected the most by the extent of calorie availability (i.e. CR vs non-CR). In this example, WT cells grown under CR conditions were compared to WT cells grown under non-CR conditions. Cells were recovered for metabolite extraction on ***Day 2 (post-diauxic phase of culturing)***. The metabolites were separated using a ***C18 column***.

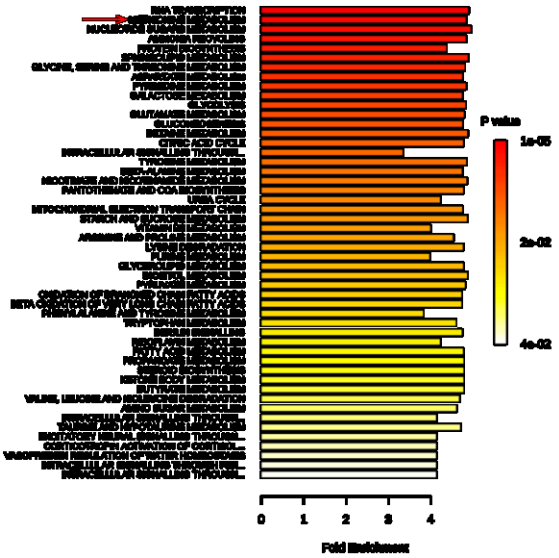

Figure 3.19. The metabolite set enrichment analysis [MSEA] (a.k.a. the pathway analysis) to establish which metabolic pathways are affected the most by the extent of calorie availability (i.e. CR vs non-CR). In this example, WT cells grown under CR conditions were compared to WT cells grown under non-CR conditions. Cells were recovered for metabolite extraction on ***Day 2 (the beginning of post-diauxic phase of culturing)***. The metabolites were separated using a ***ZIC-pHILIC column***.

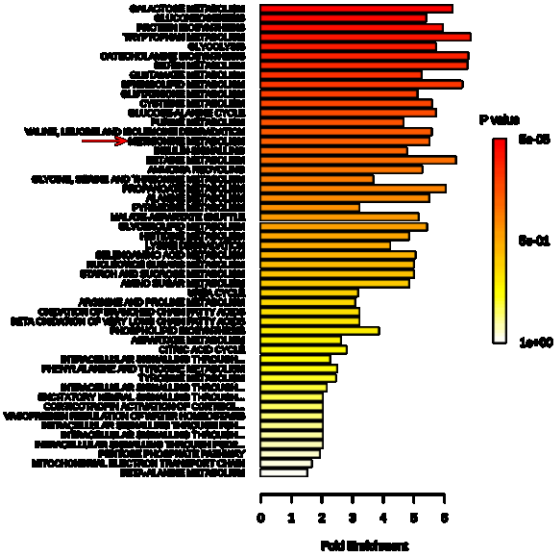

Figure 3.20. The metabolite set enrichment analysis [MSEA] (a.k.a. the pathway analysis) to establish which metabolic pathways are affected the most by the *tor1Δ* mutation. In this example, WT cells grown under non-CR conditions were compared to *tor1Δ* cells grown under non-CR conditions. Cells were recovered for metabolite extraction on ***Day 2 (the beginning of post-diauxic phase of culturing)***. The metabolites were separated using a ***C18 column***.

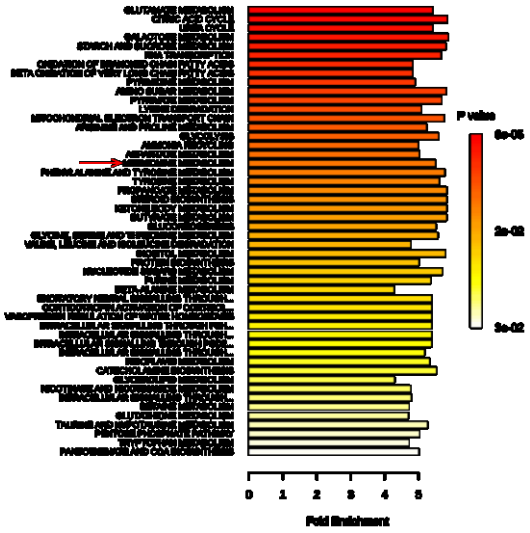

Figure 3.21. The metabolite set enrichment analysis [MSEA] (a.k.a. the pathway analysis) to establish which metabolic pathways are affected the most by the *tor1Δ* mutation. In this example, WT cells grown under non-CR conditions were compared to *tor1Δ* cells grown under non-CR conditions. Cells were recovered for metabolite extraction on ***Day 2 (the beginning of post-diauxic phase of culturing)***. The metabolites were separated using a ***ZIC-pHILIC column.***

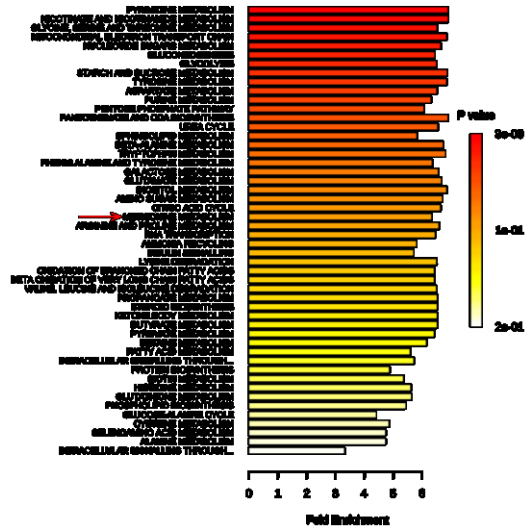

Figure 3.22. The metabolite set enrichment analysis [MSEA] (a.k.a. the pathway analysis) to establish which metabolic pathways are affected the most by the extent of calorie availability (i.e. CR vs non-CR) and/or by the *tor1Δ* mutation. In this example, *tor1Δ* cells grown under CR conditions were compared to *tor1Δ* cells grown under non-CR conditions. Cells were recovered for metabolite extraction on ***Day 7 (the end of post-diauxic phase of culturing/the beginning of stationary phase of culturing)***. The metabolites were separated using a ***C18 column***.

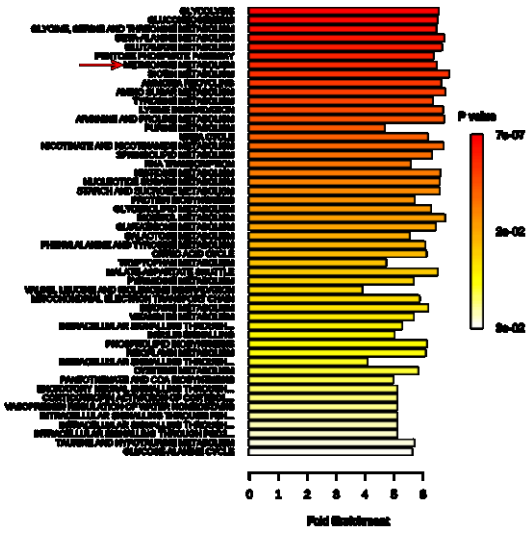

Figure 3.23. The metabolite set enrichment analysis [MSEA] (a.k.a. the pathway analysis) to establish which metabolic pathways are affected the most by the extent of calorie availability (i.e. CR vs non-CR) and/or by the *tor1Δ* mutation. In this example, *tor1Δ* cells grown under CR conditions were compared to *tor1Δ* cells grown under non-CR conditions. Cells were recovered for metabolite extraction on ***Day 7 (the end of post-diauxic phase of culturing/the beginning of stationary phase of culturing)***. The metabolites were separated using a ***ZIC-pHILIC column***.

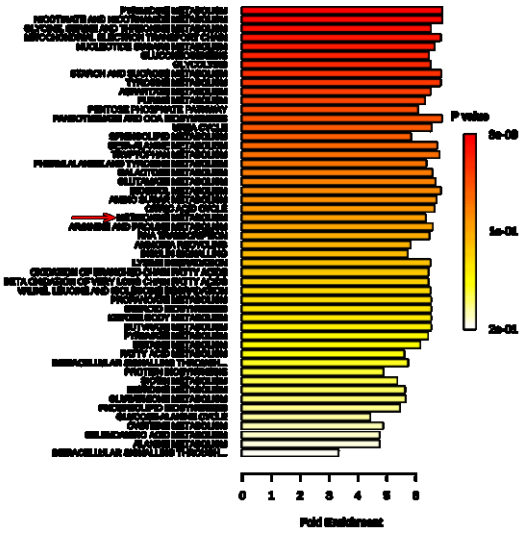

Figure 3.24. The metabolite set enrichment analysis [MSEA] (a.k.a. the pathway analysis) to establish which metabolic pathways are affected the most by the extent of calorie availability (i.e. CR vs non-CR). In this example, WT cells grown under CR conditions were compared to WT cells grown under non-CR conditions. Cells were recovered for metabolite extraction on ***Day 7 (the end of post-diauxic phase of culturing/the beginning of stationary phase of culturing)***. The metabolites were separated using a ***C18 column***.

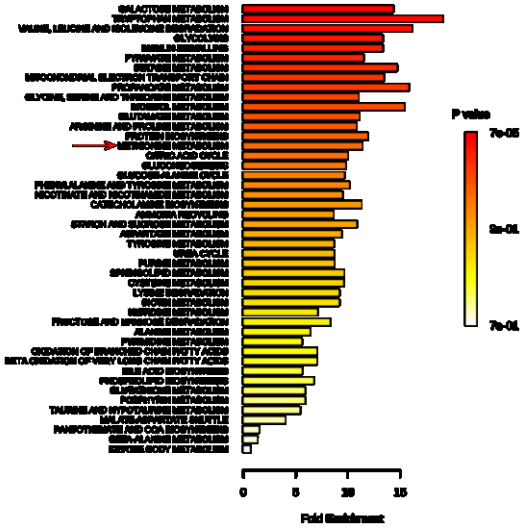

Figure 3.25. The metabolite set enrichment analysis [MSEA] (a.k.a. the pathway analysis) to establish which metabolic pathways are affected the most by the extent of calorie availability (i.e. CR vs non-CR). In this example, WT cells grown under CR conditions were compared to WT cells grown under non-CR conditions. Cells were recovered for metabolite extraction on ***Day 7 (the end of post-diauxic phase of culturing/the beginning of stationary phase of culturing)***. The metabolites were separated using a ***ZIC-pHILIC column***.

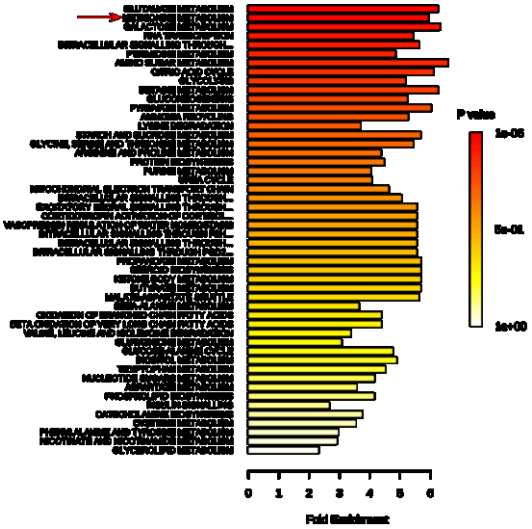

Figure 3.26. The metabolite set enrichment analysis [MSEA] (a.k.a. the pathway analysis) to establish which metabolic pathways are affected the most by the *tor1Δ* mutation. In this example, WT cells grown under non-CR conditions were compared to *tor1Δ* cells grown under non-CR conditions. Cells were recovered for metabolite extraction on ***Day 7 (the end of post-diauxic phase of culturing/the beginning of stationary phase of culturing)***. The metabolites were separated using a ***C18 column***.

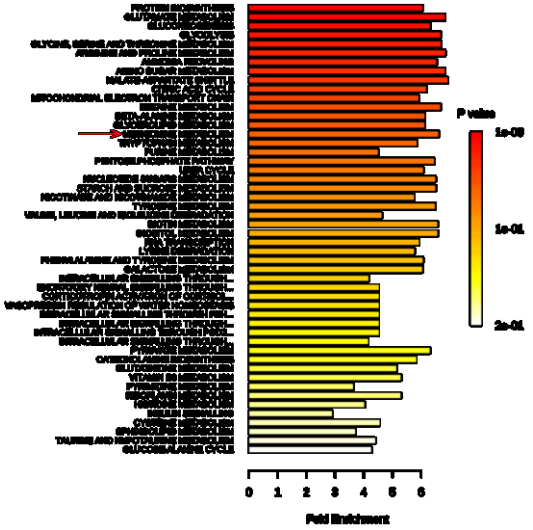

Figure 3.27. The metabolite set enrichment analysis [MSEA] (a.k.a. the pathway analysis) to establish which metabolic pathways are affected the most by the *tor1Δ* mutation. In this example, WT cells grown under non-CR conditions were compared to *tor1Δ* cells grown under non-CR conditions. Cells were recovered for metabolite extraction on ***Day 7 (the end of post-diauxic phase of culturing/the beginning of stationary phase of culturing)***. The metabolites were separated using a ***ZIC-pHILIC column***.

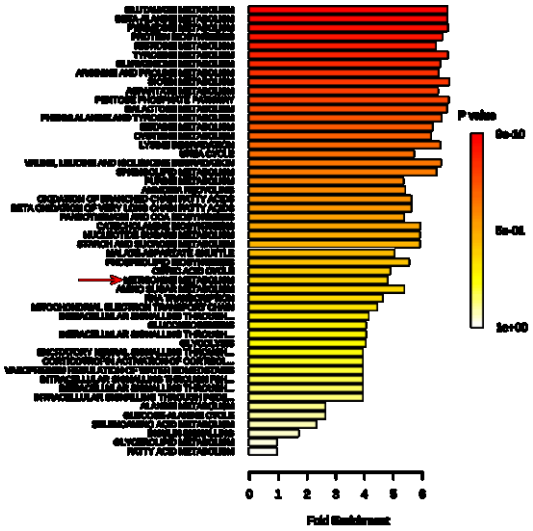

Figure 3.28. The metabolite set enrichment analysis [MSEA] (a.k.a. the pathway analysis) to establish which metabolic pathways are affected the most by the extent of calorie availability (i.e. CR vs non-CR). In this example, *tor1Δ* cells grown under CR conditions were compared to *tor1Δ* cells grown under non-CR conditions. Cells were recovered for metabolite extraction on ***Day 10 (stationary phase of culturing)***. The metabolites were separated using a ***C18 column***.

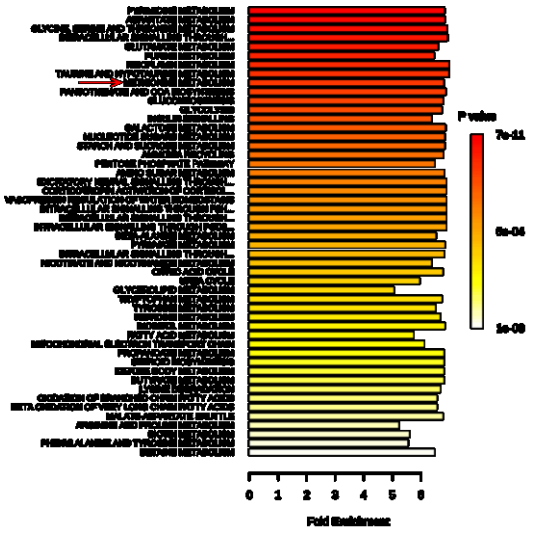

Figure 3.29. The metabolite set enrichment analysis [MSEA] (a.k.a. the pathway analysis) to establish which metabolic pathways are affected the most by the extent of calorie availability (i.e. CR vs non-CR). In this example, *tor1Δ* cells grown under CR conditions were compared to *tor1Δ* cells grown under non-CR conditions. Cells were recovered for metabolite extraction on ***Day 10 (stationary phase of culturing)***. The metabolites were separated using a ***ZIC-pHILIC column***.

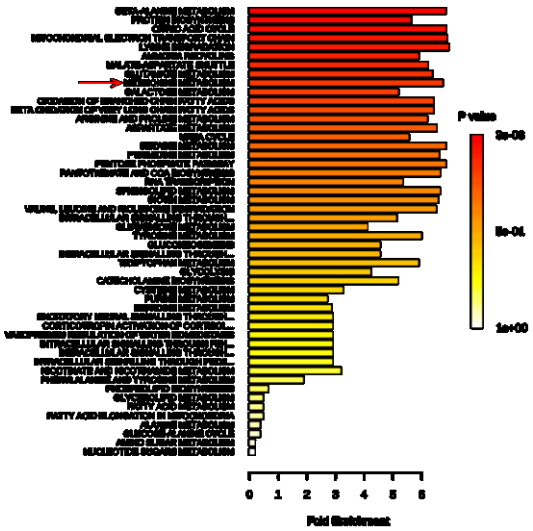

Figure 3.30. The metabolite set enrichment analysis [MSEA] (a.k.a. the pathway analysis) to establish which metabolic pathways are affected the most by the extent of calorie availability (i.e. CR vs non-CR). In this example, WT cells grown under CR conditions were compared to WT cells grown under non-CR conditions. Cells were recovered for metabolite extraction on ***Day 10 (stationary phase of culturing)***. The metabolites were separated using a **C18 column**.

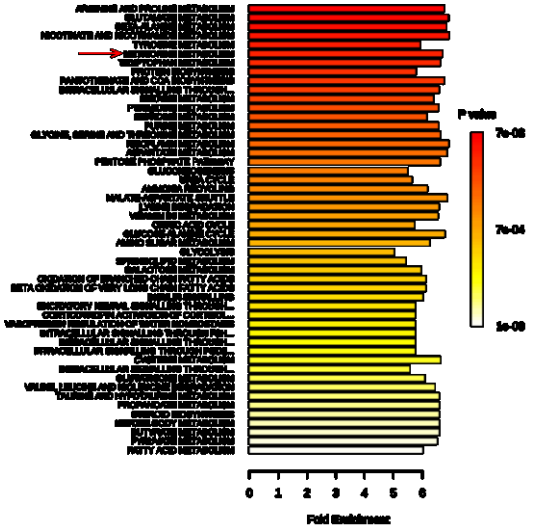

Figure 3.31. The metabolite set enrichment analysis [MSEA] (a.k.a. the pathway analysis) to establish which metabolic pathways are affected the most by the extent of calorie availability (i.e. CR vs non-CR). In this example, WT cells grown under CR conditions were compared to WT cells grown under non-CR conditions. Cells were recovered for metabolite extraction on ***Day 10 (stationary phase of culturing)***. The metabolites were separated using a ***ZIC-pHILIC column***.

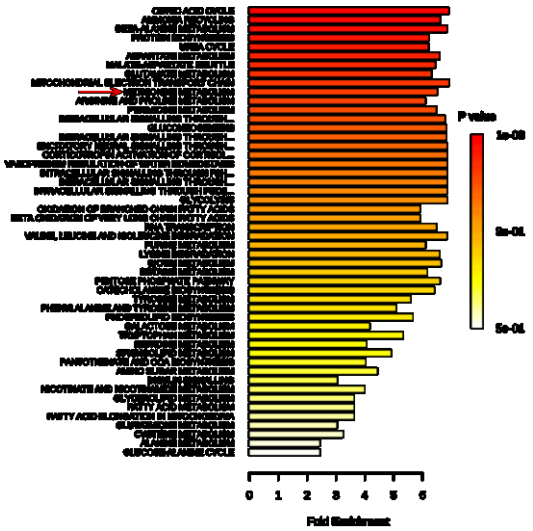

Figure 3.32. The metabolite set enrichment analysis [MSEA] (a.k.a. the pathway analysis) to establish which metabolic pathways are affected the most by the *tor1Δ* mutation. In this example, WT cells grown under non-CR conditions were compared to *tor1Δ* cells grown under non-CR conditions. Cells were recovered for metabolite extraction on ***Day 10 (stationary phase of culturing)***. The metabolites were separated using a ***C18 column***.

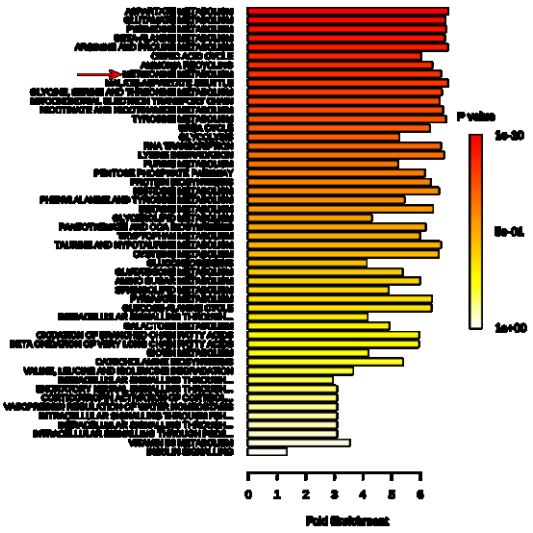

Figure 3.33. The metabolite set enrichment analysis [MSEA] (a.k.a. the pathway analysis) to establish which metabolic pathways are affected the most by the *tor1Δ* mutation. In this example, WT cells grown under non-CR conditions were compared to *tor1Δ* cells grown under non-CR conditions. Cells were recovered for metabolite extraction on ***Day 10 (stationary phase of culturing)***. The metabolites were separated using a ***ZIC-pHILIC column***.

3.3.5 In chronologically aging cells, both CR and the *tor1Δ* mutation establish a distinct pattern of methionine metabolism

The principal PCA of the concentrations of methionine metabolism intermediates in extracts of WT and *tor1Δ* cells (the metabolites were normalized to an internal standard and auto-scaled) has revealed that CR elicits a distinct pattern of methionine metabolism that significantly differs from the methionine metabolism pattern of these cells cultured under non-CR conditions. Indeed, the PCs of methionine metabolism intermediates in cells cultured under CR or non-CR conditions were well separated from each other in both WT and *tor1Δ* cells recovered on days 1, 7 and 10 of culturing (Figures 3.34-3.36). Thus, the CR-specific pattern of methionine metabolism exists in both WT and *tor1Δ* cells through all phases of the chronological aging process.

Of note, the longevity-extending *tor1Δ* mutation did not cause a significant change in the pattern of methionine metabolism in cells cultured under non-CR conditions and recovered on day 1 of culturing; this conclusion is based on the observation that the PCs of methionine metabolism intermediates in WT and *tor1Δ* cells cultured under non-CR conditions were not separated from each other (Figure 3.34). However, on days 7 and 10 of culturing, the PCs of methionine metabolism intermediates in WT and *tor1Δ* cells cultured under non-CR conditions were well separated from each other (Figures 3.35 and 3.36). Thus, the ability of the *tor1Δ* mutation to extend longevity under non-CR conditions coincides (and may cause) the ability of this mutation to remodel the pattern of methionine metabolism under these conditions.

Furthermore, the PCs of methionine metabolism intermediates in WT and *tor1Δ* cells cultured under CR conditions were not separated from each other in cells recovered on day 1, day

y and Day10 of culturing (Figures 3.34-3.36). Thus, through the entire process of chronological aging, CR establishes the same pattern of methionine metabolism in both WT and *tor1Δ* cells.

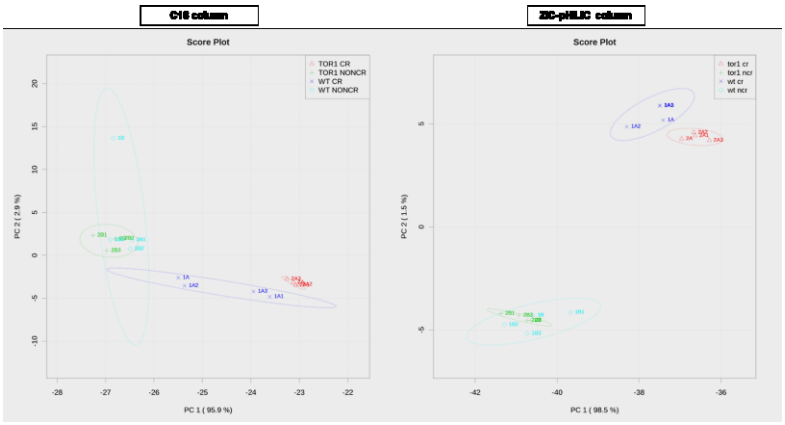

Figure 3.34. Scores plots from the principal components analysis (PCA) of the concentrations of METHIONINE METABOLISM intermediates in extracts of wild-type and *tor1Δ* cells (the metabolites were normalized to an internal standard and auto-scaled). Cells grown under CR or non-CR conditions were recovered for metabolite extraction on ***Day 1 (logarithmic phase of culturing)***.

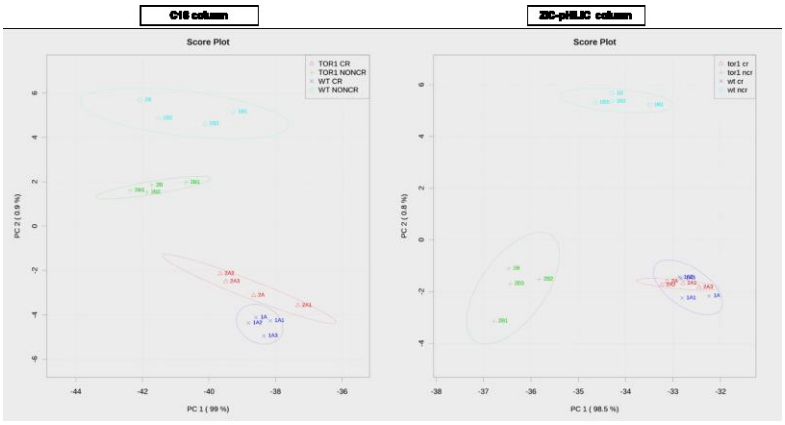

Figure 3.35. Scores plots from the principal components analysis (PCA) of the concentrations of METHIONINE METABOLISM intermediates in extracts of wild-type and *tor1Δ* cells (the metabolites were normalized to an internal standard and auto-scaled). Cells grown under CR or non-CR conditions were recovered for metabolite extraction on ***Day 7 (the end of post-diauxic/beginning of stationary phase of culturing)***.

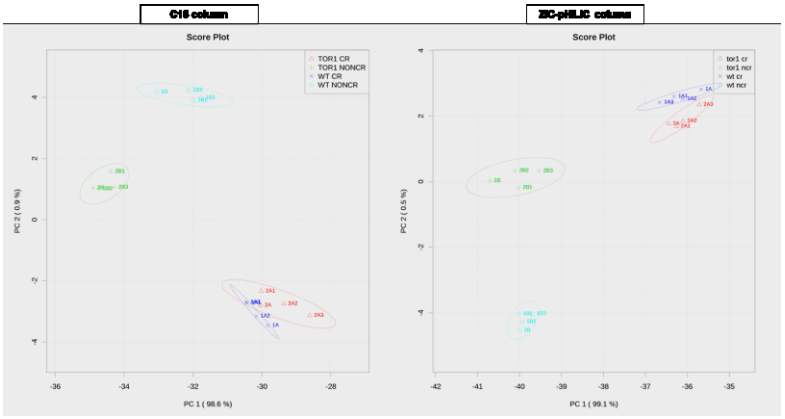

Figure 3.36. Scores plots from the principal components analysis (PCA) of the concentrations of METHIONINE METABOLISM intermediates in extracts of wild-type and *tor1Δ* cells (the metabolites were normalized to an internal standard and auto-scaled). Cells grown under CR or non-CR conditions were recovered for metabolite extraction on ***Day 10 (stationary phase of culturing)***.

3.3.6 Through the entire process of chronological aging, both CR and the *tor1Δ* mutation alter concentrations of methionine metabolism intermediates

Our LC-MS/MS analysis has revealed that CR alters concentrations of methionine metabolism intermediates in WT cells recovered on days 1, 2, 4, 7 and 10 of culturing (Figures 3.37-3.41).

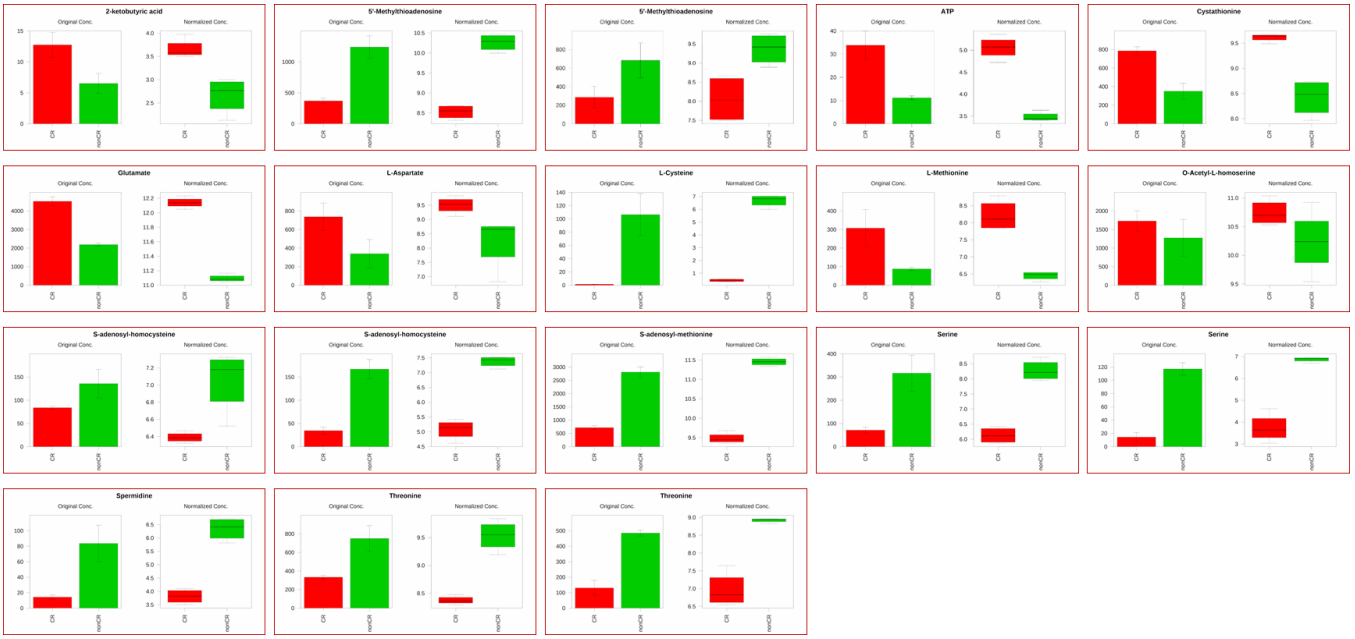

Figure 3.37. In WT cells, the CR diet alters concentrations of METHIONINE METABOLISM intermediates. Cells grown under CR or non-CR conditions were recovered for metabolite extraction on ***Day 1 (logarithmic phase).***

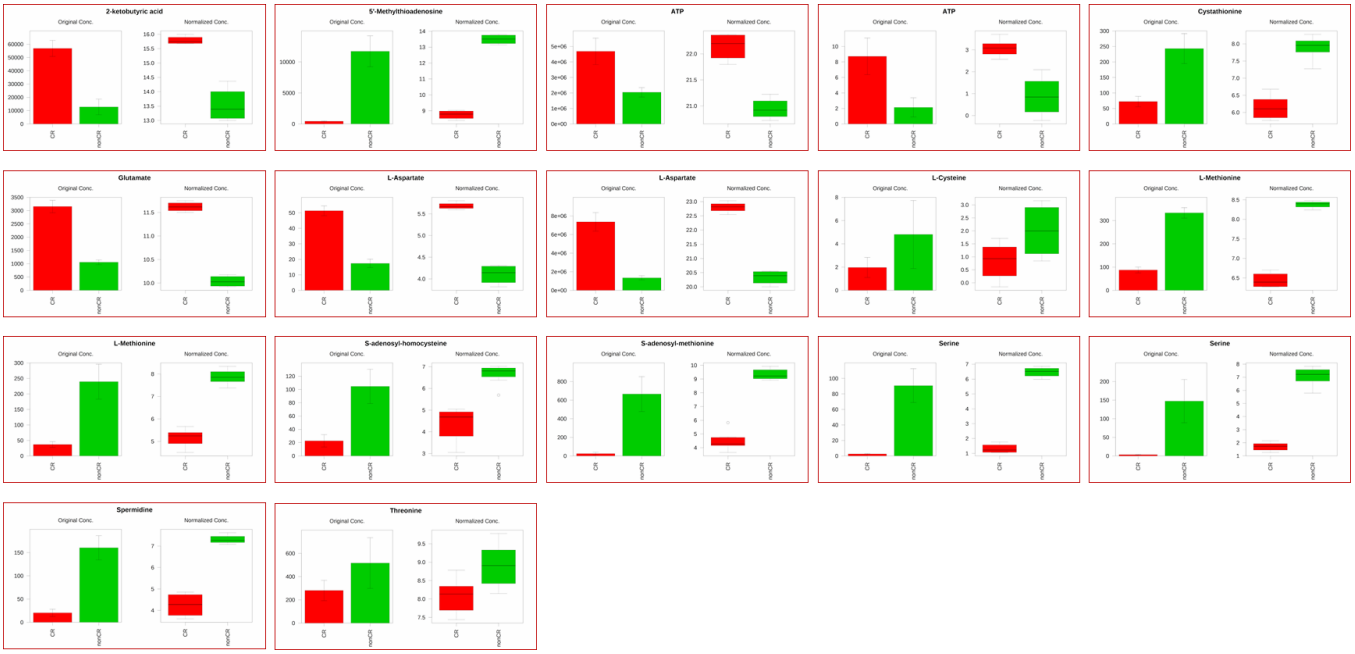

Figure 3.38. In WT cells, the CR diet alters concentrations of METHIONINE METABOLISM intermediates. Cells grown under CR or non-CR conditions were recovered for metabolite extraction on ***Day 2 (the beginning of post-diauxic phase)***.

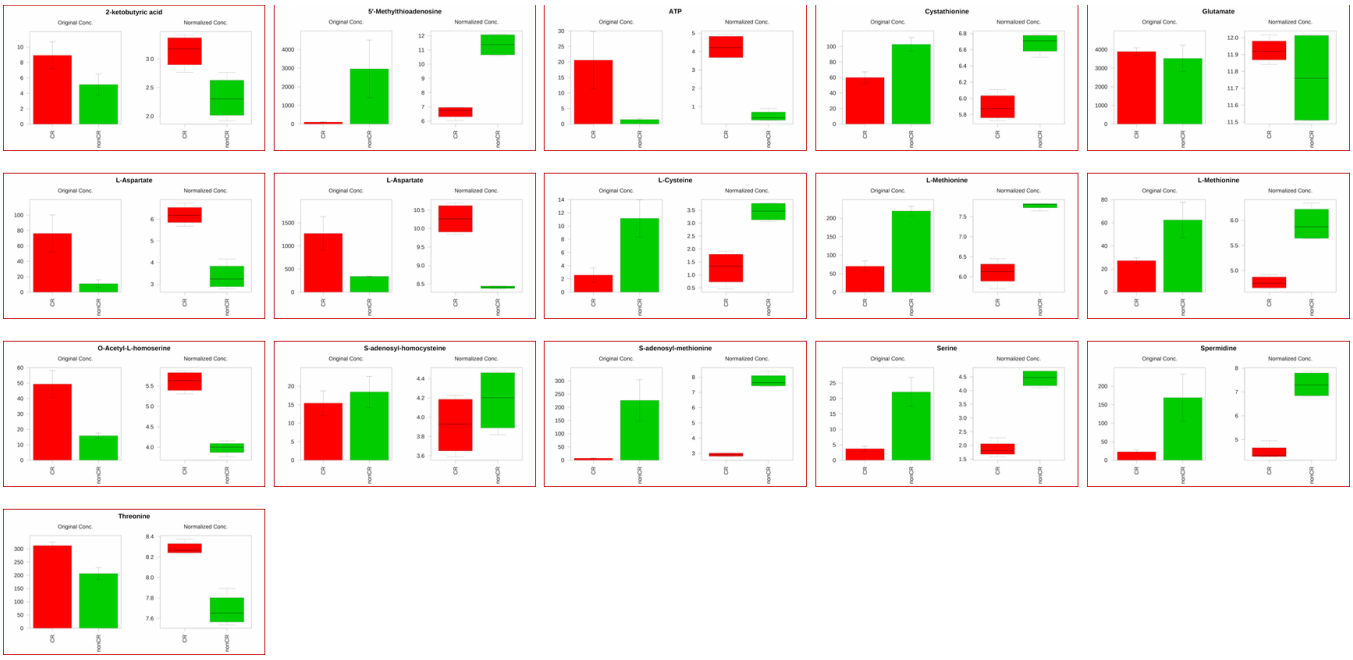

Figure 3.39. In WT cells, the CR diet alters concentrations of METHIONINE METABOLISM intermediates. Cells grown under CR or non-CR conditions were recovered for metabolite extraction on ***Day 4 (mid-post-diauxic phase)***.

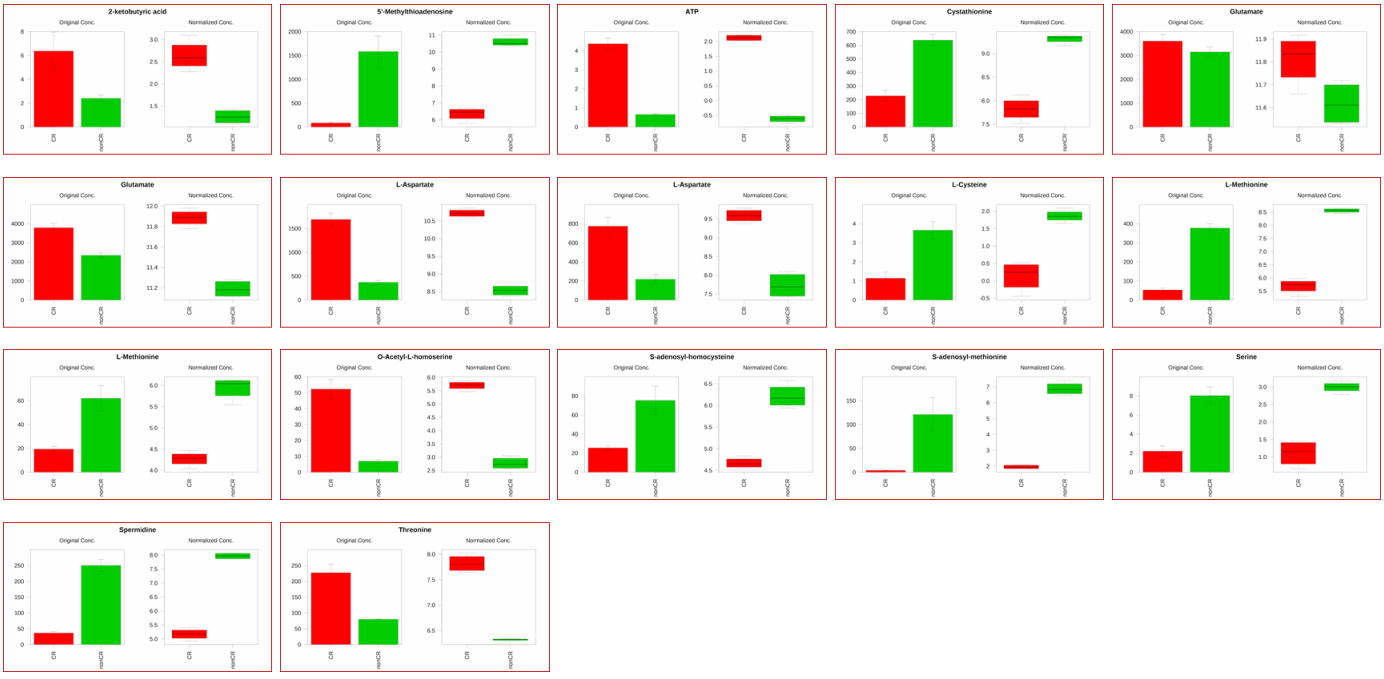

Figure 3.40. In WT cells, the CR diet alters concentrations of METHIONINE METABOLISM intermediates. Cells grown under CR or non-CR conditions were recovered for metabolite extraction on ***Day 7 (the end of post-diauxic phase/beginning of stationary phase)***.

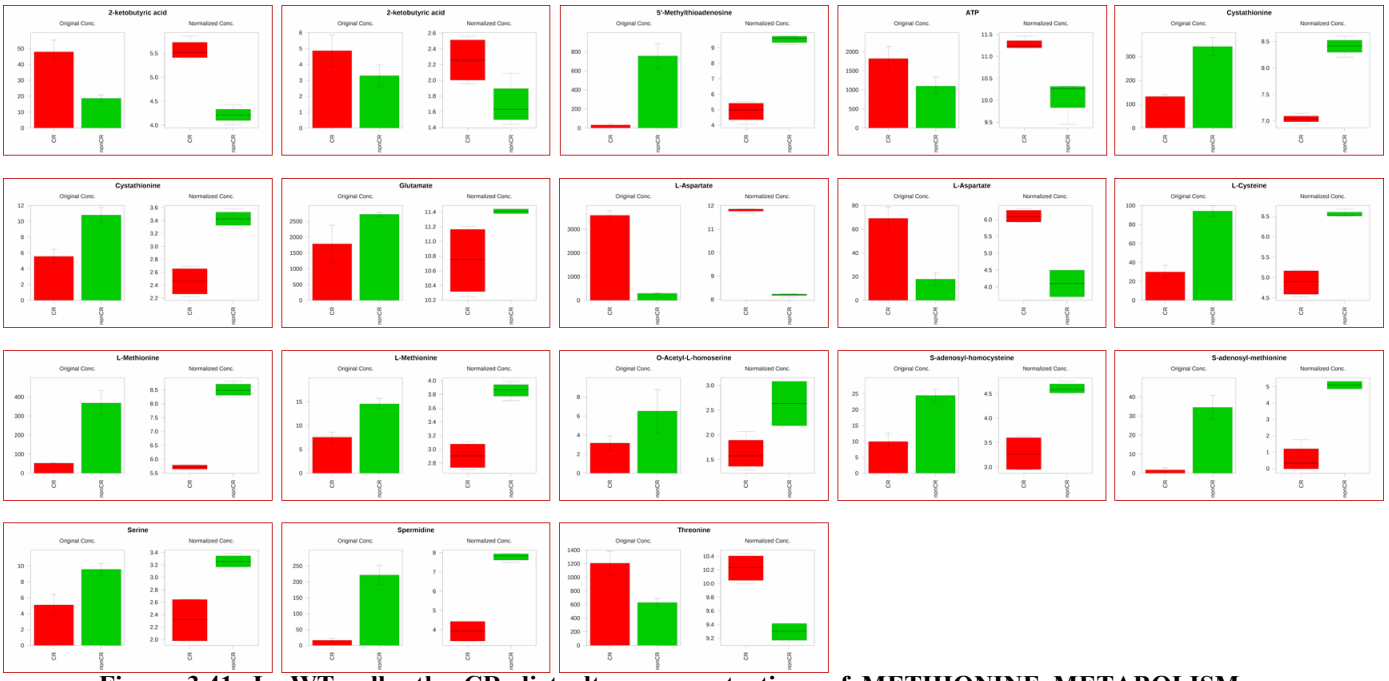

Figure 3.41. In WT cells, the CR diet alters concentrations of METHIONINE METABOLISM intermediates. Cells grown under CR or non-CR conditions were recovered for metabolite extraction on ***Day 10 (stationary phase)***.

These metabolites include ATP, 2-ketobutyric acid, 5'-methylthioadenosine, cystathionine, glutamate, aspartate, cysteine, methionine, *O*-acetyl-*L*-homoserine, *S*-adenosyl-homocysteine, *S*-adenosyl-methionine, serine, spermidine and threonine (Figures 3.37-3.41). As it has been mentioned above, these methionine metabolism intermediates comprise a network which integrates the following pathways of intermediary metabolism: 1) the biosynthesis of methionine from aspartate; 2) the biosynthesis of threonine from aspartate; 3) the biosynthesis of both cysteine and glutathione from homocysteine, an intermediate in the biosynthetic pathway for methionine; and 4) the biosynthesis of spermidine and other polyamines from S-adenosylmethionine, an intermediate in the biosynthetic pathway for methionine (Figure 3.9).

Our LC-MS/MS analysis also demonstrated that the *tor1Δ* mutation alters concentrations of methionine metabolism intermediates in chronologically aging yeast cells cultured under non-CR conditions and recovered on days 2, 7 and 10 of culturing (Table 3.2). Of note, the pattern of methionine-related metabolome that was established by the *tor1Δ* mutation was like that established by the CR diet.

Table 3.2. Cellular concentrations of METHIONINE METABOLISM intermediates are significantly increased or decreased by the *tor1Δ* mutation in yeast cultured under non-CR conditions. Cells grown under non-CR conditions were recovered for metabolite extraction on ***Day 2 (diauxic phase), Day 7 (the end of post-diauxic phase/beginning of stationary phase) and Day 10 (stationary phase)***.

	***tor1Δ*/wild-type**					
	Day 2		**Day 7**		**Day 10**	
	log2(FC)	**p-value**	**log2(FC)**	**p-value**	**log2(FC)**	**p-value**
***S*-adenosyl methionine (SAM)**	0.91	0.00338	-2.20	0.00115	-1.78	0.00030
***S*-adenosyl homocysteine**	-0.73	0.00028	-2.54	0.00047	-2.68	0.00047
Serine	-0.62	0.00740	3.82	0.00030	0.39	-
Glutamate	0.85	0.01395	0.69	0.00604	-1.13	0.03118
***L*-Aspartate**	1.73	0.00311	3.47	0.00000	3.67	0.00000
***O*-acetyl *L*-homoserine**	1.56	0.01238	1.84	0.00000	0.10	-
***L*-cysteine**	-2.73	0.00064	-0.72	-	0.85	0.00005
Spermidine	2.10	0.00589	0.87	0.04060	0.94	0.02183
Cystathionine	0.18	-	-0.38	0.03699	-0.77	0.00046
Methionine	0.97	0.03844	-1.25	0.00058	-1.78	0.00016

3.4 Discussion

Recent studies have demonstrated that a characteristic age-related remodeling of cellular metabolism may play essential roles in regulating cellular aging, influencing age-related pathologies and defining organismal longevity in evolutionarily distant eukaryotes [149, 213-227]. However, mechanisms underlying such remodeling and mechanisms by which longevity-extending dietary and genetic interventions regulate such remodeling remain unknown. This study provided the first evidence that both the longevity-extending diet CR and the-longevity extending mutation *tor1Δ* establish a similar pattern of relative concentrations of methionine metabolism intermediates through the entire process of chronological aging in *S. cerevisiae* (Figure 3.42). The methionine metabolism intermediates whose concentrations are increased by both these longevity-extending interventions include ATP, aspartate, *O*-acetyl-*L*-homoserine, glutamate and cysteine, whereas among methionine metabolism intermediates whose concentrations are decreased by both these longevity-extending interventions are threonine, methionine, serine, glutathione, spermidine, *S*-adenosyl-homocysteine and *S*-adenosyl-methionine (Figure 3.42). All these methionine metabolism intermediates are integrated into a network which integrates the following pathways of intermediary metabolism: 1) the biosynthesis of methionine from aspartate; 2) the biosynthesis of threonine from aspartate; 3) the biosynthesis of both cysteine and glutathione from homocysteine, an intermediate in the biosynthetic pathway for methionine; and 4) the biosynthesis

of spermidine and other polyamines from *S*-adenosylmethionine, an intermediate in the biosynthetic pathway for methionine (Figure 3.42).

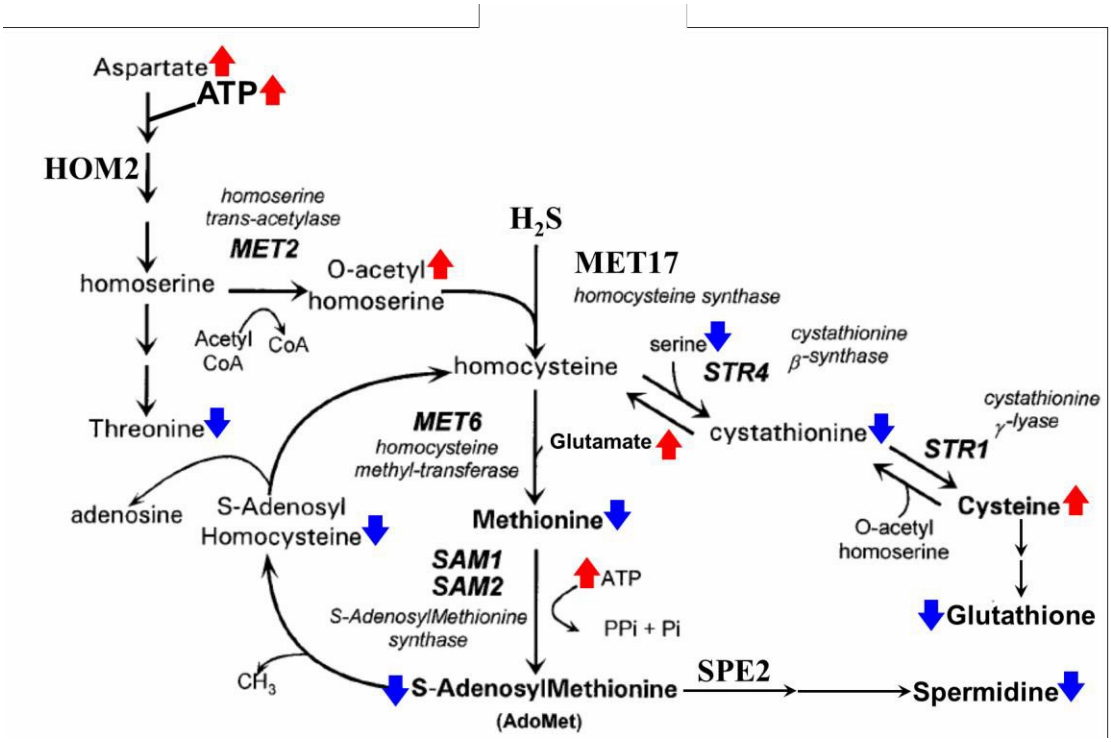

Figure 3.42. The CR diet and the *tor1Δ* mutation establish a similar pattern of methionine-related metabolome in chronologically aging yeast.

Based on these findings, we hypothesize that the observed redirection of metabolite flow within the network from the biosynthesis of methionine and spermidine to the biosynthesis of cysteine and glutathione may represent an anti-aging pattern characteristic of the ″metabolic signature″ of longevity extension in chronologically aging yeast cells placed on the CR diet or having the TOR pro-aging signaling pathway inhibited (Figure 3.42).

Future studies in the Titorenko laboratory need to address the following 2 important questions.

First, it remains unclear if the observed remodeling of methionine-related metabolome indeed represents an anti-aging ″metabolic signature″ of longevity extension in chronologically aging yeast. To address this question, it will be interesting to examine how mutations eliminating individual enzymes involved in various pathways within the network of methionine-related intermediary metabolism influence yeast longevity. The chronological lifespans of the following mutant strains will be measured under both CR and non-CR conditions: 1) *hom2Δ*, *hom3Δ* and

hom6Δ, each lacking a non-essential enzyme involved in the biosynthesis of threonine from aspartate; 2) *met2Δ*, *met6Δ*, *met7Δ*, *met17Δ*, *sam1Δ* and *sam2Δ*, each lacking a non-essential enzyme involved in the biosynthesis of methionine from homoserine; 3) *spe2Δ* and *spe3Δ*, each lacking a non-essential enzyme involved in the biosynthesis of spermidine and other polyamines from *S*-adenosylmethionine; 4) *cys3Δ* and *cys4Δ*, each lacking a non-essential enzyme involved in the biosynthesis of cysteine from homocysteine and serine; 5) *str2Δ* and *str3Δ*, each lacking a non-essential enzyme involved in the conversion of cysteine to homocysteine; and 6) *gsh1Δ* and *gsh2Δ*, each lacking a non-essential enzyme involved in the biosynthesis of glutathione from cysteine [212]. LC-MS/MS will then be used to determine the concentrations of various intermediates within the network of methionine-related intermediary metabolism in cells of each of these mutants recovered at different stages of the aging process under CR and non-CR conditions. If mutations that reverse the proposed anti-aging ″metabolic signature″ decrease the extent of longevity extension by CR, whereas mutations that enhance the proposed anti-aging ″metabolic signature″ increase the extent of longevity extension by CR, our hypothesis on the existence of the ″metabolic signature″ of longevity extension in chronologically aging yeast will be confirmed.

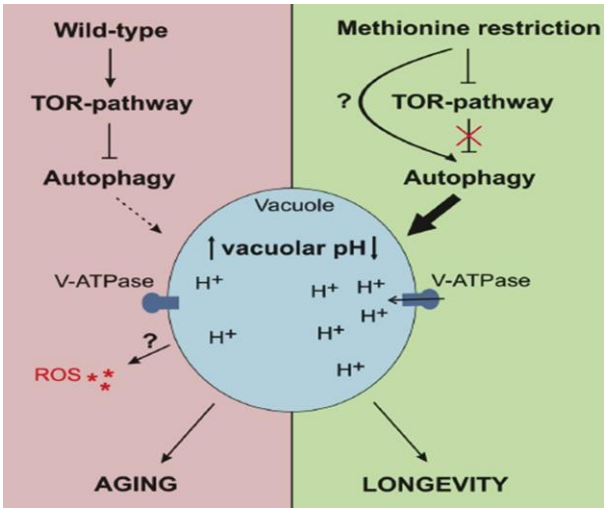

Figure 3.43. Methionine restriction extends longevity of chronologically aging yeast by attenuating the pro-aging TOR pathway, thereby stimulating autophagy-dependent acidification of vacuoles [228].

Second, it remains unclear how the observed remodeling of methionine-related metabolome may delay yeast chronological aging and extend yeast longevity. A recent study has revealed that methionine restriction extends longevity of chronologically aging yeast by attenuating the pro-aging TOR pathway, thereby stimulating autophagy-dependent acidification of vacuoles (Figure 3.43) [228]. A decreased concentration of methionine is one of the characteristic

features of the observed remodeling of methionine-related metabolome (Figure 3.42). Therefore, it will be interesting to investigate how mutations eliminating individual enzymes involved in various pathways within the network of methionine-related intermediary metabolism (see above) influence the following: 1) functional states of protein components of the TOR pathway and their phosphorylation status; 2) the extent of vacuole acidification; and 3) the intensity of autophagic vesicular flow.

4 LCA-dependent changes in mitochondrial lipidome alter mitochondrial proteome and increase the geroprotective efficiency of LCA in chronologically aging yeast

4.1 Introduction

As described in the ″Introduction″ section, studies in the Titorenko laboratory have revealed that in chronologically aging yeast under CR conditions exogenously added LCA delays yeast chronological aging, enters the yeast cell, is sorted to mitochondria, resides in both mitochondrial membranes, changes the relative concentrations of different membrane phospholipids, triggers changes in the concentrations of many mitochondrial proteins, and alters some key aspects of mitochondrial functionality. Based on the above findings, we hypothesized that the LCA-driven changes in mitochondrial lipidome may have a causal role in the age-related remodeling of proteome, thus eliciting changes in mitochondrial functionality and delaying yeast chronological aging. The objectives of studies described in this chapter was to test this hypothesis by investigating how certain mutations that eliminate enzymes involved in mitochondrial phospholipid metabolism influence the mitochondrial proteome and how they affect the geroprotective efficiency of LCA in chronologically aging yeast.

4.2 Materials and methods

4.2.1 Yeast strains, media and growth conditions

The wild-type (WT) strain *Saccharomyces cerevisiae* BY4742 (*MATα his3Δ1 leu2Δ0 lys2Δ0 ura3Δ0*) and the *ups1Δ* and *ups2Δ* single-gene-deletion mutant strains in the BY4742 genetic background from Open Biosystems/Dharmacon (a part of GE Healthcare) were grown in YP medium (1% yeast extract, 2% peptone; both from Fisher Scientific; #BP1422-2 and #BP1420-2, respectively) initially containing 0.2% (w/v) glucose (#D16-10; Fisher Scientific) with 50 μM LCA or without it. Cells were cultured at 30ºC with rotational shaking at 200 rpm in Erlenmeyer flasks at a ″flask volume/medium volume″ ratio of 5:1.

4.2.2 Purification of mitochondria

Yeast cells were harvested at 3,000 × g for 5 min at room temperature, washed with water and resuspended in DTT buffer (100 mM Tris-H_2SO_4, pH 9.4, 10 mM dithiothreitol [DTT]). The cells were then incubated in DTT buffer for 20 min at 30°C to weaken the cell wall. The cells were

washed with Zymolyase buffer (1.2 M sorbitol, 20 mM potassium phosphate, pH 7.4) and centrifuged at 3,000 × g for 5 min at room temperature. The cells were then incubated with 3 mg/g (wet weight) of Zymolyase-100T in 7 ml/g (wet weight) Zymolyase buffer for 45 min at 30°C. Following an 8-min centrifugation at 2,200 × g at 4°C, the isolated spheroplasts were washed in ice-cold homogenization buffer (5 ml/g) (0.6 M sorbitol, 10 mM Tris-HCl, pH7.4, 1 mM EDTA, 0.2% (w/v) BSA) and centrifuged at 2,200 × g for 8 min at 4°C. The spheroplasts were homogenized in ice-cold homogenization buffer using 15 strokes. Cell debris was removed by centrifuging the resulting homogenates at 3,000 × g for 10 min at 4°C. The resulting supernatant was then centrifuged at 12,000 × g for 15 min at 4°C to pellet mitochondria. The remnant cell debris was removed by centrifuging the mitochondrial fraction at 3,000 × g for 5 min at 4°C. The resulting supernatant was centrifuged at 12,000 × g for 15 min at 4°C to obtain the crude mitochondrial pellet, which was then resuspended in 3 ml of SEM Buffer (250 mM sucrose, 1 mM EDTA, 10 mM MOPS, pH 7.2) and used for further purification of mitochondria. A sucrose gradient was made by overlaying 1.5 ml of 60% sucrose with 4 ml of 32% sucrose, 1.5 ml of 23% sucrose, and then 1.5 ml of 15% sucrose (all in EM buffer; 1 mM EDTA, 10 mM MOPS, pH 7.2). Finally, a 3-ml aliquot of the crude mitochondrial fraction in SEM buffer was applied to the gradient and centrifuged at 134,000 × g (33,000 rpm) for three hours at 4°C in vacuum (Rotor SW40Ti, Beckman). The purified mitochondria found at the 60%/32% sucrose interface were carefully removed and stored at - 80°C until mass spectrometric identification of phosphorylated mitochondrial proteins.

4.2.3 Identification and quantification of proteins by mass spectrometry (MS)

Protein bands stained with QC Colloidal Coomassie Blue was cut out from an SDS-PAGE gel with a razor blade. The gel pieces were placed in individual 0.5-ml siliconized Eppendorf tubes. The bands were destained by washing twice with distilled water for 1 h. The bands were then incubated in 50 µl of acetonitrile (ACN) for 5 min at 37°C, after which ACN was removed and the bands were dried at 37°C. Next, the destained bands were incubated in 50 µl of 10 mM dithiothreitol for 30 min at 37°C to reduce thiol groups in peptides. DTT was discarded and the bands were incubated in 50 µl of 55 mM iodoacetamide (IAA) for 20 min at 37°C in the dark to remove the residual DTT. IAA was removed, and the bands were incubated in 50 µl of a 1:1 mixture of 100 mM ABC and 50% acetonitrile for 10 min at 37°C. The mixture was discarded,

and the bands were incubated twice in 50 µl of ACN under the same conditions and dried at 37°C. The trypsin and trypsin buffer were prepared as follows: (1) 1.6 ml of a 1:1 mixture of 100 mM ABC and 10mM $CaCl_2$ were used to resuspend 20 µg of trypsin; and (2) for protein digest, 50 µl of trypsin solution (1 mg/ml) was added to the bands, which were then incubated overnight at 37°C.

The following day, the samples were spun down and the supernatants containing peptides were transferred to new 0.5-ml siliconized Eppendorf tubes. To extract more peptides, the gel pieces were subjected to several washes and treatments at room temperature; the supernatants were conserved and combined with the first set to extracted peptides. For the first extraction, the bands were initially incubated in 50 µl of 25 mM ABC for 10 min and then in 50 µl of ACN for 10 min. The samples were spun down, and the supernatant were added to the first set of extracted peptides. For the second extraction, the bands were incubated in 50 µl of 5% formic acid for 10 min and then in 50 µl of ACN for 10 min. The samples were spun down, and the supernatant were combined with the first set of extracted peptides. The gel pieces were no longer used and discarded. To prevent possible oxidation during storage, 12.5 µl of 100 mM DTT was added to each set of peptides. The peptides were completely dried in a Speed-Vac at medium temperature settings (37°C) for 2 h and stored at -20°C until MS analysis.

Dried peptides were resuspended in 20 µl of 5% ACN. For each recovered protein band, an aliquot of 10 µl of dried peptides in 5% ACN was diluted 2-fold in Nano pure water for MS analysis. Samples can be stored at -20°C until being subjected to MS analysis. Individual proteins composing each band were then identified by reverse phase high performance liquid chromatography coupled to mass spectrometry (RP-HPLC/MS) using an LTQ Orbitrap. 3-µl aliquots of peptides were separated in ACN gradient using a 100-µM capillary column packed with C18 mobile phase.

Once acquiring time was completed using the LTQ Orbitrap, the raw mass spectrometry data file obtained by Xcalibur were analyzed using the Thermo Scientific Xcalibur Proteome Discoverer application (version 1.3) hereafter referred to as the Proteome Discoverer. The Proteome Discoverer was used to identify individual proteins by comparing the raw data of mass spectra of digested fragments to the mass spectra of peptides within the Uniprot FASTA database. The analysis by the Proteome Discoverer coupled to the FASTA database was enabled by using

the peak-finding search engine SEQUEST. The SEQUEST engine processes MS data using a peak-finding algorithm to search the raw data for generating a peak probability list with relative protein abundances.

The following settings of the SEQUEST search wizard within the Proteome Discoverer application were used:

Raw file and Scan Range Selection Parameters: The raw file was selected, and the Base peak ion chromatogram appeared to reveal: 1) the "Intensity (counts)" corresponding to the intensity of the largest peak in the spectrum; and 2) the "Time (min)" showing the retention time (RT). The following algorithm and settings were used:

Lower RT Limit (min): The beginning of the RT of the scan range of interest: 10 min.

Upper RT Limit (min): The end of the retention time of the scan range of interest: 18 min.

Scan Extraction Parameters

First mass: The mass of the first precursor ion in the range of ion fragments to search for in the database: 350 Daltons (Da).

Last mass: The mass of the last precursor ion in the range of ion fragments to search for in the database: 5000 Daltons (Da).

Activation type: The fragmentation method to use for activating the scan: Collision Induced Dissociation (CID).

Unrecognized charge replacement: Specifies the charge number of the precursor ions: Automatic (Default), assigns a charge number of +2 and +3 to the spectrum.

Intensity threshold: Specifies the intensity threshold below which ions are filtered out. The default value of 0.0 was used.

Minimum ion count: The minimum ion count corresponds to the minimum number of ions that must be present in an MS/MS spectrum for it to be included in a search. The default value of 1 was used.

S/N threshold: The signal-to-noise threshold is the intensity of the signal to the intensity of the background noise. The use of this threshold filters out low-intensity ions that function as a noise. The value of 1.5 was used.

Database: Uniprot_sprot FASTA

Enzyme: Trypsin

Missed Cleavages: The maximum number of internal cleavage sites per peptide fragment that is acceptable for an enzyme to miss during proteolytic digest. The default value of 2 was used.

Precursor mass tolerance: The precursor mass tolerance value used for finding peptide candidates. The possible range of values is 0.01 to 5000 ppm. The default value of 10 ppm was used.

Fragment mass tolerance: The default mass tolerance value of 0.8 Da was used for matching fragment peaks. The possible range of values was 0.0001 to 2.0 Da.

Ions series calculated: Specifies the ion factors for a, b, c, x, y, and z ions for the experiment type. The possible range is 0 through 1.0 for all ion factors. The ion factors used are b ions: 1 and y ions :1.

Search against decoy database: Specifies if the application uses a decoy database in the search; the "yes" was used.

Target FDR (strict): Specifies a strict target false discovery rate (FDR) for peptide matches with high confidence. The possible value range of 0.0 to 1.0 was used. The default value of 0.01 (1% FDR) was used.

Target FDR (relaxed): Specifies a relaxed target false discovery rate (FDR) for peptide matches with moderate confidence. The possible value ranges from 0.0 to 1.0 was used. The default value of 0.05 (5% FDR) was used.

The Thermo Proteome Search Results Report for the identification of proteins was created. The protein page displays all the proteins and their corresponding peptides found in the sample during the database search. For each protein, the report shows the following results:

Accession: The unique identifier was assigned to the protein by the Uniprot FASTA database.

Description: The name and description of the protein of the identifier appeared in the corresponding Accession column.

Score: The SEQUEST protein score is the sum of all peptide XCorr values above the specified score threshold. The score threshold was calculated as *"0.8 + peptide charge * peptide relevance factor", where peptide relevance factor* has a default value of 0.4. For each spectrum, only the highest-scoring match was used. For each spectrum and sequence, the Proteome Discoverer application uses only the highest scored peptide.

Coverage: Represents the percentage of the protein sequence covered by the identified peptides.

 # Proteins: Represents the number of identified proteins in the protein group of a master protein. When the Protein Grouping setting is disabled, the #Proteins is always equal to 1.

 # Unique Peptides: Represents the number of peptide sequences unique to a protein.

 # Peptides: Represents the number of different peptide sequences identified in the protein.

 # PSMs: The peptide spectrum matches (PSMs) value corresponds to the total number of identified peptide sequences for the protein, including those that have been identified redundantly.

 # AAs: Represents the number of amino acid in the sequence length of the protein.

MW kDa: Represents the calculated molecular weight of the protein.

Calc. pI: Represents the theoretically calculated isoelectric point, *i.e.* the pH value at which a molecule carries no net electrical charge.

Peptides Results Parameters: For each identified peptide, the report shows the following results:

Protein Descriptions: Identifies a protein associated with the peptides. This description is taken from the Uniprot FASTA file.

 # Proteins: Represents the total number of proteins in which this peptide can be found.

Probability: Represents the probability score for the peptide.

SpScore (search-dependent): Represents the raw value of the preliminary score of the SEQUEST algorithm.

XCorr (search-dependent): Scores the number of fragment ions that are common to two different peptides with the same precursor mass; calculates the cross-correlation score for all candidate peptides queried from the database.

Δ Score: A measure of the difference between the top two scores for the peptides identified by that spectrum; the Proteome Discoverer application calculates this score as follows: ΔScore = Score (Rank N Peptide) – Score (Rank 1 Peptide)/Score (Rank 1 Peptide).

ΔCn: Represents the normalized score difference between the currently selected PSM and the highest-scoring PSM for that spectrum.

 # Missed Cleavages: Represents the number of cleavage sites in a peptide sequence that trypsin did not cleave, excluding the cases where the presence of proline prevents trypsin from cleaving the peptide bond.

Peptides Matched: Represents the number of peptides included in the precursor mass tolerance window set for the search.

Charge: Represents the charge state of the peptide.

Intensity: Represents the intensity of the precursor ion.

MH+ ^{Da}: Represents the protonated monoisotopic mass of the peptide, in Daltons.

ΔM ^{ppm}: Represents the difference between the theoretical mass of the peptide and the experimental mass of the precursor ion.

RT ^{min}: Represents the retention time when the peptide was observed, in minutes.

Xcalibur is a registered trademark of Thermo Fisher Scientific Inc. in the United States. SEQUEST is a registered trademark of the University of Washington in the United States.

The ″Proteome Discoverer″ software was used to calculate the exponentially modified protein abundance index (emPAI), a measure of the relative abundance of mitochondrial proteins in a pair of analyzed datasets.

4.2.4 A plating assay for the analysis of chronological lifespan

Cells were grown in YEPD (0.2% glucose) medium at 30ºC with rotational shaking at 200 rpm in Erlenmeyer flasks at a flask volume/medium volume ratio of 5:1. A sample of cells was removed from each culture at various time points. A fraction of the cell sample was diluted to determine the total number of cells per ml of culture using a hemacytometer. 10 µl of serial dilutions (1:10 to $1:10^3$) of cells were applied to the hemacytometer, where each large square is calibrated to hold 0.1 µl. The number of cells in 4 large squares was then counted and an average was taken to ensure greater accuracy. The concentration of cells was calculated as follows: number of cells per large square x dilution factor x 10 x 1,000 = total number of cells per ml of culture. A second fraction of the cell sample was diluted and serial dilutions ($1:10^2$ to $1:10^5$) of cells were plated onto YEPD (2% glucose) plates in triplicate to count the number of viable cells per ml of each culture. 100 µl of diluted culture was plated onto each plate. After a 48-h incubation at 30ºC, the number of colonies per plate was counted. The number of colony forming units (CFU) equals to the number of viable cells in a sample. Therefore, the number of viable cells was calculated as follows: number of colonies x dilution factor x 10 = number of viable cells per ml. For each culture assayed, % viability of the cells was calculated as follows: number of viable cells per ml / total number of cells per ml x 100%. The % viability of cells in mid-logarithmic phase was set at 100%

viability for that culture. The life span curves for wild-type and some of the mutant strains were also validated using a LIVE/DEAD yeast viability kit (Invitrogen) following the manufacturer's instructions for stationary-phase cultures.

4.2.5 Statistical analysis

Statistical analysis was performed using Microsoft Excel's (2010) Analysis ToolPak - VBA. All data on cell survival are presented as mean ± SEM. The p values for comparing the means of two groups using an unpaired two-tailed *t* test were calculated with the help of the GraphPad Prism 7 statistics software. The logrank test for comparing each pair of survival curves was performed with GraphPad Prism 7. Two survival curves were considered statistically different if the *p* value was less than 0.05.

4.3 Results

4.3.1 The concentrations of membrane phospholipids in yeast mitochondria depends on several processes of phospholipid synthesis and transfer

A spatiotemporal dynamic of processes that define the relative concentrations of different classes of membrane phospholipids in yeast mitochondria is well-understood [152, 229-235]. These processes are catalyzed by enzymes that reside in both mitochondria and the endoplasmic reticulum (ER). These processes include the following steps of phospholipid synthesis and transfer: 1) the synthesis of phosphatidic acid (PA), cytidine diphosphate-diacylglycerol (CDP-DAG), diacylglycerol (DAG), phosphatidylserine (PS), phosphatidylcholine (PC) and phosphatidylinositol (PI) in the ER; 2) the movement of PA from the ER to the OMM through mitochondria-ER contact sites at zones of a juxtaposition between the OMM and the mitochondria-associated membrane (MAM) domain of the ER; 3) the transfer of PA from the OMM across the intermembrane space (IMS) to the IMM, which is catalyzed by the Ups1/Mdm35 protein complex and inhibited by CL; 4) the conversion of ER-derived PA into CDP-DAG, phosphatidylglycerol-phosphate (PGP), phosphatidylglycerol (PG), cardiolipin (CL) and monolysocardiolipin (MLCL) in a series of reactions that are catalyzed by Tam41, Pgs1, Gep4, Crd1, Cld1 and Taz1 (respectively) in the IMM; 5) the transfer of PS from the ER to the OMM via mitochondria-ER contact sites by an unidentified mechanism; 6) the Ups2/Mdm35-dependent transport of PS from

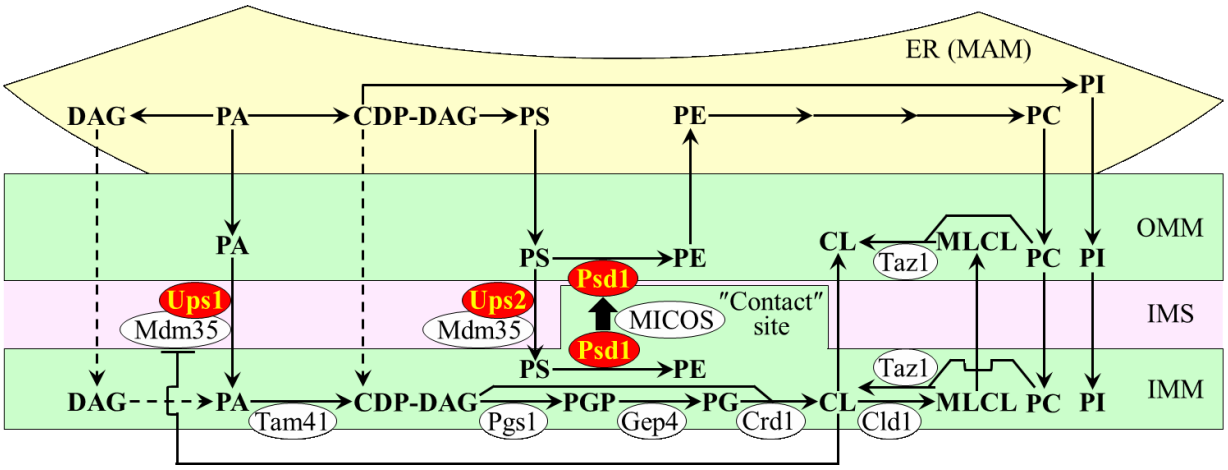

Figure 4.1. The relative concentrations of different classes of membrane phospholipids in yeast mitochondria depend on several processes of phospholipid synthesis and transfer. These processes are catalyzed by enzymes that reside in the inner mitochondrial membrane (IMM), intermembrane space (IMS), outer mitochondrial membrane (OMM) and endoplasmic reticulum (ER). Only enzymes catalyzing these processes in the IMM, IMS and OMM are shown. A T bar denotes a cardiolipin (CL)-dependent inhibition of phosphatidic acid (PA) transfer from the OMM across the IMS to the IMM. In this study we investigated various effects of single-gene-deletion mutations that eliminate enzymes displayed in red color. See text for more details. Abbreviations: CDP-DAG, cytidine diphosphate-diacylglycerol; DAG, diacylglycerol; MAM, the mitochondria-associated membrane domain of the ER; MICOS, the mitochondrial contact site protein complex; MLCL, monolysocardiolipin; PC, phosphatidylcholine; PG, phosphatidylglycerol; PGP, phosphatidylglycerol-phosphate; PI, phosphatidylinositol; PS, phosphatidylserine. This figure was prepared by Anna Leonov and me. It has been published in Leonov A, Arlia-Ciommo A, Bourque SD, Koupaki O, Kyryakov P, Dakik P, McAuley M, Medkour Y, Mohammad K, Di Maulo T, Titorenko VI. Specific changes in mitochondrial lipidome alter mitochondrial proteome and increase the geroprotective efficiency of lithocholic acid in chronologically aging yeast. Oncotarget. 2017; 8(19):30672-91.

the OMM via the IMS to the IMM, where PS is converted into phosphatidylethanolamine (PE) in a reaction catalyzed by Psd1; 7) the synthesis of PE from PS in the OMM, which is catalyzed by Psd1, requires a close apposition between the two mitochondrial membranes and is assisted by the mitochondrial contact site (MICOS) protein complex; 8) the transfer of PC and PI from the ER to the OMM via mitochondria-ER contact sites, which is followed by the movement of PC and PI from the OMM to the IMM; mechanisms of both these processes remain obscure; and 9) the movement of DAG and CDP-DAG from the ER to the OMM across mitochondria-ER contact sites, and the subsequent transfer of these two phospholipids to the IMM by currently unknown mechanisms (Figure 4.1) [152, 229-235].

4.3.2 The *ups1Δ* and *ups2Δ* mutations differently alter mitochondrial membrane lipidome and have different effects on the geroprotective efficiency of LCA

Studies by Anna Leonov, a former Doctoral student in the Titorenko laboratory, have demonstrated that, in cells cultured with or without LCA, the *ups1Δ* mutation (which eliminates a

component of the Ups1/Mdm35 protein complex involved in the transfer of PA from the OMM across the IMS to the IMM; Figure 4.1) exhibits the following effects on mitochondrial membrane lipidome: 1) it increases the PA/PS, PA/PC and PA/PI ratios for non-bilayer forming PA vs. bilayer forming PS, PC and PI; 2) it does not alter the PE/PS, PE/PC and PE/PI ratios for non-bilayer forming PE vs. PS, PC and PI; 3) it decreases the CL/PS, CL/PC and CL/PI ratios for non-bilayer forming CL vs. PS, PC and PI; 4) it does not change the PS/PI, PS/PC and PI/PC ratios for all these bilayer forming phospholipid classes; and 5) it increases the PA/PE, PA/CL and PE/CL ratios for all these non-bilayer forming phospholipid classes [236]. Thus, while the *ups1Δ* mutation alters the relative to each other concentrations for all non-bilayer forming phospholipids, it has no effect on the relative to each other concentrations for phospholipids that exhibit the bilayer forming shape. Of note, PA, PE and CL are phospholipid classes that have the non-bilayer forming shape of a cone; they increase the extent of membrane curving for the IMM, thereby raising the abundance of mitochondrial cristae (formed by the IMM) and mitochondrial contact cites (formed between the IMM and OMM) [64, 234, 235, 237-242]. In contrast, PS, PC and PI are phospholipid classes that exhibit the bilayer forming shape of a cylinder; they decrease the extent of membrane curving for the IMM, thus 1) increasing the abundance of the IMM domains having ″flat″ bilayer conformation; 2) decreasing the abundance of the IMM domains exhibiting negative curvature typical of mitochondrial contact sites; and 3) decreasing the abundance of the IMM domains displaying positive curvature characteristic of mitochondrial cristae [64, 234, 235, 237-242].

Anna Leonov has also found that the *ups1Δ* mutation 1) significantly shortens yeast chronological lifespan (CLS) in the absence of LCA; and 2) substantially lowers the geroprotective efficiency of LCA by almost eliminating the ability of LCA to increase both the mean and the maximum CLS [236].

Anna Leonov's studies also revealed that, in cells cultured in the presence or absence of LCA, the *ups2Δ* mutation (which eliminates a component of the Ups2/Mdm35 protein complex involved in the transfer of PS from the OMM across the IMS to the IMM; Figure 4.1) exhibits the following effects on mitochondrial membrane lipidome: 1) it raises the PA/PS, PA/PC and PA/PI ratios for non-bilayer forming PA vs. bilayer forming PS, PC and PI; 2) it lowers the PE/PS, PE/PC and PE/PI ratios for non-bilayer forming PE vs. PS, PC and PI; 3) it lessens the CL/PS, CL/PC and CL/PI ratios for non-bilayer forming CL vs. PS, PC and PI; 4) it does not alter the PS/PI, PS/PC and PI/PC ratios for all these bilayer forming classes of phospholipids; 5) it rises the PA/PE and

PA/CL ratios for all these non-bilayer forming phospholipid classes; and 6) it does not alter the PE/CL ratio for these two non-bilayer forming phospholipids [236]. Thus, unlike the *ups1Δ* mutation, *ups2Δ* allows to maintain the equimolar concentrations of two non-bilayer forming phospholipids, PE and CL, by proportionally decreasing their concentrations.

According to Anna Leonov's data, the *ups1Δ* mutation 1) extends yeast CLS in the absence of LCA; and 2) significantly amplifies the geroprotective efficiency of LCA by enhancing the ability of this bile acid to increase both the mean and the maximum CLS [236].

Based on these findings, it was suggested (and then confirmed by other studies in the Titorenko laboratory) that the *ups2Δ* mutation may slow down yeast chronological aging and increase the geroprotective efficiency of LCA because it establishes a distinctive aging-delaying pattern of mitochondrial lipidome [236]. This *ups2Δ*-specific pattern may consist of the following distinct changes in the relative concentrations of different phospholipid classes: 1) an increase of the PA/PS, PA/PC and PA/PI ratios for non-bilayer forming PA vs. bilayer forming PS, PC and PI; 2) a decrease of the PE/PS, PE/PC and PE/PI ratios for non-bilayer forming PE vs. bilayer forming PS, PC and PI; 3) a decline of the CL/PS, CL/PC and CL/PI ratios for non-bilayer forming CL vs. bilayer forming PS, PC and PI; and 4) a rise of the PA/PE and PA/CL ratios for these non-bilayer forming classes of phospholipids [236].

4.3.3 The *ups1Δ* and *ups2Δ* mutations alter the concentrations of many mitochondrial proteins in yeast cultured with or without LCA

Based on the above findings, we hypothesized that the LCA-dependent creation and preservation of a distinctive pro-longevity pattern of mitochondrial lipidome may cause a remodeling of mitochondrial proteome to establish a pro-longevity pattern of mitochondrial protein composition. To test this hypothesis, we used quantitative mass spectrometry to compare the identities and relative concentrations of proteins that were recovered in mitochondria purified from WT, *ups1Δ* and *ups2Δ* cells cultured with or without LCA. The *ups1Δ* mutation establishes and maintains a distinct pro-aging pattern of mitochondrial lipidome, shortens CLS, and lowers the geroprotective efficiency of LCA (see above; [236]). In contrast, the *ups2Δ* mutation institutes and preserves a specific pro-longevity pattern of mitochondrial lipidome, extends CLS, and amplifies the geroprotective efficiency of LCA (see above; [236]).

We found that both mutations, *ups1Δ* and *ups2Δ*, alter the age-related chronology of changes in concentrations of numerous mitochondrial proteins in yeast cultured in the presence of LCA or in its absence; these proteins have been implicated in many essential mitochondrial functions (see Figure 4.2 and Suppl. Tables S1 - S9 for *ups1Δ* on http://www.oncotarget.com/index.php?journal=oncotarget&page=rt&op=suppFiles&path[]=16766&path[]=0, andFigure 4.3 and Suppl. Tables S10 – S15 for *ups2Δ* on http://www.oncotarget.com/index.php?journal=oncotarget&page=rt&op=suppFiles&path[]=16766&path[]=0).

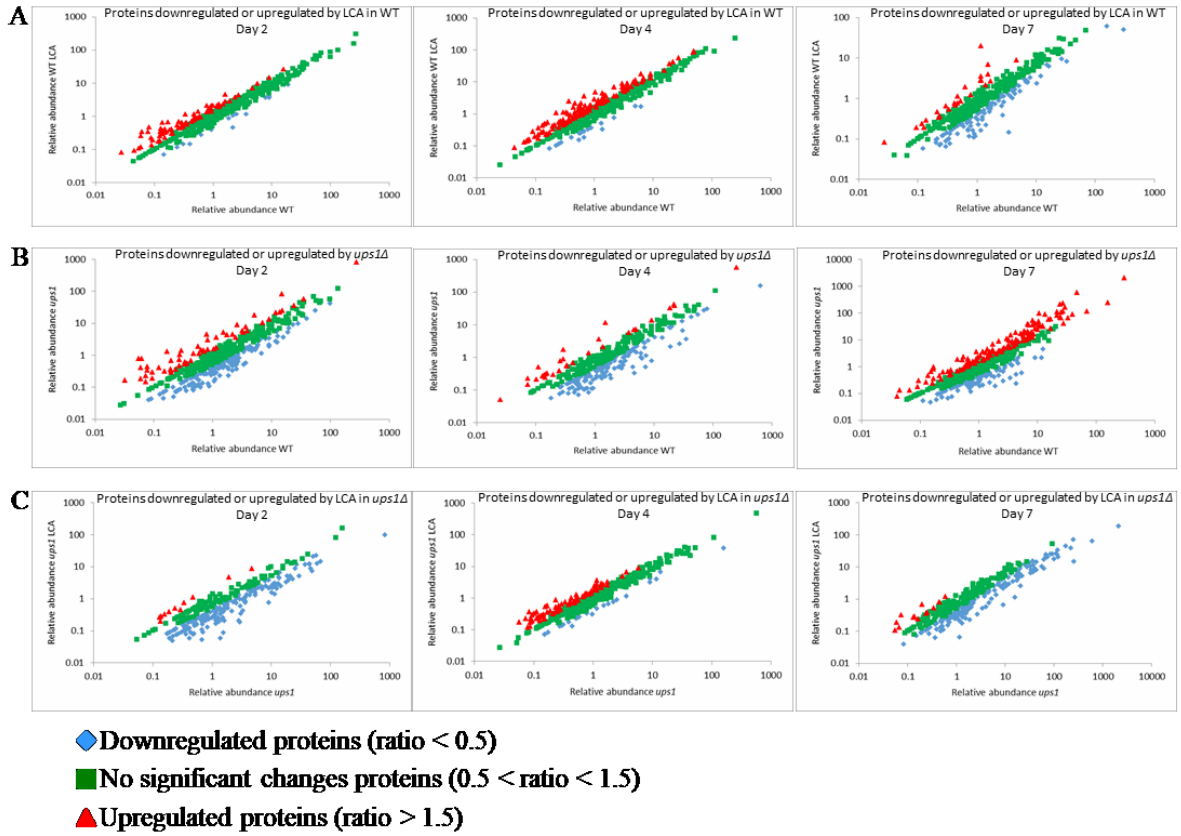

Figure 4.2. Scatter plots comparing the relative concentrations of proteins in mitochondria purified from WT or *ups1Δ* (short-lived) cells cultured with or without LCA. Mitochondria were purified from WT or *ups1Δ* cells recovered on day 2, 4 or 7 of cell culturing. Mass spectrometry-based identification and quantitation of proteins recovered in purified mitochondria were performed as described in Materials and methods. Scatter plots comparing the relative abundance of mitochondrial proteins between specified datasets were plotted on a log-log scale spanning six orders of magnitude. Data on the relative abundance of mitochondrial proteins are presented as means of 2 independent experiments.

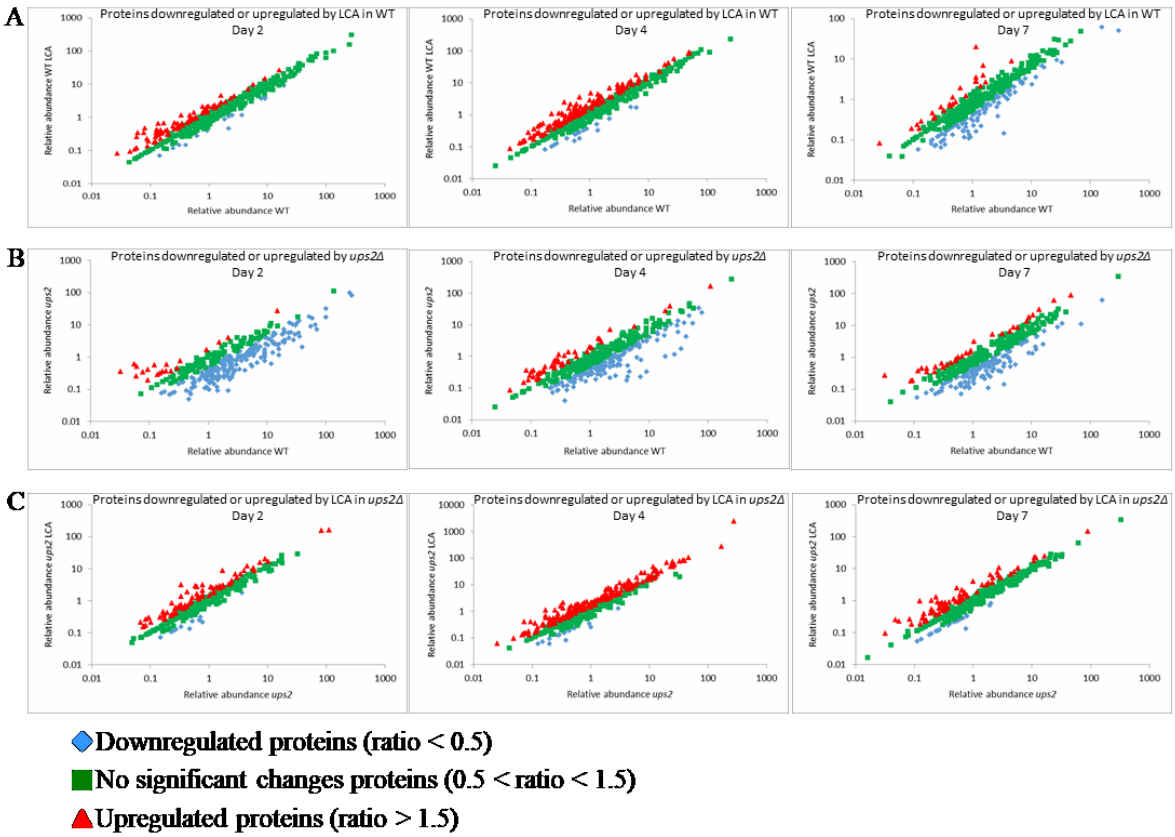

Figure 4.3. Scatter plots comparing the relative concentrations of proteins in mitochondria purified from WT or *ups2Δ* (long-lived) cells cultured with or without LCA. Mitochondria were purified from WT or *ups2Δ* cells recovered on day 2, 4 or 7 of cell culturing. Mass spectrometry-based identification and quantitation of proteins recovered in purified mitochondria were performed as described in Materials and methods. Scatter plots comparing the relative abundance of mitochondrial proteins between specified datasets were plotted on a log-log scale spanning six orders of magnitude. Data on the relative abundance of mitochondrial proteins are presented as means of 2 independent experiments.

We then compared the datasets of relative concentrations of mitochondrial proteins that are statistically significantly downregulated or upregulated 1) by LCA in WT; 2) by the *ups1Δ* or *ups2Δ* mutation in the absence of LCA; and 3) by LCA in *ups1Δ* or *ups2Δ* cells.

Our comparative analysis of these datasets for *ups1Δ* revealed the following: 1) many mitochondrial proteins that are downregulated or upregulated in *ups1Δ* cells cultured without LCA are unique to these datasets (i.e. these proteins are not present in the datasets of mitochondrial proteins that are downregulated or upregulated by LCA in WT or by LCA in *ups1Δ* cells) (Figures 4.4A – 4.4F); and 2) the total number and identities of mitochondrial proteins that are downregulated or upregulated in *ups1Δ* cells cultured with or without LCA fluctuate significantly in cells recovered on day 2, 4 or 7 of cell culturing (i.e. at different stages of chronological aging) (Figures 4.4H – 4.4L).

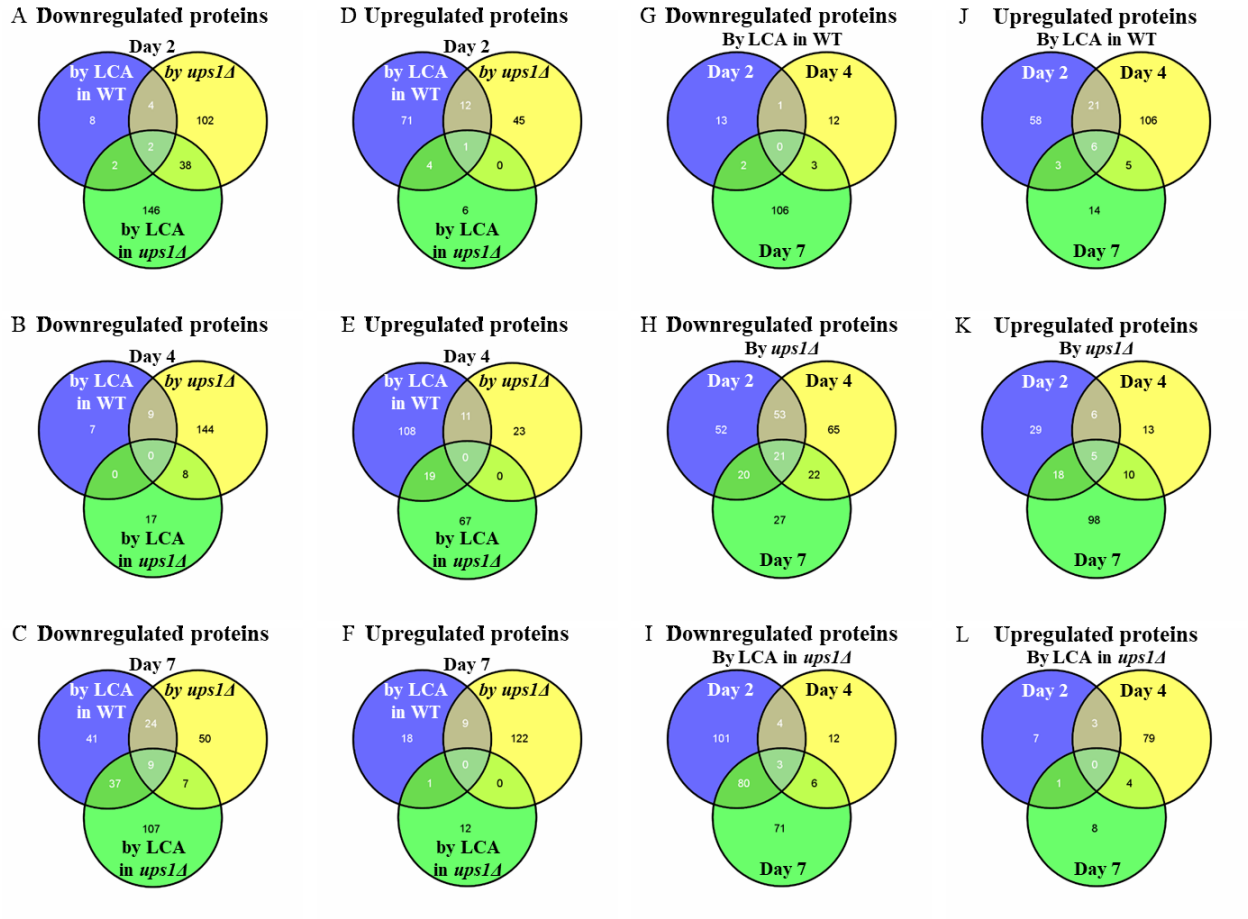

Figure 4.4. The *ups1Δ* mutation alters the concentrations of many mitochondrial proteins in yeast cultured with or without LCA. (**A** – **F**) Venn diagrams showing a comparison of the datasets of relative concentrations of mitochondrial proteins that are statistically significantly downregulated or upregulated by LCA in WT, by the *ups1Δ* mutation in the absence of LCA, and by LCA in *ups1Δ* cells; WT cells were recovered on day 2, 4 or 7 of culturing. (**G** and **J**) Venn diagrams showing a comparison of the datasets of relative concentrations of mitochondrial proteins that are statistically significantly downregulated or upregulated by LCA in WT cells recovered on day 2, 4 or 7 of culturing. (**H** and **K**) Venn diagrams showing a comparison of the datasets of relative concentrations of mitochondrial proteins that are statistically significantly downregulated or upregulated by the *ups1Δ* mutation in the absence of LCA; *ups1Δ* cells were recovered on day 2, 4 or 7 of culturing. (**I** and **L**) Venn diagrams showing a comparison of the datasets of relative concentrations of mitochondrial proteins that are statistically significantly downregulated or upregulated by LCA in *ups1Δ* cells recovered on day 2, 4 or 7 of culturing.

For *ups2Δ*, we found that: 1) a number of mitochondrial proteins that are downregulated or upregulated in *ups2Δ* cells cultured in the absence of LCA cannot be found in the datasets of mitochondrial proteins downregulated or upregulated by LCA in WT or by LCA in *ups2Δ* cells (Figures 4.5A – 4.5F); 2) the total number and identities of mitochondrial proteins that are downregulated or upregulated in *ups2Δ* cells cultured in the absence of LCA vary substantially with the chronological age of cells (Figures 4.5H and 4.5K); 3) numerous mitochondrial proteins that are downregulated or upregulated by LCA in *ups2Δ* cells are unique to these datasets as they

cannot be found in the datasets of mitochondrial proteins downregulated or upregulated by LCA in WT or by the *ups2Δ* mutation in the absence of LCA (Figures 4.5A – 4.5F); and 4) the total number and identities of mitochondrial proteins that are downregulated or upregulated by LCA in *ups2Δ* cells fluctuate significantly with the chronological age of cells (Figures 4.5I and 4.5L).

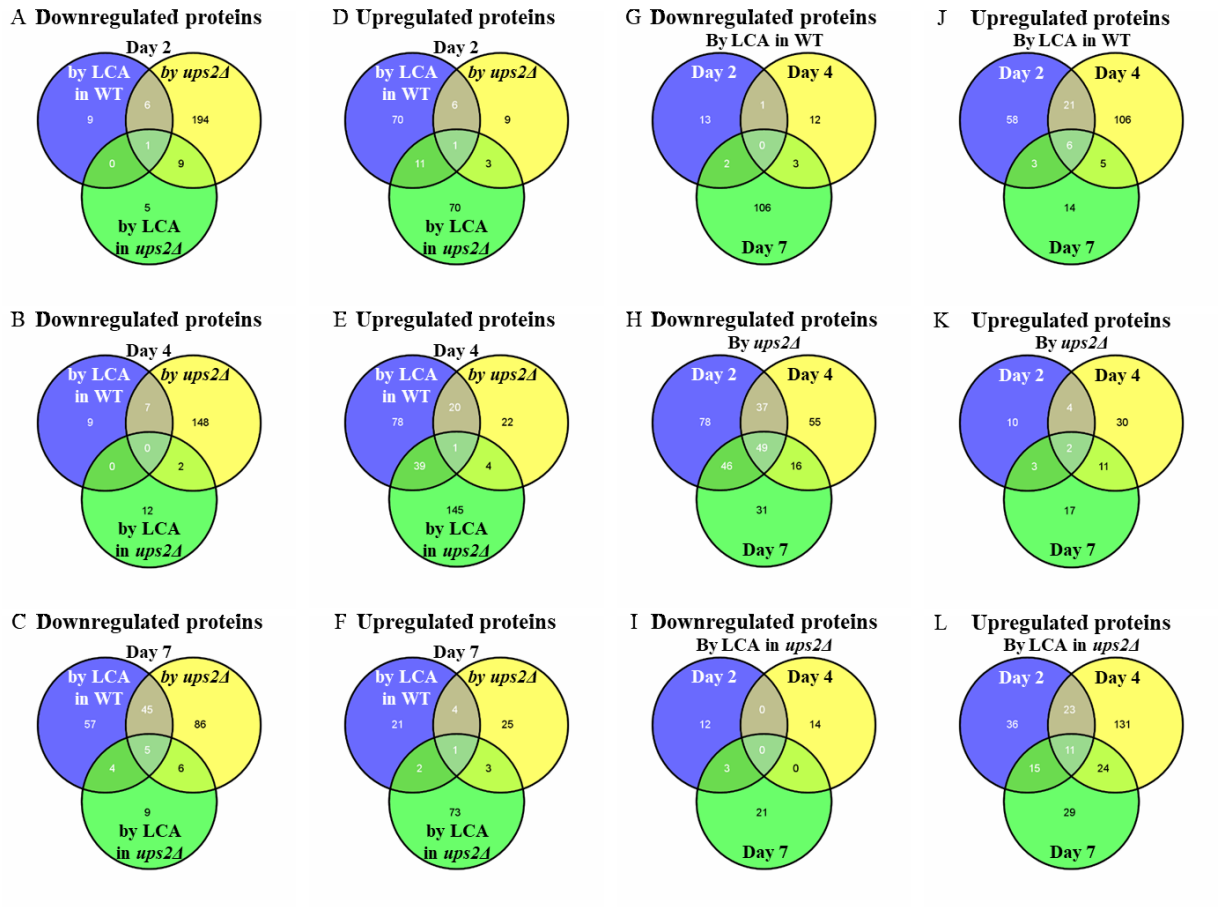

Figure 4.5. The *ups2Δ* mutation alters the concentrations of many mitochondrial proteins in yeast cultured with or without LCA. (**A** – **F**) Venn diagrams showing a comparison of the datasets of relative concentrations of mitochondrial proteins that are statistically significantly downregulated or upregulated by LCA in WT, by the *ups2Δ* mutation in the absence of LCA, and by LCA in *ups2Δ* cells; WT cells were recovered on day 2, 4 or 7 of culturing. (**G** and **J**) Venn diagrams showing a comparison of the datasets of relative concentrations of mitochondrial proteins that are statistically significantly downregulated or upregulated by LCA in WT cells recovered on day 2, 4 or 7 of culturing. (**H** and **K**) Venn diagrams showing a comparison of the datasets of relative concentrations of mitochondrial proteins that are statistically significantly downregulated or upregulated by the *ups2Δ* mutation in the absence of LCA; *ups2Δ* cells were recovered on day 2, 4 or 7 of culturing. (**I** and **L**) Venn diagrams showing a comparison of the datasets of relative concentrations of mitochondrial proteins that are statistically significantly downregulated or upregulated by LCA in *ups2Δ* cells recovered on day 2, 4 or 7 of culturing.

Taken together, these findings indicate that in yeast cultured with or without LCA 1) the establishment and maintenance of a distinct pro-aging pattern of mitochondrial lipidome in short-

lived *ups1Δ* cells [236] correlate with the establishment and maintenance of a specific aging-accelerating pattern of mitochondrial proteome in these mutant cells (this study); and 2) the institution and preservation of a specific pro-longevity pattern of mitochondrial lipidome in long-lived *ups2Δ* cells [236] correlate with the institution and preservation of a distinctive aging-delaying pattern of mitochondrial proteome in these mutant cells (this study).

4.3.4 The mitochondrial proteomes of *ups1Δ* and *ups2Δ* differ substantially

Because our findings suggest that in yeast cultured with or without LCA the *ups1Δ* and *ups2Δ* mutations can establish and maintain either an aging-accelerating or an aging-delaying (respectively) pattern of mitochondrial proteome, we compared the datasets of relative concentrations of mitochondrial proteins that are statistically significantly downregulated or upregulated in *ups1Δ* or *ups2Δ* cells in the absence or presence of LCA.

For *ups1Δ* and *ups2Δ* cells cultured without LCA, we found the following: 1) many mitochondrial proteins that are downregulated or upregulated in long-lived *ups2Δ* cells are not present in the datasets of mitochondrial proteins that are downregulated or upregulated in short-lived *ups1Δ* cells (Figures 4.6A – 4.69F; Suppl. Tables S16 and S17 on http://www.oncotarget.com/index.php?journal=oncotarget&page=rt&op=suppFiles&path[]=16766&path[]=0); and 2) the total number and identities of mitochondrial proteins that are downregulated or upregulated only in long-lived *ups2Δ* cells fluctuate significantly in cells recovered at different stages of chronological aging (Figures 4.6A – 4.6F; Suppl. Tables S16 and S17 on http://www.oncotarget.com/index.php?journal=oncotarget&page=rt&op=suppFiles&path[]=16766&path[]=0). Functions of some mitochondrial proteins that are downregulated or upregulated only in long-lived *ups2Δ* cells remain to be established (Figures 4.6G – 4.6L; Suppl. Tables S16 and S17 on http://www.oncotarget.com/index.php?journal=oncotarget&page=rt&op=suppFiles&path[]=16766&path[]=0). Many mitochondrial proteins that are downregulated or upregulated only in long-lived *ups2Δ* cells have been implicated in essential mitochondrial functions, including the electron transport chain (ETC), respiration, the tricarboxylic acid (TCA) cycle, ribosome assembly, amino acid metabolism, carbohydrate metabolism, protein import, proteostasis, metabolite synthesis, protein synthesis, ATP synthesis, metabolite transport, lipid metabolism, contact sites and cristae

maintenance, redox homeostasis, mitochondrial DNA (mtDNA) maintenance, stress response, mRNA synthesis and processing, the maintenance of contact sites between mitochondria and vacuoles, and mitochondrial fusion (Figures 4.6G – 4.6L; Suppl. Tables S16 and S17 on http://www.oncotarget.com/index.php?journal=oncotarget&page=rt&op=suppFiles&path[]=16766&path[]=0).

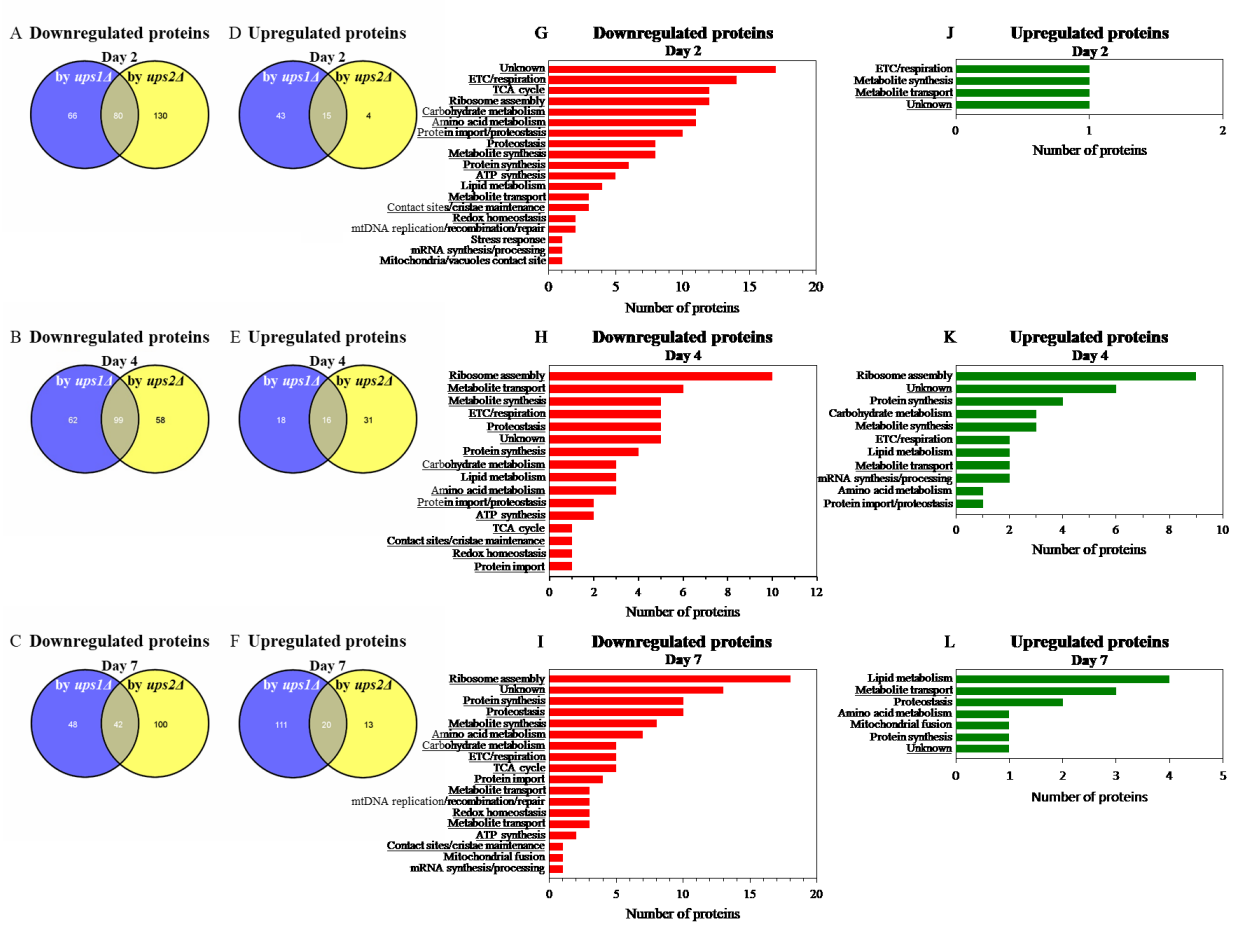

Figure 4.6. In cells cultured without LCA, many mitochondrial proteins that are downregulated or upregulated in long-lived *ups2Δ* cells are not downregulated or upregulated in short-lived *ups1Δ* cells. (**A** – **F**) Venn diagrams showing a comparison of the datasets of relative concentrations of mitochondrial proteins that are statistically significantly downregulated or upregulated in *ups1Δ* or *ups2Δ* cells cultured in the absence of LCA; cells were recovered on day 2, 4 or 7 of culturing. (**G** – **L**) Mitochondrial proteins that are downregulated or upregulated only in long-lived *ups2Δ* cells belong to various functional categories. The names of functional categories whose protein representatives were downregulated or upregulated in *ups2Δ* cells recovered on every of the three days are underlined. Functions of some mitochondrial proteins that are downregulated or upregulated only in *ups2Δ* cells are currently unknown. Abbreviations: ETC, electron transport chain; mtDNA, mitochondrial DNA; TCA, the tricarboxylic acid cycle.

For *ups1Δ* and *ups2Δ* cells cultured with LCA, we found the following: 1) many mitochondrial proteins that are downregulated or upregulated by LCA in long-lived *ups2Δ* cells

cannot be found in the datasets of mitochondrial proteins that are downregulated or upregulated by LCA in WT or short-lived *ups1Δ* cells (Figures 4.7A – 4.7F; Suppl. Tables S18 and S19 on http://www.oncotarget.com/index.php?journal=oncotarget&page=rt&op=suppFiles&path[]=16766&path[]=0); and 2) the total number and identities of mitochondrial proteins that are downregulated or upregulated by LCA only in long-lived *ups2Δ* cells vary notably in cells recovered at different stages of chronological aging (Figures 4.7A – 4.7F; Suppl. Tables S18 and S19 on http://www.oncotarget.com/index.php?journal=oncotarget&page=rt&op=suppFiles&path[]=16766&path[]=0).

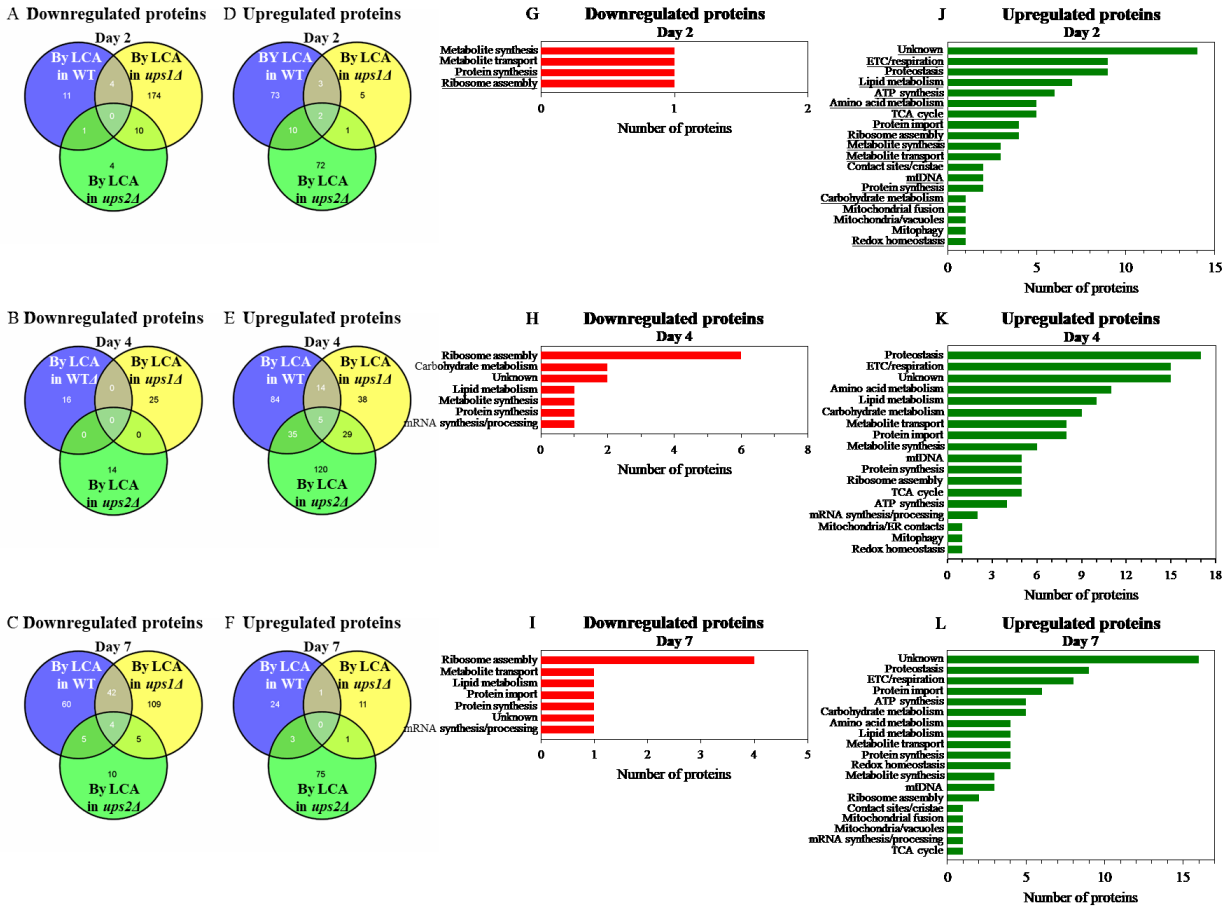

Figure 4.7. In cells cultured with LCA, many mitochondrial proteins that are downregulated or upregulated by LCA in long-lived *ups2Δ* cells are not downregulated or upregulated by LCA in WT or short-lived *ups1Δ* cells. (**A** – **F**) Venn diagrams showing a comparison of the datasets of relative concentrations of mitochondrial proteins that are statistically significantly downregulated or upregulated by LCA in WT, *ups1Δ* or *ups2Δ*; cells were recovered on day 2, 4 or 7 of culturing. (**G** – **L**) Mitochondrial proteins that are downregulated or upregulated by LCA only in long-lived *ups2Δ* cells belong to many different functional categories. The names of functional categories whose protein representatives were downregulated or upregulated by LCA in *ups2Δ* cells recovered on every of the three days are underlined. Functions of some mitochondrial proteins that are downregulated

or upregulated by LCA only in *ups2Δ* cells are currently unknown. Abbreviations: ETC, electron transport chain; mtDNA, mitochondrial DNA; TCA, the tricarboxylic acid cycle.

Functions of some mitochondrial proteins that are downregulated or upregulated by LCA only in long-lived *ups2Δ* cells remain unknown (Figures 4.7G – 4.7L; Suppl. Tables S18 and S19 on http://www.oncotarget.com/index.php?journal=oncotarget&page=rt&op=suppFiles&path[]=16766&path[]=0). Numerous mitochondrial proteins that are downregulated or upregulated by LCA only in long-lived *ups2Δ* cells are known for their essential roles in the same set of mitochondrial functions as the ones played by proteins that are downregulated or upregulated only in long-lived *ups2Δ* cells culture without LCA (compare Figures 4.6G – 4.6L and Suppl. Tables S16 and S17 on http://www.oncotarget.com/index.php?journal=oncotarget&page=rt&op=suppFiles&path[]=16766&path[]=0 to Figures 4.7G – 4.7L and Suppl. Tables S18 and S19on http://www.oncotarget.com/index.php?journal=oncotarget&page=rt&op=suppFiles&path[]=16766&path[]=0).

In sum, these findings suggest that in yeast cultured with or without LCA the *ups2Δ* mutation may establish and maintain an aging-delaying pattern of mitochondrial proteome.

4.3.4 Many mitochondrial proteins that are downregulated or upregulated by LCA only in long-lived *ups2Δ* cells play essential roles in aging delay by LCA

Because our findings suggest that in yeast cultured with LCA the *ups2Δ* mutation may establish and maintain a distinct pattern of mitochondrial proteome that is essential for the ability of LCA to delay aging, we investigated how single-gene-deletion mutations eliminating the key proteins constituting such pattern affect the geroprotective efficiency of LCA.

We thought that some of the proteins downregulated by LCA in *ups2Δ* may function in attenuating the geroprotective efficiency of LCA, and thus the elimination of these proteins by mutations may increase such efficiency. We also thought that some of the proteins upregulated by LCA in *ups2Δ* may act as facilitators of aging delay by LCA, and therefore the elimination of these proteins by mutations may decrease the geroprotective efficiency of LCA.

We found that mutants that lack 10 out of 12 proteins most highly downregulated by LCA in *ups2Δ* exhibit a statistically significantly increase of the aging-delaying efficiency of LCA; a

slight increase of such efficiency seen in mutants that lack 2 other downregulated by LCA proteins was not statistically significant (Figures 4.8A – 4.8C). We also found that mutants that lack 11 out of 12 proteins vastly upregulated by LCA in *ups2Δ* display a statistically significantly decrease of the geroprotective efficiency of LCA; a minor decrease of such efficiency observed in a mutant lacking one of the downregulated by LCA proteins was not statistically significant (Figures 4.8D – 4.8F). Of note, none of these mutants exhibits such robust change of the aging-delaying efficiency of LCA as the changes seen in the *ups1Δ*, *ups2Δ* and *psd1Δ* mutants [236]. This finding suggests that Ups1, Ups2 and Psd1 may function as upstream regulators of various mitochondrial processes whose synergistic action defines the efficiency of aging delay by LCA.

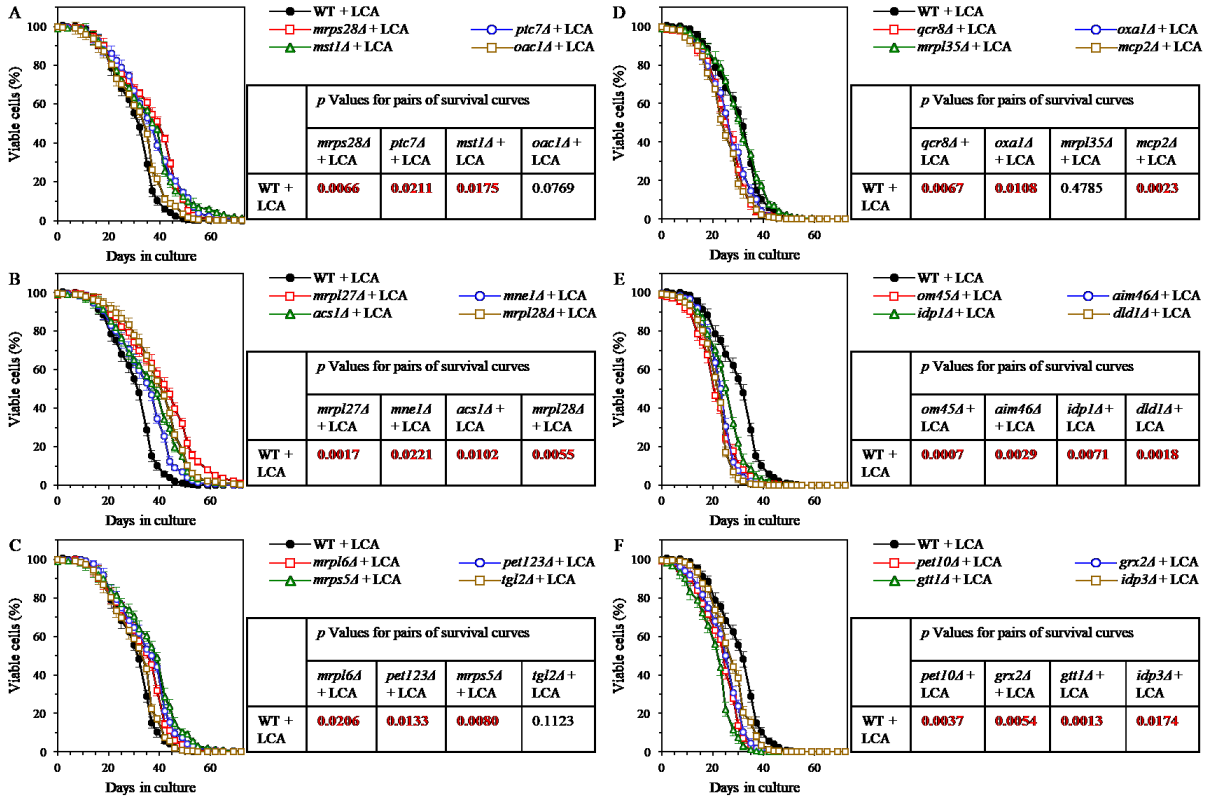

Figure 4.8. Many mutations eliminating proteins downregulated by LCA in *ups2Δ* increase the aging-delaying efficiency of LCA, while many mutations eliminating proteins upregulated by LCA in *ups2Δ* decrease such efficiency. WT and mutant cells were cultured in the nutrient-rich YP medium initially containing 0.2% glucose with 50 μM LCA. (**A** - **C**) Survival curves of chronologically aging WT and mutant strains that lack proteins most highly downregulated by LCA in *ups2Δ* are shown. Data are presented as means ± SEM (n = 3). Also shown are *p* values for different pairs of survival curves of WT and mutant strains cultured with LCA. Survival curves shown in (**A** - **C**) were compared. Two survival curves were considered statistically different if the *p* value was less than 0.05. The *p* values for comparing pairs of survival curves using the logrank test were calculated as described in Materials and methods. (**D** - **F**) Survival curves of chronologically aging WT and mutant strains that lack proteins most substantially upregulated by LCA in *ups2Δ* are shown. Data are presented as means ± SEM (n = 3). Also shown are *p* values for different pairs of survival curves of WT and mutant strains cultured with LCA. Survival curves shown in (**D** - **F**) were compared. Two survival curves were considered statistically different if the *p* value was less than 0.05. The *p* values for comparing pairs of survival curves using the logrank test were calculated as described in Materials

and methods. These experiments were performed by Pavlo Kyryakov, Pamela Dakik, Melissa McAuley, Younes Medkour and Tamara Di Maulo.

Taken together, these findings further support the notion that the *ups2Δ* mutation may allow to sustain a distinct aging-delaying pattern of mitochondrial proteome that is essential for the ability of LCA to delay aging.

4.4 Discussion

This study, along with studies described elsewhere [236], provide evidence that the mitochondrial lipidome defines not only the rate of yeast chronological aging but also the geroprotective efficiency of LCA in chronologically aging yeast. We demonstrated the existence of a distinct pro-longevity pattern of mitochondrial lipidome, which extends yeast CLS in the absence of LCA and amplifies the geroprotective efficiency of LCA [236]. This pattern consists in a proportional decrease of PE and CL concentrations, and in a concomitant increase of PA concentration. PE, CL and PA are non-bilayer forming, cone-shaped phospholipid classes that increase the extent of membrane curving for the IMM to rise the abundance of mitochondrial cristae (formed by the IMM) and mitochondrial contact cites (formed between the IMM and OMM) [236]. We also show that these LCA-driven specific changes in the composition of mitochondrial membrane lipids cause a distinct remodeling of mitochondrial proteome by decreasing and increasing concentration of many mitochondrial proteins (this study). These proteins have been implicated in such vital mitochondrial functions as the ETC and respiration, the TCA cycle, ribosome assembly, amino acid metabolism, carbohydrate metabolism, protein import, proteostasis, metabolite synthesis, protein synthesis, ATP synthesis, metabolite transport, lipid metabolism, contact sites and cristae maintenance, redox homeostasis, mtDNA maintenance, stress response, mRNA synthesis and processing, the maintenance of contact sites between mitochondria and vacuoles, and mitochondrial fusion (this study). We provided evidence that the LCA-dependent remodeling of mitochondrial lipidome and the resulting changes in mitochondrial proteome allow to change the age-related chronology of changes in such vital mitochondrial processes as respiration, electrochemical potential maintenance, ROS homeostasis preservation and ATP synthesis [236]. These changes facilitate the establishment and maintenance of an aging-delaying pattern of mitochondrial functionality that is essential for the ability of LCA to delay aging.

The Titorenko laboratory has previously demonstrated that LCA causes major changes not only in mitochondrial membrane lipidome but also in the size, number and morphology of mitochondria [64]. One could envision that these LCA-driven changes in mitochondrial abundance and morphology may affect mitochondrial protein import, folding, assembly and other aspects of mitochondrial proteostasis, thereby altering mitochondrial proteome. The ongoing studies in the Titorenko laboratory address the validity of this assumption.

5 Mechanisms through which lithocholic acid delays yeast chronological aging under caloric restriction conditions

5.1 Introduction

As described in the ″Introduction″ section, our recent studies have indicated that under CR conditions lithocholic acid (LCA) influences not only the composition and functionality of mitochondria but also some cellular processes confined to other cellular compartments. Based on these recent studies, we hypothesized that LCA may delay chronological aging of yeast limited in calorie supply also because it affects these other cellular processes taking place in various cellular locations. The objectives of studies described in Chapter 5 was to test this hypothesis by investigating mechanisms through which LCA controls the spatiotemporal dynamics of these other cellular processes in different cellular locations under CR conditions.

5.2 Materials and methods

5.2.1 Yeast strains, media and growth conditions

The WT strain BY4742 (*MATα his3Δ1 leu2Δ0 lys2Δ0 ura3Δ0*) and single-gene-deletion mutant strains in the BY4742 genetic background (all from Open Biosystems/Dharmacon, a part of GE Healthcare) were grown in YP medium (1% yeast extract, 2% peptone; both from Fisher Scientific; #BP1422-2 and #BP1420-2, respectively) initially containing 0.2% glucose (#D16-10; Fisher Scientific) with 50 μM LCA (#L6250; Sigma) or without it. Cells were cultured at 30ºC with rotational shaking at 200 rpm in Erlenmeyer flasks at a ″flask volume/medium volume″ ratio of 5:1.

5.2.2 Chronological life span assay

A sample of cells was taken from a culture at a certain time-point. A fraction of the sample was diluted to determine the total number of cells using a hemocytometer. Another fraction of the cell sample was diluted, and serial dilutions of cells were plated in duplicate onto YP plates containing 2% glucose as carbon source. After 2 d of incubation at 30ºC, the number of colony forming units (CFU) per plate was counted. The number of CFU was defined as the number of viable cells in a sample. For each culture, the percentage of viable cells was calculated as follows: (number of viable cells per ml/total number of cells per ml) × 100. The percentage of viable cells

in mid-logarithmic phase was set at 100%. The life span curves were validated using a LIVE/DEAD yeast viability kit (Invitrogen) following the manufacturer's instructions.

5.2.3 Mass spectrometric identification and quantitation of cellular lipids

Extraction of cellular lipids and their mass spectrometric identification and quantitation were performed as previously described [227]. A sample of cells was taken from a culture on a certain day of culturing. A fraction of the sample was diluted to determine the total number of cells using a hemocytometer (# 3200; Hausser Scientific). 5×10^7 cells were harvested by centrifugation in a Centra CL2 clinical centrifuge for 5 min at 3,000 × g at room temperature. The cell pellet was washed once in ice-cold nanopure water and once in ice-cold 155 mM ammonium bicarbonate (pH 8.0), and the cells were harvested by centrifugation at 16,000 × g for 1 min at 4ºC. The cell pellet was stored at -80ºC until lipid extraction. For lipid extraction, the pelleted cells kept at -80ºC were thawed on ice before being resuspended in 200 µl of ice-cold nanopure water. The re-suspended sample was transferred to a 15-ml high-strength glass screw top centrifuge tube with a Teflon lined cap (#0556912; Fisher Scientific). The volume of each sample was topped off to 1 ml with ice-cold nanopure water. To each tube the following was added: 20 µL of the internal standard mix prepared in Chromasolv HPLC (>99.9%) chloroform (Sigma-Aldrich) as described [215], 800 µl of 425-600 µM acid-washed glass beads to break open the cells (#G8772; Sigma-Aldrich) and 3 ml of a Chromasolv HPLC (>99.9%) chloroform-methanol mixture (both from Sigma-Aldrich) at a 17:1 ratio. The samples were then vortexed vigorously for 2 h at 4ºC and subjected to centrifugation in a Centra CL2 clinical centrifuge at 3,000 × g for 5 min at room temperature. The lower organic phase was then transferred to another 15-ml high-strength glass screw top centrifuge tube using a glass Pasteur pipette with careful attention not to disrupt the glass beads or upper aqueous phase. 1.5 ml of chloroform-methanol (2:1) solution was added to the remaining upper aqueous phase. The samples were again vortexed vigorously at 4ºC for 2 h. The initial separated organic band was kept at 4ºC for the duration of the second vortexing. At the end of 2-h vortexing, the samples were again centrifuged for 5 min at 3,000 × g at room temperature; the lower organic phase was then separated and added to the corresponding initial organic phase with a glass Pasteur pipette. With both lower organic phases combined, the solvent was evaporated off by nitrogen gas flow. Once all solvent was evaporated, the remaining lipid film was dissolved in 100 µl of chloroform-methanol (1:2) and immediately transferred into 2-ml glass vials with Teflon screw

tops to avoid evaporation until samples were analyzed by mass spectrometry. Samples were then stored at -80ºC and ran on the LTQ Orbitrap Mass Spectrometer within one week of the extraction. Samples were diluted (1:1) with chloroform/methanol (1:2) mixture supplemented with 0.1% ammonium hydroxide. Lipids were resolved by direct injection using a Thermo Orbitrap Velos mass spectrometer equipped with a HESI-II ion source (Thermo Scientific, Waltham, MA, USA) at a flow rate of 5 µl/min. The optimized tune setting and instrument methods for mass spectrometric analysis of lipids were previously described [227]. Mass spectra were converted to open format mzXML using the ProteoWizard MSConvert software (http://proteowizard.sourceforge.net/), the file format used by the Lipid Identification Software LipidXplorer (https://wiki.mpi-cbg.de/lipidx/Main_Page) for the automated detection and quantitation of lipid species. Data were normalized by taking the ratio of signal intensity of precursor ions to that of their respective lipid class-specific internal standard (spiked standard), multiplied by the concentration of that standard to give a molar quantity.

5.2.4 Fluorescence microscopy

BODIPY 493/503 (#D3922, Thermo Fisher Scientific) staining for monitoring neutral lipids deposited in lipid droplets [23], propidium iodide (PI; #P4170, Sigma) staining for visualizing the extent of plasma membrane permeability for small molecules was performed as described previously [243], 4′,6-diamidino-2-phenylindole dihydrochloride (DAPI; #D9542; Sigma) staining for visualizing nuclei [243] and Annexin V (#A13201; Thermo Fisher Scientific) staining for visualizing externalized phosphatidylserine [243] were performed according to established procedures. Live imaging was performed on a Leica DM6000B epifluorescence microscope equipped with a high-resolution Hamamatsu Orca ER CCD camera using oil immersion and a 100× objective. Images were acquired with 20-ms exposures using PerkinElmer Volocity software. Image files were exported as TIFFs then opened in ImageJ, where the percentage of BODIPY 493/503-, PI- and Annexin V-positive cells or cells with fragmented nucleus was calculated.

5.2.5 Cell viability assay for monitoring the susceptibility of yeast to a mode of cell death induced by palmitoleic acid (POA)

A sample of cells was taken from a culture on a certain day of culturing. A fraction of the sample was diluted to determine the total number of cells using a hemocytometer. 8×10^7 cells were harvested by centrifugation for 1 min at 21,000 × g at room temperature and resuspended in 8 ml of YP medium containing 0.2% glucose as carbon source. Each cell suspension was divided into 8 equal aliquots. Three pairs of aliquots were supplemented with POA (#P9417; Sigma) from a 50-mM stock solution (in 10% chloroform, 45% hexane and 45% ethanol; #650498, #248878 and #34852, respectively; all from Sigma). The final concentration of POA was 0.05 mM, 0.1 mM or 0.15 mM for each pair of aliquots; in all these aliquots, the final concentrations of chloroform, hexane and ethanol were 0.03%, 0.135% and 0.135%, respectively. One pair of aliquots was supplemented only with chloroform, hexane and ethanol added to the final concentrations of 0.03%, 0.135% and 0.135%, respectively. All aliquots were then incubated for 2 h at 30ºC on a Labquake rotator (#400110; Thermolyne/Barnstead International) set for 360º rotation. Serial dilutions of cells were plated in duplicate onto plates containing YP medium with 2% glucose as carbon source. After 2 d of incubation at 30ºC, the number of colony forming units (CFU) per plate was counted. The number of CFU was defined as the number of viable cells in a sample. For each aliquot of cells exposed to POA, the % of viable cells was calculated as follows: (number of viable cells per ml in the aliquot exposed to POA/number of viable cells per ml in the control aliquot that was not exposed to POA) × 100.

5.2.6 Cell viability assay for monitoring the susceptibility of yeast to a mode of cell death induced by hydrogen peroxide

A sample of cells was taken from a culture on a certain day of culturing. A fraction of the sample was diluted to determine the total number of cells using a hemocytometer. 8×10^7 cells were harvested by centrifugation for 1 min at 21,000 × g at room temperature and resuspended in 8 ml of YP medium containing 0.2% glucose as carbon source. Each cell suspension was divided into 8 equal aliquots. Three pairs of aliquots were supplemented with hydrogen peroxide (#H325-500; Fisher Scientific) to the final concentration of 0.5 mM, 1.5 mM or 2.5 mM for each pair. One pair of aliquots remained untreated. All aliquots were then incubated for 2 h at 30ºC on a Labquake rotator (#400110; Thermolyne/Barnstead International) set for 360º rotation. Serial dilutions of cells were plated in duplicate onto plates containing YP medium with 2% glucose as carbon source. After 2 d of incubation at 30ºC, the number of CFU per plate was counted. The number of CFU

was defined as the number of viable cells in a sample. For each aliquot of cells exposed to hydrogen peroxide, the % of viable cells was calculated as follows: (number of viable cells per ml in the aliquot exposed to hydrogen peroxide/number of viable cells per ml in the control aliquot that was not exposed to hydrogen peroxide) × 100.

5.2.7 Statistical analysis

Statistical analysis was performed using Microsoft Excel's (2010) Analysis ToolPak - VBA. All data on cell survival are presented as mean ± SEM. The *p* values for comparing the means of two groups using an unpaired two-tailed *t* test were calculated with the help of the GraphPad Prism 7 statistics software. The logrank test for comparing each pair of survival curves was performed with GraphPad Prism 7. Two survival curves were considered statistically different if the *p* value was less than 0.05. The Pearson correlation coefficient (r) and the R-squared values were computed using Microsoft Excel's (2010) Analysis ToolPak - VBA. The Pearson's correlation coefficient (r) values ranging from 0.9 to 1.0 (-0.9 to -1.0) were considered a very high positive (negative) correlation between the two variables, whereas the Pearson's correlation coefficient (r) values ranging from 0.7 to 0.9 (-0.7 to -0.9) were considered a high positive (negative) correlation between the two variables [244].

5.3 Results

5.3.1 Our hypothesis on mechanisms through which LCA may delay yeast chronological aging under CR conditions

Our recent studies have revealed that LCA not only alters mitochondrial lipidome and proteome, enlarges mitochondria, decreases mitochondrial number, modifies mitochondrial cristae structure, and changes vital aspects of mitochondrial functionality [14, 59, 64, 70, 107, 145, 221, 236, 245-248], but also affects some other cellular processes in different cellular locations. Specifically, during post-diauxic (PD) and the non-proliferative stationary (ST) phases of culturing yeast under CR conditions on 0.2% glucose, LCA also affects the following cellular processes: 1) it increases the concentration of triacylglycerols (TAG), so-called ″neutral″ (uncharged) lipids initially synthesized in the endoplasmic reticulum (ER) and then deposited in lipid droplets (LD) (Figure 5.1); 2) it decreases the concentration of free fatty acids (FFA), which can be used as

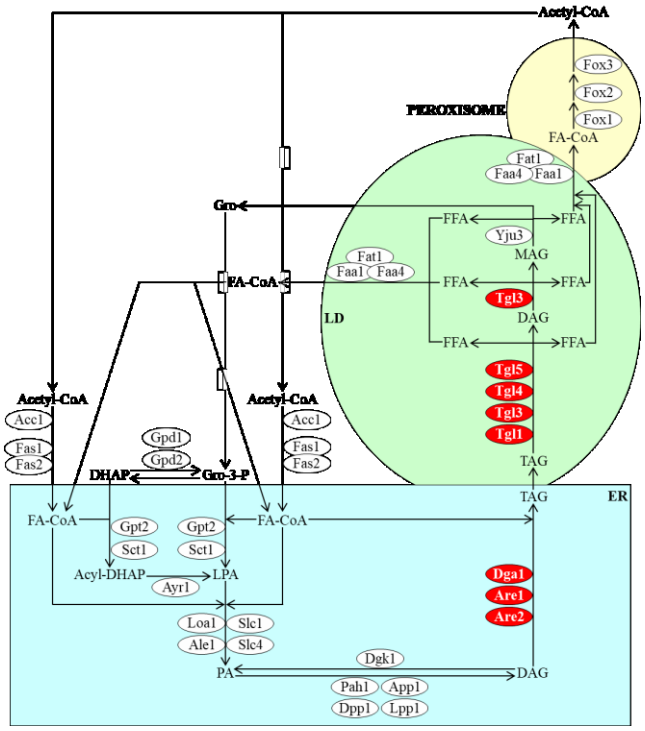

Figure 5.1. The anabolic branch of TAG metabolism occurs in the endoplasmic reticulum (ER), whereas the catabolic branch of TAG metabolism is confined to lipid droplets (LD) and peroxisomes. TAG are ″neutral″ (uncharged) lipids initially synthesized in the ER from free fatty acids (FFA). FFA can also be formed as the products of TAG lipolysis in LD. Moreover, FFA can undergo β-oxidation in peroxisomes. Proteins displayed in red color: proteins that are eliminated by the single-gene-deletion mutations whose effects on yeast chronological lifespan, lipid concentrations, percent of cells exhibiting propidium iodide positive staining characteristic of necrotic cell death and cell viability following a short-term treatment with palmitoleic acid were studied. See text for more details. Abbreviations: Acc1, acetyl-CoA carboxylase 1; Ale1, acyltransferase for lysophosphatidylethanolamine 1; App1, actin patch protein 1; Are1/2, acyl-coenzyme A: cholesterol acyl transferase-related enzymes 1 and 2; Dga1, diacylglycerol acyltransferase 1; Dgk1, diacylglycerol kinase 1; Dpp1, diacylglycerol pyrophosphate phosphatase 1; DHAP, dihydroxyacetone phosphate; Faa1/4, fatty acid activation 1 and 2; FA-CoA, fatty acyl-CoA ester; Fas1/2, fatty acid synthetases 1 and 2; Fat1, fatty acid transporter 1; Fox1/2/3, fatty acid oxidation 1, 2 and 3; Gpd1/2, glycerol-3-phosphate dehydrogenases 1 and 2; Gpt2, glycerol-3-phosphate acyltransferase; Gro, glycerol; Gro-3-P, glycerol-3-phosphate; Loa1, lysophosphatidic acid: oleoyl-CoA acyltransferase 1; Lpp1, lipid phosphate phosphatase 1; LPA, lysophosphatidic acid; MAG, monoacylglycerol; PA, phosphatidic acid; Pah1, phosphatidic acid phosphohydrolase 1; Sct1, suppressor of choline-transport mutants 1; Slc1/4, sphingolipid compensation 1 and 4; Tgl1/3/4/5, triglyceride lipases 1, 3, 4 and 5.

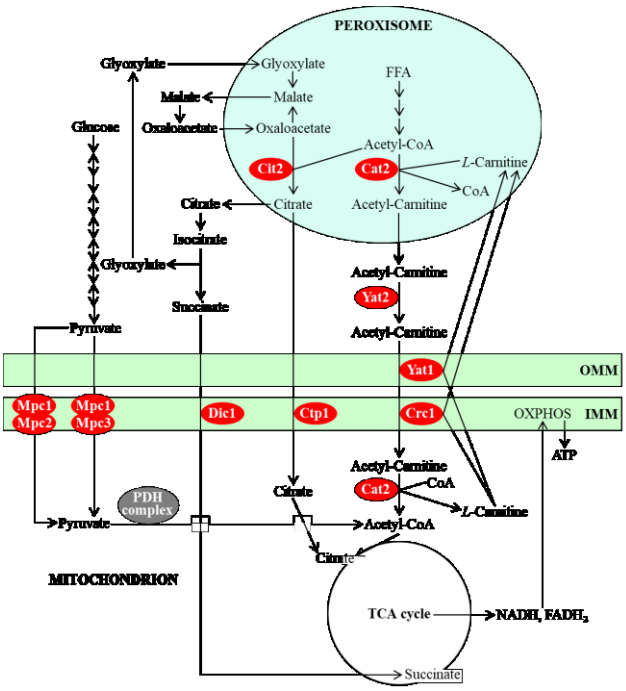

Figure 5.2. As the final product of the β-oxidation of free fatty acids (FFA) in peroxisomes, acetyl-CoA: 1) is transported to mitochondria via the carnitine shuttle; 2) is oxidized in mitochondria through the TCA cycle, thus providing reducing equivalents NADH and $FADH_2$ for ATP synthesis via oxidative phosphorylation (OXPHOS); and 3) is transported to mitochondria in the forms of the glyoxylate cycle intermediates citrate and succinate to replenish the mitochondrial pool of TCA cycle intermediates. As the final product of glycolysis, pyruvate: 1) is transported to mitochondria via mitochondrial pyruvate carrier; and 2) is converted to acetyl-CoA, which is oxidized in mitochondria through the TCA cycle. Proteins displayed in red color: proteins that are eliminated by the single-gene-deletion mutations whose effects on yeast chronological lifespan were studied. See text for more details. Abbreviations: Cat2, carnitine acetyl-CoA transferase; Cit2, citrate synthase; Crc1, carnitine transporter; Ctp1, citrate transporter; Dic1, dicarboxylate carrier; Mpc1, Mpc2 and Mpc3, mitochondrial pyruvate carrier1 1, 2 and 3; PDH, pyruvate dehydrogenase; Yat1, mitochondrial

carnitine acetyltransferase; Yat2, cytosolic carnitine acetyltransferase. IMM and OMM, inner and outer mitochondrial membranes.

substrates for TAG synthesis in the ER and can also be formed as the products of TAG lipolysis in LD; FFA can then undergo β-oxidation in peroxisomes (Figure 5.1); 3) it increases the concentrations of the Gpd2, Gpt2, Slc1, Are1 and Dga1 proteins, all of which reside in the ER and are involved in the synthesis of TAG from FFA (Figure 5.1); 4) it decreases the concentrations of the Tgl1, Tgl3, Tgl4 and Tgl5 proteins, all of which exist in LD and catalyze TAG lipolysis that yields FFA (Figure 5.1); 5) it increases the concentrations of Cat2, Crc1, Yat1 and Yat2; these proteins are required for the carnitine-dependent transport of acetyl-CoA from peroxisomes (where acetyl-CoA is formed as the final product of the β-oxidation of FFA) to mitochondria (Figure 5.2); 6) it decreases the concentrations of the Cit2, Ctp1 and Dic1 proteins (Cit2 catalyzes a peroxisomal anaplerotic reaction transforming acetyl-CoA into citrate; this reaction is followed by the conversion of citrate into succinate and then by the Ctp1- and Dic1-dependent delivery of citrate and succinate (respectively) to mitochondria) (Figure 5.2); 7) it increases the concentrations of Mpc1 and Mpc3, the two protein components of a mitochondrial pyruvate carrier involved in pyruvate transport to mitochondria during respiratory growth; it does not, however, alter the concentration of the Mpc2 protein component of the mitochondrial pyruvate carrier Mpc1/Mpc2 that assembles and operates during fermentative growth (Figure 5.2); 8) it increases the percentage of cells exhibiting a tubular mitochondrial network and decreases the percentage of cells displaying fragmented mitochondria; 9) it lowers cell susceptibility to an apoptotic mode of regulated cell death (RCD) caused by an exposure to hydrogen peroxide or acetic acid; and 9) it decreases cell susceptibility to liponecrotic RCD triggered by a treatment with FFA [14, 54, 59, 145, 236, 246, 248]. It remained unclear how LCA regulates the anabolic and catabolic branches of TAG metabolism in the ER, LD and peroxisomes (Figure 5.1), and how it regulates other cellular processes named in this section. It was also unknown if and how such LCA-dependent regulation of some (or all) of these cellular processes contributes to the ability of LCA to delay yeast chronological aging. We put forward the hypothesis that LCA may delay chronological aging of yeast under CR also because this bile acid affects these other cellular processes confined to different cellular locations. To test this hypothesis, we examined mechanisms underlying the ability of LCA to regulate the spatiotemporal dynamics of these other cellular processes confined to several compartments of yeast cells limited in calorie supply. We also assessed a possibility that

there is a causal relationship between such LCA-driven regulation of these other cellular processes and the LCA-dependent delay of yeast chronological aging under CR conditions.

5.3.2 LCA increases the abundance of LD in an age-related manner

We have previously found that, during PD and ST phases of culturing yeast under CR on 0.2% glucose, LCA rises the abundance of TAG and increases the concentrations of enzymes involved in the synthesis of this class of neutral lipids from FFA in the ER [14, 236, 246]. We have also noticed that, in these yeast cells, LCA decreases the abundance of FFA and decreases the concentrations of enzymes involved in the lipolytic conversion of TAG into FFA in LD [14, 236, 246]. Based on the above observations, we hypothesized that LCA may have the following effects on TAG metabolism and transport in yeast limited in calorie supply: 1) it may accelerate TAG synthesis in the ER and, perhaps, the ensuing TAG deposition in LD; and 2) it may decelerate TAG lipolysis in LD. This hypothesis posits that LCA may increase the abundance of LD in chronologically aging yeast under CR conditions, perhaps during certain stages of the aging process (i.e. in an age-related manner). To test this hypothesis, we used live-cell fluorescence microscopy with BODIPY 493/503, a stain for neutral lipids, to assess the percentage of cells that contain LD in wild-type (WT) strain cultured under CR conditions with or without LCA; the cells were recovered on different days (i.e. in different phases) of culturing. We found that LCA has the following effects: 1) it increases the percentage of cells with LD in logarithmic (L) phase (Figures 5.3A and 5.3B), when neutral lipids are known to be synthesized in the ER and deposited in LD [23]; and 2) it rises the percentage of cells with LD in PD and ST phases (Figures 5.3A and 5.3B), when neutral lipids are known to be lipolytically degraded in LD [23].

These findings support our hypothesis on the following effects of LCA in yeast cells of WT strain limited in calorie supply: 1) LCA accelerates TAG synthesis in the ER and the subsequent TAG deposition in LD; and 2) LCA decelerates TAG lipolysis in LD. The first effect of LCA prevails during L phase of culturing under CR conditions, whereas the second effect of LCA predominates during PD and ST phases of such culturing.

5.3.3 LCA decreases the concentration of FFA during several consecutive stages of the aging process

As we found, LCA accelerates TAG synthesis from FFA during L phase and decelerates TAG lipolysis into FFA during PD and ST phases of culturing under CR conditions. We therefore hypothesized that LCA may decrease the concentration of FFA through several phases of culturing under CR conditions. To test this hypothesis, we used quantitative mass spectrometry to compare cellular lipidomes of WT yeast cultured under CR conditions with or without LCA. In support of our hypothesis, we found that LCA causes a significant decline in the concentration of FFA in L, diauxic (D), PD and the beginning of ST phases (Figure 5.4A).

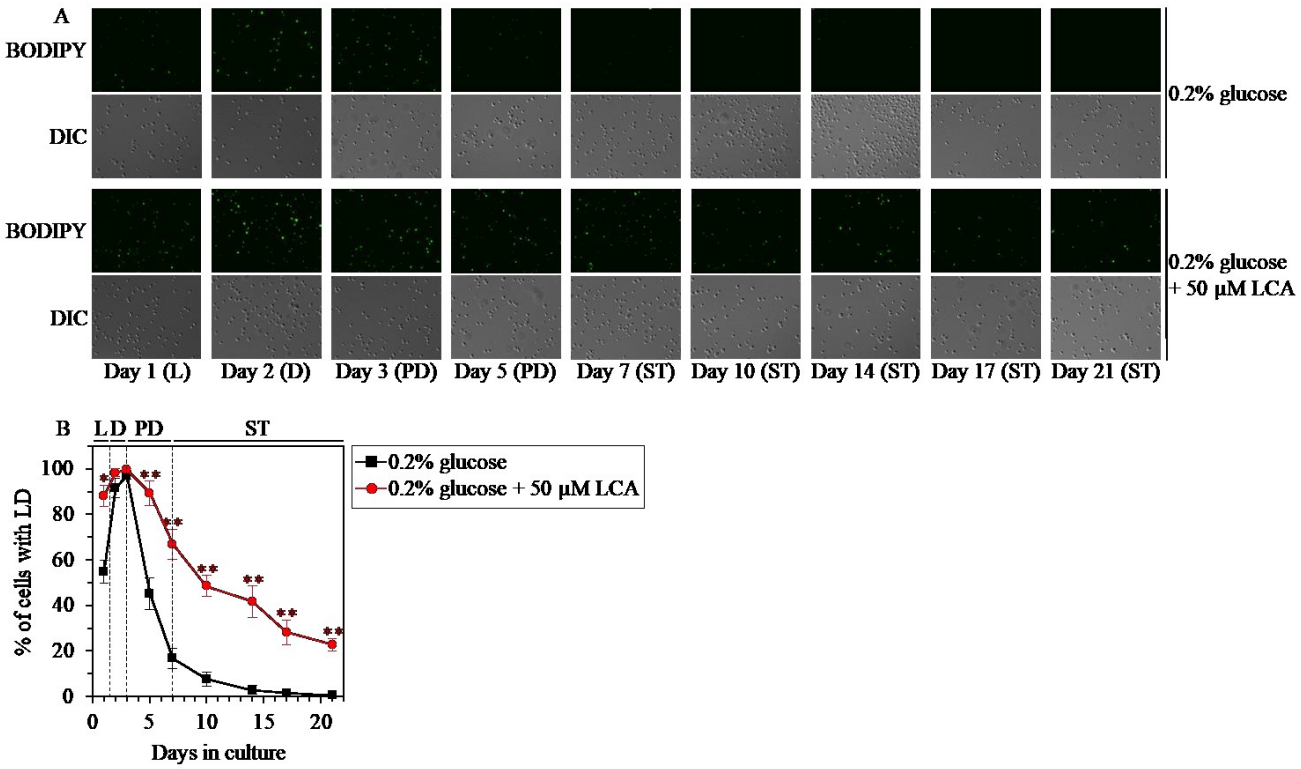

Figure 5.3. Under CR conditions, LCA causes an age-related increase in the percentage of wild-type (WT) cells that contain lipid droplets (LD). WT cells were cultured in the nutrient-rich YP medium initially containing 0.2% glucose with 50 µM LCA or without it. (**A**) Cells recovered on different days of culturing were visualized using the differential interference contrast (DIC) microscopy and stained with BODIPY 493/503, which was used to detect neutral lipids of LD as described in Materials and Methods. (**B**) Percentage of cells that contain LD. Images like the representative images shown in (**A**) were quantitated. Data are presented as means ± SEM (n = 3; *p < 0.05; **p < 0.01). Abbreviations: L, D, PD and ST, logarithmic, diauxic, post-diauxic and stationary growth phases (respectively).

Furthermore, almost mirroring the effects of LCA on the temporal dynamics of TAG-containing LD (Figure 5.3B), LCA affected the intracellular concentration of TAG as follows: 1)

LCA increased TAG concentration in L phase; 2) LCA had no significant effect on TAG concentration in D phase; and 3) LCA increased TAG concentration in PD and ST phases (Figure 2J).

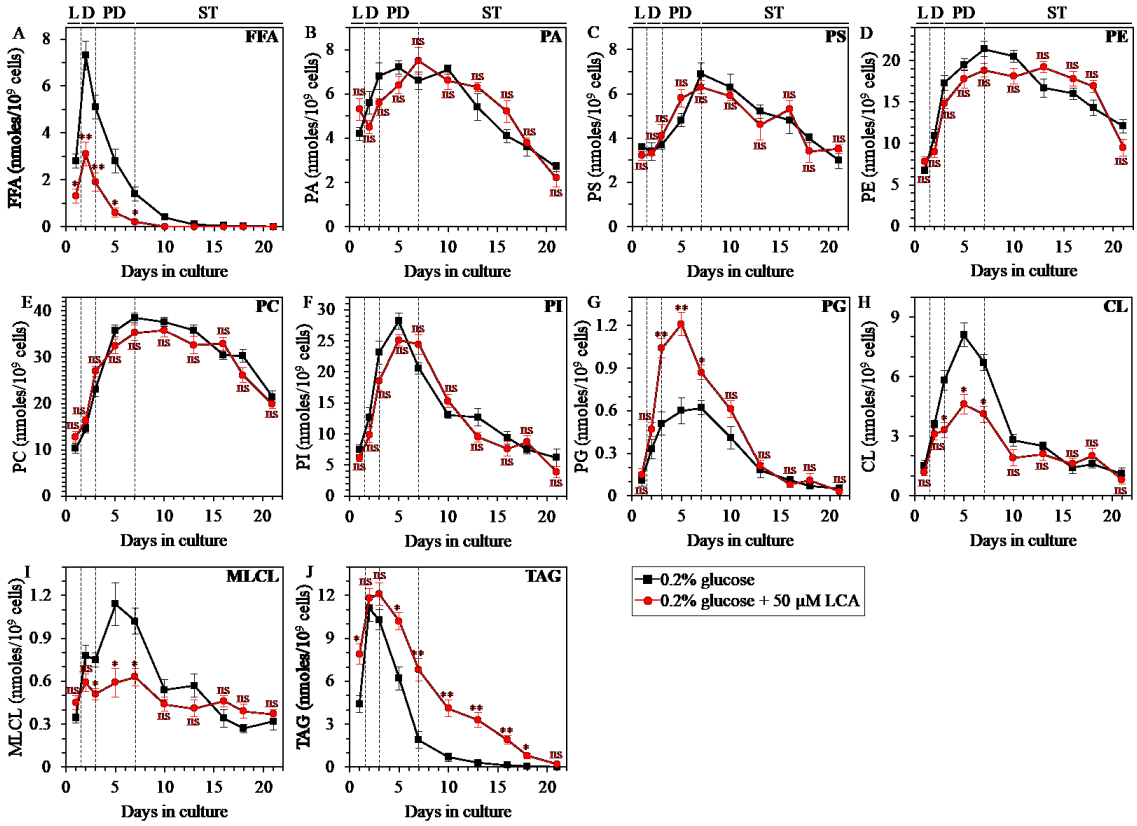

Figure 5.4. Under CR conditions, LCA exhibits age-related differential effects on the concentrations of several classes of cellular lipids in WT yeast. WT cells were cultured in the nutrient-rich YP medium initially containing 0.2% glucose with 50 µM LCA or without it. Following extraction of lipids from cells recovered on different days of culturing, various lipid classes were identified and quantitated by mass spectrometry as described in Materials and Methods. Data are presented as means ± SEM (n = 3; *p < 0.05; **p < 0.01; ns, not significant). Abbreviations: CL, cardiolipin; FFA, free fatty acids; L, D, PD and ST, logarithmic, diauxic, post-diauxic and stationary growth phases (respectively); MLCL, monolysocardiolipin; PA, phosphatidic acid; PC, phosphatidylcholine; PE, phosphatidylethanolamine; PG, phosphatidylglycerol; PI, phosphatidylinositol; PS, phosphatidylserine; TAG, triacylglycerol. These experiments were performed by Simon Bourque, Vincent Richard, Karamat Mohammad and me.

Moreover, as we have described previously [64, 145, 236, 248], because within a yeast cell LCA amasses primarily in both mitochondrial membranes and specifically alters phospholipid metabolism and transport in these membranes, LCA exhibited the following effects on the cellular concentrations of the signature mitochondrial membrane lipids cardiolipin (CL), monolysocardiolipin (MLCL) and phosphatidylglycerol (PG): 1) in D and PD phases, LCA decreased the concentrations of CL and MLCL, both of which are synthesized in the IMM from

PG (Figures 2H and 2I, respectively); and 2) in D and PD phases, LCA also increased the concentration of PG (Figure 5.4G).

Unlike the ability of LCA to alter the cellular concentrations of FFA, TAG, CL, MLCL and PG, this bile acid had no significant effect on the concentrations of the following phospholipids: phosphatidic acid (PA), phosphatidylserine (PS), phosphatidylethanolamine (PE), phosphatidylcholine (PC) and phosphatidylinositol (PI) (Figures 5.4B, 5.4C, 5.4D, 5.4E and 5.4F, respectively).

In sum, these findings further support our hypothesis on the mechanism through which LCA regulates the anabolic branch of TAG metabolism in the ER and the catabolic branch of TAG metabolism in LD. In this mechanism: 1) by accelerating TAG synthesis from FFA within the ER and the subsequent TAG deposition within LD during L and, likely, D phases of culturing under CR conditions, LCA decreases the concentration of FFA during these two phases; and 2) by decelerating TAG lipolysis into FFA within LD during PD and ST phases of culturing under CR conditions, LCA decreases the concentration of FFA during these two phases (Figure 5.5).

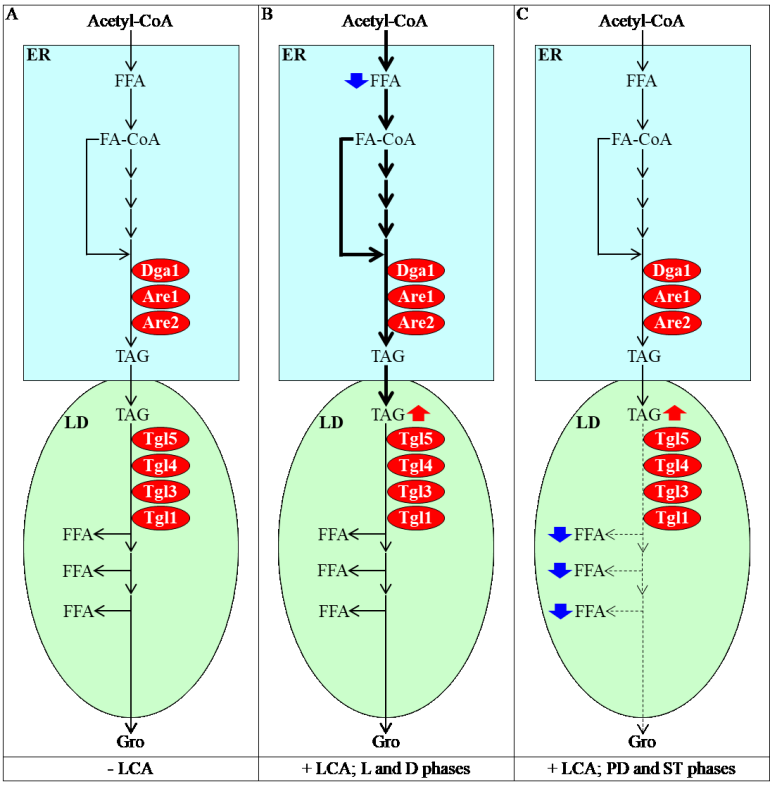

Figure 5.5. Mechanism through which LCA regulates the anabolic branch of triacylglycerol (TAG) metabolism in the endoplasmic reticulum (ER) and the catabolic branch of TAG metabolism in lipid droplets (LD). (**A**) Relative rates of reactions and relative concentrations of metabolites in the anabolic branch of TAG metabolism in the ER and the catabolic branch of TAG metabolism in LD in yeast cells cultured under CR conditions without LCA. (**B**) During logarithmic (L) and diauxic (D) phases of culturing under CR conditions with LCA, this bile acid accelerates TAG synthesis from free fatty acids (FFA) within the ER and the subsequent TAG deposition within LD, thereby decreasing the concentration of FFA during these phases. (**C**) During post-diauxic (PD) and stationary (ST) phases of culturing under CR conditions with LCA, this bile acid decelerates TAG lipolysis into FFA within LD, thus decreasing the concentration of FFA during PD and ST phases. The thickness of black arrows is proportional to the rates of the corresponding metabolic reactions. Arrows next to the names of lipid classes denote those of them whose concentrations are increased (red arrows) or decreased (blue arrows) in yeast cultured under CR conditions with LCA. Abbreviations: Are1/2, acyl-coenzyme A: cholesterol acyl transferase-related enzymes 1 and 2; Dga1, diacylglycerol acyltransferase 1; FA-CoA, fatty acyl-CoA ester; Gro, glycerol; MAG, monoacylglycerol; Tgl1/3/4/5, triglyceride lipases 1, 3, 4 and 5.

5.3.4 The efficiency of longevity extension by LCA inversely correlates with the intracellular concentration of FFA

Because LCA causes a significant decline in the concentration of FFA during several consecutive phases of culturing under CR conditions, we sought to determine if the extent of such decline correlates with the efficiency of longevity extension by LCA under these conditions.

We first assessed how a single-gene-deletion mutation eliminating the Dga1, Are1 or Are2 protein, each catalyzing the synthesis of TAG from FFA in the ER (Figure 5.5), influences the efficiency of yeast chronological lifespan (CLS) extension by LCA and how it affects the cellular concentration of FFA under CR conditions. We found that the *dga1Δ*, *are1Δ* and *are2Δ* mutations exhibit the following effects: 1) each of them significantly decreases the extent to which LCA can extend both the mean and maximum CLS (Figures 5.6A-5.6D for *dga1Δ*, Figures 5.6F-5.6I for *are1Δ* and Figures 5.6K-5.6N for *are2Δ*); and 2) each of them significantly increases the cellular concentration of FFA (Figures 5.6E, 5.6J and 5.6O for *dga1Δ*, *are1Δ* and *are2Δ* [respectively]).

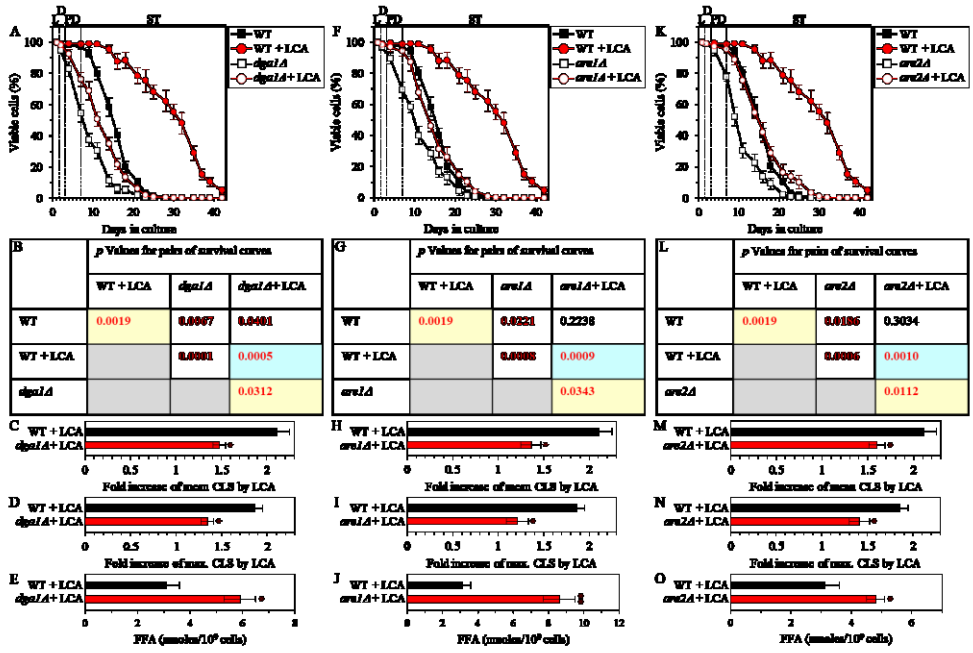

Figure 5.6. Under CR conditions in the presence of LCA, lack of any of the three enzymes involved in the synthesis of TAG from FFA increases the concentration of FFA and decreases the extent to which LCA can extend yeast chronological lifespan (CLS). WT cells and mutant cells carrying a single-gene-deletion mutation eliminating either the Dga1, Are1 or Are2 protein were cultured in the nutrient-rich YP medium initially containing 0.2% glucose with 50 μM LCA or without it. (**A**, **F**, **K**) Survival curves of the chronologically aging WT and *dga1Δ* (**A**), WT and *are1Δ* (**F**) or WT and *are2Δ* (**K**) strains are shown. Data are presented as means ± SEM (n = 3). Data for the WT strain cultured with or without LCA are replicated in graphs **A**, **F**, **K** of this Figure. (**B**, **G**, **L**) *p* Values for different pairs of survival curves of the WT and *dga1Δ* (**B**), WT and *are1Δ* (G) or WT and *are2Δ* (**L**) strains cultured with or without LCA. Survival curves shown in (**A**, **F** or **K**, respectively) were compared. Two survival curves were considered statistically different if the *p* value was less than 0.05. The *p* values for comparing pairs of survival curves using the logrank test were calculated as described in Materials and Methods. The *p* values displayed on a yellow color background indicate that LCA extends the CLS of the WT, *dga1Δ* (**B**), *are1Δ* (**G**) and *are2Δ* (**L**) strains. The *p* values displayed on a blue color background indicate that LCA extends the CLS of the *dga1Δ* (**B**), *are1Δ* (**G**) and *are2Δ* (**L**) strains to a lower extent than that of the WT strain. (**C**, **D**, **H**, **I**,

M, **N**) Survival curves shown in (**A**, **F**, **K**) were used to calculate the fold of increase of the mean (**C**, **H**, **M**) and maximum (**D**, **I**, **N**) CLS by LCA for the WT and *dga1Δ* (**C**, **D**), WT and *are1Δ* (**H**, **I**) or WT and *are2Δ* (**M**, **N**) strains. Data are presented as means ± SEM (n = 3; **p* < 0.05). (**E**, **J**, **O**) The maximum concentration of FFA, which was observed in WT and *dga1Δ* (**E**), WT and *are1Δ* (**J**) or WT and *are2Δ* (**O**) cells recovered on day 2 of culturing with LCA, is shown. Data are presented as means ± SEM (n = 3; **p* < 0.05; ***p* < 0.01). Abbreviations: FFA, free fatty acids; L, D, PD and ST, logarithmic, diauxic, post-diauxic and stationary growth phases (respectively). These experiments were performed by Alexander Goldberg, Pavlo Kyryakov, Alejandra Gomez-Perez and Olivia Koupaki.

Using these data, we compared the fold increase of mean or maximum CLS and the maximum intracellular concentration of FFA (which was observed in WT, *dga1Δ*, *are1Δ* and *are2Δ* cells recovered on day 2 of culturing with LCA under CR conditions). We found that the Pearson's correlation coefficient (r) values for the correlation between these two compared variables are less than -0.8 for both possible pairwise combinations of the mean or maximum CLS and the maximum intracellular concentration of FFA (Figure 5.7). Because the Pearson's r value ranging from -0.7 to -0.9 is considered a high negative correlation between the two variables [244], we concluded that the fold increase of mean or maximum CLS has a high negative correlation with the intracellular concentration of FFA. Thus, the efficiency of longevity extension by LCA inversely correlates with the intracellular concentration of FFA.

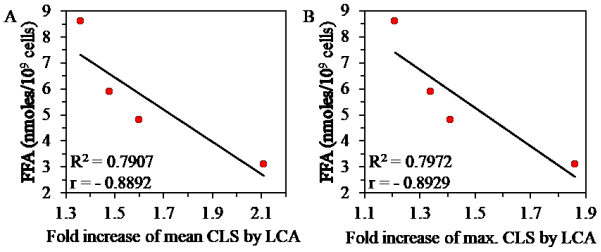

C

Genetic background	Fold increase of mean CLS by LCA	Fold increase of max. CLS by LCA	FFA concentration (nmoles/10^9 cells)
WT	2.11 ± 0.14	1.86 ± 0.09	3.1 ± 0.5
are2Δ	1.6 ± 0.09	1.41 ± 0.11	4.8 ± 0.3
dga1Δ	1.48 ± 0.07	1.34 ± 0.07	5.9 ± 0.6
are1Δ	1.36 ± 0.11	1.21 ± 0.12	8.6 ± 0.9

Figure 5.7. Under CR conditions in the presence of LCA, lack of any of the three enzymes involved in the synthesis of TAG from FFA decreases the extent to which LCA can extend yeast CLS proportionally to the cellular concentration of FFA. WT cells and mutant cells carrying a single-gene-deletion mutation eliminating either Dga1, Are1 or Are2 were cultured in the nutrient-rich YP medium initially containing 0.2% glucose with 50 μM LCA. Survival curves shown in Figures **3A**, **3F** and **3K** were used to calculate the folds of increase of the mean and maximum CLS by LCA for the WT and *dga1Δ*, *are1Δ* or *are2Δ* strains. (**A**, **B**) Plots comparing the folds increase of mean (**A**) or maximum (**B**) CLS and the maximum intracellular concentration of FFA (which was observed in WT and mutant cells recovered on day 2 of culturing with LCA). Different points show the data for WT, *dga1Δ*, *are1Δ* or *are2Δ* cells. Linear trendlines and the R-squared values are displayed; these values demonstrate a good fit of the line to the data. The Pearson's correlation coefficient (r) values are also shown; because the r value ranging from -0.7 to -0.9 is considered a high negative correlation between the two variables, the fold increase of the mean (**A**) or maximum (**B**) CLS has a high negative correlation with the intracellular concentration of FFA. (**C**) The experimental data used to create plots shown in (**A** and **B**). Genetic backgrounds of strains, the folds of increase of the mean and maximum CLS by LCA, and the maximum concentration of FFA (which was observed in WT and mutant cells recovered on day 2 of culturing with LCA) are shown. Data are presented as means ± SEM (n = 3). Abbreviation: FFA, free fatty acids. These experiments were performed by Simon Bourque, Vincent Richard, Karamat Mohammad and me.

We then investigated how a single-gene-deletion mutation eliminating the Tgl1, Tgl3, Tgl4 or Tgl5 protein, each catalyzing TAG lipolysis that yields FFA in LD (Figure 5.5), affects the efficiency of yeast CLS extension by LCA and how it influences the cellular concentration of FFA under CR conditions. We found that the *tgl1Δ*, *tgl3Δ*, *tgl4Δ* and *tgl5Δ* mutations have the following effects: 1) each of them significantly increases the extent to which LCA can prolong both the mean and maximum CLS (Figures 5.8A-5.8D for *tgl1Δ*, Figures 5.8F-5.8I for *tgl3Δ*, Figures 5.9A-5.9D for *tgl4Δ* and Figures 5.9F-5.9I for *tgl5Δ*); and 2) each of them significantly decreases the cellular concentration of FFA (Figures 5.8E, 5.8J, 5.9E and 5.9J for *tgl1Δ*, *tgl3Δ*, *tgl4Δ* and *tgl5Δ* [respectively]). We used these data to compare the fold increase of mean or maximum CLS and the maximum intracellular concentration of FFA (which was observed in WT, *tgl1Δ*, *tgl3Δ*, *tgl4Δ* and *tgl5Δ* cells recovered on day 2 of culturing with LCA under CR conditions). The Pearson's r values for the correlation between these two variables were less than -0.9 for both possible pairwise combinations (Figure 5.10). Hence, the fold increase of mean or maximum CLS has a very high negative correlation with the intracellular concentration of FFA. These results confirm our assumption that the efficiency of longevity extension by LCA inversely correlates with the intracellular concentration of FFA.

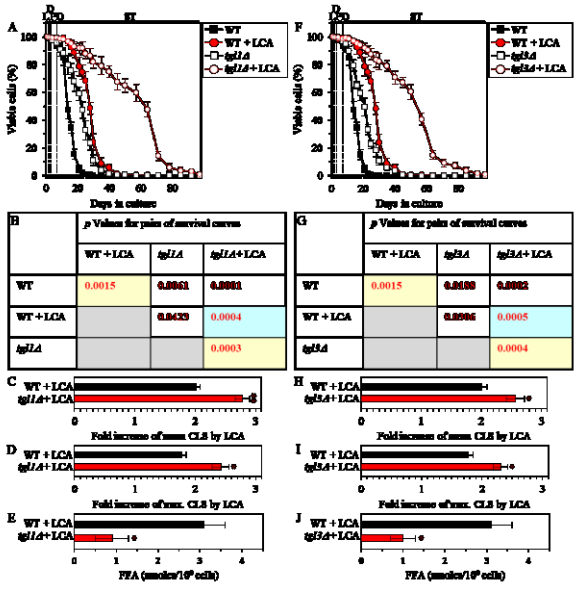

Figure 5.8. Under CR conditions in the presence of LCA, lack of the Tgl1 or Tgl3 enzymes involved in the TAG lipolysis that yields FFA decreases the concentration of FFA and increases the extent to which LCA can extend yeast CLS. WT cells and mutant cells carrying a single-gene-deletion mutation eliminating either the Tgl1 or Tgl3 protein were cultured in the nutrient-rich YP medium initially containing 0.2% glucose with 50 μM LCA or without it. (**A**, **F**) Survival curves of the chronologically aging WT and *tgl1Δ* (**A**) or WT and *tgl3Δ* (F) strains are shown. Data are presented as means ± SEM (n = 3). Data for the WT strain cultured with or without LCA are replicated in graphs **A**, **F** of this Figure and in graphs **A**, **F** of Figure 5. (**B**, **G**) *p* Values for different pairs of survival curves of the WT and *tgl1Δ* (**B**) or WT and *tgl3Δ* (G) strains cultured with or without LCA. Survival curves shown in **A** or **F** (respectively) were compared. Two survival curves were considered statistically different if the *p* value was less than 0.05. The *p* values for comparing pairs of survival curves using the logrank test were calculated as described in Materials and Methods. The *p* values displayed on a yellow color background indicate that LCA extends the CLS of the WT (**B** and **G**), *tgl1Δ* (**B**) and *tgl3Δ* (**G**) strains. The *p* values displayed on a blue color background indicate that LCA extends the CLS of the *tgl1Δ* (**B**) and *tgl3Δ* (**G**) strains to a higher extent that that of the WT strain. (**C**, **D**, **H**, **I**) Survival curves shown in (**A**, **F**) were used to calculate the fold of increase of the mean (**C**, **H**) and maximum (**D**, **I**) CLS by LCA for the WT and *tgl1Δ* (**C**, **D**) or WT and *tgl3Δ* (**H**, **I**) strains. Data are presented as means ± SEM (n = 3; **p* < 0.05; ***p* < 0.01). (**E**, **J**) The maximum concentration of FFA, which was observed in WT

and *tgl1Δ* (**E**) or WT and *tgl3Δ* (**J**) cells recovered on day 2 of culturing with LCA, is shown. Data are presented as means ± SEM (n = 3; **p* < 0.05). Abbreviations: FFA, free fatty acids; L, D, PD and ST, logarithmic, diauxic, post-diauxic and stationary growth phases (respectively). These experiments were performed by Alexander Goldberg, Pavlo Kyryakov, Alejandra Gomez-Perez and Olivia Koupaki.

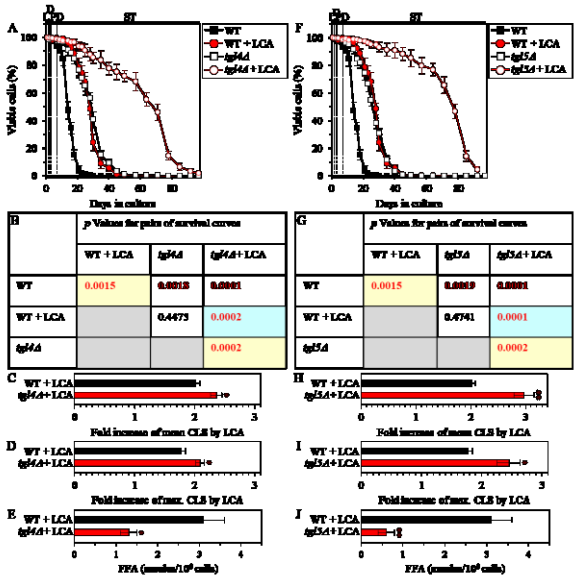

Figure 5.9. Under CR conditions in the presence of LCA, lack of the Tgl4 or Tgl5 enzymes involved in the TAG lipolysis that yields FFA decreases the concentration of FFA and increases the extent to which LCA can extend yeast CLS. WT cells and mutant cells carrying a single-gene-deletion mutation eliminating either the Tgl4 or Tgl5 protein were cultured in the nutrient-rich YP medium initially containing 0.2% glucose with 50 μM LCA or without it. (**A**, **F**) Survival curves of the chronologically aging WT and *tgl4Δ* (**A**) or WT and *tgl5Δ* (F) strains are shown. Data are presented as means ± SEM (n = 3). Data for the WT strain cultured with or without LCA are replicated in graphs **A**, **F** of this Figure and in graphs **A**, **F** of Figure 4. (**B**, **G**) *p* Values for different pairs of survival curves of the WT and *tgl4Δ* (**B**) or WT and *tgl5Δ* (G) strains cultured with or without LCA. Survival curves shown in **A** or **F** (respectively) were compared. Two survival curves were considered statistically different if the *p* value was less than 0.05. The *p* values for comparing pairs of survival curves using the logrank test were calculated as described in Materials and Methods. The *p* values displayed on a yellow color background indicate that LCA extends the CLS of the WT (**B** and **G**), *tgl4Δ* (**B**) and *tgl5Δ* (**G**) strains. The *p* values displayed on a blue color background indicate that LCA extends the CLS of *tgl4Δ* (**B**) and *tgl5Δ* (**G**) strains to a higher extent that that of the WT strain. (**C**, **D**, **H**, **I**) Survival curves shown in (**A**, **F**) were used to calculate the fold of increase of the mean (**C**, **H**) and maximum (**D**, **I**) CLS by LCA for the WT and *tgl4Δ* (**C**, **D**) or WT and *tgl5Δ* (**H**, **I**) strains. Data are presented as means ± SEM (n = 3; **p* < 0.05; ***p* < 0.01). (**E**, **J**) The maximum concentration of FFA, which was observed in WT and *tgl4Δ* (**E**) or WT and *tgl5Δ* (**J**) cells recovered on day 2 of culturing with LCA, is shown. Data are presented as means ± SEM (n = 3; **p* < 0.05; ***p* <0.01). Abbreviations: FFA, free fatty acids; L, D, PD and ST, logarithmic, diauxic, post-diauxic and stationary growth phases (respectively). These experiments were performed by Alexander Goldberg, Pavlo Kyryakov, Alejandra Gomez-Perez and Olivia Koupaki.

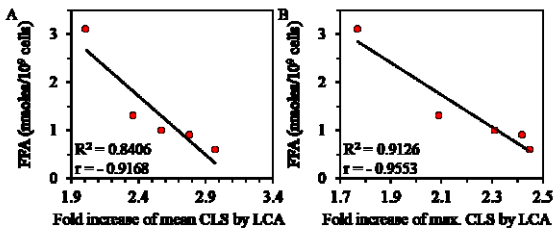

C

Genetic background	Fold increase of mean CLS by LCA	Fold increase of max. CLS by LCA	FFA concentration (nmoles/10⁹ cells)
WT	2.01 ± 0.08	1.77 ± 0.08	3.1 ± 0.5
tgl4Δ	2.36 ± 0.09	2.09 ± 0.07	1.3 ± 0.2
tgl3Δ	2.57 ± 0.15	2.31 ± 0.12	1.0 ± 0.3
tgl1Δ	2.78 ± 0.12	2.42 ± 0.14	0.9 ± 0.4
tgl5Δ	2.97 ± 0.18	2.45 ± 0.19	0.6 ± 0.2

Figure 5.10 Under CR conditions in the presence of LCA, lack of any of the four enzymes involved in the TAG lipolysis that yields FFA increases the extent to which LCA can extend yeast CLS proportionally to the cellular concentration of FFA. WT cells and mutant cells carrying a single-gene-deletion mutation eliminating either Tgl1, Tgl3, Tgl4 or Tgl5 were cultured in the nutrient-rich YP medium initially containing 0.2% glucose with 50 μM LCA. Survival curves shown in Figures **4A**, **4F**, **5A** and **5F** were used to calculate the folds of increase of the mean and maximum CLS by LCA for the WT, *tgl1Δ*, *tgl3Δ*, *tgl4Δ* and *tgl5Δ* strains. (**A**, **B**) Plots comparing the folds increase of mean (**A**) or maximum (**B**) CLS and the maximum intracellular concentration of FFA (which was observed in WT and mutant cells recovered on day 2 of culturing with LCA). Different points show the data for WT, *tgl1Δ*, *tgl3Δ*, *tgl4Δ* or *tgl5Δ* cells. Linear trendlines and the R-squared values are displayed; these values demonstrate a good fit of the line to the data. The Pearson's correlation coefficient (r) values are also shown; because the r value ranging from -0.9 to -1.0 is considered a very high negative correlation

between the two variables, the fold increase of the mean (**A**) or maximum (**B**) CLS has a high negative correlation with the intracellular concentration of FFA. (**C**) The experimental data used to create plots shown in (**A** and **B**). Genetic backgrounds of strains, the folds of increase of the mean and maximum CLS by LCA, and the maximum concentration of FFA (which was observed in WT and mutant cells recovered on day 2 of culturing with LCA) are shown. Data are presented as means ± SEM (n = 3). Abbreviation: FFA, free fatty acids. These experiments were performed by Simon Bourque, Vincent Richard, Karamat Mohammad and me.

In sum, the above findings indicate that LCA delays yeast chronological aging in part because it decreases the intracellular concentration of FFA.

5.3.5 LCA delays the age-related onset and decelerates progression of liponecrosis and decreases cell susceptibility to this form of RCD in an age-dependent manner

Our recent study has revealed that CR extends yeast CLS in part because this low-calorie diet allows cells to maintain a low concentration of FFA during PD and ST phases, thereby postponing the onset of the liponecrotic mode of RCD [249]. The present study indicates that in yeast cultured under CR conditions, LCA causes further decline in the concentration of FFA in L, D, PD and the beginning of ST phases (Figure 5.4A). We therefore sought to determine if LCA may further postpone the age-related onset of liponecrotic RCD in chronologically aging yeast under CR conditions.

We first used live-cell fluorescence microscopy with propidium iodide (PI), a stain for visualizing the loss of plasma membrane (PM) integrity (a hallmark event of necrosis), to monitor how LCA influences age-related changes in the percentage of calorically restricted WT cells exhibiting PI positive staining; this staining is characteristic of necrotic cell death. We found that in WT cells LCA delays the onset of necrosis in the end of PD phase and slows down the progression of this cell death mode during ST phase of culturing under CR conditions (Figures 5.11A and 5.11B).

We then examined if LCA influences the susceptibility of calorically restricted WT cells to liponecrotic RCD; this mode of age-related RCD can be triggered by a short-term treatment of yeast with FFA [14, 103, 185, 186, 238]. We found that in WT yeast cultured under CR conditions, LCA significantly increases clonogenic survival of cells briefly (for 2 h) treated with palmitoleic acid (POA; a monounsaturated form of FFA) if these cells were recovered during PD or ST phase of culturing (Figure 5.11C).

These findings indicate that in WT yeast limited in calorie supply, LCA postpones the age-related onset and slows down the progression of liponecrotic RCD and decreases cell susceptibility

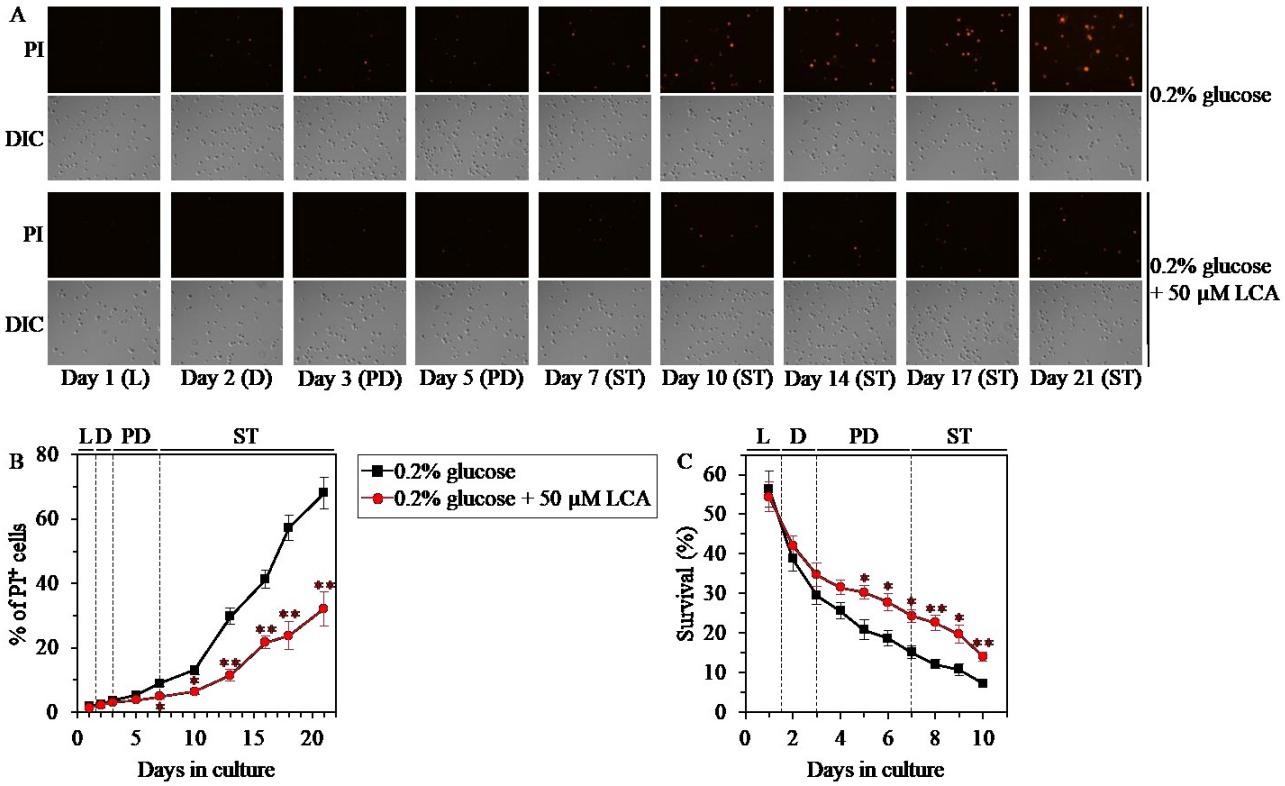

Figure 5.11. Under CR conditions, LCA postpones the age-related onset of necrotic cell death and decreases cell susceptibility to a liponecrotic mode of regulated cell death (RCD). WT cells were cultured in the nutrient-rich YP medium initially containing 0.2% glucose with 50 µM LCA or without it. (**A**) Cells recovered on different days of culturing were visualized using the DIC microscopy and stained with propidium iodide (PI) for visualizing the loss of plasma membrane integrity (a hallmark event of necrosis) as described in Materials and Methods. (**B**) Percentage of cells exhibiting PI positive staining characteristic of necrotic cell death. Images like the representative images shown in (**A**) were quantitated. Data are presented as means ± SEM (n = 3; *p < 0.05; **p < 0.01). Data for the WT strain cultured with LCA are replicated in graph **A** of Figure 7. (**C**) Clonogenic survival of cells recovered on different days of culturing and then treated for 2 h with 0.15 mM palmitoleic acid (POA, a monounsaturated form of FFA) to elicit a liponecrotic mode of RCD as described in Materials and Methods. Data are presented as means ± SEM (n = 3; *p < 0.05; **p < 0.01). Data for the WT strain cultured with LCA are replicated in graph **D** of Figure 7. Abbreviations: L, D, PD and ST, logarithmic, diauxic, post-diauxic and stationary growth phases (respectively).

to this mode of RCD in an age-dependent manner. It is conceivable that LCA may extend longevity of chronologically aging WT cells under CR conditions in part by decreasing the risk of liponecrotic RCD during PD and ST phases and actively increasing the chance of cell survival during these phases.

5.3.6 The efficiency with which LCA decreases the risk of age-related liponecrotic RCD inversely correlates with the intracellular concentration of FFA

Since LCA elicits a substantial reduction in the concentration of FFA in yeast cultured under CR conditions, we assessed if the extent of such reduction correlates with the efficiencies of the following LCA-dependent processes: 1) the delay of the age-related onset of liponecrotic RCD; 2) the deceleration of progression of liponecrotic RCD; and 3) the decrease in cell susceptibility to liponecrotic RCD.

We initially tested how a single-gene-deletion mutation eliminating the Dga1, Are1 or Are2 protein, each catalyzing the synthesis of TAG from FFA in the ER (Figure 5.5), influences age-related changes in the following traits of yeast cells limited in calorie supply: 1) the percentage of cells that display PI positive staining characteristic of necrotic cell death; 2) the susceptibility of cells to liponecrotic RCD caused by a brief (for 2 h) treatment of these cells with POA; and 3) the intracellular concentration of FFA. We found that the *dga1Δ*, *are1Δ* and *are2Δ* mutations have the following effects: 1) since the middle of PD phase of cell culturing, each of them significantly increases the percentage of cells exhibiting PI positive staining typical of necrotic cell death (Figure 5.12A); 2) since the middle of PD phase of cell culturing, each of them significantly increases cell susceptibility to liponecrotic RCD caused by a 2-h treatment with POA (Figure 5.12D); 3) each of them significantly increases the cellular concentration of FFA (Figures 5.6E, 5.6J and 5.6O for *dga1Δ*, *are1Δ* and *are2Δ* [respectively]). We used these data to compare the maximum intracellular concentration of FFA (which was observed in WT, *dga1Δ*, *are1Δ* and *are2Δ* cells recovered on day 2 of culturing with LCA under CR conditions) as one variable and each of the following two variables: 1) the maximum percentages of cells exhibiting PI positive staining (which were observed in WT and mutant cells recovered on day 21, the last day of culturing with LCA); or 2) the minimum percentages of clonogenic survival of POA-treated cells (which were observed in WT and mutant cells recovered on day 10, the last day of cell recovery from the culture for the treatment with POA). The Pearson's r value for the correlation between the maximum intracellular concentration of FFA and the maximum percentage of cells exhibiting PI positive staining was more than 0.8 (Figure 5.12B). Thus, the maximum percentage of cells exhibiting PI positive staining has a high positive correlation with the intracellular concentration of FFA. The Pearson's r value for the correlation between the maximum intracellular concentration of FFA and the minimum percentage of clonogenic survival of POA-treated cells was less than -0.8 (Figure 5.12E). Hence, the minimum percentage of clonogenic survival of POA-treated cells has a high negative correlation with the intracellular concentration of FFA. We therefore

concluded that there is an inverse relationship between the extent of the LCA-dependent decline in the concentration of FFA and the efficiencies of the following LCA-dependent processes: 1) the delay of the age-related onset of liponecrotic RCD; 2) the deceleration of progression of liponecrotic RCD; and 3) the decrease in cell susceptibility to liponecrotic RCD.

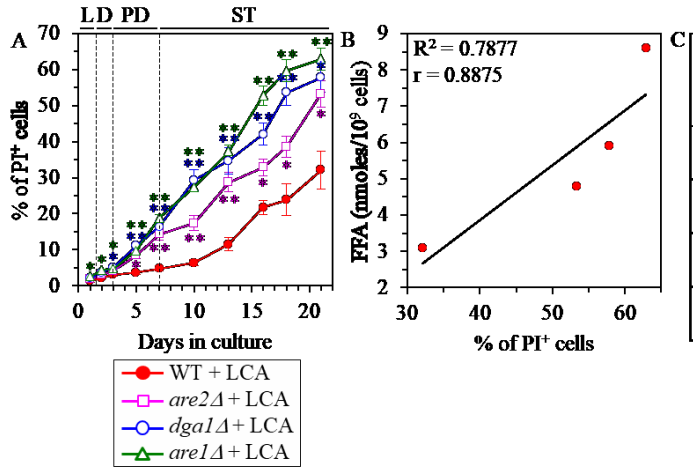

Genetic background	% of PI⁺ cells	FFA conc. (nmoles/10^9 cells)
WT	32.1 ± 5.3	3.1 ± 0.5
are2Δ	53.3 ± 3.7	4.8 ± 0.3
dga1Δ	57.8 ± 4.0	5.9 ± 0.6
are1Δ	62.9 ± 3.1	8.6 ± 0.9

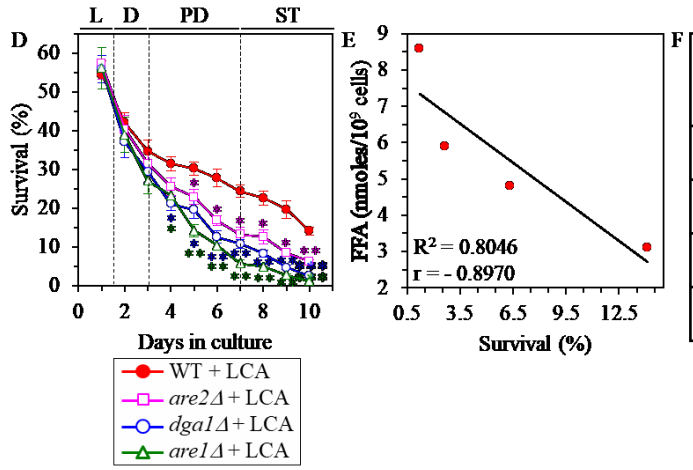

Genetic background	Survival (%)	FFA conc. (nmoles/10^9 cells)
WT	14.1 ± 1.1	3.1 ± 0.5
are2Δ	6.3 ± 0.5	4.8 ± 0.3
dga1Δ	2.6 ± 0.3	5.9 ± 0.6
are1Δ	1.2 ± 0.4	8.6 ± 0.9

Figure 5.12. Under CR conditions in the presence of LCA, lack of any of the three enzymes involved in the synthesis of TAG from FFA accelerates the age-related onset of necrotic cell death and increases cell susceptibility to liponecrotic RCD proportionally to the cellular concentration of FFA. WT cells and mutant cells carrying a single-gene-deletion mutation eliminating either the Dga1, Are1 or Are2 protein were cultured in the nutrient-rich YP medium initially containing 0.2% glucose with 50 µM LCA. (**A**) Cells recovered on different days of culturing were visualized using the DIC microscopy and stained with PI for visualizing the loss of plasma membrane integrity (a hallmark event of necrosis) as described in Materials and Methods. Percentage of cells exhibiting PI positive staining characteristic of necrotic cell death is shown. Data are presented as means ± SEM (n = 3; *p < 0.05; **p < 0.01). Data for the WT strain cultured with LCA are replicated in graph **B** of Figure 6. (**B**) Plot comparing the maximum percentage of cells exhibiting PI positive staining (which was observed in WT and mutant cells recovered on day 21, the last day of culturing with LCA) and the maximum concentration of FFA (which was observed in WT and mutant cells recovered on day 2 of culturing with LCA). Different points show the data for WT, *dga1Δ*, *are1Δ* or *are2Δ* cells. Linear trendline and the R-squared value are displayed; the R-squared value demonstrates a good fit of the line to the data. The Pearson's correlation coefficient (r) value is also shown; because the r value ranging from 0.7 to 0.9 is considered a high positive correlation between the two variables, the percentage of cells exhibiting PI positive staining has a high positive correlation with the intracellular concentration of FFA. (**C**) The experimental data used to

create the plot shown in (**B**). Genetic backgrounds of strains, the percentage of cells exhibiting PI positive staining on day 21 (the last day) of culturing with LCA and the maximum concentration of FFA, which was observed in WT and mutant cells recovered on day 2 of culturing with LCA, are shown. Data are presented as means ± SEM (n = 3). (**D**) Clonogenic survival of cells recovered on different days of culturing and then treated for 2 h with 0.15 mM POA (a monounsaturated form of FFA) to elicit a liponecrotic mode of RCD as described in Materials and Methods. Data are presented as means ± SEM (n = 3; *p < 0.05; **p < 0.01). Data for the WT strain cultured with LCA are replicated in graph **C** of Figure 6. (**E**) Plot comparing the minimum percentage of clonogenic survival of POA-treated cells (which was observed in WT and mutant cells recovered on day 10, the last day of cell recovery from the culture for the treatment with POA) and the maximum concentration of FFA (which was observed in WT and mutant cells recovered on day 2 of culturing with LCA). Different points show the data for WT, *dga1Δ*, *are1Δ* or *are2Δ* cells. Linear trendline and the R-squared value are displayed; the R-squared value demonstrates a good fit of the line to the data. The Pearson's correlation coefficient (r) value is also shown; because the r value ranging from -0.7 to -0.9 is considered a high negative correlation between the two variables, the percentage of clonogenic survival of POA-treated cells has a high negative correlation with the intracellular concentration of FFA. (**F**) The experimental data used to create the plot shown in (**E**). Genetic backgrounds of strains, the percentage of clonogenic survival of POA-treated cells on day 10 (the last day of cell recovery from the culture for the treatment with POA) and the maximum concentration of FFA, which was observed in WT and mutant cells recovered on day 2 of culturing with LCA, are shown. Data are presented as means ± SEM (n = 3). Abbreviations: FFA, free fatty acids; L, D, PD and ST, logarithmic, diauxic, post-diauxic and stationary growth phases (respectively); PI, propidium iodide.

We then investigated how a single-gene-deletion mutation eliminating the Tgl1, Tgl3, Tgl4 or Tgl5 protein, each catalyzing TAG lipolysis that yields FFA in LD (Figure 5.5), affects age-related changes in the above traits of liponecrotic RCD and how it influences the cellular concentration of FFA under CR conditions. We found that the *tgl1Δ*, *tgl3Δ*, *tgl4Δ* and *tgl5Δ* mutations exhibit the following effects: 1) since the beginning of ST phase of cell culturing, each of them significantly decreases the the percentage of cells exhibiting PI positive staining characteristic of necrotic cell death (Figure 5.13A); 2) since the end of PD phase of cell culturing, each of them significantly decreases cell susceptibility to liponecrotic RCD elicited in response to a 2-h treatment with POA (Figure 5.13D); 3) each of them significantly decreases the cellular concentration of FFA (Figures 5.8E, 5.8J, 5.9E and 5.9J for *tgl1Δ*, *tgl3Δ*, *tgl4Δ* and *tgl5Δ* [respectively]). Using these data, we compared the maximum intracellular concentration of FFA (which was observed in WT, *tgl1Δ*, *tgl3Δ*, *tgl4Δ* and *tgl5Δ* cells recovered on day 2 of culturing with LCA under CR conditions) as one variable and each of the above traits of liponecrotic RCD as another variable. The Pearson's r value for the correlation between the maximum intracellular concentration of FFA and the maximum percentage of cells exhibiting PI positive staining was more than 0.9 (Figure 5.13B). Hence, the maximum percentage of cells exhibiting PI positive staining has a very high positive correlation with the intracellular concentration of FFA. The Pearson's r value for the correlation between the maximum intracellular concentration of FFA and the minimum percentage of clonogenic survival of POA-treated cells was less than -0.9 (Figure

5.13E). Thus, the minimum percentage of clonogenic survival of POA-treated cells has a very high negative correlation with the intracellular concentration of FFA. These results confirm our assumption that the extent of the LCA-dependent decline in the concentration of FFA is in an inverse relationship with the LCA-dependent postponement of the age-related onset of liponecrotic RCD, the LCA-dependent slowing of progression of liponecrotic RCD and the LCA-dependent decline in cell susceptibility to liponecrotic RCD.

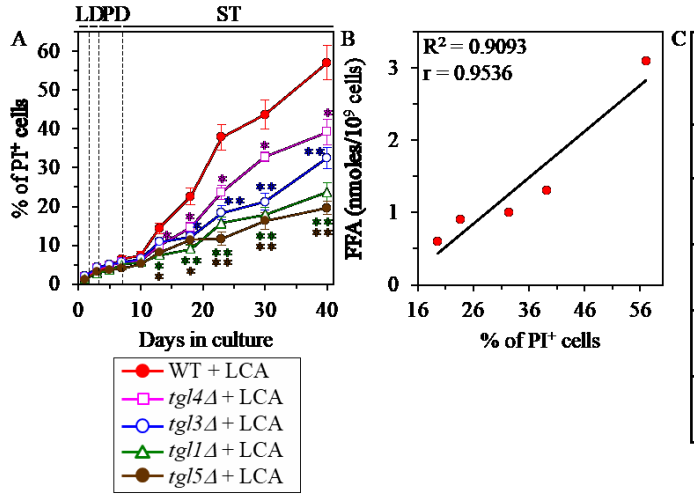

C

Genetic background	% of PI⁺ cells	FFA conc. (nmoles/10^9 cells)
WT	57.1 ± 4.4	3.1 ± 0.5
tgl4Δ	39.2 ± 3.3	1.3 ± 0.2
tgl3Δ	32.5 ± 2.8	1.0 ± 0.3
tgl1Δ	23.7 ± 2.4	0.9 ± 0.4
tgl5Δ	19.6 ± 1.7	0.6 ± 0.2

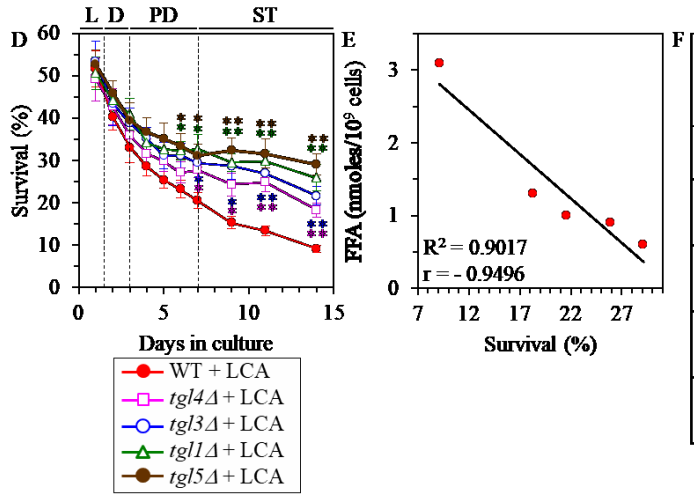

F

Genetic background	Survival (%)	FFA conc. (nmoles/10^9 cells)
WT	9.1 ± 0.9	3.1 ± 0.5
tgl4Δ	18.3 ± 1.7	1.3 ± 0.2
tgl3Δ	21.6 ± 2.2	1.0 ± 0.3
tgl1Δ	25.9 ± 3.1	0.9 ± 0.4
tgl5Δ	29.1 ± 2.5	0.6 ± 0.2

Figure 5.13. Under CR conditions in the presence of LCA, lack of any of the four enzymes involved in the TAG lipolysis that yields FFA decelerates the age-related onset of necrotic cell death and decreases cell susceptibility to liponecrotic RCD proportionally to the cellular concentration of FFA. WT cells and mutant cells carrying a single-gene-deletion mutation eliminating either the Tgl1, Tgl3, Tgl4 or Tgl5 protein were cultured in the nutrient-rich YP medium initially containing 0.2% glucose with 50 μM LCA. (**A**) Cells recovered on different days of culturing were visualized using the DIC microscopy and stained with PI for visualizing the loss of plasma membrane integrity (a hallmark event of necrosis) as described in Materials and Methods. Percent of cells exhibiting PI positive staining characteristic of necrotic cell death is shown. Data are presented as means ± SEM (n = 3; *p < 0.05; **p < 0.01). (**B**) Plot comparing the maximum percentage of cells exhibiting PI positive staining (which was observed in WT and mutant cells recovered on day 40, the last day of culturing with LCA) and the maximum concentration of FFA (which was observed in WT and mutant cells recovered on day 2 of culturing with LCA). Different points show

the data for WT, *tgl1Δ*, *tgl3Δ*, *tgl4Δ* or *tgl5Δ* cells. Linear trendline and the R-squared value are displayed; the R-squared value demonstrates a good fit of the line to the data. The Pearson's correlation coefficient (r) value is also shown; because the r value ranging from 0.9 to 1.0 is considered a very high positive correlation between the two variables, the percentage of cells exhibiting PI positive staining has a very high positive correlation with the intracellular concentration of FFA. (**C**) The experimental data used to create the plot shown in (**B**). Genetic backgrounds of strains, the percentage of cells exhibiting PI positive staining on day 40 (the last day) of culturing with LCA and the maximum concentration of FFA, which was observed in WT and mutant cells recovered on day 2 of culturing with LCA, are shown. Data are presented as means ± SEM (n = 3). (**D**) Clonogenic survival of cells recovered on different days of culturing and then treated for 2 h with 0.15 mM POA (a monounsaturated form of FFA) to elicit a liponecrotic mode of RCD as described in Materials and Methods. Data are presented as means ± SEM (n = 3; *p < 0.05; **p < 0.01). (**E**) Plot comparing the minimum percentage of clonogenic survival of POA-treated cells (which was observed in WT and mutant cells recovered on day 14, the last day of POA treatment) and the maximum concentration of FFA (which were observed in WT and mutant cells recovered on day 2 of culturing with LCA). Different points show the data for WT, *tgl1Δ*, *tgl3Δ*, *tgl4Δ* or *tgl5Δ* cells. Linear trendline and the R-squared value are displayed; the R-squared value demonstrates a good fit of the line to the data. The Pearson's correlation coefficient (r) value is also shown; because the r value ranging from -0.9 to -1.0 is considered a very high negative correlation between the two variables, the percentage of clonogenic survival of POA-treated cells has a very high negative correlation with the intracellular concentration of FFA. (**F**) The experimental data used to create the plot shown in (**E**). Genetic backgrounds of strains, the percentage of clonogenic survival of POA-treated cells on day 14 (the last day of POA treatment) and the maximum concentration of FFA, which was observed in WT and mutant cells recovered on day 2 of culturing with LCA, are shown. Data are presented as means ± SEM (n = 3). Abbreviations: FFA, free fatty acids; L, D, PD and ST, logarithmic, diauxic, post-diauxic and stationary growth phases (respectively); PI, propidium iodide.

It needs to be noted that the age-related onset of liponecrotic RCD and the rate of its progression in the above experiments were monitored in the absence of endogenous POA (a monounsaturated form of FFA), whereas cell susceptibility to liponecrotic RCD in these experiments was measured in yeast exposed to exogenous POA. Our previous studies have revealed that the buildup of POA-containing phospholipids in the PM and the excessive accumulation of POA-containing phospholipids in both mitochondrial membranes are direct pro-death processes in yeast treated with POA, whereas the assimilation of POA into TAG in the ER and the ensuing buildup of POA-containing TAG in LD are direct pro-survival processes in this yeast [103, 197, 198, 250]. We have also previously demonstrated that the *dga1Δ* and *are2Δ* mutations, both of which decelerate the synthesis of TAG from FFA in the ER (Figure 5.5) and decrease the incorporation of POA into TAG, increase cell susceptibility to liponecrotic RCD [103, 197]. These previous findings indicate the following: 1) an increase in the intracellular concentration of POA (a 16-carbon monounsaturated form of FFA) and the subsequent incorporation of POA into phospholipids increase the risk of liponecrotic RCD; and 2) a decrease in the intracellular concentration of POA caused by the assimilation of this form of FFA into TAG decreases the risk of liponecrotic RCD.

Altogether, the above findings and our previously published data [103, 197, 198, 250] indicate that the efficiency of decreasing the risk of age-related liponecrotic RCD by LCA inversely correlates with the intracellular concentration of FFA. Thus, in support of our hypothesis proposed at the end of the previous section, LCA delays yeast chronological aging under CR conditions in part by decreasing the risk of liponecrotic RCD during PD and ST phases and actively increasing the chance of cell survival during these phases.

5.3.7 The peroxisome-to-mitochondrion transport of acetyl-CoA via the carnitine shuttle is essential for the delay of yeast chronological aging by LCA

We have previously noticed that, during PD and ST phases of culturing yeast under CR on 0.2% glucose, LCA increases the concentrations of Cat2, Crc1, Yat1 and Yat2 [14, 236, 246]. All these proteins are known to be required for the carnitine-dependent transport of acetyl-CoA from peroxisomes (where acetyl-CoA is made as the final product of the β-oxidation of FFA) to mitochondria [251, 252] (Figure 5.2). We hypothesized that such peroxisome-to-mitochondrion transport of acetyl-CoA via the carnitine shuttle may contribute to the ability of LCA to postpone chronological aging of yeast limited in calorie supply. To test this hypothesis, we investigated how a single-gene-deletion mutation eliminating the Cat2, Crc1, Yat1 or Yat2 protein influences the efficiency of yeast CLS extension by LCA under CR conditions. We found that each of these mutations significantly decreases the extent to which LCA can prolong both the mean and maximum CLS (Figures 5.14A, 5.14E, 5.14I and 5.14J for *cat2Δ*; Figures 5.14B, 5.14F, 5.14I and 5.14J for *crc1Δ*; Figures 5.14C, 5.14G, 5.14I and 5.14J for *yat1Δ*; and Figures 5.14D, 5.14H, 5.14I and 5.14J for *yat2Δ*). We therefore concluded that the carnitine-dependent transport of acetyl-CoA from peroxisomes to mitochondria makes an essential contribution to the LCA-dependent delay of yeast chronological aging under CR conditions.

5.3.8 The peroxisome-to-mitochondrion transport of acetyl-CoA in the forms of the glyoxylate cycle intermediates citrate and succinate is dispensable for the delay of yeast chronological aging by LCA

Our previous studies have revealed that, during PD and ST phases of culturing yeast under CR on 0.2% glucose, LCA decreases the concentrations of the Cit2, Ctp1 and Dic1 proteins [14, 236, 246]. Cit2 is known to catalyze a peroxisomal reaction of the glyoxylate cycle leading to the

conversion of acetyl-CoA into citrate [253] (Figure 5.2). Ctp1 has been implicated in the delivery of this peroxisomally produced citrate to mitochondria, whereas Dic1 has been shown to be a mitochondrial transporter for another intermediate of the glyoxylate cycle, succinate [254]; both these transport proteins enable the replenishment of TCA cycle intermediates in mitochondria [57] (Figure 5.2).

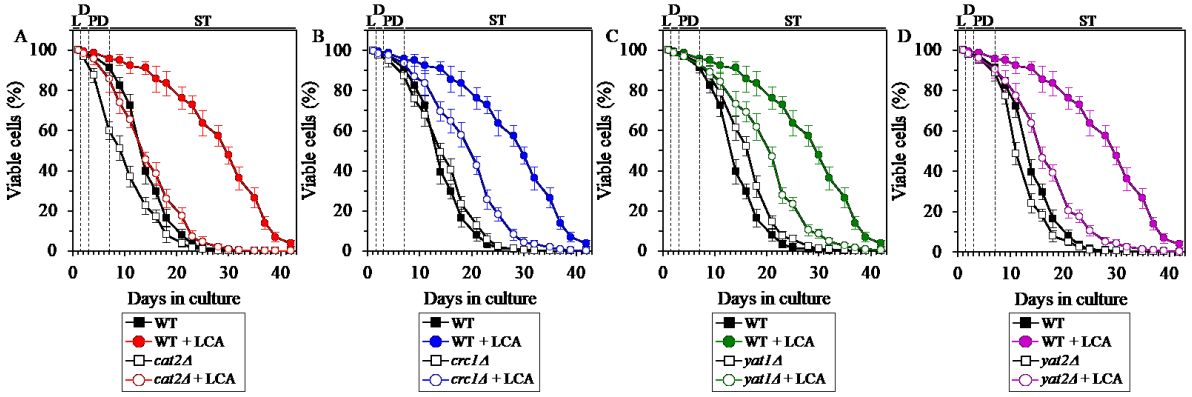

E

	p Values for pairs of survival curves		
	WT + LCA	*cat2Δ*	*cat2Δ* + LCA
WT	0.0009	**0.0343**	0.4810
WT + LCA		**0.0002**	0.0007
cat2Δ			0.0355

F

	p Values for pairs of survival curves		
	WT + LCA	*crc1Δ*	*crc1Δ* + LCA
WT	0.0009	0.4386	**0.0140**
WT + LCA		**0.0008**	0.0066
crc1Δ			0.0259

G

	p Values for pairs of survival curves		
	WT + LCA	*yat1Δ*	*yat1Δ* + LCA
WT	0.0009	0.0527	**0.0094**
WT + LCA		**0.0016**	0.0079
yat1Δ			0.0303

H

	p Values for pairs of survival curves		
	WT + LCA	*yat2Δ*	*yat2Δ* + LCA
WT	0.0009	0.0661	0.0581
WT + LCA		**0.0003**	0.0017
yat2Δ			0.0311

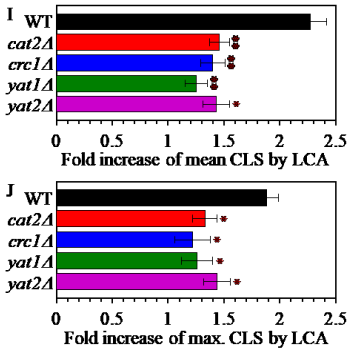

Figure 5.14. Under CR conditions in the presence of LCA, lack of any of the four proteins required for the transport of acetyl-CoA from peroxisomes to mitochondria via the carnitine shuttle decreases the efficiency of yeast CLS extension by LCA. WT cells and mutant cells carrying a single-gene-deletion mutation eliminating either the Cat2, Crc1, Yat1 or Yat2 protein were cultured in the nutrient-rich YP medium initially containing 0.2% glucose with 50 µM LCA or without it. (**A**, **B**, **C**, **D**) Survival curves of the chronologically aging WT and *cat2Δ* (**A**), WT and *crc1Δ* (**B**), WT and *yat1Δ* (**C**) or WT and *yat2Δ* (**D**) strains are shown. Data are presented as means ± SEM (n = 3). Data for the WT strain cultured with or without LCA are replicated in graphs **A**, **B**, **C**, **D** of this Figure. (**E**, **F**, **G**, **H**) *p* Values for different pairs of survival curves of the WT and *cat2Δ* (**E**), WT and *crc1Δ* (**F**), WT and *yat1Δ* (**G**) or WT and *yat2Δ* (**H**) strains cultured with or without LCA. Survival curves shown in (**A**, **B**, **C** or **D**, respectively) were compared. Two survival curves were considered statistically different if the *p* value was less than 0.05. The *p* values for comparing pairs of survival curves using the logrank test were calculated as described in Materials and Methods. The *p* values displayed on a yellow color background indicate that LCA extends the CLS of the WT, *cat2Δ* (**E**), *crc1Δ* (**F**), *yat1Δ* (**G**) and *yat2Δ* (**H**) strains. The *p* values displayed on a blue color background indicate that LCA extends the CLS of the *cat2Δ* (**E**), *crc1Δ* (**F**), *yat1Δ* (**G**) and *yat2Δ* (**H**) strains to a lower extent than that of the WT strain. (**I**, **J**) Survival curves shown in (**A**, **B**, **C**, **D**) were used to calculate the fold of increase of the mean (**I**) and maximum (**J**) CLS by LCA for the WT, *cat2Δ*, *crc1Δ*, *yat1Δ* and *yat2Δ* strains. Data are presented as means ± SEM (n = 3; **p* < 0.05; ***p* < 0.01). Abbreviations: L, D, PD and ST, logarithmic, diauxic, post-diauxic and stationary

growth phases (respectively). These experiments were performed by Alexander Goldberg, Pavlo Kyryakov, Alejandra Gomez-Perez and Olivia Koupaki.

We sought to determine whether the transport of acetyl-CoA from peroxisomes to mitochondria in the forms of citrate and succinate plays a role in the LCA-dependent delay of yeast chronological aging under CR conditions. We therefore assessed how a single-gene-deletion mutation eliminating the Cit2, Ctp1 or Dic1 protein affects the extent to which LCA can increase yeast CLS under CR conditions. We found that none of these mutations has a significant effect on the efficiency with which LCA can extend CLS under CR conditions (Figures 5.15A, 5.15D, 5.15G and 5.15H for *cit2Δ*; Figures 5.15B, 5.15E, 5.15G and 5.15H for *ctp1Δ*; and Figures 5.15C, 5.15F, 5.15G and 5.15H for *dic1Δ*). Hence, in yeast limited in calorie supply, the peroxisome-to-mitochondrion transport of acetyl-CoA in the forms of the glyoxylate cycle intermediates citrate and succinate does not make an essential contribution to the delay of yeast chronological aging by LCA.

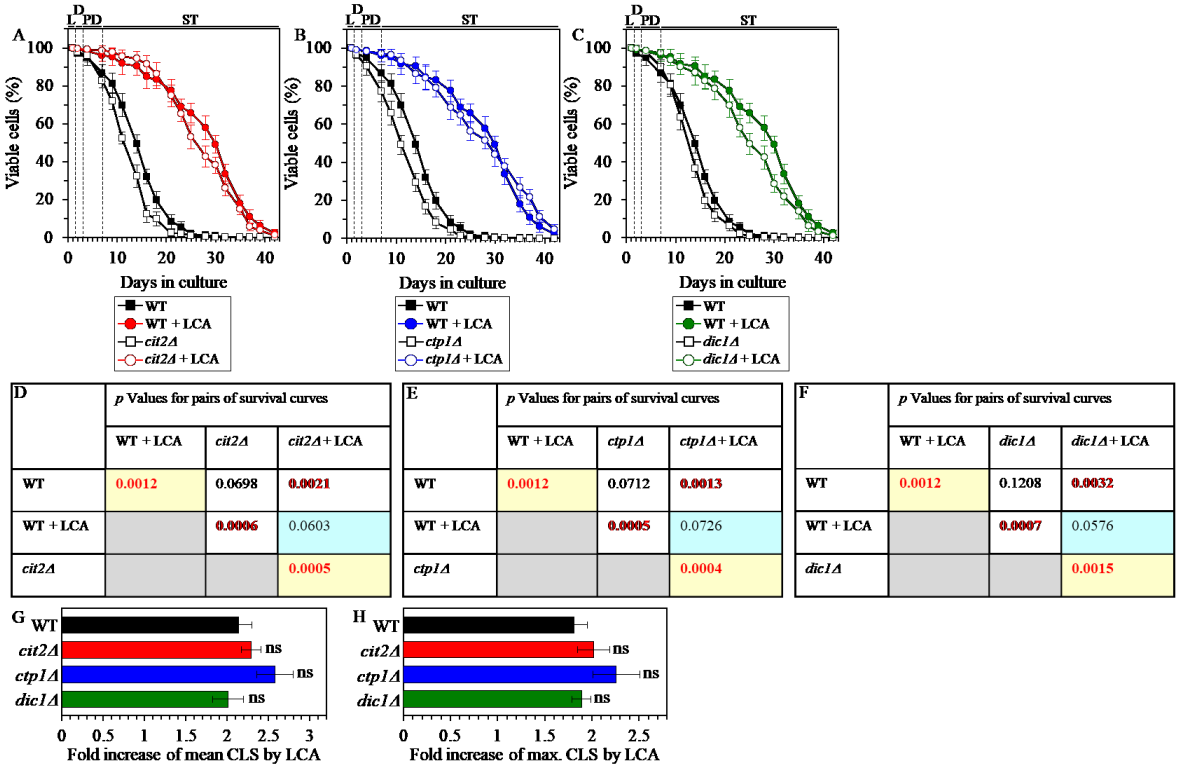

D

	p Values for pairs of survival curves		
	WT + LCA	*cit2Δ*	*cit2Δ* + LCA
WT	0.0012	0.0698	**0.0021**
WT + LCA		**0.0006**	0.0603
cit2Δ			0.0005

E

	p Values for pairs of survival curves		
	WT + LCA	*ctp1Δ*	*ctp1Δ* + LCA
WT	0.0012	0.0712	**0.0013**
WT + LCA		**0.0005**	0.0726
ctp1Δ			0.0004

F

	p Values for pairs of survival curves		
	WT + LCA	*dic1Δ*	*dic1Δ* + LCA
WT	0.0012	0.1208	**0.0032**
WT + LCA		**0.0007**	0.0576
dic1Δ			0.0015

Figure 5.15. Under CR conditions in the presence of LCA, lack of any of the three proteins required for the peroxisome-to-mitochondrion transport of acetyl-CoA in the forms of the glyoxylate cycle intermediates citrate and succinate does not alter the efficiency of yeast CLS extension by LCA. WT cells and mutant cells carrying a single-gene-deletion mutation eliminating either the Cit2, Ctp1 or Dic1 protein were cultured in the nutrient-rich YP medium initially containing 0.2% glucose with 50 μM LCA or without it. (**A**, **B**, **C**) Survival curves of the chronologically aging WT and *cit2Δ* (**A**), WT and *ctp1Δ* (**B**) or WT and *dic1Δ* (**C**) strains are shown. Data are

presented as means ± SEM (n = 3). Data for the WT strain cultured with or without LCA are replicated in graphs **A**, **B**, **C** of this Figure and in graphs **A**, **B**, **C** of Supplemental figure S7. (**D**, **E**, **F**) *p* Values for different pairs of survival curves of the WT and *cit2Δ* (**D**), WT and *ctp1Δ* (**E**) or WT and *dic1Δ* (**F**) strains cultured with or without LCA. Survival curves shown in (**A**, **B**, or **C**, respectively) were compared. Two survival curves were considered statistically different if the *p* value was less than 0.05. The *p* values for comparing pairs of survival curves using the logrank test were calculated as described in Materials and Methods. The *p* values displayed on a yellow color background indicate that LCA extends the CLS of the WT, *cit2Δ* (**D**), *ctp1Δ* (**E**) and *dic1Δ* (**F**) strains. The *p* values displayed on a blue color background indicate that LCA extends the CLS of the *cit2Δ* (**D**), *ctp1Δ* (**E**) and *dic1Δ* (**F**) strains as efficiently as it extends the CLS of the WT strain. (**G**, **H**) Survival curves shown in (**A**, **B**, **C**) were used to calculate the fold of increase of the mean (**G**) and maximum (**H**) CLS by LCA for the WT, *cit2Δ*, *ctp1Δ* and *dic1Δ* strains. Data are presented as means ± SEM (n = 3; ns, not significant). Abbreviations: L, D, PD and ST, logarithmic, diauxic, post-diauxic and stationary growth phases (respectively). These experiments were performed by Alexander Goldberg, Pavlo Kyryakov, Alejandra Gomez-Perez and Olivia Koupaki.

5.3.9 The Mpc1/Mpc3 mitochondrial pyruvate carrier is necessary for the delay of yeast chronological aging by LCA

As we have previously found, during PD and ST phases of culturing yeast under CR on 0.2% glucose, LCA exhibits the following effects [14, 236, 246]: 1) it rises the concentrations of Mpc1 and Mpc3, the two protein components of a mitochondrial pyruvate carrier involved in pyruvate transport to mitochondria during respiratory growth [255, 256]; and 2) it does not change the concentration of the Mpc2 protein component of the mitochondrial pyruvate carrier Mpc1/Mpc2 formed during fermentative growth [255, 256] (Figure 5.2). Based on these findings, we hypothesized that the Mpc1/Mpc2 and/or Mpc1/Mpc3 mitochondrial pyruvate carriers may contribute to the LCA-dependent delay of yeast chronological aging under CR conditions. To test this hypothesis, we examined the effect of a single-gene-deletion mutation eliminating the Mpc1, Mpc2 or Mpc3 protein on the efficiency with which LCA can increase yeast CLS under CR conditions. We found the following: 1) the *mpc1Δ* and *mpc3Δ* mutations decrease the efficiency of yeast CLS extension by LCA (Figures 5.16A, 5.16D, 5.16G and 5.16H for *mpc1Δ*; and Figures 5.16C, 5.16F, 5.16G and 5.16H for *mpc3Δ*); and 2) the *mpc2Δ* mutation does not affect such efficiency (Figures 5.16B, 5.16E, 5.16G and 5.16H). These findings indicate that the Mpc1/Mpc3 mitochondrial pyruvate carrier (which is formed during respiratory growth) plays an essential role in the LCA-dependent delay of chronological aging in yeast limited in calorie supply. In contrast, the Mpc1/Mpc2 mitochondrial pyruvate carrier (which is formed during fermentative growth) is dispensable for the delay of yeast chronological aging by LCA under CR conditions.

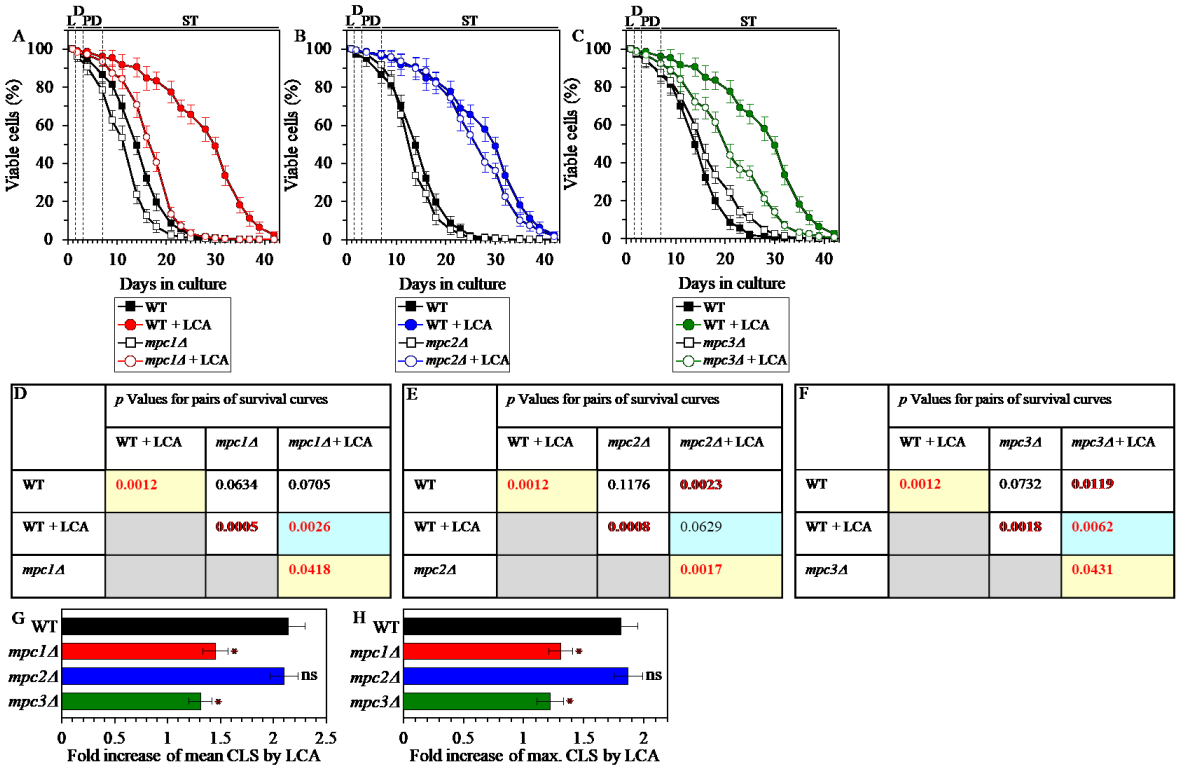

D

	p Values for pairs of survival curves		
	WT + LCA	*mpc1Δ*	*mpc1Δ* + LCA
WT	0.0012	0.0634	0.0705
WT + LCA		0.0005	0.0026
mpc1Δ			0.0418

E

	p Values for pairs of survival curves		
	WT + LCA	*mpc2Δ*	*mpc2Δ* + LCA
WT	0.0012	0.1176	0.0023
WT + LCA		0.0008	0.0629
mpc2Δ			0.0017

F

	p Values for pairs of survival curves		
	WT + LCA	*mpc3Δ*	*mpc3Δ* + LCA
WT	0.0012	0.0732	0.0119
WT + LCA		0.0018	0.0062
mpc3Δ			0.0431

Figure 5.16. Under CR conditions in the presence of LCA, lack of the Mpc1 or Mpc3 protein component of the Mpc1/Mpc3 mitochondrial pyruvate carrier decreases the efficiency of yeast CLS extension by LCA, whereas lack of the Mpc2 protein component of the Mpc1/Mpc2 mitochondrial pyruvate carrier does not affect such efficiency. WT cells and mutant cells carrying a single-gene-deletion mutation eliminating either the Mpc1, Mpc2 or Mpc3 protein were cultured in the nutrient-rich YP medium initially containing 0.2% glucose with 50 μM LCA or without it. (**A**, **B**, **C**) Survival curves of the chronologically aging WT and *mpc1Δ* (**A**), WT and *mpc2Δ* (**B**) or WT and *mpc3Δ* (**C**) strains are shown. Data are presented as means ± SEM (n = 3). Data for the WT strain cultured with or without LCA are replicated in graphs **A**, **B**, **C** of this Figure and in graphs **A**, **B**, **C** of Supplemental figure S6. (**D**, **E**, **F**) *p* Values for different pairs of survival curves of the WT and *mpc1Δ* (**D**), WT and *mpc2Δ* (**E**) or WT and *mpc3Δ* (**F**) strains cultured with or without LCA. Survival curves shown in (**A**, **B** or **C**, respectively) were compared. Two survival curves were considered statistically different if the *p* value was less than 0.05. The *p* values for comparing pairs of survival curves using the logrank test were calculated as described in Materials and Methods. The *p* values displayed on a yellow color background indicate that LCA extends the CLS of the WT, *mpc1Δ* (**D**), *mpc2Δ* (**E**) and *mpc3Δ* (**F**) strains. The *p* values displayed on a blue color background in **D** and **F** indicate that LCA extends the CLS of the *mpc1Δ* (**D**) and *mpc3Δ* (**F**) strains to a lower extent than that of the WT strain. The *p* value displayed on a blue color background in **E** indicates that LCA extends the CLS of the *mpc2Δ* strain as efficiently as it extends the CLS of the WT strain. (**G**, **H**) Survival curves shown in (**A**, **B**, **C**) were used to calculate the fold of increase of the mean (**G**) and maximum (**H**) CLS by LCA for the WT, *mpc1Δ*, *mpc2Δ* and *mpc3Δ* strains. Data are presented as means ± SEM (n = 3; **p* < 0.05; ns, not significant). Abbreviations: L, D, PD and ST, logarithmic, diauxic, post-diauxic and stationary growth phases (respectively). These experiments were performed by Alexander Goldberg, Pavlo Kyryakov, Alejandra Gomez-Perez and Olivia Koupaki.

5.3.10 The ability of LCA to shift a balance between the processes of mitochondrial fusion and fission toward fusion is essential for the delay of yeast chronological aging by LCA

We have previously noticed that, during PD and ST phases of culturing yeast under CR on 0.2% glucose, LCA has the following effects on the morphology and protein composition of

mitochondria: 1) it increases the percentage of cells exhibiting a tubular mitochondrial network [14]; 2) it decreases the percentage of cells displaying fragmented mitochondria [14]; 3) it causes a major enlargement of mitochondria [64]; 4) it significantly decreases mitochondrial number [64]; 5) it decreases the concentrations of the Caf4 and Mdv1 protein components of the mitochondrial fission machine [246]; and 6) it increases the concentrations of the Fzo1 and Ugo1 protein components of the mitochondrial fusion machine [236]. Because mitochondrial morphology is known to be defined by a balance between the processes of mitochondrial fusion and fission [257, 258], it is feasible that all these effects of LCA are due to its ability to shift this balance toward mitochondrial fusion. In support of this assumption, the mitochondrial membranes of LCA-treated yeast are enriched in PA [64, 236], a phospholipid known to increase mitochondrial size and to decrease mitochondrial number by causing the following two effects: 1) PA activates mitochondrial fusion [259-263]; in yeast treated with LCA, this effect of PA is due to its ability to stimulate the biogenesis of the Ugo1 protein component of the mitochondrial fusion machine [264]; and 2) PA inhibits mitochondrial fission because it decreases the efficiency with which the oligomerized dynamin-related protein component of the mitochondrial fission machine (Drp1 in mammals and Dnm1 in yeast) can constrict mitochondria [263, 265, 266]. We sought to determine whether the ability of LCA to shift a balance between the processes of mitochondrial fusion and fission toward fusion may play a role in the LCA-dependent delay of yeast chronological aging under CR conditions. We therefore examined how the extent to which LCA prolongs the CLS of yeast limited in calorie supply is influenced by the single-gene-deletion mutations eliminating protein components of the mitochondrial fusion or fission machine. We found the following: 1) the *fzo1Δ*, *mgm1Δ* and *ugo1Δ* mutations, each eliminating a protein component of the mitochondrial fusion machine, decrease the efficiency of yeast CLS extension by LCA (Figures 5.17A, 5.17D, 5.17G and 5.17H for *fzo1Δ*; Figures 5.17B, 5.17E, 5.17G and 5.17H for *mgm1Δ*; and Figures 5.17C, 5.17F, 5.17G and 5.17H for *ugo1Δ*); and 2) the *caf4Δ*, *dnm1Δ* and *mdv1Δ* mutations, each eliminating a protein component of the mitochondrial fission machine, increase the efficiency of yeast CLS extension by LCA (Figures 5.18A, 5.18D, 5.18G and 5.18H for *caf4Δ*; Figures 5.18B, 5.18E, 5.18G and 5.18H for *dnm1Δ*; and Figures 5.18C, 5.18F, 5.18G and 5.18H for *mdv1Δ*). We therefore concluded that the ability of LCA to shift a balance between the processes of mitochondrial fusion and fission toward fusion makes an essential contribution to the LCA-dependent delay of chronological aging in yeast limited in calorie supply.

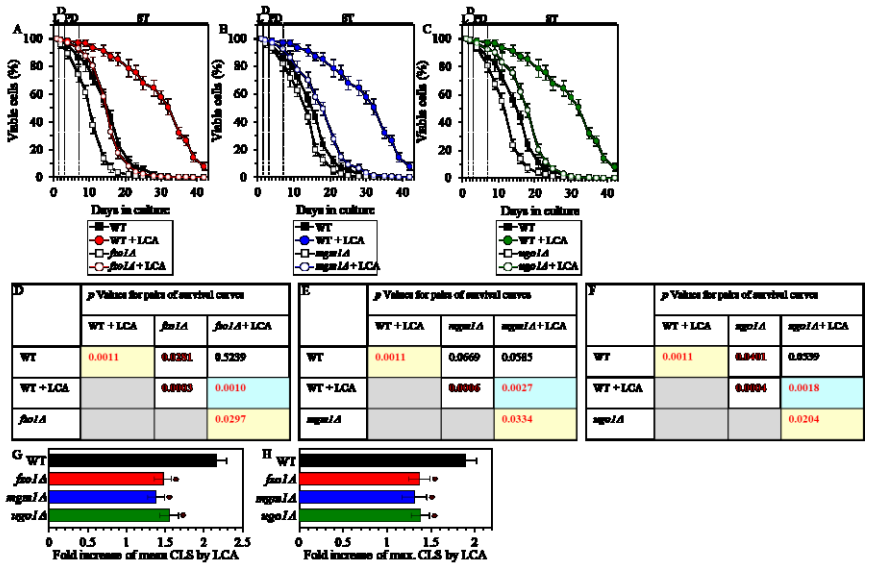

Figure 5.17. Under CR conditions in the presence of LCA, lack of the Fzo1, Mgm1 or Ugo1 protein component of the mitochondrial fusion machine decreases the efficiency of yeast CLS extension by LCA. WT cells and mutant cells carrying a single-gene-deletion mutation eliminating either the Fzo1, Mgm1 or Ugo1 protein were cultured in the nutrient-rich YP medium initially containing 0.2% glucose with 50 μM LCA or without it. (**A**, **B**, **C**) Survival curves of the chronologically aging WT and *fzo1Δ* (**A**), WT and *mgm1Δ* (**B**) or WT and *ugo1Δ* (**C**) strains are shown. Data are presented as means ± SEM (n = 3). Data for the WT strain cultured with or without LCA are replicated in graphs **A**, **B**, **C** of this Figure. (**D**, **E**, **F**) *p* Values for different pairs of survival curves of the WT and *fzo1Δ* (**D**), WT and *mgm1Δ* (**E**) or WT and *ugo1Δ* (**F**) strains cultured with or without LCA. Survival curves shown in (**A**, **B** or **C**, respectively) were compared. Two survival curves were considered statistically different if the *p* value was less than 0.05. The *p* values for comparing pairs of survival curves using the logrank test were calculated as described in Materials and Methods. The *p* values displayed on a yellow color background indicate that LCA extends the CLS of the WT, *fzo1Δ* (**D**), *mgm1Δ* (**E**) and *ugo1Δ* (**F**) strains. The *p* values displayed on a blue color background in **D**, **E** and **F** indicate that LCA extends the CLS of the *fzo1Δ* (**D**), *mgm1Δ* (**E**) and *ugo1Δ* (**F**) strains to a lower extent than that of the WT strain. (**G**, **H**) Survival curves shown in (**A**, **B**, **C**) were used to calculate the fold of increase of the mean (**G**) and maximum (**H**) CLS by LCA for the WT, *fzo1Δ*, *mgm1Δ* and *ugo1Δ* strains. Data are presented as means ± SEM (n = 3; **p* < 0.05). Abbreviations: L, D, PD and ST, logarithmic, diauxic, post-diauxic and stationary growth phases (respectively). These experiments were performed by Alexander Goldberg, Pavlo Kyryakov, Alejandra Gomez-Perez and Olivia Koupaki.

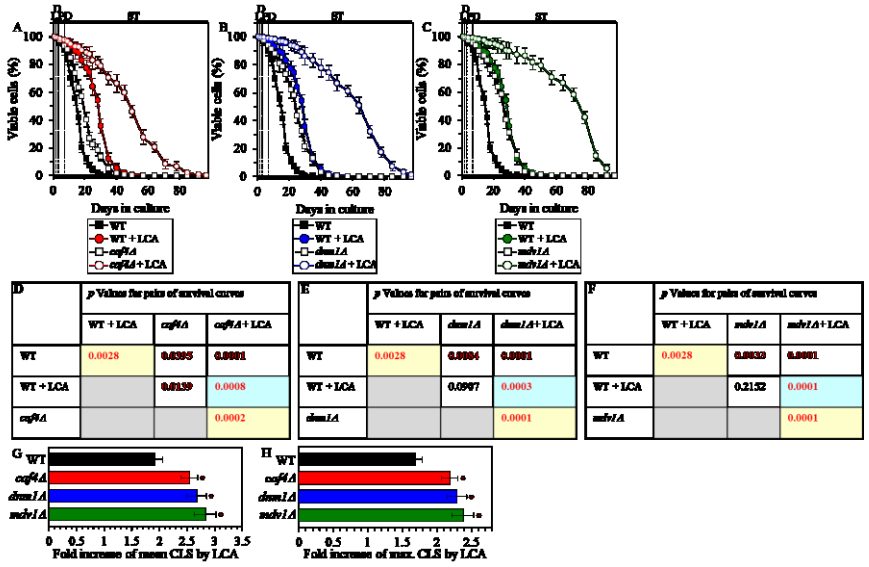

Figure 5.18. Under CR conditions in the presence of LCA, lack of the Caf4, Dnm1 or Mdv1 protein component of the mitochondrial fission machine increases the efficiency of yeast CLS extension by LCA. WT cells and mutant cells carrying a single-gene-deletion mutation eliminating either the Caf4, Dnm1 or Mdv1 protein were cultured in the nutrient-rich YP medium initially containing 0.2% glucose with 50 μM LCA or without it. (**A**, **B**, **C**) Survival curves of the chronologically aging WT and *caf4Δ* (**A**), WT and *dnm1Δ* (**B**) or WT and *mdv1Δ* (**C**) strains are shown. Data are presented as means ± SEM (n = 3). Data for the WT strain cultured with or without LCA are replicated in graphs **A**, **B**, **C** of this Figure. (**D**, **E**, **F**) *p* Values for different pairs of survival curves

of the WT and *caf4Δ* (**D**), WT and *dnm1Δ* (**E**) or WT and *mdv1Δ* (**F**) strains cultured with or without LCA. Survival curves shown in (**A**, **B** or **C**, respectively) were compared. Two survival curves were considered statistically different if the *p* value was less than 0.05. The *p* values for comparing pairs of survival curves using the logrank test were calculated as described in Materials and Methods. The *p* values displayed on a yellow color background indicate that LCA extends the CLS of the WT, *caf4Δ* (**D**), *dnm1Δ* (**E**) and *mdv1Δ* (**F**) strains. The *p* values displayed on a blue color background in **D**, **E** and **F** indicate that LCA extends the CLS of the *caf4Δ* (**D**), *dnm1Δ* (**E**) and *mdv1Δ* (**F**) strains to a higher extent than that of the WT strain. (**G**, **H**) Survival curves shown in (**A**, **B**, **C**) were used to calculate the fold of increase of the mean (**G**) and maximum (**H**) CLS by LCA for the WT, *caf4Δ*, *dnm1Δ* and *mdv1Δ* strains. Data are presented as means ± SEM (n = 3; $*p < 0.05$). Abbreviations: L, D, PD and ST, logarithmic, diauxic, post-diauxic and stationary growth phases (respectively). These experiments were performed by Alexander Goldberg, Pavlo Kyryakov, Alejandra Gomez-Perez and Olivia Koupaki.

5.3.11 LCA delays the age-related onset and slows progression of mitochondria-controlled apoptosis and decreases cell susceptibility to this form of RCD in an age-dependent manner

Mitochondrial network fragmentation is known as one of the hallmarks of a mitochondria-controlled form of age-related apoptotic RCD [23, 249, 267-277]. We have demonstrated that, during PD and ST phases of culturing yeast under CR on 0.2% glucose, LCA attenuates mitochondrial network fragmentation [14, 64, 236, 246] by shifting a balance between the processes of mitochondrial fusion and fission toward fusion (this study), and that this effect of LCA is essential for its ability to delay yeast chronological aging under CR conditions (this study). We therefore sought to determine whether in yeast limited in calorie supply LCA may affect age-related changes in some other hallmark events of this mitochondria-controlled form of apoptotic RCD. We found that the ability of LCA to delay mitochondrial network fragmentation during PD and ST phases coincides with its ability to postpone the age-related onset and decelerate progression of such characteristic event in apoptotic RCD as cytochrome *c* efflux from mitochondria during ST phase (Figure 5.19A); cytochrome *c* is known as a pro-apoptotic protein whose release from fragmented mitochondria into the cytosol of yeast cells is a late event in mitochondria-controlled apoptotic RCD [23, 249, 267-277]. We also found that LCA delays the age-related onset and slows progression of nuclear fragmentation during ST phase (Figures 5.19B and 5.19C); nuclear fragmentation in yeast is known as another characteristic late event of age-related apoptotic RCD [23, 249, 267-277]. Moreover, we noticed that LCA postpones the age-related onset and slows progression of phosphatidylserine (PS) translocation from the inner to the outer leaflet of the plasma membrane during PD and ST phases (Figures 5.20A and 5.20B); this so-called externalization of PS in yeast is known as an early event in age-related apoptotic RCD [278, 279].

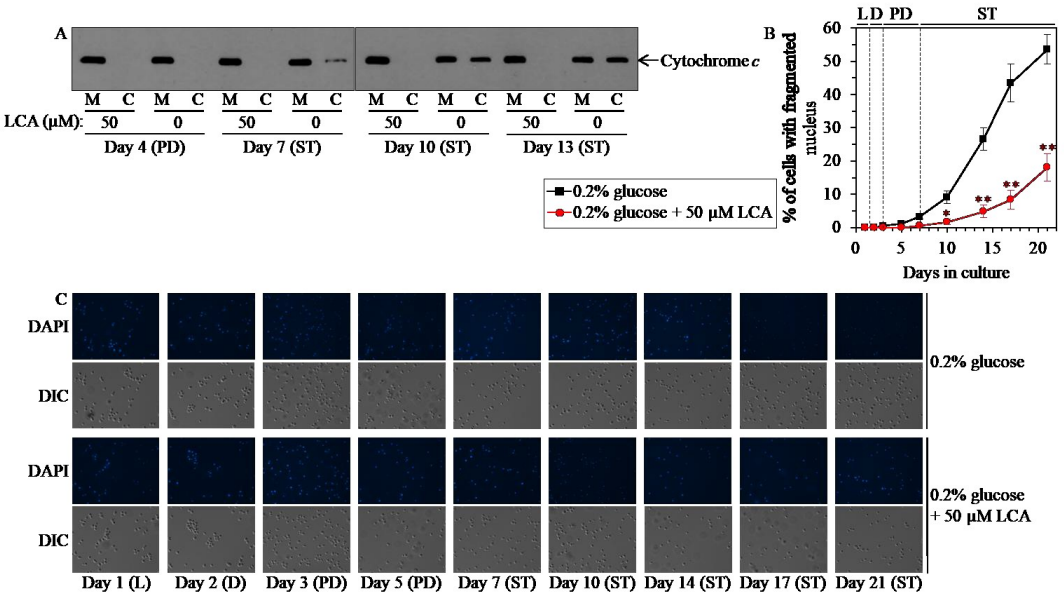

Figure 5.19. Under CR conditions, LCA postpones the age-related onset and decelerates progression of such late events in apoptotic RCD as cytochrome *c* efflux from mitochondria and nuclear fragmentation. WT cells were cultured in the nutrient-rich YP medium initially containing 0.2% glucose with 50 μM LCA or without it. (**A**) Western blot analysis of cytochrome *c* in purified mitochondria (M) and in the cytosolic fraction (C) recovered from cells that were taken on different days of culturing. Equal portions of mitochondrial and cytosolic fractions were analyzed by immunoblotting to cytochrome *c*. (**B**) Percentage of cells exhibiting fragmented nucleus, a characteristic trait of apoptotic RCD. Images like the representative images shown in (**C**) were quantitated as described in Materials and Methods. Data are presented as means ± SEM (n = 3; *p < 0.05; **p < 0.01). (**C**) Cells recovered on different days of culturing were visualized using the DIC microscopy and stained with 4′,6-diamidino-2-phenylindole dihydrochloride (DAPI) to detect nuclei as described in Materials and Methods. Abbreviations: L, D, PD and ST, logarithmic, diauxic, post-diauxic and stationary growth phases (respectively).

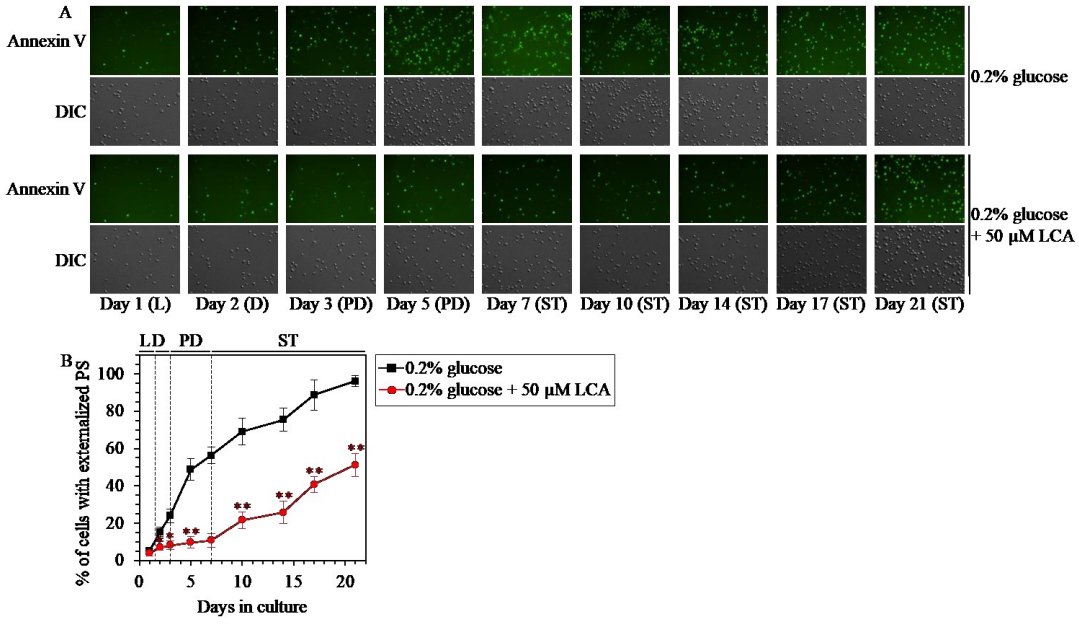

Figure 5.20. Under CR conditions, LCA postpones the age-related onset and slows progression of such early event in apoptotic RCD as phosphatidylserine (PS) translocation from the inner to the outer leaflet of the plasma membrane. WT cells were cultured in the nutrient-rich YP medium initially containing 0.2% glucose with

50 µM LCA or without it. (**A**) Cells recovered on different days of culturing were visualized using the DIC microscopy and stained with Annexin V to detect the presence of PS in the outer leaflet of the plasma membrane as described in Materials and Methods. (**B**) Percentage of cells exhibiting externalized PS, a characteristic trait of apoptotic RCD consisting in the translocation of PS from the inner to the outer leaflet of the plasma membrane. Images like the representative images shown in (**A**) were quantitated as described in Materials and Methods. Data are presented as means ± SEM (n = 3; *p < 0.05; **p < 0.01). Abbreviations: L, D, PD and ST, logarithmic, diauxic, post-diauxic and stationary growth phases (respectively).

Mitochondrial network fragmentation and the efflux of several pro-apoptotic proteins (including cytochrome *c*) from the intermediate space of fragmented mitochondria are known to be characteristic traits of mitochondria-controlled apoptotic RCD induced by a short-term exposure of yeast cells to exogenous hydrogen peroxide [23, 249, 267-277]. Our assessment of how LCA influences cell susceptibility to this mode of apoptotic RCD under CR conditions has revealed the following: 1) LCA significantly increases clonogenic survival of cells briefly (for 2 h) treated with hydrogen peroxide if these cells were recovered during PD or ST phase of culturing (Figure 5.21); and 2) LCA does not alter clonogenic survival of cells subjected to such treatment if these cells were recovered during L or D phase of culturing (Figure 5.21).

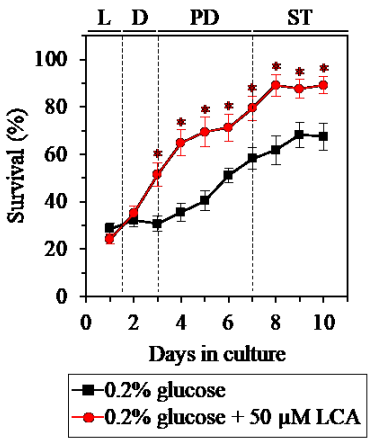

Figure 5.21. Under CR conditions, LCA decreases cell susceptibility to mitochondria-controlled apoptotic RCD in an age-dependent manner. WT cells were cultured in the nutrient-rich YP medium initially containing 0.2% glucose with 50 µM LCA or without it. An assay for measuring clonogenic survival of cells recovered on different days of culturing and then treated for 2 h with 2.5 mM hydrogen peroxide to elicit a mitochondria-controlled mode of apoptotic RCD was performed as described in Materials and Methods. Data are presented as means ± SEM (n = 3; *p < 0.05). Abbreviations: L, D, PD and ST, logarithmic, diauxic, post-diauxic and stationary growth phases (respectively).

In sum, the above findings indicate that LCA delays yeast chronological aging in part because it attenuates mitochondrial network fragmentation, thereby delaying the onset of an age-related mode of mitochondria-controlled apoptotic RCD during PD and ST phases of culturing under CR conditions.

5.4 Discussion

This study and our previously published data [14, 64, 236, 246] suggest a hypothetical model for the mechanisms through which LCA delays chronological aging of yeast limited in calorie supply. This model is depicted in Figure 5.22. The key aspects of this model are as follows:

1) if LCA is added to culture medium at the time of cell inoculation, it elicits an aging-delaying cellular pattern and preserves such pattern throughout the entire chronological lifespan of the yeast culture, before an arrest of cell growth and division (i.e. during L, D and PD phases of culturing) and after such arrest (i.e. during ST phase of culturing); 2) LCA causes the stepwise development and maintenance of the aging-delaying cellular pattern in part because it alters various intercompartmental communications; these communications involve movements of certain intermediates of lipid and carbohydrate metabolism between the ER and LD, LD and peroxisomes, peroxisomes and mitochondria, the ER and mitochondria, and the cytosol and mitochondria; 3) LCA attenuates mitochondrial network fragmentation by shifting a balance between the processes of mitochondrial fusion and fission toward fusion;

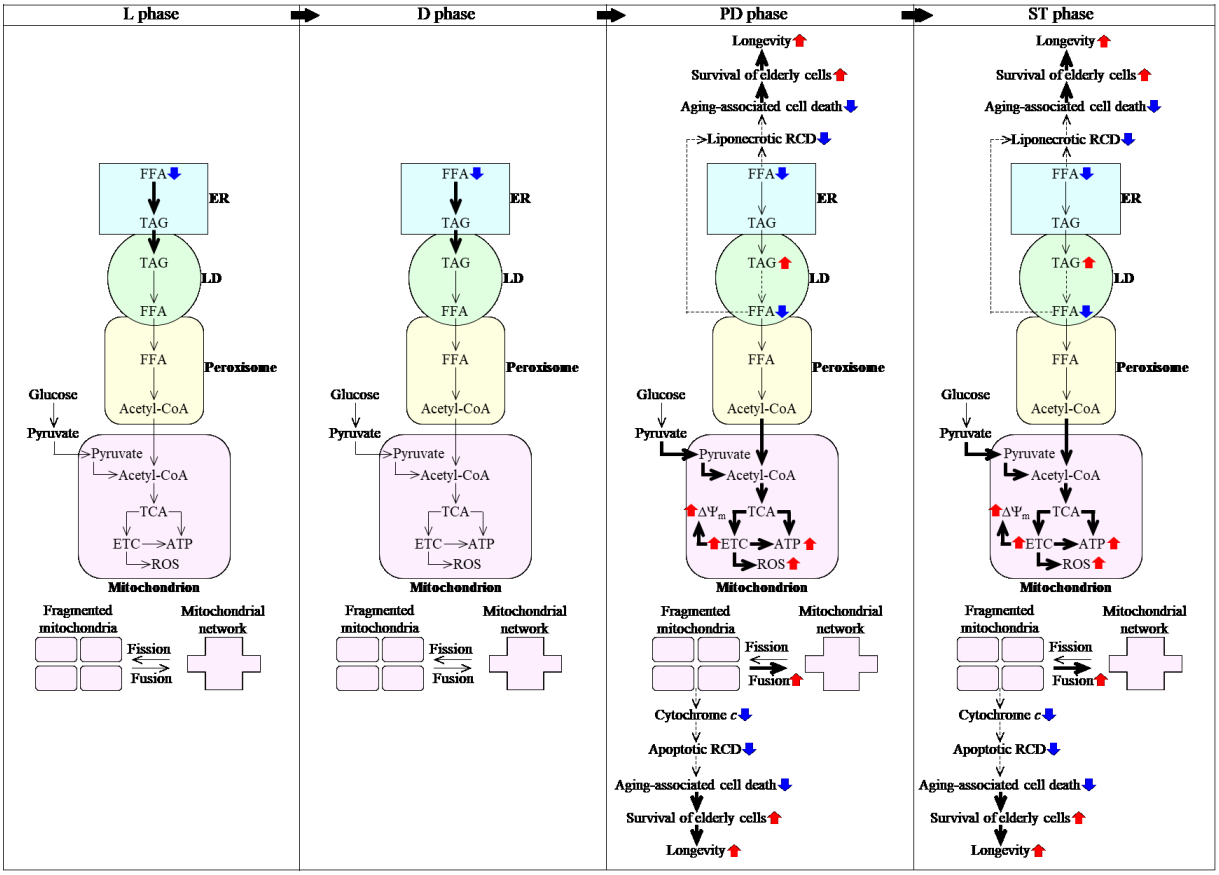

Figure 5.22. Mechanisms through which LCA delays chronological aging of yeast limited in calorie supply. In yeast cultured under CR conditions, LCA elicits an aging-delaying cellular pattern and preserves such pattern throughout the entire chronological lifespan, before an arrest of cell growth and division (i.e. during L, D and PD phases of culturing) and after such arrest (i.e. during ST phase of culturing). Under these conditions, LCA causes the stepwise development and maintenance of the aging-delaying cellular pattern because it alters the spatiotemporal dynamics of a cellular network integrating certain pathways of lipid and carbohydrate metabolism, some intercompartmental communications, specific aspects of mitochondrial morphology and functionality, and liponecrotic and apoptotic modes of RCD. Because LCA decreases the risk of aging-associated cell death to increase the chance of elderly cells to survive, it extends longevity of chronologically aging yeast. The thickness of black

arrows is proportional to the rates of processes. Arrows next to the names of affected processes denote those of them that are intensified (red arrows) or weakened (blue arrows). Arrows next to the names of affected metabolites signify those of them whose concentrations are increased (red arrows) or decreased (blue arrows). Please see text for additional details. Abbreviations: Ac-CoA, acetyl-CoA; ER, endoplasmic reticulum; ETC, electron transport chain; FFA, free fatty acids; L, D, PD and ST, logarithmic, diauxic, post-diauxic and stationary growth phases (respectively); LD, lipid droplets; RCD, regulated cell death; ROS, reactive oxygen species; TAG, triacylglycerols; TCA, tricarboxylic acid cycle; $\Delta\Psi_m$, mitochondrial electrochemical membrane potential.

4) the LCA-dependent changes in the communications between different cellular compartments and the LCA-driven weakening of mitochondrial network fragmentation decrease the risk of the cell commitment to liponecrotic and apoptotic RCD modes during PD and ST phases, thereby increasing the chance of cell survival during these phases of culturing; and 5) because LCA decreases the risk of aging-associated cell death to increase the chance of elderly cells to survive, it prolongs longevity of chronologically aging yeast (Figure 5.22).

Our findings indicate that LCA decreases the cellular concentration of FFA through the entire chronological lifespan of yeast limited in calorie supply. In our model, two mechanisms underlie this effect of LCA. One mechanism consists in the ability of LCA to regulate the anabolic branch of TAG metabolism by accelerating TAG synthesis from FFA within the ER and the ensuing TAG deposition within LD during L and D phases of culturing (Figure 5.22). The other mechanism involves an LCA-dependent regulation of the catabolic branch of TAG metabolism through the deceleration of TAG lipolysis into FFA within LD during PD and ST phases of culturing (Figure 5.22). By decreasing the cellular concentration of FFA through the entire chronological lifespan, LCA delays the age-related onset and decelerates the progression of FFA-induced liponecrotic RCD during PD and ST phases of culturing under CR conditions (Figure 5.22). This LCA-dependent decrease of the risk of aging-associated cell death increases the chance of elderly cells to survive and makes an essential contribution to the ability of LCA to extend longevity of chronologically aging yeast.

Our model further posits that the LCA-dependent stimulation of the peroxisome-to-mitochondrion transport of acetyl-CoA via the carnitine shuttle during PD and ST phases [236, 246] is indispensable for the delay of yeast chronological aging by LCA under CR conditions (Figure 5.22). Another essential contributor to this aging-delaying effect of LCA is the Mpc1/Mpc3 mitochondrial pyruvate carrier involved in the cytosol-to-mitochondrion transport of pyruvate during respiratory growth (Figure 5.22); akin to the carnitine-dependent transport of acetyl-CoA from peroxisomes to mitochondria, this mitochondrial pyruvate carrier is activated

during PD and ST phases of culturing yeast under CR conditions [236, 246]. It is conceivable that these stimulating, aging-delaying effects of LCA on the peroxisome-to-mitochondrion transport of acetyl-CoA and the cytosol-to-mitochondrion transport of pyruvate may be involved in the following cause-effect relationship with other mitochondrial processes known to be elicited by LCA: 1) these effects may be caused by the accumulation of LCA in both mitochondrial membranes and by the subsequent remodeling of mitochondrial membrane lipidome during PD and ST phases of culturing under CR conditions [64, 107, 145, 221, 248]; and 2) these effects may cause the LCA-dependent changes in some vital aspects of mitochondrial functionality; these changes include a rise in mitochondrial respiration/electron transport chain, electrochemical membrane potential, reactive oxygen species concentration and ATP synthesis during PD and ST phases of culturing under CR conditions [64, 107, 145, 221, 248].

LCA is known to inhibit mitochondrial network fragmentation during PD and ST phases of culturing yeast under CR conditions [14, 64, 236, 246]. This study provides evidence that, during these phases of culturing, such effect of LCA on mitochondrial morphology is in the following cause-effect relationship with other cellular processes affected by LCA: 1) it is caused by the ability of LCA to shift a balance between the processes of mitochondrial fusion and fission toward fusion; 2) it causes a delay in the onset and a deceleration in the progression of an age-related mode of mitochondria-controlled apoptotic RCD (Figure 5.22). Like for the FFA-induced liponecrotic mode of RCD, the LCA-dependent decrease of the risk of aging-associated apoptotic mode of RCD increases the chance of elderly cells to survive and, thus, is an important contributing factor to longevity extension by LCA in chronologically aging yeast limited in calorie supply (Figure 5.22).

In sum, this study provides important new insights into the mechanisms by which LCA delays yeast chronological aging under CR conditions by altering the spatiotemporal dynamics of a cellular network that integrates certain pathways of lipid and carbohydrate metabolism, some intercompartmental communications, specific aspects of mitochondrial morphology and functionality, and liponecrotic and apoptotic modes of RCD. In the future, it would be interesting to investigate how LCA influences a novel mechanism of longevity extension by CR in chronologically aging yeast. This recently discovered mechanism has been shown to link cellular aging to cell cycle regulation, maintenance of a quiescent state, entry into a non-quiescent state and survival in the non-quiescent state [162].

6 LCA elicits the establishment of a distinct phosphoprotein profile of mitochondria, which significantly differs from the phosphoprotein profile of mitochondria in yeast cells cultured without LCA

6.1 Introduction

As described in the ″Introduction″ section, because LCA triggers major changes in the age-related chronology of several vital processes taking place in mitochondria, we hypothesized that LCA may cause these changes by eliciting a reversible phosphorylation of some mitochondrial proteins. The objectives of studies described in Chapter 6 was to test this hypothesis by investigating if an exposure of chronologically aging yeast to exogenous LCA can trigger such phosphorylation of some mitochondrial proteins.

6.2 Materials and methods

6.2.1 Yeast strains, media and growth conditions

The WT strain BY4742 (*MATα his3Δ1 leu2Δ0 lys2Δ0 ura3Δ0*) was grown in YP medium (1% yeast extract, 2% peptone; both from Fisher Scientific; #BP1422-2 and #BP1420-2, respectively) initially containing 0.2% glucose (#D16-10; Fisher Scientific) with 50 μM LCA (#L6250; Sigma) or without it. Cells were cultured at 30ºC with rotational shaking at 200 rpm in Erlenmeyer flasks at a ″flask volume/medium volume″ ratio of 5:1.

6.2.2 Purification of mitochondria

Yeast cells were harvested at 3,000 × g for 5 min at room temperature, washed with water and resuspended in DTT buffer (100 mM Tris-H_2SO_4, pH 9.4, 10 mM dithiothreitol [DTT]). Cells were incubated in DTT buffer for 20 min at 30°C to weaken the cell wall. The cells were washed with Zymolyase buffer (1.2 M sorbitol, 20 mM potassium phosphate, pH 7.4) and centrifuged at 3,000 × g for 5 min at room temperature. The cells were then incubated with 3 mg/g (wet weight) of Zymolyase-100T in 7 ml/g (wet weight) Zymolyase buffer for 45 min at 30°C. Following an 8-min centrifugation at 2,200 × g at 4°C, the isolated spheroplasts were washed in ice-cold homogenization buffer (5 ml/g) (0.6 M sorbitol, 10 mM Tris-HCl, pH7.4, 1 mM EDTA, 0.2% (w/v) BSA) and centrifuged at 2,200 × g for 8 min at 4°C. The spheroplasts were homogenized in ice-cold homogenization buffer using 15 strokes. Cell debris was removed by centrifuging the

resulting homogenates at 3,000 × g for 10 min at 4°C. The resulting supernatant was then centrifuged at 12,000 × g for 15 min at 4°C to pellet mitochondria. The remnant cell debris were removed by centrifuging the mitochondrial fraction at 3,000 × g for 5 min at 4°C. The resulting supernatant was then centrifuged at 12,000 × g for 15 min at 4°C to obtain the crude mitochondrial pellet, which were then resuspended in 3 ml of SEM Buffer (250 mM sucrose, 1 mM EDTA, 10 mM MOPS, pH 7.2) and used for further purification of mitochondria. A sucrose gradient was made by overlaying 1.5 ml of 60% sucrose with 4 ml of 32% sucrose, 1.5 ml of 23% sucrose, and then 1.5 ml of 15% sucrose (all in EM buffer; 1 mM EDTA, 10 mM MOPS, pH 7.2). Finally, a 3-ml aliquot of the crude mitochondrial fraction in SEM buffer was applied to the gradient and centrifuged at 134,000 × g (33,000 rpm) for three hours at 4°C in vacuum (Rotor SW40Ti, Beckman). The purified mitochondria found at the 60%/32% sucrose interface were carefully removed and stored at -80°C until mass spectrometric identification of phosphorylated mitochondrial proteins.

6.2.3 Mass spectrometric identification of phosphorylated mitochondrial proteins

Purified mitochondria were resuspended in TCL buffer (25 mM Tris/HCl pH 8.5, 150 mM NaCl, 1 mM EDTA, 0.1 mM DTT, 4% CHAPS, 1 mM PMSF, protease inhibitor cocktail) and subjected to vortexing with glass beads for 10 min at 4ºC. The sample was subjected to centrifugation for 5 min at 16,000 × g at 4ºC. Immediately after centrifugation, the supernatant was placed into a pre-chilled Eppendorf tube. The extracted mitochondrial proteins were precipitated with 10% TCA, washed with 80% acetone, dried, resuspended in the sample buffer for SDS-PAGE and then subjected to SDS-PAGE at 200 V until the sample reaches the running gel. After staining the running gel with QC Colloidal Coomassie Blue and destaining, protein bands were cut out from the SDS-PAGE gel with a razor blade. The gel pieces were placed in individual 0.5-ml siliconized Eppendorf tubes and incubated with 50 µl of acetonitrile (ACN) for 5 min at 37ºC. ACN was removed and the gel pieces will be dried at 37ºC. The gel pieces were incubated in 50 µl of 10 mM dithiothreitol (DTT) for 30 min at 37ºC to reduce thiol groups in peptides. DTT was discarded and the gel pieces were incubated in 50 µl of 55 mM iodoacetamide (IAA) for 20 min at 37ºC in the dark to remove the residual DTT. IAA was removed, and the gel pieces was incubated in 50 µl of a 1:1 mixture of 100 mM ABC and 50% acetonitrile for 10 min at 37ºC. The mixture was discarded, and the gel pieces were incubated twice in 50 µl of ACN

under the same conditions and dried at 37°C. The trypsin and trypsin buffer were prepared as follows: 1) 1.6 ml of a 1:1 mixture of 100 mM ABC and 10mM $CaCl_2$ was used to resuspend 20 µg of trypsin; and 2) for protein digest, 50 µl of trypsin solution (1 mg/ml) was added to the gel piece, which was then incubated overnight at 37°C. The following day, the gel pieces were spun down and the supernatants containing peptides were transferred to new 0.5-ml siliconized Eppendorf tubes. To extract more peptides, the gel pieces were subjected to several washes and treatments at room temperature; the gel pieces were conserved and combined with the first set to extracted peptides. For the first extraction, the gel pieces were initially incubated in 50 µl of 25 mM ABC for 10 min and then in 50 µl of ACN for 10 min. The samples were spun down, and the supernatant was added to the first set of extracted peptides. For the second extraction, the gel pieces were incubated in 50 µl of 5% formic acid for 10 min and then in 50 µl of ACN for 10 min. The samples were spun down, and the supernatant was combined with the first set of extracted peptides. For phosphopeptide enrichment using TiO_2, the peptides obtained from the digestion step were dried down, re-dissolved in 100 µl of binding buffer (1 M glycolic acid, 80% acetonitrile, and 5% trifluoroacetic acid [TFA]) and mixed with 50 µl of TiO_2 magnetic beads (Roche) pre-equilibrated with 500 µl of binding buffer. The beads were incubated for 30 min in a mixer, washed once with 500 µl of binding buffer, and then washed twice with 500 µl of wash buffer (80% acetonitrile, 1% TFA). The bound peptides were eluted twice with 50 µl of elution buffer (5% ammonium hydroxide, pH 12), dried and re-dissolved in 15 µl of 2% acetonitrile and 1% formic acid before LC-MS/MS analysis. Phosphorylated peptides were identified by reverse phase high performance liquid chromatography coupled to mass spectrometry (RP-HPLC/MS) using an LTQ Orbitrap. 3-µl aliquots of peptides were separated in ACN gradient using a 100-µM capillary column packed with C18 mobile phase.

6.3 Results

6.3.1 Several proteins are differently phosphorylated in mitochondria of cells cultured in the presence or absence of LCA

We have used centrifugation to equilibrium in a sucrose density gradient to purify mitochondria from yeast cells cultured in the nutrient-rich YP medium containing 0.2% glucose with 50 µM LCA or without LCA. The shape of this gradient has been previously optimized for

the purification of mitochondria devoid of contamination by other organelles, such as the nucleus, endoplasmic reticulum, Golgi apparatus, plasma membrane and vacuole (Figure 6.1).

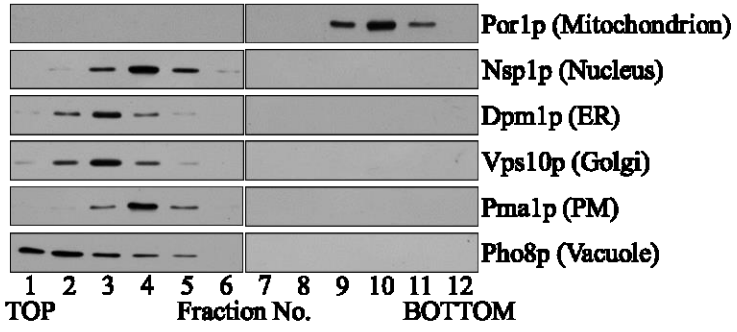

Figure 6.1. Purification of mitochondria from yeast cells using centrifugation to equilibrium in a sucrose density gradient. Equal volumes of gradient fractions were analyzed by immunoblotting with antibodies to Por1p (a protein marker of mitochondria), Nsp1p (a protein marker of the nucleus), Dpm1p (a protein marker of the endoplasmic reticulum [ER]), Vps10p (a protein marker of the Golgi), Pma1p (a protein marker of the plasma membrane [PM]) and Pho8p (a protein marker of the vacuole).

We then used a quantitative, label-free mass spectrometry approach to compare phosphoproteomes of mitochondria from yeast cells that were cultured with or without LCA and recovered for mitochondria purification at day 2 (i.e. at diauxic phase of culturing), day 4 (i.e. at post-diauxic phase of culturing) or day 7 (i.e. at stationary phase of culturing). Cells for mitochondria purification were recovered at different days of culturing because we sought to assess how chronological age of these cells influences the mitochondrial proteome in yeast exposed to LCA or remained untreated. Cells for mitochondria purification were recovered at days 2, 4 and 7 because our previous study has revealed that the first 7 days of culturing (but not the time after this critical period) are indispensable for the delay of yeast chronological aging by LCA [59].

We have detected and identified numerous phosphopeptides and phosphoproteins in mitochondria of yeast cells cultured with or without LCA and recovered for mitochondria purification at days 2, 4 and 7 of culturing, as outlined in Table 6.1.

Table 6.1. Numbers of phosphopeptides and phosphoproteins that were detected and identified in mitochondria of yeast cells cultured with or without LCA and recovered for mitochondria purification at different days of culturing.

+ or - LCA	Day	Number of phosphoproteins	Number of phosphopeptides
- LCA	2	173	295
	4	211	375
	7	248	433
+ LCA	2	178	302
	4	220	390
	7	261	447

We have then analyzed the mitochondrial phosphoproteome data using principal component analysis (PCA). PCA of was performed for mitochondrial phosphoproteins and phosphopeptides that were found in cells cultured with or without LCA and recovered for mitochondria purification at days 2, 4 and 7 of culturing.

PCA for mitochondrial phosphoproteins revealed that LCA elicits a distinct phosphoprotein profile that significantly differs from that of mitochondria in yeast cells cultured without LCA (Figure 6.2). This distinct LCA-driven phosphoprotein profile was observed in mitochondria of cells recovered at any of the three days of culturing. The sample with LCA and the reference without LCA were separated farthest from each other in case of mitochondrial phosphoproteins from chronologically old cells recovered at day 7 (Figure 6.2). Although the sample with LCA and the reference without LCA were also separated from each other in case of mitochondrial phosphoproteins from chronologically young cells recovered at day 2, they were clustered much closer to each other than those from chronologically old cells recovered at day 7 (Figure 6.2). We therefore concluded that the ability of LCA to alter the mitochondrial phosphoproteome is gradually enhanced with the chronological age of yeast cells.

PCA for mitochondrial phosphopeptides has supported my conclusions that 1) LCA prompts the establishment of a distinct phosphoprotein profile of mitochondria, which significantly differs from the phosphoprotein profile of mitochondria in yeast cells cultured without LCA; and 2) the efficiency with which LCA changes the mitochondrial phosphoproteome is progressively increased with the chronological age of yeast cells (Figure 6.3).

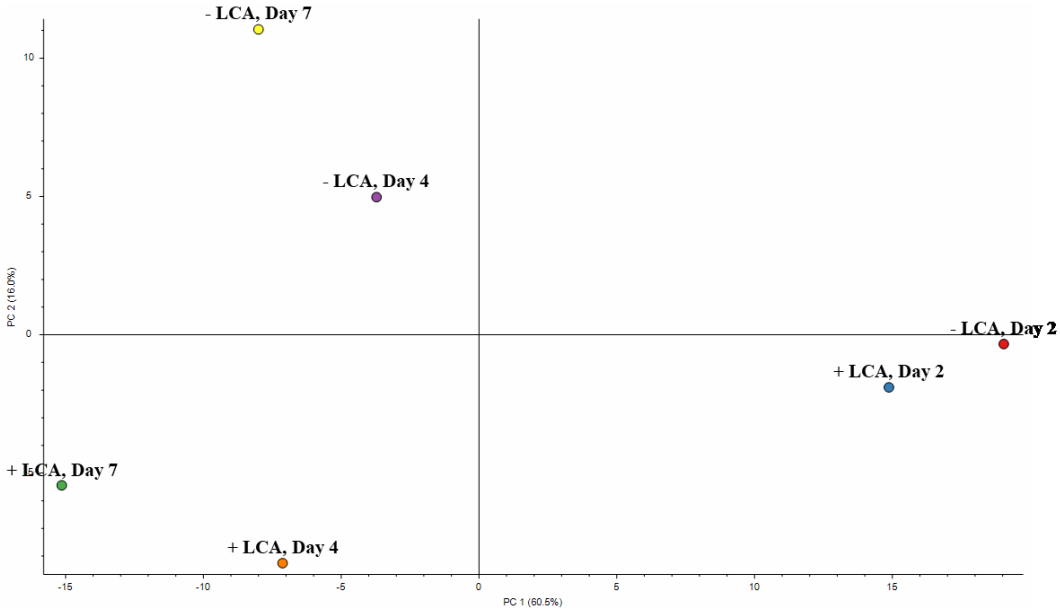

Figure 6.2. Principal component analysis for mitochondrial phosphoproteins found in cells cultured with or without LCA and recovered for mitochondria purification at days 2, 4 and 7 of culturing. See text for discussion.

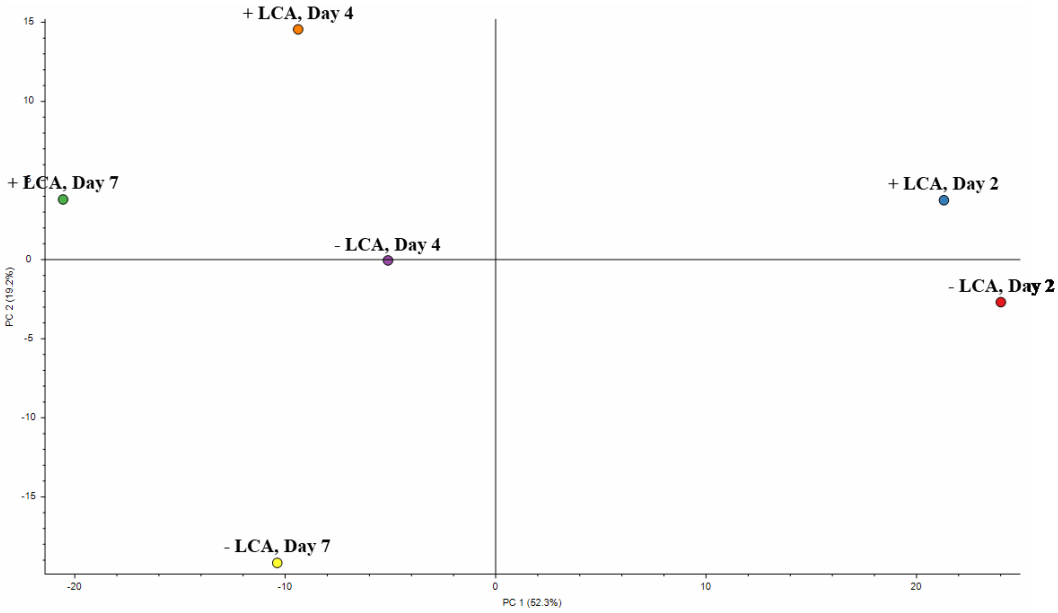

Figure 6.3. Principal component analysis for mitochondrial phosphopeptides found in cells cultured with or without LCA and recovered for mitochondria purification at days 2, 4 and 7 of culturing. See text for discussion.

Our further analysis of the mitochondrial phosphoproteome data allowed to identify several proteins that are phosphorylated only in mitochondria of cells cultured with or without LCA (Table 6.2). We found that the number of such proteins differently phosphorylated in mitochondria of cells cultured in the presence or absence of LCA is gradually enhanced with the chronological age of yeast cells (Table 6.2).

Table 6.2. The number of phosphorylated proteins present only in mitochondria of cells cultured with or without LCA. See text for discussion.

Day	Number of mitochondrial phosphoproteins present only in yeast cultured without LCA	Number of mitochondrial phosphoproteins present only in yeast cultured with LCA
2	3	8
4	3	12
7	7	20

The identities of proteins that are phosphorylated only in mitochondria of cells cultured with or without LCA and recovered at day 2, 4 or 7 of culturing are presented in Tables 6.3, 6.4 and 6.5. Some of these proteins have been previously found only in mitochondria where they participate in carbohydrate metabolism and co-translational mitochondrial import (Tables 6.3, 6.4 and 6.5). Many of these mitochondrial phosphoproteins 1) have also been found in other cellular locations; and 2) have been shown to participate in essential cellular processes most of which are not directly linked to mitochondria (Tables 6.3, 6.4 and 6.5). More than 30% of the proteins that have been found in other cellular locations have been previously shown by others to be associated

with mitochondria only in phosphorylated forms and only in yeast cells cultured in media with alternative carbon sources or exposed to various mild stresses; the names of the proteins in Tables 6.3, 6.4 and 6.5are shown in red color. The proteins that are phosphorylated only in mitochondria of cells cultured with or without LCA and recovered at day 2, 4 or 7 of culturing have been implicated in regulating PKA, protein phosphorylation, lipid metabolism, ion transport, endocytosis, TOR2-dependent regulation of lipid metabolism, G protein coupled receptor signaling, HOG signaling, cytoskeleton organization, stress response, nitrogen starvation response, cell wall maintenance, glucose-deprivation induced stress response, tubular ER morphology maintenance and proteostasis (Tables 6.3, 6.4 and 6.5).

Table 6.3. The names, functions, phosphorylation sites and cellular locations of proteins that are phosphorylated only in mitochondria of cells cultured with or without LCA and recovered at day 2. See text for discussion. The names of proteins that have been found in other cellular locations and shown (by others) to be associated with mitochondria only in phosphorylated forms are shown in red color.

+ or - LCA	Protein name (SGD), function (SGD), phosphorylation site (my data) and cellular location (SGD)
+ LCA	**BCY1** (YIL033C): Regulatory subunit of the cyclic AMP-dependent protein kinase (PKA); PKA is a component of a signaling pathway that controls a variety of cellular processes, including metabolism, cell cycle, stress response, stationary phase, and sporulation; Position in a master protein: [143-167; 1xPhospho [T/S]; Location: Cytoplasm, Nucleus
	YCK1 (YHR135C): Palmitoylated plasma membrane-bound casein kinase I (CK1) isoform; Is involved in glucose sensing; Causes glucose repression of respiratory metabolism; Is involved in the phosphorylation and regulation of glucose sensor Rgt2p; ***Also found on the outer surface of mitochondria***; Position in a master protein: [43-59; 1xPhospho [S/T]; Location: Plasma membrane
	YCK2 (YNL154C): Palmitoylated plasma membrane-bound casein kinase I (CK1) isoform; Is involved in glucose sensing; Causes glucose repression of respiratory metabolism; Is involved in the phosphorylation and regulation of glucose sensor Rgt2p; ***Also found on the outer surface of mitochondria***; Position in a master protein: [448-481; 1xPhospho [S/Y]; Location: Plasma membrane
	SPO14 (YKR031C): Phospholipase D; Catalyzes the hydrolysis of phosphatidylcholine, producing choline and phosphatidic acid; Position in a master protein: [1234-1252; 1xPhospho [S1244]; Location: Nucleus, Endosome
	CTR1 (YPR124W): High-affinity copper transporter of plasma membrane; Mediates copper uptake under low copper conditions; Protein increases in abundance and relocates from nucleus to plasma membrane upon DNA replication stress; Position in a master protein: [191-204; 1xPhospho [S]; Location: Nucleus, Plasma membrane
	PKH1 (YDR490C): Serine/threonine protein kinase; involved in sphingolipid-mediated signaling pathway that controls endocytosis and activates the signaling cascade required for maintenance of cell wall integrity; Position in a master protein: [491-503; 1xPhospho [S493]; Location: Cytoplasm
	LSP1 (YPL004C): Sphingolipid long chain base-responsive protein LSP1; A core component of eisosomes, large immobile patch structures at the cell cortex associated with endocytosis; Phosphorylated on Thr233 upon Pkc1p hyperactivation in a Slt2p MAPK-dependent fashion; Represses Pkc1p/Ypk1p stress resistance pathways Position in a master protein: [134-143; 1xPhospho [S138]; Location: Cytoplasm
	GPR1 (YDL035C): Plasma membrane G protein coupled receptor (GPCR); Interacts with the heterotrimeric G protein alpha subunit, Gpa2p, and with Plc1p; Sensor that integrates nutritional signals with the modulation of cell fate via PKA and cAMP synthesis; Position in a master protein: [368-384; 1xPhospho [S373]; Location: Plasma membrane

- LCA	**OM14** (YBR230C): Mitochondrial outer membrane receptor for cytosolic ribosomes; Integral protein of the outer membrane that interacts with the nascent chain-associated complex (NAC) bound to ribosomes, contributing to co-translational mitochondrial import; Interacts with porin (Por1p) and Om45p; Position in a master protein: [7-26; 2xPhospho [S15; S]; Location: Mitochondrion
	PTK2 (YJR059W): Serine/threonine protein kinase; Involved in regulation of ion transport across plasma membrane; Is essential for glucose-dependent Pma1p activation via phosphorylation of Pma1p-Ser899; Enhances spermine uptake; Position in a master protein: [584-613; 1xPhospho [S592]; Location: Nucleus
	HSP42 (YDR171W): Small heat shock protein with chaperone activity; Suppresses unfolded protein aggregation; Involved in cytoskeleton reorganization after heat shock; Protein abundance increases and forms cytoplasmic foci in response to DNA replication stress; Position in a master protein: [213-237; 2xPhospho [S215; S223]; Location: Cytoskeleton

Table 6.4. The names, functions, phosphorylation sites and cellular locations of proteins that are phosphorylated only in mitochondria of cells cultured with or without LCA and recovered at day 4. See text for discussion. The names of proteins that have been found in other cellular locations and shown (by others) to be associated with mitochondria only in phosphorylated forms are shown in red color.

+ or - LCA	Protein name (SGD), function (SGD), phosphorylation site (my data) and cellular location (SGD)
+ LCA	**PIL1** (YGR086C): Sphingolipid long chain base-responsive protein PIL1; Eisosome core component; Eisosomes are large immobile cell cortex structures associated with endocytosis; ***detected in phosphorylated state in mitochondria***; phosphorylated on Thr233 upon Pkc1p hyperactivation in a Slt2p MAPK-dependent fashion; represses Pkc1p/Ypk1p stress resistance pathways; Relocates from plasma membrane to cytoplasm upon DNA replication stress; Position in a master protein: [45-56; 1xPhospho [S45]; Location: Plasms membrane, Mitochondrion, Lipid droplet
	RAS2 (YNL098C): Ras-like protein 2; Regulates nitrogen starvation response, sporulation, and filamentous growth; Farnesylation and palmitoylation required for activity and localization to plasma membrane; Position in a master protein: [233-251; 1xPhospho [S/T]; Location: Plasma membrane
	VIP1 (YLR410W): Inositol hexakisphosphate and diphosphoinositol-pentakisphosphate kinase; Is involved in such diverse processes as vacuolar biogenesis, t*he stress response, cell wall synthesis*, actin cytoskeleton function, and phosphate signaling and homeostasis; Position in a master protein: [891-907; 1xPhospho [S895]; Location: Cytoskeleton
	YDL218W: Uncharacterized membrane protein; Is induced by starvation and aerobic conditions, as well as in response to treatment with the mycotoxin patulin; Position in a master protein: [293-311; 1xPhospho [S]; Location: A Membrane
	FMP45 (YDL222C): SUR7 family integral membrane protein that is localized to ***mitochondria*** and plasma membrane; required for cell wall maintenance, sporulation and sphingolipid content maintenance; Position in a master protein: [242-277; 1xPhospho [T/S/Y]; Location: ***Mitochondria***, Plasma membrane
	ZEO1 (YOL109W): Peripheral membrane protein of the plasma membrane; Regulates the cell integrity pathway mediated by Pkc1p and Slt2p; Is detected in a phosphorylated state in highly purified ***mitochondria***; Position in a master protein: [30-45; 1xPhospho [S40]; Location: Plasma membrane, Mitochondria
	PKH2 (YOL100W): Serine/threonine protein kinase; Is involved in sphingolipid-mediated signaling pathway that controls endocytosis; activates the signaling cascade required for maintenance of *cell wall integrity*; Position in a master protein: [1007-1018; 1xPhospho [S1009]; Location: Cytoplasm, Nucleus
	OM14 (YBR230C): Mitochondrial outer membrane receptor for cytosolic ribosomes; Integral protein of the outer membrane that interacts with the nascent chain-associated complex (NAC) bound to ribosomes, contributing to co-translational mitochondrial import; Interacts with porin (Por1p) and Om45p; Position in a master protein: [7-26; 2xPhospho [S15; S]; Location: Mitochondrion
	MSS4 (YDR208W): Phosphatidylinositol-4-phosphate 5-kinase; involved in actin cytoskeleton organization and cell morphogenesis; Position in a master protein: [266-284; 1xPhospho [S/T]; Location: Plasma membrane, Nucleus

	MYO3 (YKL129C): One of two type I myosins; localizes to actin cortical patches; Position in a master protein: [774-782; 1xPhospho [S777]; Location: Cytoplasm, Cytoskeleton
	PBP1 (YGR178C): PAB1-binding protein 1; Component of *glucose-deprivation induced stress granules*; Involved in P-body-dependent granule assembly; Represses mRNA polyadenylation; Position in a master protein: [345-369; 1xPhospho [T353]; Location: Cytoplasm, Mitochondrion, Nucleus
	CCC1 (YLR220W); Vacuolar Fe^{2+}/Mn^{2+} transporter; *Prevents mitochondrial iron accumulation*; Position in a master protein: [60-77; 1xPhospho [S68]; Location: Cytoplasm, Vacuole, Golgi
- LCA	**RTN2** (YDL204W): Reticulon-like protein involved in the maintenance of tubular ER morphology; promotes membrane curvature; regulates the ER asymmetry-induced inheritance block during ER stress; Is involved in ER-derived peroxisomal biogenesis; Position in a master protein: [240-259; 1xPhospho [S]; Location: Endoplasmic reticulum
	ENT4 (YLL038C): Putative clathrin binding protein, that is localized to cortical actin patches; it has a predicted role in actin filament organization and actin patch assembly, and endocytosis; Position in a master protein: [163-170; 1xPhospho [T/S]; Location: Cytoskeleton
	SEG2 (YKL105C): Eisosome component involved in the assembly of eisosomes, large immobile patch structures at the cell cortex associated with endocytosis; Position in a master protein: [920-925; 1xPhospho [S922]; Location: Plasma membrane

Table 6.5. The names, functions, phosphorylation sites and cellular locations of proteins that are phosphorylated only in mitochondria of cells cultured with or without LCA and recovered at day 7. See text for discussion. The names of proteins that have been found in other cellular locations and shown (by others) to be associated with mitochondria only in phosphorylated forms are shown in red color.

+ or - LCA	Protein name (SGD), function (SGD), phosphorylation site (my data) and cellular location (SGD)
+ LCA	**SUR7** (YML052W): Plasma membrane protein; Component of eisosomes; Is involved in sporulation and plasma membrane sphingolipid content; Position in a master protein: [***239-283; 1xPhospho [S***]; Location: Plasma membrane
	YDL218W: Uncharacterized membrane protein; Is induced by starvation and aerobic conditions, as well as in response to treatment with the mycotoxin patulin; Position in a master protein: [257-292; 257-287; 263-292; 263-287; 293-311; 1xPhospho [S/Y]; 1xPhospho [S/Y/T]; 1xPhospho [S/Y/T]; 1xPhospho [S]; 1xPhospho [S305]; Location: A Membrane
	RAS2 (YNL098C): Ras-like protein 2; Regulates nitrogen starvation response, sporulation, and filamentous growth; Farnesylation and palmitoylation required for activity and localization to plasma membrane; Position in a master protein: [181-196; 233-251; 233-239; 197-211; [197-211; 2xPhospho [S188; S192]; 2xPhospho [S235; S238]; 2xPhospho [S235; S238]; 1xPhospho [S207]; 2xPhospho [S202; S207]; Location: Plasma membrane
	UIP4 (YPL186C): a Ubl (ubiquitin-like protein)-specific protease; ***Detected in a phosphorylated state in the mitochondrial outer membrane***; Position in a master protein: [197-214; 1xPhospho [S205]; Location: ***Mitochondrial outer membrane***, Endoplasmic reticulum, Nucleus
	EIS1 (YMR031C): Component of the eisosome required for proper eisosome assembly; ***Is detected in a phosphorylated state in highly purified mitochondria***; Position in a master protein: [128-137; 2xPhospho [S130; S133]; Location: Plasma membrane, ***Mitochondria***
	RTN1 (YDR233C): Reticulon protein; Is involved in the maintenance of tubular ER morphology; Regulates the ER asymmetry-induced inheritance block during ER stress; Is involved in ER-derived peroxisomal biogenesis; ***Is involved in phosphatidylserine transfer between the ER and mitochondria***; Position in a master protein: [***219-247; 1xPhospho [S/T***]; Location: Endoplasmic reticulum
	PKH1 (YDR490C): Serine/threonine protein kinase; involved in sphingolipid-mediated signaling pathway that controls endocytosis and activates the signaling cascade required for maintenance of cell wall integrity; Position in a master protein: [294-317; 1xPhospho [S/Y/T]; Location: Cytoplasm
	ALD4 (YOR374W): ***Mitochondrial aldehyde dehydrogenase***; required for growth on ethanol and conversion of acetaldehyde to acetate; ***phosphorylated***; ***expression is glucose repressed***; Position in a master protein: [498-511; 1xPhospho [S500]; Location: ***Mitochondrial matrix***

	YKL050C (YKL050C): Protein of unknown function; Position in a master protein: [450-463; 1xPhospho [S460]; Location: Unknown
	MCK1 (YNL307C): Protein serine/threonine/tyrosine kinase involved in protein phosphorylation and breakdown; cyclin-binding protein; Is involved in chromosome segregation, meiotic entry, genome stability, phosphorylation-dependent protein degradation, ***inhibition of protein kinase A***, transcriptional regulation, inhibition of RNA pol III, and calcium stress; Position in a master protein: [14-31; 1xPhospho [S24]; Location: Unknown
	FMP45 (YDL222C): SUR7 family integral membrane protein that is localized to ***mitochondria*** and plasma membrane; required for cell wall maintenance, sporulation and sphingolipid content maintenance; Position in a master protein: [215-241; 1xPhospho [T/S]; Location: ***Mitochondria***, Plasma membrane
	YCK2 (YNL154C): Palmitoylated plasma membrane-bound casein kinase I (CK1) isoform; Is involved in glucose sensing; Causes glucose repression of respiratory metabolism; Is involved in the phosphorylation and regulation of glucose sensor Rgt2p; ***Also found on the outer surface of mitochondria***; Position in a master protein: [448-481; 1xPhospho [S/Y/T]; Location: Plasma membrane
	HER1 (YOR227W): HMG2-induced ER-remodeling protein 1; Is required for proliferation or remodeling of the ER that is caused by overexpression of Hmg2p; Position in a master protein: [1010-1035; 1xPhospho [S1013]; Location: Cytoplasm, ***Mitochondria***
	IST2 (YBR086C): Cortical ER protein involved in ER-plasma membrane tethering; one of 6 proteins that connect ER to the plasma membrane (PM) and regulate PM phosphatidylinositol-4-phosphate (PI4P) levels by controlling access of Sac1p phosphatase to its substrate PI4P in the PM; Position in a master protein: [828-855; 1xPhospho [S847]; Location: Plasma membrane, Endoplasmic reticulum (cortical)
	TCB3 (YML072C): Cortical ER protein involved in ER-plasma membrane tethering; one of 6 proteins that connect ER to the plasma membrane (PM) and regulate PM phosphatidylinositol-4-phosphate (PI4P) levels by controlling access of Sac1p phosphatase to its substrate PI4P in the PM; ***Is detected in a phosphorylated state in mitochondria***; Position in a master protein: [101-124; 1xPhospho [S112]; Location: Plasma membrane, Endoplasmic reticulum (cortical)
	TCB1 (YOR086C): Lipid-binding ER protein involved in ER-plasma membrane tethering; one of 6 proteins that connect ER to plasma membrane (PM) and regulate PI4P levels by controlling access of Sac1p phosphatase to its substrate PI4P in PM; ***Is also localizes to mitochondria***; Position in a master protein: [33-47; 3xPhospho [S40; S42; S44]; Location: Plasma membrane, Endoplasmic reticulum (cortical), ***Mitochondria***
	GPD1 (YDL022W): NAD-dependent glycerol-3-phosphate dehydrogenase; key enzyme of glycerol synthesis, essential for growth under osmotic stress; expression regulated by high-osmolarity glycerol response pathway; protein abundance increases in response to DNA replication stress; ***constitutively inactivated via phosphorylation*** by the protein kinases Ypk1p and Ypk2p, ***dephosphorylation increases catalytic activity***; Position in a master protein: [22-36; 2xPhospho [S25; S]; Location: Cytoplasm, Peroxisome
	ORM2 (YLR350W): Protein that mediates sphingolipid homeostasis; Is required for resistance to agents that induce unfolded protein response; Orm1p and Orm2p together control membrane biogenesis by coordinating lipid homeostasis with protein quality control; Position in a master protein: [7-33; 1xPhospho [S]; Location: Endoplasmic reticulum
	MYO5 (YMR109W): One of two type I myosin motors; Position in a master protein: [1134-1158; 1xPhospho [T1153]; Location: Cytoplasm, Actin Cytoskeleton
	SEG1 (YMR086W): Component of eisosome required for proper eisosome assembly; Controls eisosome length and shape; Forms heterogeneous patches at plasma membrane in small, medium and large buds; ***Expression is repressed by cAMP***; Position in a master protein: [215-225; 296-329; 654-667; 442-460; 2xPhospho [S217; S220]; 1xPhospho [S]; 2xPhospho [S656; S]; 1xPhospho [T/S]; Location: Plasma membrane
- LCA	**VTC2** (YFL004W): Regulatory subunit of the vacuolar transporter chaperone (VTC) complex; Is involved in membrane trafficking, vacuolar polyphosphate accumulation, microautophagy and non-autophagic vacuolar fusion; Position in a master protein: [176-190; 1xPhospho [S187]; Location: Vacuole membrane

	SUR7 (YML052W): Plasma membrane protein; Component of eisosomes; Is involved in sporulation and plasma membrane sphingolipid content; Position in a master protein: [***216-226; 1xPhospho [S221***]; Location: Plasma membrane
	HSP42 (YDR171W): Small heat shock protein with chaperone activity; Suppresses unfolded protein aggregation; Involved in cytoskeleton reorganization after heat shock; Protein abundance increases and forms cytoplasmic foci in response to DNA replication stress; Position in a master protein: [213-237; 1xPhospho [S]; Location: Cytoskeleton
	TY1B-DR6 (YDR365W-B): Transposon Ty1-DR6 Gag-Pol polyprotein; Position in a master protein: [363-381; 1xPhospho [S/Y]; Location: Cytoplasm, Nucleus
	SYP1 (YCR030C); Negative regulator of WASP-Arp23 complex; Is involved in endocytic site formation; Inhibits actin assembly in vitro; Regulate assembly and disassembly of the septin ring; Potential role in actin cytoskeletal organization; Position in a master protein: [257-285; 1xPhospho [S]; Location: The mother-bud neck
	EDE1 (YBL047C): Scaffold protein involved in the formation of early endocytic sites; Putative regulator of cytokinesis; Is required for localization to and organization of endocytic sites; Interacts with other endocytic proteins; Functions upstream of CMK2 in regulating non-apoptotic cell death; Position in a master protein: [524-531; 1xPhospho [S]; Location: Cytoplasm, Cytoskeleton
	RTN1 (YDR233C): Reticulon protein; Is involved in the maintenance of tubular ER morphology; Regulates the ER asymmetry-induced inheritance block during ER stress; Is involved in ER-derived peroxisomal biogenesis; ***Is involved in phosphatidylserine transfer between the ER and mitochondria***; Position in a master protein: [***217-235; 1xPhospho [T/S***]; Location: Endoplasmic reticulum

6.4 Discussion

Based on the above data on the LCA-driven remodeling of the mitochondrial phosphoproteome, we propose the following hypothesis. LCA is known to be a mildly toxic molecule with detergent-like properties that elicits a hormetic stress response, which is in part responsible for the delay of yeast chronological aging [14, 250]. Exogenous LCA has been shown to enter calorically restricted yeast cells, be sorted to mitochondria, amass in the IMM and OMM, and alter the concentrations of certain mitochondrial membrane phospholipids [248]. We hypothesize that the created by LCA mild stress and/or changes in mitochondrial membrane lipidome may convert the mitochondrion into a signaling platform stimulating activities of a distinct set of protein kinases and protein phosphatases confined to mitochondria as well as to some other cellular compartments. After being activated, these protein kinases and protein phosphatases that phosphorylate or dephosphorylate (respectively) certain target proteins; some of these target proteins reside in mitochondria, whereas other are in other cellular compartments. Following their phosphorylation or dephosphorylation, the phosphorylated or dephosphorylated forms of proteins in these other cellular compartments are sorted to mitochondria; they are likely not imported into these organelles but attached to their outer surface. The phosphorylated and dephosphorylated forms of proteins associated with mitochondria in response to LCA treatment may delay yeast chronological aging via the following two groups of mechanisms: 1) some of

these mitochondria-associated phosphorylated or dephosphorylated proteins alter mitochondrial functionality and/or allow mitochondria to operate as a signaling platform orchestrating certain aging-delaying processes in other cellular locations; and 2) the re-location of phosphorylated or dephosphorylated form of some other proteins from their initial cellular sites to mitochondria may allow to alter the rates of efficiencies of cellular processes in these initial sites in a way that causes a delay of yeast chronological aging.

To test the above hypothesis, the Titorenko laboratory will attempt to identify protein kinases and protein phosphatases responsible for the phosphorylation or dephosphorylation of proteins whose phosphorylated or dephosphorylated forms associate with mitochondria in response to LCA treatment. The names of protein kinases and protein phosphatases that will be interesting to test for their possible involvement in the phosphorylation or dephosphorylation of proteins associated with mitochondria in LCA-treated cells are shown in Table 6.6; this table also specifies the reason why such involvement needs to be tested. WT and mutant strains carrying single-gene-deletion mutations eliminating each of these protein kinases or protein phosphatases will be cultured in the nutrient-rich YP (1% yeast extract, 2% peptone) medium containing 0.2% glucose with 50 μM LCA (the concentration of LCA that elicits the highest aging-delaying effect) or without LCA. Yeast cells will be recovered at days 2, 4 and 7 of culturing to analyze the mitochondrial proteome in cells of different chronological ages. A quantitative, label-free mass spectrometry approach will be then used to compare phosphoproteomes of mitochondria purified from WT and mutant cells that were cultured with or without LCA and recovered for mitochondria purification at different days of culturing.

It will then be tested if single-gene-deletion mutations eliminating each of the protein kinases and protein phosphatases of interest influence the extent of yeast longevity extension by LCA. Our hypothesis predicts that 1) mutations eliminating protein kinases and protein phosphatases that phosphorylate or dephosphorylate proteins associated with mitochondria in response to LCA treatment are expected to weaken the extent of yeast longevity extension by LCA; and 2) mutations eliminating protein kinases and protein phosphatases that do not phosphorylate or dephosphorylate proteins associated with mitochondria in response to LCA treatment are expected to have no effect on the extent of yeast longevity extension by LCA.

Table 6.6. The names of protein kinases and phosphatases need to be tested (and the reason why they need to be tested) for the possible involvement in the phosphorylation or dephosphorylation of proteins associated with mitochondria in LCA-treated cells.

Name	Reason
Tpk1	A catalytic subunit of PKA, which phosphorylates core protein components of mitochondrial protein import machinery
Yck1	An isoform of CK1, which phosphorylates core protein components of mitochondrial protein import machinery
Yck2	An isoform of CK1, which phosphorylates core protein components of mitochondrial protein import machinery
Cka1	A catalytic subunit of CK2, which phosphorylates core protein components of mitochondrial protein import machinery and mitophagy
Cka2	A catalytic subunit of CK2, which phosphorylates core protein components of mitochondrial protein import machinery and mitophagy
Hog1	The MAPK which in response to cell-surfaces stresses stimulates the Cka2-dependent phosphorylation of Atg32, a mitochondrial receptor for mitophagy
Tor1	A protein kinase subunit of the target of rapamycin complex 1 (TORC1), the key nutrient sensor
Tap42	A downstream effector of TORC1, which regulates PP2a and PP2A-like protein phosphatases
Sch9	A downstream effector of TORC1 and a nutrient-sensing protein kinase, which regulates oxidative phosphorylation and protein synthesis in mitochondria
Pkp1	A mitochondrial protein kinase, which inhibits mitochondrial pyruvate dehydrogenase by phosphorylating its E1 α subunit; found only in mitochondria
Pkp2	A mitochondrial protein kinase, which inhibits mitochondrial pyruvate dehydrogenase by phosphorylating its E1 α subunit; found only in mitochondria
Ptc5	A mitochondrial protein phosphatase, which activates mitochondrial pyruvate dehydrogenase by dephosphorylating the phosphorylated form of its E1 α subunit; found only in mitochondria
Ptc6	A mitochondrial protein phosphatase, which activates mitochondrial pyruvate dehydrogenase by dephosphorylating the phosphorylated form of its E1 α subunit; found only in mitochondria
Fmp48	A mitochondrial protein kinase of unknown function; found only in mitochondria
Ptc7	A mitochondrial protein phosphatase of unknown function; found only in mitochondria

The above analysis is expected to identify protein kinases and protein phosphatases responsible for the phosphorylation or dephosphorylation of proteins whose phosphorylated or dephosphorylated forms associate with mitochondria in response to LCA treatment. The Titorenko laboratory will use this knowledge to formulate and to test further hypotheses on how the regulated protein phosphorylation and dephosphorylation of certain mitochondrial proteins by a distinct set of protein kinases and protein phosphatases may underlie the delay of yeast chronological aging by LCA.

Although some of the single-gene-deletion mutations eliminating each of the protein kinases or protein phosphatases of interest may weaken or enhance the extent of yeast longevity extension by LCA, these effects may be non-specific (i.e. may not be due to changes in the phosphorylation state of specific mitochondrial proteins). Indeed, some of the protein kinases and protein phosphatases are known for their abilities to phosphorylate and dephosphorylate (respectively) proteins outside of mitochondria. Further assessment of the proposed hypothesis

may therefore require testing how phosphomimetic and non-phosphorylatable mutations at the critical phosphorylation sites of each of the mitochondrial proteins of interest influence the extent of yeast longevity extension by LCA; mitochondrial proteins of interest are the ones whose phosphorylated or dephosphorylated forms associate with mitochondria in response to LCA treatment. Phosphomimetic mutations at the phosphorylation sites are known to result in amino acid substitutions that mimic a phosphorylated protein; such substitutions include serine for aspartate as well as serine or threonine for glutamate. Non-phosphorylatable mutations at the phosphorylation sites yield amino acid substitutions that prevent protein phosphorylation at a serine, tyrosine or threonine site; such substitutions include serine or threonine for alanine as well as tyrosine for phenylalanine or alanine.

7 General conclusions

Studies described in this thesis have revealed that some of the molecular and cellular mechanisms through which CR and LCA delay yeast chronological aging are common to these two longevity-extending interventions. Among the mechanisms of aging delay that CR and LCA have in common are the following ones: 1) both CR and LCA shift a balance between the processes of mitochondrial fusion and fission toward fusion, thus postponing the age-related onset and slowing the progression of the mitochondria-controlled apoptotic mode of regulated cell death; and 2) both CR and LCA stimulate the peroxisome-to-mitochondrion transport of acetyl-CoA via the carnitine shuttle, thereby delaying the age-related onset of the decline in mitochondrial functionality.

We found that some mechanisms of yeast chronological aging delay are specific only to CR or LCA. Indeed, only CR (but not LCA) decelerates the chronological aging process in part because it causes a significant rise in the concentration of trehalose, thus postponing the age-related onset of the deterioration in cellular proteostasis. Moreover, only LCA (but not CR) slows down the chronological aging process in part because it stimulates the Mpc1/Mpc3 mitochondrial pyruvate carrier involved in the cytosol-to-mitochondrion transport of pyruvate, thereby postponing the age-related onset of the decline in mitochondrial functionality.

Finally, although both CR and LCA delay the age-related onset and decelerate the progression of the FFA-driven liponecrotic form of regulated cell death, these two longevity-extending interventions decrease the concentration of FFA via different mechanisms. CR lowers the concentration of FFA by stimulating both TAG lipolysis in LD and the subsequent peroxisomal β-oxidation of FFA (the product of such lipolysis). In contrast, LCA lessens the concentration of FFA by promoting TAG synthesis from FFA in LD.

In sum, studies described in this thesis have demonstrated that intercompartmental communications between the ER, LD, peroxisomes, mitochondria and the cytosol play essential roles in regulating the pace of chronological aging in *S. cerevisiae*. Furthermore, CR and LCA control some of these intercompartmental communications through similar mechanisms. However, other intercompartmental communications are controlled by CR and LCA via mechanisms that are specific for each of these two longevity-extending interventions. Based on these findings, we hypothesize that some of the molecular and cellular mechanisms of aging delay and longevity

extension represent the core mechanisms that are controlled by many aging-delaying and longevity-extending interventions, whereas other such mechanisms have evolved as an adaptation to specific changes in the availability of certain nutrients or particular mildly toxic molecules.

References

1. Fontana L, Partridge L, Longo VD. Extending healthy life span--from yeast to humans. Science. 2010; 328:321-6.

2. Kaeberlein M. Lessons on longevity from budding yeast. Nature. 2010; 464:513-9.

3. Longo VD, Shadel GS, Kaeberlein M, Kennedy B. Replicative and chronological aging in Saccharomyces cerevisiae. Cell Metab. 2012; 16:18-31.

4. Váchová L, Cáp M, Palková Z. Yeast colonies: a model for studies of aging, environmental adaptation, and longevity. Oxid Med Cell Longev. 2012; 2012:601836.

5. Denoth Lippuner A, Julou T, Barral Y. Budding yeast as a model organism to study the effects of age. FEMS Microbiol Rev. 2014; 38:300-25.

6. Nyström T, Liu B. Protein quality control in time and space - links to cellular aging. FEMS Yeast Res. 2014; 14:40-8.

7. Weissman J, Guthrie C, Fink GR (editors). Guide to Yeast Genetics: Functional Genomics, Proteomics, and Other Systems Analysis. 2010; Academic Press, Burlington.

8. Botstein D, Fink GR. Yeast: an experimental organism for 21st Century biology. Genetics. 2011; 189:695-704.

9. Lee SS, Avalos Vizcarra I, Huberts DH, Lee LP, Heinemann M. Whole lifespan microscopic observation of budding yeast aging through a microfluidic dissection platform. Proc Natl Acad Sci USA. 2012; 109:4916-20.

10. Sutphin GL, Olsen BA, Kennedy BK, Kaeberlein M. Genome-wide analysis of yeast aging. Subcell Biochem. 2012; 57:251-89.

11. Xie Z, Zhang Y, Zou K, Brandman O, Luo C, Ouyang Q, Li H. Molecular phenotyping of aging in single yeast cells using a novel microfluidic device. Aging Cell. 2012; 11:599-606.

12. Zhang Y, Luo C, Zou K, Xie Z, Brandman O, Ouyang Q, Li H. Single cell analysis of yeast replicative aging using a new generation of microfluidic device. PloS One. 2012; 7:e48275.

13. Eisenberg T, Knauer H, Schauer A, Büttner S, Ruckenstuhl C, Carmona-Gutierrez D, Ring J, Schroeder S, Magnes C, Antonacci L, Fussi H, Deszcz L, Hartl R, Schraml E, Criollo A, Megalou E, Weiskopf D, Laun P, Heeren G, Breitenbach M, Grubeck-Loebenstein B, Herker E, Fahrenkrog B, Fröhlich KU, Sinner F, Tavernarakis N, Minois N, Kroemer G, Madeo F. Induction of autophagy by spermidine promotes longevity. Nat Cell Biol. 2009; 11:1305-14.

14. Goldberg AA, Richard VR, Kyryakov P, Bourque SD, Beach A, Burstein MT, Glebov A, Koupaki O, Boukh-Viner T, Gregg C, Juneau M, English AM, Thomas DY, Titorenko VI. Chemical genetic screen identifies lithocholic acid as an anti-aging compound that extends yeast chronological life span in a TOR-independent manner, by modulating housekeeping longevity assurance processes. Aging. 2010; 2:393-414.

15. Kapahi P, Chen D, Rogers AN, Katewa SD, Li PW, Thomas EL, Kockel L. With TOR, less is more: a key role for the conserved nutrient-sensing TOR pathway in aging. Cell Metab. 2010; 11:453-65.

16. Evans DS, Kapahi P, Hsueh WC, Kockel L. TOR signaling never gets old: aging, longevity and TORC1 activity. Ageing Res Rev. 2011; 10:225-37.

17. Minois N, Carmona-Gutierrez D, Madeo F. Polyamines in aging and disease. Aging. 2011; 3:716-32.

18. Jazwinski SM. The retrograde response retrograde response and other pathways of interorganelle communication interorganelle communication in yeast replicative aging. Subcell Biochem. 2012; 57:79-100.

19. Jazwinski SM. The retrograde response: when mitochondrial quality control is not enough. Biochim Biophys Acta. 2013; 1833:400-9.

20. Leonov A, Titorenko VI. A network of interorganellar communications underlies cellular aging. IUBMB Life. 2013; 65:665-74.

21. Hubbard BP, Sinclair DA. Small molecule SIRT1 activators for the treatment of aging and age-related diseases. Trends Pharmacol Sci. 2014; 35:146-54.

22. Sinclair DA, Guarente L. Small-molecule allosteric activators of sirtuins. Annu Rev Pharmacol Toxicol. 2014; 54:363-80.

23. Goldberg AA, Bourque SD, Kyryakov P, Gregg C, Boukh-Viner T, Beach A, Burstein MT, Machkalyan G, Richard V, Rampersad S, Cyr D, Milijevic S, Titorenko VI. Effect of calorie restriction on the metabolic history of chronologically aging yeast. Exp Gerontol. 2009; 44:555-71.

24. Steffen KK, Kennedy BK, Kaeberlein M. Measuring replicative life span in the budding yeast. J Vis Exp. 2009; 28:1209.

25. Hu J, Wei M, Mirisola MG, Longo VD. Assessing chronological aging in Saccharomyces cerevisiae. Methods Mol Biol. 2013; 965:463-72.

26. Sinclair DA. Studying the replicative life span of yeast cells. Methods Mol Biol. 2013; 1048:49-63.

27. Burtner CR, Murakami CJ, Kaeberlein M. A genomic approach to yeast chronological aging. Methods Mol Biol. 2009; 548:101-14.

28. Murakami C, Kaeberlein M. Quantifying yeast chronological life span by outgrowth of aged cells. J Vis Exp. 2009; 27:1156.

29. Wu Z, Song L, Liu SQ, Huang D. A high throughput screening assay for determination of chronological lifespan of yeast. Exp Gerontol. 2011; 46:915-22.

30. Fabrizio P, Longo VD. The chronological life span of Saccharomyces cerevisiae. Methods Mol Biol. 2007; 371:89-95.

31. Piper PW. Maximising the yeast chronological lifespan. Subcell Biochem. 2012; 57:145-59.

32. Longo VD, Kennedy BK. Sirtuins in aging and age-related disease. Cell. 2006; 126:257-68.

33. Longo VD, Fabrizio P. Chronological aging in Saccharomyces cerevisiae. Subcell Biochem. 2012; 57:101-21.

34. Bitterman KJ, Medvedik O, Sinclair DA. Longevity regulation in Saccharomyces cerevisiae: linking metabolism, genome stability, and heterochromatin. Microbiol Mol Biol Rev. 2003; 67:376-99.

35. Steinkraus KA, Kaeberlein M, Kennedy BK. Replicative aging in yeast: the means to the end. Annu Rev Cell Dev Biol. 2008; 24:29-54.

36. St'ovíček V, Váchová L, Kuthan M, Palková Z. General factors important for the formation of structured biofilm-like yeast colonies. Fungal Genet Biol. 2010; 47:1012-22.

37. Váchová L, Palková Z. Aging and longevity of yeast colony populations: metabolic adaptation and differentiation. Biochem Soc Trans. 2011; 39:1471-5.

38. Cáp M, Stěpánek L, Harant K, Váchová L, Palková Z. Cell differentiation within a yeast colony: metabolic and regulatory parallels with a tumor-affected organism. Mol Cell. 2012; 46:436-48.

39. Cáp M, Váchová L, Palková Z. Reactive oxygen species in the signaling and adaptation of multicellular microbial communities. Oxid Med Cell Longev. 2012; 2012:976753.

40. Mazzoni C, Mangiapelo E, Palermo V, Falcone C. Hypothesis: is yeast a clock model to study the onset of humans aging phenotypes? Front Oncol. 2012; 2:203.

41. Váchová L, Hatáková L, Cáp M, Pokorná M, Palková Z. Rapidly developing yeast microcolonies differentiate in a similar way to aging giant colonies. Oxid Med Cell Longev. 2013; 2013:102485.

42. Palková Z, Wilkinson D, Váchová L. Aging and differentiation in yeast populations: elders with different properties and functions. FEMS Yeast Res. 2014; 14:96-108.

43. Šťovíček V, Váchová L, Begany M, Wilkinson D, Palková Z. Global changes in gene expression associated with phenotypic switching of wild yeast. BMC Genomics. 2014; 15:136.

44. Howitz KT, Sinclair DA. Xenohormesis: sensing the chemical cues of other species. Cell. 2008; 133:387-91.

45. Goldberg AA, Kyryakov P, Bourque SD, Titorenko VI. Xenohormetic, hormetic and cytostatic selective forces driving longevity at the ecosystemic level. Aging. 2010; 2:461-70.

46. Burstein MT, Beach A, Richard VR, Koupaki O, Gomez-Perez A, Goldberg AA, Kyryakov P, Bourque SD, Glebov A, Titorenko VI. Interspecies Chemical Signals Released into the Environment May Create Xenohormetic, Hormetic and Cytostatic Selective Forces that Drive the Ecosystemic Evolution of Longevity Regulation Mechanisms. Dose Response. 2012; 10:75-82.

47. Howitz KT, Bitterman KJ, Cohen HY, Lamming DW, Lavu S, Wood JG, Zipkin RE, Chung P, Kisielewski A, Zhang LL, Scherer B, Sinclair DA. Small molecule activators of sirtuins extend Saccharomyces cerevisiae lifespan. Nature. 2003; 425:191-6.

48. Lamming DW, Wood JG, Sinclair DA. Small molecules that regulate lifespan: evidence for xenohormesis. Mol Microbiol. 2004; 53:1003-9.

49. Bonawitz ND, Shadel GS. Rethinking the mitochondrial theory of aging: the role of mitochondrial gene expression in lifespan determination. Cell Cycle. 2007; 6:1574-8.

50. Bonawitz ND, Chatenay-Lapointe M, Pan Y, Shadel GS. Reduced TOR signaling extends chronological life span via increased respiration and upregulation of mitochondrial gene expression. Cell Metab. 2007; 5:265-77.

51. Pan Y, Shadel GS. Extension of chronological life span by reduced TOR signaling requires down-regulation of Sch9p and involves increased mitochondrial OXPHOS complex density. Aging. 2009; 1:131-45.

52. Wei M, Fabrizio P, Madia F, Hu J, Ge H, Li LM, Longo VD. Tor1/Sch9-regulated carbon source substitution is as effective as calorie restriction in life span extension. PLoS Genet. 2009; 5:e1000467.

53. Mesquita A, Weinberger M, Silva A, Sampaio-Marques B, Almeida B, Leão C, Costa V, Rodrigues F, Burhans WC, Ludovico P. Caloric restriction or catalase inactivation extends yeast chronological lifespan by inducing H2O2 and superoxide dismutase activity. Proc Natl Acad Sci USA. 2010; 107:15123-8.

54. Beach A, Titorenko VI. In search of housekeeping pathways that regulate longevity. Cell Cycle. 2011; 10:3042-4.

55. Pan Y. Mitochondria, reactive oxygen species, and chronological aging: a message from yeast. Exp Gerontol. 2011; 46:847-52.

56. Pan Y, Schroeder EA, Ocampo A, Barrientos A, Shadel GS. Regulation of yeast chronological life span by TORC1 via adaptive mitochondrial ROS signaling. Cell Metab. 2011; 13:668-78.

57. Titorenko VI, Terlecky SR. Peroxisome metabolism and cellular aging. Traffic. 2011; 12: 252-9.

58. Beach A, Burstein MT, Richard VR, Leonov A, Levy S, Titorenko VI. Integration of peroxisomes into an endomembrane system that governs cellular aging. Front Physiol. 2012; 3: 283.

59. Burstein MT, Kyryakov P, Beach A, Richard VR, Koupaki O, Gomez-Perez A, Leonov A, Levy S, Noohi F, Titorenko VI. Lithocholic acid extends longevity of chronologically aging yeast only if added at certain critical periods of their lifespan. Cell Cycle. 2012; 11:3443-62.

60. Cai L, Tu BP. Driving the cell cycle through metabolism. Annu Rev Cell Dev Biol. 2012; 28:59-87.

61. Kyryakov P, Beach A, Richard VR, Burstein MT, Leonov A, Levy S, Titorenko VI. Caloric restriction extends yeast chronological lifespan by altering a pattern of age-related changes in trehalose concentration. Front Physiol. 2012; 3:256.

62. Ocampo A, Liu J, Schroeder EA, Shadel GS, Barrientos A. Mitochondrial respiratory thresholds regulate yeast chronological life span and its extension by caloric restriction. Cell Metab. 2012; 16:55-67.

63. Barral Y. A new answer to old questions. eLife. 2013; 2:e00515.

64. Beach A, Richard VR, Leonov A, Burstein MT, Bourque SD, Koupaki O, Juneau M, Feldman R, Iouk T, Titorenko VI (2013). Mitochondrial membrane lipidome defines yeast longevity. Aging. 2013; 5:551-74.

65. Beach A, Titorenko VI. Essential roles of peroxisomally produced and metabolized biomolecules in regulating yeast longevity. Subcell Biochem. 2013; 69:153-67.

66. Brandes N, Tienson H, Lindemann A, Vitvitsky V, Reichmann D, Banerjee R, Jakob U. Time line of redox events in aging postmitotic cells. eLife. 2013; 2:e00306.

67. Hachinohe M, Yamane M, Akazawa D, Ohsawa K, Ohno M, Terashita Y, Masumoto H. A reduction in age-enhanced gluconeogenesis extends lifespan. PLoS One. 2013; 8:e54011.

68. Mirisola MG, Longo VD. A radical signal activates the epigenetic regulation of longevity. Cell Metab. 2013; 17:812-3.

69. Orlandi I, Ronzulli R, Casatta N, Vai M. Ethanol and acetate acting as carbon/energy sources negatively affect yeast chronological aging. Oxid Med Cell Longev. 2013; 2013:802870.

70. Richard VR, Leonov A, Beach A, Burstein MT, Koupaki O, Gomez-Perez A, Levy S, Pluska L, Mattie S, Rafesh R, Iouk T, Sheibani S, Greenwood M, Vali H, Titorenko VI. Macromitophagy is a longevity assurance process that in chronologically aging yeast limited in calorie supply sustains functional mitochondria and maintains cellular lipid homeostasis. Aging. 2013; 5:234-69.

71. Schroeder EA, Raimundo N, Shadel GS. Epigenetic silencing mediates mitochondria stress-induced longevity. Cell Metab. 2013; 17:954-64.

72. Tahara EB, Cunha FM, Basso TO, Della Bianca BE, Gombert AK, Kowaltowski AJ. Calorie restriction hysteretically primes aging Saccharomyces cerevisiae toward more effective oxidative metabolism. PLoS One. 2013; 8:e56388.

73. Martins D, Titorenko VI, English AM. Cells with impaired mitochondrial H2O2 sensing generate less •OH radicals and live longer. Antioxid Redox Signal. 2014; 21:1490-503.

74. Chen B, Retzlaff M, Roos T, Frydman J. Cellular strategies of protein quality control. Cold Spring Harb Perspect Biol. 2011; 3:a004374.

75. Lindquist SL, Kelly JW. Chemical and biological approaches for adapting proteostasis to ameliorate protein misfolding and aggregation diseases: progress and prognosis. Cold Spring Harb Perspect Biol. 2011; 3:a004507.

76. Taylor RC, Dillin A. Aging as an event of proteostasis collapse. Cold Spring Harb Perspect Biol. 2011; 3:a004440.

77. Kim YE, Hipp MS, Bracher A, Hayer-Hartl M, Hartl FU. Molecular chaperone functions in protein folding and proteostasis. Annu Rev Biochem. 2013; 82:323-55.

78. Legakis JE, Koepke JI, Jedeszko C, Barlaskar F, Terlecky LJ, Edwards HJ, Walton PA, Terlecky SR. Peroxisome senescence in human fibroblasts. Mol Biol Cell. 2002; 13:4243-55.

79. Terlecky SR, Koepke JI, Walton PA. Peroxisomes and aging. Biochim Biophys Acta. 2006; 1763:1749-54.

80. Ma C, Agrawal G, Subramani S. Peroxisome assembly: matrix and membrane protein biogenesis. J Cell Biol. 2011; 193:7-16.

81. Liu X, Ma C, Subramani S. Recent advances in peroxisomal matrix protein import. Curr Opin Cell Biol. 2012; 24:484-9.

82. Hasan S, Platta HW, Erdmann R. Import of proteins into the peroxisomal matrix. Front Physiol. 2013; 4:261.

83. Titorenko VI, Rachubinski RA. The peroxisome: orchestrating important developmental decisions from inside the cell. J Cell Biol. 2004; 164:641-5.

84. Goldberg AA, Bourque SD, Kyryakov P, Boukh-Viner T, Gregg C, Beach A, Burstein MT, Machkalyan G, Richard V, Rampersad S, Titorenko VI. A novel function of lipid droplets in regulating longevity. Biochem Soc Trans. 2009; 37:1050-5.

85. Ivashchenko O, Van Veldhoven PP, Brees C, Ho YS, Terlecky SR, Fransen M. Intraperoxisomal redox balance in mammalian cells: oxidative stress and interorganellar cross-talk. Mol Biol Cell. 2011; 22:1440-51.

86. Islinger M, Grille S, Fahimi HD, Schrader M. The peroxisome: an update on mysteries. Histochem Cell Biol. 2012; 137:547-74.

87. Walton PA, Pizzitelli M. Effects of peroxisomal catalase inhibition on mitochondrial function. Front Physiol. 2012; 3:108.

88. Wang B, Van Veldhoven PP, Brees C, Rubio N, Nordgren M, Apanasets O, Kunze M, Baes M, Agostinis P, Fransen M. Mitochondria are targets for peroxisome-derived oxidative stress in cultured mammalian cells. Free Radic Biol Med. 2013; 65:882-94.

89. Nordgren M, Fransen M. Peroxisomal metabolism and oxidative stress. Biochimie. 2014; 98:56-62.

90. Hiltunen JK, Mursula AM, Rottensteiner H, Wierenga RK, Kastaniotis AJ, Gurvitz A. The biochemistry of peroxisomal beta-oxidation in the yeast Saccharomyces cerevisiae. FEMS Microbiol Rev. 2003; 27:35-64.

91. Kawałek A, Lefevre SD, Veenhuis M, van der Klei IJ. Peroxisomal catalase deficiency modulates yeast lifespan depending on growth conditions. Aging. 2013; 5:67-83.

92. Lefevre SD, van Roermund CW, Wanders RJ, Veenhuis M, van der Klei IJ. The significance of peroxisome function in chronological aging of Saccharomyces cerevisiae. Aging Cell. 2013; 12:784-93.

93. Minois N. Molecular basis of the 'anti-aging' effect of spermidine and other natural polyamines - a mini-review. Gerontology. 2014; 60:319-26.

94. Morselli E, Galluzzi L, Kepp O, Criollo A, Maiuri MC, Tavernarakis N, Madeo F, Kroemer G. Autophagy mediates pharmacological lifespan extension by spermidine and resveratrol. Aging. 2009; 1:961-70.

95. Morselli E, Mariño G, Bennetzen MV, Eisenberg T, Megalou E, Schroeder S, Cabrera S, Bénit P, Rustin P, Criollo A, Kepp O, Galluzzi L, Shen S, Malik SA, Maiuri MC, Horio Y, López-Otín C, Andersen JS, Tavernarakis N, Madeo F, Kroemer G. Spermidine and resveratrol induce autophagy by distinct pathways converging on the acetylproteome. J Cell Biol. 2011; 192:615-29.

96. Binns D, Januszewski T, Chen Y, Hill J, Markin VS, Zhao Y, Gilpin C, Chapman KD, Anderson RG, Goodman JM. An intimate collaboration between peroxisomes and lipid bodies. J Cell Biol. 2006; 173:719-31.

97. D'Autréaux B, Toledano MB. ROS as signalling molecules: mechanisms that generate specificity in ROS homeostasis. Nat Rev Mol Cell Biol. 2007; 8:813-24.

98. Giorgio M, Trinei M, Migliaccio E, Pelicci PG. Hydrogen peroxide: a metabolic by-product or a common mediator of ageing signals? Nat Rev Mol Cell Biol. 2007; 8:722-8.

99. Veal EA, Day AM, Morgan BA. Hydrogen peroxide sensing and signaling. Mol Cell. 2007; 26:1-14.

100. Goodman JM. The gregarious lipid droplet. J Biol Chem. 2008; 283:28005-9.

101. Adeyo O, Horn PJ, Lee S, Binns DD, Chandrahas A, Chapman KD, Goodman JM. The yeast lipin orthologue Pah1p is important for biogenesis of lipid droplets. J Cell Biol. 2011; 192:1043-55.

102. Kohlwein SD, Veenhuis M, van der Klei IJ. Lipid droplets and peroxisomes: key players in cellular lipid homeostasis or a matter of fat - store 'em up or burn 'em down. Genetics. 2013; 193:1-50.

103. Sheibani S, Richard VR, Beach A, Leonov A, Feldman R, Mattie S, Khelghatybana L, Piano A, Greenwood M, Vali H, Titorenko VI. Macromitophagy, neutral lipids synthesis, and peroxisomal fatty acid oxidation protect yeast from "liponecrosis", a previously unknown form of programmed cell death. Cell Cycle. 2014; 13:138-47.

104. van der Klei IJ, Yurimoto H, Sakai Y, Veenhuis M. The significance of peroxisomes in methanol metabolism in methylotrophic yeast. Biochim Biophys Acta. 2006; 1763:1453-62.

105. Piper PW, Harris NL, MacLean M. Preadaptation to efficient respiratory maintenance is essential both for maximal longevity and the retention of replicative potential in chronologically ageing yeast. Mech Ageing Dev. 2006; 127:733-40.

106. Lavoie H, Whiteway M. Increased respiration in the sch9Δ mutant is required for increasing chronological life span but not replicative life span. Eukaryot Cell. 2008; 7:1127-35.

107. Burstein MT, Titorenko VI. A mitochondrially targeted compound delays aging in yeast through a mechanism linking mitochondrial membrane lipid metabolism to mitochondrial redox biology. Redox Biol. 2014; 2:305-7.

108. Schroeder EA, Shadel GS. Crosstalk between mitochondrial stress signals regulates yeast chronological lifespan. Mech Ageing Dev. 2014; 135:41-9.

109. Broach JR. Nutritional control of growth and development in yeast. Genetics. 2012; 192:73-105.

110. De Virgilio C. The essence of yeast quiescence. FEMS Microbiol Rev. 2012; 36:306-39.

111. Orzechowski Westholm J, Tronnersjö S, Nordberg N, Olsson I, Komorowski J, Ronne H. Gis1 and Rph1 regulate glycerol and acetate metabolism in glucose depleted yeast cells. PLoS One. 2012; 7(2):e31577.

112. Fabrizio P, Gattazzo C, Battistella L, Wei M, Cheng C, McGrew K, Longo VD (2005). Sir2 blocks extreme life-span extension. Cell. 2005; 123:655-67.

113. Burtner CR, Murakami CJ, Kennedy BK, Kaeberlein M. A molecular mechanism of chronological aging in yeast. Cell Cycle. 2009; 8:1256-70.

114. Burtner CR, Murakami CJ, Olsen B, Kennedy BK, Kaeberlein M. A genomic analysis of chronological longevity factors in budding yeast. Cell Cycle; 2011; 10:1385-96.

115. Murakami C, Delaney JR, Chou A, Carr D, Schleit J, Sutphin GL, An EH, Castanza AS, Fletcher M, Goswami S, Higgins S, Holmberg M, Hui J, Jelic M, Jeong KS, Kim JR, Klum S, Liao E, Lin MS, Lo W, Miller H, Moller R, Peng ZJ, Pollard T, Pradeep P, Pruett D, Rai D, Ros V, Schuster A, Singh M, Spector BL, Vander Wende H, Wang AM, Wasko BM, Olsen B, Kaeberlein M. pH neutralization protects against reduction in replicative lifespan following chronological aging in yeast. Cell Cycle. 2012; 11:3087-96.

116. Eisenberg T, Schroeder S, Andryushkova A, Pendl T, Küttner V, Bhukel A, Mariño G, Pietrocola F, Harger A, Zimmermann A, Moustafa T, Sprenger A, Jany E, Büttner S, Carmona-Gutierrez D, Ruckenstuhl C, Ring J, Reichelt W, Schimmel K, Leeb T, Moser C, Schatz S, Kamolz LP, Magnes C, Sinner F, Sedej S, Fröhlich KU, Juhasz G, Pieber TR, Dengjel J, Sigrist SJ, Kroemer G, Madeo F. Nucleocytosolic depletion of the energy metabolite acetyl-coenzyme A stimulates autophagy and prolongs lifespan. Cell Metab. 2014; 19:431-44.

117. Hu J, Wei M, Mirzaei H, Madia F, Mirisola M, Amparo C, Chagoury S, Kennedy B, Longo VD. Tor-Sch9 deficiency activates catabolism of the ketone body-like acetic acid to promote trehalose accumulation and longevity. Aging Cell. 2014; 13:457-67.

118. Fraenkel DG. Yeast intermediary metabolism. 2011; Cold Spring Harbor Laboratory Press, Cold Spring Harbor.

119. Crespo JL, Powers T, Fowler B, Hall MN. The TOR-controlled transcription activators GLN3, RTG1, and RTG3 are regulated in response to intracellular levels of glutamine. Proc Natl Acad Sci USA. 2002; 99:6784-9.

120. Powers RW 3rd, Kaeberlein M, Caldwell SD, Kennedy BK, Fields S. Extension of chronological life span in yeast by decreased TOR pathway signaling. Genes Dev. 2006; 20:174-84.

121. Jewell JL, Russell RC, Guan KL. Amino acid signalling upstream of mTOR. Nat Rev Mol Cell Biol. 2013; 14:133-9.

122. Conrad M, Schothorst J, Kankipati HN, Van Zeebroeck G, Rubio-Texeira M, Thevelein JM. Nutrient sensing and signaling in the yeast Saccharomyces cerevisiae. FEMS Microbiol Rev. 2014; 38:254-99.

123. Shimobayashi M, Hall MN. Making new contacts: the mTOR network in metabolism and signalling crosstalk. Nat Rev Mol Cell Biol. 2014; 15:155-62.

124. Swinnen E, Ghillebert R, Wilms T, Winderickx J. Molecular mechanisms linking the evolutionary conserved TORC1-Sch9 nutrient signalling branch to lifespan regulation in Saccharomyces cerevisiae. FEMS Yeast Res. 2014; 14:17-32.

125. Barea F, Bonatto D. Aging defined by a chronologic-replicative protein network in Saccharomyces cerevisiae: an interactome analysis. Mech Ageing Dev. 2009; 130:444-60.

126. Lorenz DR, Cantor CR, Collins JJ. A network biology approach to aging in yeast. Proc Natl Acad Sci USA. 2009; 106:1145-50.

127. Borklu Yucel E, Ulgen KO. A network-based approach on elucidating the multi-faceted nature of chronological aging in S. cerevisiae. PLoS One. 2011; 6:e29284.

128. Gozuacik D, Bialik S, Raveh T, Mitou G, Shohat G, Sabanay H, Mizushima N, Yoshimori T, Kimchi A. DAP-kinase is a mediator of endoplasmic reticulum stress-induced caspase activation and autophagic cell death. Cell Death Differ. 2008; 15:1875-86.

129. Eisenberg-Lerner A, Bialik S, Simon HU, Kimchi A. Life and death partners: apoptosis, autophagy and the cross-talk between them. Cell Death Differ. 2009; 16:966-75.

130. Bialik S, Zalckvar E, Ber Y, Rubinstein AD, Kimchi A. Systems biology analysis of programmed cell death. Trends Biochem Sci. 2010; 35:556-64.

131. Zalckvar E, Bialik S, Kimchi A. The road not taken: a systems level strategy for analyzing the cell death network. Autophagy. 2010; 6:813-5.

132. Zalckvar E, Yosef N, Reef S, Ber Y, Rubinstein AD, Mor I, Sharan R, Ruppin E, Kimchi A. A systems level strategy for analyzing the cell death network: implication in exploring the apoptosis/autophagy connection. Cell Death Differ. 2010; 17:1244-53.

133. Munoz AJ, Wanichthanarak K, Meza E, Petranovic D. Systems biology of yeast cell death. FEMS Yeast Res. 2012; 12:249-65.

134. Rubinstein AD, Kimchi A. Life in the balance - a mechanistic view of the crosstalk between autophagy and apoptosis. J Cell Sci. 2012; 125:5259-68.

135. Young MM, Kester M, Wang HG. Sphingolipids: regulators of crosstalk between apoptosis and autophagy. J Lipid Res. 2013; 54:5-19.

136. Büttner S, Eisenberg T, Herker E, Carmona-Gutierrez D, Kroemer G, Madeo F. Why yeast cells can undergo apoptosis: death in times of peace, love, and war. J Cell Biol. 2006; 175:521-5.

137. Carmona-Gutierrez D, Eisenberg T, Büttner S, Meisinger C, Kroemer G, Madeo F. Apoptosis in yeast: triggers, pathways, subroutines. Cell Death Differ. 2010; 17:763-73.

138. Gems D, Partridge L. Genetics of longevity in model organisms: Debates and paradigm shifts. Annu. Rev. Physiol. 2013; 75:621–44.

139. López-Otín C, Blasco MA, Partridge L, Serrano M, Kroemer G. The hallmarks of aging. Cell, 2013; 153:1194–1217.

140. Kenyon CJ. The genetics of ageing. Nature. 2010; 464;504–12.

141. De Cabo R, Carmona-Gutierrez D, Bernier M, Hall MN, Madeo F. The search for antiaging interventions: From elixirs to fasting regimens. Cell. 2014; 157:1515–26.

142. Bjedov I, Toivonen JM, Kerr F, Slack C, Jacobson J, Foley A, Partridge L. Mechanisms of life span extension by rapamycin in the fruit fly Drosophila melanogaster. Cell Metab. 2010; 11:35–46.

143. Russell SJ, Kahn CR. Endocrine regulation of ageing. Nat. Rev. Mol. Cell Biol. 2007; 8:681–91.

144. Huang X, Withers BR, Dickson RC. Sphingolipids and lifespan regulation. Biochim. Biophys. Acta. 2014; 1841:657–64.

145. Mitrofanova D, Dakik P, McAuley M, Medkour Y, Mohammad K, Titorenko VI. Lipid metabolism and transport define longevity of the yeast Saccharomyces cerevisiae. Front Biosci (Landmark Ed). 2018; 23:1166-94.

146. Wang MC, O'Rourke EJ, Ruvkun G. Fat metabolism links germline stem cells and longevity in C. elegans. Science. 2008; 322:957–60.

147. O'Rourke EJ, Kuballa P, Xavier R, Ruvkun G. ω-6 Polyunsaturated fatty acids extend life span through the activation of autophagy. Genes Dev. 2013; 27:429–40.

148. Jové M, Naudí A, Aledo JC, Cabré R, Ayala V, Portero-Otin M, Barja G, Pamplona R. Plasma long-chain free fatty acids predict mammalian longevity. Sci Rep. 2013; 3:3346.

149. Arlia-Ciommo A, Leonov A, Piano A, Svistkova V, Titorenko VI. Cell-autonomous mechanisms of chronological aging in the yeast Saccharomyces cerevisiae. Microb Cell. 2014; 1:163-78.

150. Leonov A, Feldman R, Piano A, Arlia-Ciommo A, Lutchman V, Ahmadi M, Elsaser S, Fakim H, Heshmati-Moghaddam M, Hussain A, Orfali S, Rajen H, Roofigari-Esfahani N, Rosanelli L, Titorenko VI. Caloric restriction extends yeast chronological lifespan via a mechanism linking cellular aging to cell cycle regulation, maintenance of a quiescent state, entry into a non-quiescent state and survival in the non-quiescent state. Oncotarget. 2017; 8:69328-50.

151. Rowland AA, Voeltz GK. Endoplasmic reticulum-mitochondria contacts: Function of the junction. Nat. Rev. Mol. Cell Biol. 2012; 13:607–25.

152. Horvath SE, Daum G. Lipids of mitochondria. Prog Lipid Res. 2013; 52:590–614.

153. Tatsuta T, Scharwey M, Langer T. Mitochondrial lipid trafficking. Trends Cell Biol. 2014; 24:44–52.

154. Hunter T. Protein kinases and phosphatases: the yin and yang of protein phosphorylation and signaling. Cell. 1995; 80:225-36.

155. Cohen P. The role of protein phosphorylation in human health and disease. The Sir Hans Krebs Medal Lecture. Eur J Biochem. 2001; 268:5001-10.

156. Rao S, Gerbeth C, Harbauer A, Mikropoulou D, Meisinger C, Schmidt O. Signaling at the gate: phosphorylation of the mitochondrial protein import machinery. Cell Cycle. 2011; 10:2083-90.

157. Kanamaru Y, Sekine S, Ichijo H, Takeda K. The phosphorylation-dependent regulation of mitochondrial proteins in stress responses. J Signal Transduct. 2012; 2012:931215.

158. Opalińska M, Meisinger C. Mitochondrial protein import under kinase surveillance. Microb Cell. 2014; 1:51-7.

159. Opalińska M, Meisinger C. Metabolic control via the mitochondrial protein import machinery. Curr Opin Cell Biol. 2015; 33:42-8.

160. Zhang F, Zhang L, Qi Y, Xu H. Mitochondrial cAMP signaling. Cell Mol Life Sci. 2016; 73:4577-90.

161. Liu J, Li H, Papadopoulos V. PAP7, a PBR/PKA-RI-associated protein: a new element in the relay of the hormonal induction of steroidogenesis. J Steroid Biochem Mol Biol. 2003; 85:275-83.

162. Gerbeth C, Mikropoulou D, Meisinger C. From inventory to functional mechanisms: regulation of the mitochondrial protein import machinery by phosphorylation. FEBS J. 2013; 280:4933-42.

163. Kanki T, Furukawa K, Yamashita S. Mitophagy in yeast: Molecular mechanisms and physiological role. Biochim Biophys Acta. 2015; 1853:2756-65.

164. Sickmann A, Reinders J, Wagner Y, Joppich C, Zahedi R, Meyer HE, Schönfisch B, Perschil I, Chacinska A, Guiard B, Rehling P, Pfanner N, Meisinger C. The proteome of Saccharomyces cerevisiae mitochondria. Proc Natl Acad Sci USA. 2003; 100:13207-12.

165. Reinders J, Zahedi RP, Pfanner N, Meisinger C, Sickmann A. Toward the complete yeast mitochondrial proteome: multidimensional separation techniques for mitochondrial proteomics. J Proteome Res. 2006; 5:1543-54.

166. Szilard RK, Titorenko VI, Veenhuis M, Rachubinski RA. Pay32p of the yeast Yarrowia lipolytica is an intraperoxisomal component of the matrix protein translocation machinery. J Cell Biol. 1995; 131:1453-69.

167. Graham JM, 1999. Purification of a crude mitochondrial fraction by density-gradient centrifugation, in: Bonifacino JS, Dasso M, Harford JB, Lippincott-Schwartz J, Yamada KM (eds.), Current Protocols in Cell Biology. John Wiley & Sons, Inc., NJ, pp. 3.4.1-3.4.22.

168. Fabrizio P, Liou LL, Moy VN, Diaspro A, Valentine JS, Gralla EB, Longo VD. SOD2 functions downstream of Sch9 to extend longevity in yeast. Genetics. 2003; 163:35-46.

169. Titorenko VI, Smith JJ, Szilard RK, Rachubinski RA. Pex20p of the yeast Yarrowia lipolytica is required for the oligomerization of thiolase in the cytosol and for its targeting to the peroxisome. J Cell Biol. 1998; 142:403-20.

170. Rieder SE, Emr SD, 2000. Isolation of subcellular fractions from the yeast Saccharomyces cerevisiae, in: Bonifacino JS, Dasso M, Harford JB, Lippincott-Schwartz J, Yamada KM (eds.), Current Protocols in Cell Biology. John Wiley & Sons, Inc., NJ, pp. 3.8.1-3.8.68.

171. Verstrepen KJ, Van Laere SD, Vercammen J, Derdelinckx G, Dufour JP, Pretorius IS, Winderickx J, Thevelein JM, Delvaux FR. The Saccharomyces cerevisiae alcohol acetyl transferase Atf1p is localized in lipid particles. Yeast. 2004; 21:367-77.

172. Fraenkel DG, 2011. Yeast intermediary metabolism. Cold Spring Harbor Laboratory Press, Cold Spring Harbor, NY.

173. Henry SA, Kohlwein SD, Carman GM. Metabolism and regulation of glycerolipids in the yeast Saccharomyces cerevisiae. Genetics. 2012; 190:317-49.

174. Kohlwein SD, Veenhuis M, van der Klei IJ. Lipid droplets and peroxisomes: key players in cellular lipid homeostasis or a matter of fat - store 'em up or burn 'em down. Genetics. 2013; 193:1-50.

175. Klug L, Daum G. Yeast lipid metabolism at a glance. FEMS Yeast Res. 2014; 14:369-88.

176. Dakik P, Titorenko VI. Communications between mitochondria, the nucleus, vacuoles, peroxisomes, the endoplasmic reticulum, the plasma membrane, lipid droplets, and the cytosol during yeast chronological aging. Front Genet. 2016; 7:177.

177. François J, Parrou JL. Reserve carbohydrates metabolism in the yeast Saccharomyces cerevisiae. FEMS Microbiol Rev. 2001; 25:125-45.

178. Eleutherio E, Panek A, De Mesquita JF, Trevisol E, Magalhães R. Revisiting yeast trehalose metabolism. Curr Genet. 2015; 61:263-74.

179. Singer MA, Lindquist S. Thermotolerance in Saccharomyces cerevisiae: The Yin and Yang of trehalose. Trends Biotechnol. 1998; 16:460-68.

180. Werner-Washburne M, Roy S, Davidson GS. Aging and the survival of quiescent and non-quiescent cells in yeast stationary-phase cultures. Subcell Biochem. 2012; 57:123-43.

181. Li L, Miles S, Melville Z, Prasad A, Bradley G, Breeden LL. Key events during the transition from rapid growth to quiescence in budding yeast require posttranscriptional regulators. Mol Biol Cell. 2013; 24:3697-709.

182. Sibirny AA, Titorenko VI, Gonchar MV, Ubiyvovk VM, Ksheminskaya GP, Vitvitskaya OP. Genetic control of methanol utilization in yeasts. J Basic Microbiol. 1988; 28:293-319.

183. van der Klei IJ, Yurimoto H, Sakai Y, Veenhuis M. The significance of peroxisomes in methanol metabolism in methylotrophic yeast. Biochim Biophys Acta. 2006; 1763:1453-62.

184. Binns D, Januszewski T, Chen Y, Hill J, Markin VS, Zhao Y, Gilpin C, Chapman KD, Anderson RG, Goodman JM. An intimate collaboration between peroxisomes and lipid bodies. J Cell Biol. 2006; 173:719-31.

185. Friedman JR, Nunnari J. Mitochondrial form and function. Nature. 2014; 505:335-43.

186. Labbé K, Murley A, Nunnari J. Determinants and functions of mitochondrial behavior. Annu Rev Cell Dev Biol. 2014; 30:357-91.

187. Hardwick JM, Cheng WC. Mitochondrial programmed cell death pathways in yeast. Dev Cell. 2004; 7:630-2.

188. Büttner S, Eisenberg T, Herker E, Carmona-Gutierrez D, Kroemer G, Madeo F. Why yeast cells can undergo apoptosis: death in times of peace, love, and war. J Cell Biol. 2006; 175:521-5.

189. Eisenberg T, Büttner S, Kroemer G, Madeo F. The mitochondrial pathway in yeast apoptosis. Apoptosis. 2007; 12:1011-23.

190. Cheng WC, Leach KM, Hardwick JM. Mitochondrial death pathways in yeast and mammalian cells. Biochim Biophys Acta. 2008; 1783:1272-9.

191. Braun RJ, Westermann B. Mitochondrial dynamics in yeast cell death and aging. Biochem Soc Trans. 2011; 39:1520-6.

192. Guaragnella N, Zdralević M, Antonacci L, Passarella S, Marra E, Giannattasio S. The role of mitochondria in yeast programmed cell death. Front Oncol. 2012; 2:70.

193. Knorre DA, Popadin KY, Sokolov SS, Severin FF. Roles of mitochondrial dynamics under stressful and normal conditions in yeast cells. Oxid Med Cell Longev. 2013; 2013:m139491.

194. Bernhardt D, Müller M, Reichert AS, Osiewacz HD. Simultaneous impairment of mitochondrial fission and fusion reduces mitophagy and shortens replicative lifespan. Sci Rep. 2015; 5:7885.

195. Strich R. Programmed cell death initiation and execution in budding yeast. Genetics. 2015; 200:1003-14.

196. Falcone C, Mazzoni C. External and internal triggers of cell death in yeast. Cell Mol Life Sci. 2016; 73:2237-50.

197. Richard VR, Beach A, Piano A, Leonov A, Feldman R, Burstein MT, Kyryakov P, Gomez-Perez A, Arlia-Ciommo A, Baptista S, Campbell C, Goncharov D, Pannu S, Patrinos D, Sadri B, Svistkova V, Victor A, Titorenko VI. Mechanism of liponecrosis, a distinct mode of programmed cell death. Cell Cycle. 2014; 13:3707-26.

198. Arlia-Ciommo A, Svistkova V, Mohtashami S, Titorenko VI. A novel approach to the discovery of anti-tumor pharmaceuticals: searching for activators of liponecrosis. Oncotarget. 2016; 7:5204-25.

199. Hiltunen JK, Mursula AM, Rottensteiner H, Wierenga RK, Kastaniotis AJ, Gurvitz A. The biochemistry of peroxisomal beta-oxidation in the yeast Saccharomyces cerevisiae. FEMS Microbiol Rev. 2003; 27:35-64.

200. Giorgio M, Trinei M, Migliaccio E, Pelicci PG. Hydrogen peroxide: a metabolic by-product or a common mediator of ageing signals? Nat Rev Mol Cell Biol. 2007; 8:722-8.

201. Balaban RS, Nemoto S, Finkel T. Mitochondria, oxidants, and aging. Cell. 2005; 120:483-95.

202. Longo VD, Liou LL, Valentine JS, Gralla EB. Mitochondrial superoxide decreases yeast survival in stationary phase. Arch Biochem Biophys. 1999; 365:131-42.

203. Lin MT, Beal MF. Mitochondrial dysfunction and oxidative stress in neurodegenerative diseases. Nature. 2006; 443:787-95.

204. Fabrizio P, Pozza F, Pletcher SD, Gendron CM, Longo VD. Regulation of longevity and stress resistance by Sch9 in yeast. Science. 2001; 292:288-90.

205. Burstein MT, Kyryakov P, Beach A, Richard VR, Koupaki O, Gomez-Perez A, Leonov A, Levy S, Noohi F, Titorenko VI. Lithocholic acid extends longevity of chronologically aging yeast only if added at certain critical periods of their lifespan. Cell Cycle. 2012; 11:3443-62.

206. Oelkers P, Cromley D, Padamsee M, Billheimer JT, Sturley SL. The DGA1 gene determines a second triglyceride synthetic pathway in yeast. J Biol Chem. 2002; 277:8877-81.

207. Sorger D, Daum G. Synthesis of triacylglycerols by the acyl-coenzyme A: diacyl-glycerol acyltransferase Dga1p in lipid particles of the yeast Saccharomyces cerevisiae. J Bacteriol. 2002; 184:519-24.

208. Athenstaedt K, Daum G. YMR313c/TGL3 encodes a novel triacylglycerol lipase located in lipid particles of Saccharomyces cerevisiae. J Biol Chem. 2003; 278:23317-23.

209. Athenstaedt K, Daum G. Tgl4p and Tgl5p, two triacylglycerol lipases of the yeast Saccharomyces cerevisiae are localized to lipid particles. J Biol Chem. 2005; 280:37301-09.

210. Jandrositz A, Petschnigg J, Zimmermann R, Natter K, Scholze H, Hermetter A, Kohlwein SD, Leber R. The lipid droplet enzyme Tgl1p hydrolyzes both steryl esters and triglycerides in the yeast, Saccharomyces cerevisiae. Biochim Biophys Acta. 2005; 1735:50-8.

211. Zhao Y, Gilliat AF, Ziehm M, Turmaine M, Wang H, Ezcurra M, Yang C, Phillips G, McBay D, Zhang WB, Partridge L, Pincus Z, Gems D. Two forms of death in ageing Caenorhabditis elegans. Nat Commun. 2017; 8:15458.

212. Thomas D, Surdin-Kerjan Y. Metabolism of sulfur amino acids in Saccharomyces cerevisiae. Microbiol Mol Biol Rev. 1997; 61:503-32.

213. Butler JA, Ventura N, Johnson TE, Rea SL. Long-lived mitochondrial (Mit) mutants of Caenorhabditis elegans utilize a novel metabolism. FASEB J. 2010; 24:4977-88.

214. Yoshida R, Tamura T, Takaoka C, Harada K, Kobayashi A, Mukai Y, Fukusaki E. Metabolomics-based systematic prediction of yeast lifespan and its application for semi-rational screening of ageing-related mutants. Aging Cell 2010; 9:616-25.

215. Houtkooper RH, Argmann C, Houten SM, Cantó C, Jeninga EH, Andreux PA, Thomas C, Doenlen R, Schoonjans K, Auwerx J. The metabolic footprint of aging in mice. Sci Rep. 2011; 1:134.

216. Yu Z, Zhai G, Singmann P, He Y, Xu T, Prehn C, Römisch-Margl W, Lattka E, Gieger C, Soranzo N, Heinrich J, Standl M, Thiering E, Mittelstraß K, Wichmann HE, Peters A, Suhre K, Li Y, Adamski J, Spector TD, Illig T, Wang-Sattler R. Human serum metabolic profiles are age dependent. Aging Cell 2012; 11:960-7.

217. Sarup P, Pedersen SM, Nielsen NC, Malmendal A, Loeschcke V. The metabolic profile of long-lived Drosophila melanogaster. PLoS One 2012; 7:e47461.

218. Butler JA, Mishur RJ, Bhaskaran S, Rea SL. A metabolic signature for long life in the Caenorhabditis elegans Mit mutants. Aging Cell 2013; 12:130-8.

219. Collino S, Montoliu I, Martin FP, Scherer M, Mari D, Salvioli S, Bucci L, Ostan R, Monti D, Biagi E, Brigidi P, Franceschi C, Rezzi S. Metabolic signatures of extreme longevity in northern Italian centenarians reveal a complex remodeling of lipids, amino acids, and gut microbiota metabolism. PLoS One 2013; 8:e56564.

220. Arlia-Ciommo A, Piano A, Leonov A, Svistkova V, Titorenko VI. Quasi-programmed aging of budding yeast: a trade-off between programmed processes of cell proliferation, differentiation, stress response, survival and death defines yeast lifespan. Cell Cycle 2014; 13:3336-49.

221. Arlia-Ciommo A, Piano A, Svistkova V, Mohtashami S, Titorenko VI. Mechanisms underlying the anti-aging and anti-tumor effects of lithocholic bile acid. Int J Mol Sci. 2014; 15:16522-43.

222. Avanesov AS, Ma S, Pierce KA, Yim SH, Lee BC, Clish CB, Gladyshev VN. Age- and diet-associated metabolome remodeling characterizes the aging process driven by damage accumulation. Elife 2014; 3:e02077.

223. Hashim Z, Mukai Y, Bamba T, Fukusaki E. Metabolic profiling of retrograde pathway transcription factors rtg1 and rtg3 knockout yeast. Metabolites 2014; 4:580-98.

224. Jové M, Naudí A, Ramírez-Núñez O, Portero-Otín M, Selman C, Withers DJ, Pamplona R. Caloric restriction reveals a metabolomic and lipidomic signature in liver of male mice. Aging Cell 2014; 13:828-37.

225. Kamei Y, Tamada Y, Nakayama Y, Fukusaki E, Mukai Y. Changes in transcription and metabolism during the early stage of replicative cellular senescence in budding yeast. J Biol Chem. 2014; 289:32081-93.

226. Mahanti P, Bose N, Bethke A, Judkins JC, Wollam J, Dumas KJ, Zimmerman AM, Campbell SL, Hu PJ, Antebi A, Schroeder FC. Comparative metabolomics reveals endogenous ligands of DAF-12, a nuclear hormone receptor, regulating C. elegans development and lifespan. Cell Metab. 2014; 19:73-83.

227. Richard VR, Bourque SD, Titorenko VI. Metabolomic and lipidomic analyses of chronologically aging yeast. Methods Mol Biol. 2014; 1205:359-73.

228. Ruckenstuhl C, Netzberger C, Entfellner I, Carmona-Gutierrez D, Kickenweiz T, Stekovic S, Gleixner C, Schmid C, Klug L, Sorgo AG, Eisenberg T, Büttner S, Mariño G, Koziel R, Jansen-Dürr P, Fröhlich KU, Kroemer G, Madeo F. Lifespan extension by methionine restriction requires autophagy-dependent vacuolar acidification. PLoS Genet. 2014; 10:e1004347.

229. Connerth M, Tatsuta T, Haag M, Klecker T, Westermann B, Langer T. Intramitochondrial transport of phosphatidic acid in yeast by a lipid transfer protein. Science. 2012; 338:815-8.

230. Baile MG, Lu YW, Claypool SM. The topology and regulation of cardiolipin biosynthesis and remodeling in yeast. Chem Phys Lipids. 2014; 179:25-31.

231. Aaltonen MJ, Friedman JR, Osman C, Salin B, di Rago JP, Nunnari J, Langer T, Tatsuta T. MICOS and phospholipid transfer by Ups2-Mdm35 organize membrane lipid synthesis in mitochondria. J Cell Biol. 2016; 213:525-534.

232. Miyata N, Watanabe Y, Tamura Y, Endo T, Kuge O. Phosphatidylserine transport by Ups2-Mdm35 in respiration-active mitochondria. J Cell Biol. 2016; 214:77-88.

233. Dimmer KS, Rapaport D. Mitochondrial contact sites as platforms for phospholipid exchange. Biochim Biophys Acta. 2017; 1862:69-80.

234. Mårtensson CU, Doan KN, Becker T. Effects of lipids on mitochondrial functions. Biochim Biophys Acta. 2017; 1862:102-13.

235. Tatsuta T, Langer T. Intramitochondrial phospholipid trafficking. Biochim Biophys Acta. 2017; 1862:81-9.

236. Leonov A, Arlia-Ciommo A, Bourque SD, Koupaki O, Kyryakov P, Dakik P, McAuley M, Medkour Y, Mohammad K, Di Maulo T, Titorenko VI. Specific changes in mitochondrial lipidome alter mitochondrial proteome and increase the geroprotective efficiency of lithocholic acid in chronologically aging yeast. Oncotarget. 2017; 8:30672-91.

237. McMahon HT, Gallop JL. Membrane curvature and mechanisms of dynamic cell membrane remodelling. Nature. 2005; 438:590-6.

238. Zimmerberg J. Membrane biophysics. Curr Biol. 2006; 16:R272- R276.

239. van Meer G, Voelker DR, Feigenson GW. Membrane lipids: where they are and how they behave. Nat Rev Mol Cell Biol. 2008; 9:112-24.

240. Shibata Y, Hu J, Kozlov MM, Rapoport TA. Mechanisms shaping the membranes of cellular organelles. Annu Rev Cell Dev Biol. 2009; 25:329-54.

241. McMahon HT, Boucrot E. Membrane curvature at a glance. J Cell Sci. 2015; 128:1065-70.

242. Jarsch IK, Daste F, Gallop JL. Membrane curvature in cell biology: An integration of molecular mechanisms. J Cell Biol. 2016; 214:375-87.

243. Madeo F, Fröhlich E, Fröhlich KU. A yeast mutant showing diagnostic markers of early and late apoptosis. J Cell Biol. 1997; 139:729-34.

244. Mukaka MM. Statistics corner: A guide to appropriate use of correlation coefficient in medical research. Malawi Med J. 2012; 24:69-71.

245. Beach A, Leonov A, Arlia-Ciommo A, Svistkova V, Lutchman V, Titorenko VI. Mechanisms by which different functional states of mitochondria define yeast longevity. Int. J. Mol. Sci. 2015, 16:5528-54.

246. Beach A, Richard VR, Bourque S, Boukh-Viner T, Kyryakov P, Gomez-Perez A, Arlia-Ciommo A, Feldman R, Leonov A, Piano A, Svistkova V, Titorenko VI. Lithocholic bile acid accumulated in yeast mitochondria orchestrates a development of an anti-aging cellular pattern by causing age-related changes in cellular proteome. Cell Cycle. 2015; 14:1643-1656.

247. Medkour Y, Titorenko VI. Mitochondria operate as signaling platforms in yeast aging. Aging (Albany NY). 2016; 8:212-213.

248. Medkour Y, Dakik P, McAuley M, Mohammad K, Mitrofanova D, Titorenko VI. Mechanisms underlying the essential role of mitochondrial membrane lipids in yeast chronological aging. Oxid Med Cell Longev. 2017; 2017:2916985.

249. Arlia-Ciommo A, Leonov A, Beach A, Richard VR, Bourque SD, Burstein MT, Kyryakov P, Gomez-Perez A, Koupaki O, Feldman R, Titorenko VI. Caloric restriction delays yeast chronological aging by remodeling carbohydrate and lipid metabolism, altering peroxisomal and mitochondrial functionalities, and postponing the onsets of apoptotic and liponecrotic modes of regulated cell death. Oncotarget. 2018; 9:16163-84.

250. Mohammad K, Dakik P, Medkour Y, McAuley M, Mitrofanova D, Titorenko VI. Yeast cells exposed to exogenous palmitoleic acid either adapt to stress and survive or commit to regulated liponecrosis and die. Oxid Med Cell Longev. 2018; 2018:3074769.

251. Swiegers JH, Dippenaar N, Pretorius IS, Bauer FF. Carnitine-dependent metabolic activities in Saccharomyces cerevisiae: three carnitine acetyltransferases are essential in a carnitine-dependent strain. Yeast. 2001; 18:585-95.

252. Franken J, Kroppenstedt S, Swiegers JH, Bauer FF. Carnitine and carnitine acetyltransferases in the yeast Saccharomyces cerevisiae: a role for carnitine in stress protection. Curr Genet. 2008; 53:347-60.

253. Lewin AS, Hines V, Small GM. Citrate synthase encoded by the CIT2 gene of Saccharomyces cerevisiae is peroxisomal. Mol Cell Biol. 1990; 10:1399-1405.

254. Kaplan RS, Mayor JA, Gremse DA, Wood DO. High level expression and characterization of the mitochondrial citrate transport protein from the yeast Saccharomyces cerevisiae. J Biol Chem. 1995; 270:4108-14.

255. Bricker DK, Taylor EB, Schell JC, Orsak T, Boutron A, Chen YC, Cox JE, Cardon CM, Van Vranken JG, Dephoure N, Redin C, Boudina S, Gygi SP, Brivet M, Thummel CS, Rutter J. A mitochondrial pyruvate carrier required for pyruvate uptake in yeast, Drosophila, and humans. Science. 2012; 337:96-100.

256. Herzig S, Raemy E, Montessuit S, Veuthey JL, Zamboni N, Westermann B, Kunji ER, Martinou JC. Identification and functional expression of the mitochondrial pyruvate carrier. Science. 2012; 337:93-6.

257. Friedman JR, Nunnari J. Mitochondrial form and function. Nature. 2014; 505:335-43.

258. Labbé K, Murley A, Nunnari J. Determinants and functions of mitochondrial behavior. Annu Rev Cell Dev Biol. 2014; 30:357-91.

259. Choi SY, Huang P, Jenkins GM, Chan DC, Schiller J, Frohman MA. A common lipid links Mfn-mediated mitochondrial fusion and SNARE-regulated exocytosis. Nat Cell Biol. 2006; 8:1255-62.

260. Huang H, Gao Q, Peng X, Choi SY, Sarma K, Ren H, Morris AJ, Frohman MA. piRNA-associated germline nuage formation and spermatogenesis require MitoPLD profusogenic mitochondrial-surface lipid signaling. Dev Cell. 2011; 20:376-87.

261. Baba T, Kashiwagi Y, Arimitsu N, Kogure T, Edo A, Maruyama T, Nakao K, Nakanishi H, Kinoshita M, Frohman MA, Yamamoto A, Tani K. Phosphatidic acid (PA)-preferring phospholipase A1 regulates mitochondrial dynamics. J Biol Chem. 2014; 289:11497-511.

262. Frohman MA. Role of mitochondrial lipids in guiding fission and fusion. J Mol Med. 2015; 93: 3-269.

263. Kameoka S, Adachi Y, Okamoto K, Iijima M, Sesaki H. Phosphatidic acid and cardiolipin coordinate mitochondrial dynamics. Trends Cell Biol. 2018; 28:67-76.

264. Vögtle FN, Keller M, Taskin AA, Horvath SE, Guan XL, Prinz C, Opalińska M, Zorzin C, van der Laan M, Wenk MR, Schubert R, Wiedemann N, Holzer M, Meisinger C. The fusogenic lipid phosphatidic acid promotes the biogenesis of mitochondrial outer membrane protein Ugo1. J Cell Biol. 2015; 210:951-60.

265. Adachi Y, Itoh K, Yamada T, Cerveny KL, Suzuki TL, Macdonald P, Frohman MA, Ramachandran R, Iijima M, Sesaki H. Coincident phosphatidic acid interaction restrains Drp1 in mitochondrial division. Mol Cell. 2016; 63:1034-43.

266. Adachi Y, Iijima M, Sesaki H. An unstructured loop that is critical for interactions of the stalk domain of Drp1 with saturated phosphatidic acid. Small GTPases. 2018; 9:472-9.

267. Hardwick JM, Cheng WC. Mitochondrial programmed cell death pathways in yeast. Dev Cell. 2004; 7:630-632.

268. Büttner S, Eisenberg T, Herker E, Carmona-Gutierrez D, Kroemer G, Madeo F. Why yeast cells can undergo apoptosis: death in times of peace, love, and war. J Cell Biol. 2006; 175:521-525.

269. Eisenberg T, Büttner S, Kroemer G, Madeo F. The mitochondrial pathway in yeast apoptosis. Apoptosis. 2007; 12:1011-1023.

270. Cheng WC, Leach KM, Hardwick JM. Mitochondrial death pathways in yeast and mammalian cells. Biochim Biophys Acta. 2008; 1783:1272-1279.

271. Braun RJ, Westermann B. Mitochondrial dynamics in yeast cell death and aging. Biochem Soc Trans. 2011; 39:1520-1526.

272. Guaragnella N, Zdralević M, Antonacci L, Passarella S, Marra E, Giannattasio S. The role of mitochondria in yeast programmed cell death. Front Oncol. 2012; 2:70.

273. Knorre DA, Popadin KY, Sokolov SS, Severin FF. Roles of mitochondrial dynamics under stressful and normal conditions in yeast cells. Oxid Med Cell Longev. 2013; 2013:m139491.

274. Bernhardt D, Müller M, Reichert AS, Osiewacz HD. Simultaneous impairment of mitochondrial fission and fusion reduces mitophagy and shortens replicative lifespan. Sci Rep. 2015; 5:7885.

275. Strich R. Programmed cell death initiation and execution in budding yeast. Genetics. 2015; 200:1003-1014.

276. Falcone C, Mazzoni C. External and internal triggers of cell death in yeast. Cell Mol Life Sci. 2016; 73:2237-2250.

277. Carmona-Gutierrez D, Bauer MA, Zimmermann A, Aguilera A, Austriaco N, Ayscough K, Balzan R, Bar-Nun S, Barrientos A, Belenky P, Blondel M, Braun RJ, Breitenbach M, Burhans WC, Büttner S, Cavalieri D, Chang M, Cooper KF, Côrte-Real M, Costa V, Cullin C, Dawes I, Dengjel J, Dickman MB, Eisenberg T, Fahrenkrog B, Fasel N, Fröhlich KU, Gargouri A, Giannattasio S, Goffrini P, Gourlay CW, Grant CM, Greenwood MT, Guaragnella N, Heger T, Heinisch J, Herker E, Herrmann JM, Hofer S, Jiménez-Ruiz A, Jungwirth H, Kainz K, Kontoyiannis DP, Ludovico P, Manon S, Martegani E, Mazzoni C, Megeney LA, Meisinger C, Nielsen J, Nyström T, Osiewacz HD, Outeiro TF, Park HO, Pendl T, Petranovic D, Picot S, Polčic P, Powers T, Ramsdale M, Rinnerthaler M, Rockenfeller P, Ruckenstuhl C, Schaffrath R, Segovia M, Severin FF, Sharon A, Sigrist SJ, Sommer-Ruck C, Sousa MJ, Thevelein JM, Thevissen K, Titorenko V, Toledano MB, Tuite M, Vögtle FN, Westermann B, Winderickx J, Wissing S, Wölfl S, Zhang ZJ, Zhao RY, Zhou B, Galluzzi L, Kroemer G, Madeo F. Guidelines and recommendations on yeast cell death nomenclature. Microb Cell. 2018; 5:4-31.

278. Herker E, Jungwirth H, Lehmann KA, Maldener C, Fröhlich KU, Wissing S, Büttner S, Fehr M, Sigrist S, Madeo F. Chronological aging leads to apoptosis in yeast. J Cell Biol. 2004; 164:501-507.

279. Carmona-Gutierrez D, Eisenberg T, Büttner S, Meisinger C, Kroemer G, Madeo F. Apoptosis in yeast: triggers, pathways, subroutines. Cell Death Differ. 2010; 17:763-773.